AD-A276 642

‖‖‖‖‖‖‖‖‖‖‖‖‖‖

AD

6294-CH-01
DTIC.

MECHANISMS OF LASER INDUCED REACTIONS IN OPAQUE HETEROGENEOUS ENVIRONMENTS

Final Technical Report

by

F. WILKINSON

November, 1993

DTIC
ELECTE
MAR 0 8 1994
S E D

United States Army
European Research Office of the U.S. Army
London, England

Contract Number   DAJA 45-90-C-0022

Loughborough University of Technology
Loughborough
Leicestershire
LE11 3TU, England

Approved for Public Release; distribution unlimited

DTIC QUALITY INSPECTED 1

94-07495

‖‖‖‖‖‖‖‖‖‖‖‖‖

94 3 7 012

Best
Available
Copy

REPORT DOCUMENTATION PAGE

ERO Proposal Number: R&D No. 6294-CH-01   **Contract Number:** DAJA 45-90-C-0022

Title of Proposal: Mechanisms of Laser Induced Reactions in Opaque Heterogeneous Environments

Report Number: _____011_____ **Period Covered: From** ___Nov 1990___ **to** ___Nov 1993___

	CRA&I	☒
..TIS	TAB	☐
JTIC	Announced	☐
Justification		

Name of Institution: Loughborough University of Technology
Administration Building
Loughborough
Leicestershire, LE11 3TU
U.K.

By _____

Jistibution/

Availability Codes

Jist	Avail and/or Special
A-1	

Principal Investigator: Professor F. Wilkinson

Abstract: (Approximately 75 words for Interim Report, 300 for Final)

The technique of laser flash photolysis has been applied to both heterogeneous and homogeneous samples in order to increase understanding of the mechanisms of laser induced reactions at surfaces. Nanosecond diffuse reflectance laser flash photolysis has been used to study triplet state absorption and fluorescence emission of monomers and dimers of acridine orange and other dyes which are shown to aggregate when adsorbed on microcrystalline cellulose and on other surfaces. The properties of excited states within dyed fabrics have been evaluated in several cases. The mechanism of the yellowing of thermomechanical paper pulp has also been investigated and transients studied on nanosecond timescales for the first time. Triplet-triplet energy transfer from benzophenone to oxazine dyes, from eosin to anthracene, and from anthracene to azomethine dyes has been studied on both cellulose and silica surfaces. This work demonstrates the occurrence of energy transfe by static and dynamic mechanisms depending on both the nature of the surface and the adsorbed species. The first picosecond studies exciting directly into the charge transfer absorption bands of aromatic hydrocarbon/oxygen complexes formed in the presence of high pressures of oxygen have been carried out to demonstrate the role of charge-transfer interactions in determining the singlet oxygen formation efficiencies during quenching of electronically excited states by molecular oxygen. Nanosecond laser excitation of a series of naphthalene and anthracene derivatives in the presence and absence of oxygen has clearly demonstrated for the first time the importance of charge transfer interactions in determining oxygen quenching constants and singlet oxygen formation efficiencies.

Thirteen papers, including a chapter in a book, have already been published, three papers are in press and these together with ten abstracts of contributions to conferences, including several plenary lectures at International Conferences, are given as Appendixes to this report.

USARDSG Form 1188

ABSTRACT

The technique of laser flash photolysis has been applied to both heterogeneous and homogeneous samples in order to increase understanding of the mechanisms of laser induced reactions at surfaces. Nanosecond diffuse reflectance laser flash photolysis has been used to study triplet state absorption and fluorescence emission of monomers and dimers of acridine orange and other dyes which are shown to aggregate when adsorbed on microcrystalline cellulose and on other surfaces. The properties of excited states within dyed fabrics have been evaluated in several cases. The mechanism of the yellowing of thermomechanical paper pulp has also been investigated and transients studied on nanosecond timescales for the first time. Triplet-triplet energy transfer from benzophenone to oxazine dyes, from eosin to anthracene, and from anthracene to azomethine dyes has been studied on both cellulose and silica surfaces. This work demonstrates the occurrence of energy transfer by static and dynamic mechanisms depending on both the nature of the surface and the adsorbed species. The first picosecond studies exciting directly into the charge transfer absorption bands of aromatic hydrocarbon/oxygen complexes formed in the presence of high pressures of oxygen have been carried out to demonstrate the role of charge-transfer interactions in determining the singlet oxygen formation efficiencies during quenching of electronically excited states by molecular oxygen. Nanosecond laser excitation of a series of naphthalene and anthracene derivatives in the presence and absence of oxygen has clearly demonstrated for the first time the importance of charge transfer interactions in determining oxygen quenching constants and singlet oxygen formation efficiencies. Thirteen papers, including a chapter in a book, have already been published, three papers are in press and these together with ten abstracts of contributions to conferences, including several plenary lectures at International Conferences, are given as Appendixes to this report.

KEYWORDS

Aggregation	Alumina
Aromatic hydrocarbons	Cellulose
Charge transfer	Diffuse reflectance
Dyed Fabrics	Emission spectroscopy
Energy transfer	Fluorescein dyes
Heterogeneous photochemistry	Interfaces
Kubelka-Munk theory	Laser flash photolysis
Metal oxide surfaces	Opaque materials
Oxygen quenching	Photochemistry
Picosecond spectroscopy	Rhodamine dyes
Sensitizers	Silica
Surfaces	Transient absorption
Transient decay	Triplet states

TABLE OF CONTENTS

LIST OF APPENDIXES

Published Papers

A. **Picosecond Absorption Studies on the Role of Charge Transfer Interactions in the Mechanism of Quenching of Triplet States by Molecular Oxygen.**
Chem. Phys. Lett., 1993, **202**, 528-534.

B. **Kinetic Spectroscopy of Pyrazolotriazole Azomethine Dyes.**
J. Chem. Soc. Faraday Trans., 1993, **89**(14), 2385-2390.

C. **The Efficiency of Singlet Oxygen Generation by Substituted Naphthalenes in Benzene. Evidence for the Participation of Charge-Transfer Interactions.**
Chem. Phys. Lett., 1992, **199**, 314-319.

D. **The Application of Diffuse Reflectance Laser Photolysis to study Photochemistry at Interfaces and in Dyed Fabrics.**
Proc. Indian Acad. Sci. (Chem. Sci.), 1992, **104**, 739-745.

E. **Photochemistry on Surfaces: Fluorescence Emission of Monomers and Dimers and Triplet State Absorption of Acridine Orange Adsorbed on Microcrystalline Cellulose.**
Spectrochemica Acta, 1992, **48A**, 135-145.

F. **Diffuse Reflectance Laser Photolysis Studies of the Mechanisms of Light-Induced Reactions in Heterogeneous Systems.**
Proc. Indian Acad. Sci. (Chem. Sci.), 1992, **104**, 287-298.

G. **Photochemistry on Surfaces: Fluorescence Emission Quantum Yield Evaluation of Dyes Adsorbed on Microcrystalline Cellulose.**
J. Chem. Soc. Faraday Trans, 1992, **88**(1), 15-22.

H. **Photochemistry on Surfaces: Triplet-Triplet Energy Transfer on Microcrystalline Cellulose Studied by Diffuse Reflectance Transient Absorption and Emission Spectroscopy.**
Photochem. Photobiol., 1991, **54**, 599-608.

I. **Diffuse Reflectance Laser Flash Photolysis of Adsorbed Molecules.**
Proc. Indian Acad. Sci. (Chem. Sci.), 1991, **103**, 305-311.

J. **Diffuse Reflectance Laser Photolysis of Adsorbed Molecules.**
Photochemical Processes in Organized Molecular Systems Ed. K. Honda *Elsevier*, 1991, 377-396.

K. **Diffuse-reflectance Laser Flash Photolysis Studies of the Photochemistry of Bleached Thermomechanical Pulp.**
J. Photochem. Photobiol, 1991, **57**, 111-125

L. **Picosecond Diffuse Reflectance and Transmission Laser Flash Photolysis Study of Various Triaryl-2-pyrazolines.**
Spectrochemica Acta, 1990, **46A**, 975-985

Chapter in Book

M. **Diffuse Reflectance Laser Flash Photolysis of Thermomechanical Pulp.**
Photochemistry of Lignocellulosic Materials, Eds C. Heitner & J.C. Scaiano,
ACS Symp. 531, 1993, 86-98

Papers to be Published

N. **Factors Governing the Efficiency of Singlet Oxygen Production During Oxygen Quenching of Singlet and Triplet States of Anthracene Derivatives in Cyclohexane Solution.**
Accepted by Amer. Chem. Soc.., 1993.

O. **Factors which Determine the Efficiency of Sensitized Singlet Oxygen Production.**
Accepted by Proc. Indian Acad. Sci (Chem. Sci.), 1993.

P. **Excited Triplet State Interactions with Molecular Oxygen: Influence of Charge Transfer on the Bimolecular Quenching Rate Constants and the Yields of Singlet Oxygen ($O_2^{*},{}^1\Delta_g$) for Substituted Naphthalenes in Various Solvents.**
Submitted to J. Chem. Phys.

Published Conference Contributions

Q. **Nanosecond and Picosecond Laser Flash Photolysis Studies of Charge Transfer Interactions in the Mechanisms of Quenching by Molecular Oxygen.**
2nd Conference on Lasers in Chemistry, Trieste, 1993.

R. **Oxygen Quenching of Excited States and Quantum Yields of Sensitized Production of Singlet Oxygen.**
Congreso de Fotoquimica, Poblet, Spain, 1993, p3.

S. **Time Resolved Diffuse Reflectance Spectroscopy involving Molecules Adsorbed on Oxide Minerals.**
Proc. Conf. Environmental Photochem., Adelboden, Switzerland, 1993, p21.

T. **Nanosecond and Picosecond Studies of the Effects of Charge Transfer Interactions Oxygen Quenching of Excited States and on Singlet Oxygen Yields.**
Proc. Int. Conf. Photochem., Vancouver, Canada, 1993, p110.

U. **The Role of Charge Transfer Interactions in the Mechanism of Quenching of Triplet States by Molecular Oxygen, - Nanosecond and Picosecond Laser Flash Photolysis Studies.**
Presented at 2nd Int. Conf. Solar Energy and Ap. Photochem., Cairo, Egypt, 1993.

V. **Diffuse Reflectance Laser Photolysis Studies of Light-Induced Reactions in Heterogeneous Systems.**
Proc. Fifth Cong. Euro. Soc. Photobiology, Marburg, Germany, 1993, p225.

W. **Luminescence, Transient Absorption and Energy Transfer Involving Monomeric and Dimeric Adsorbed Dyes on Surfaces.**
Proc. IUPAC Symp. Photochem., Leuven, Belgium, 1992, p546.

X. **Picosecond Absorption Studies of Organic Molecule-Molecular Oxygen Excited Charge Transfer Complexes.**
Proc. IUPAC Symp. Photochem., Leuven, Belgium, 1992, p328.

Y. **Dynamic Energy and Electron Transfer on Surfaces.**
Proc. XVth Int. Conf. Photochem., Paris, France, 1991, III-41.

Z. **Primary Photochemical Processes of Dyes Adsorbed on Surfaces.**
Proc. XVth Int. Conf. Photochem., Paris, France, 1991, III-7.

1. INTRODUCTION

In 1981 Wilkinson and Kessler demonstrated that for opaque samples diffuse reflected light can be used as an analysing source in laser flash photolysis studies [1]. This extended to opaque heterogeneous and often highly scattering samples, the advantages of being able to subject them to laser flash photolysis investigations using diffuse reflected light in place of transmitted light as the analysing source on time scales later extended into the picosecond domain by Wilkinson et al [2]. In the three year period covered by this report, Dr. D. J. McGarvey and Dr. D. R. Worrall (for the last three months), have been working full time as postdoctoral research assistants on this project and Professor F Wilkinson, Principal Investigator, has devoted 30% of his time to this project. Thirteen papers have been published [3-15], two other papers are in press [16,17] and one has been submitted recently [18]. These papers together with abstracts of conference contributions [19-28] are included as appendixes to this report. Since most experimental detail are given in these papers, only a brief survey is given here. In the Results and Discussion section of this report a summary of the published results is given, full details of which are to be found in the papers attached as Appendixes A-Z.

2. EXPERIMENTAL

The equipment used in nanosecond transmission flash photolysis in our laboratories is described elsewhere [4]. Figure 1 shows a schematic diagram of the apparatus and typical time resolved transient absorption spectra are shown in figure 2. In diffuse reflectance laser flash photolysis, the main difference is the geometrical arrangement of the analysing light, compare figure 1 with figure 3. Figure 4 shows a typical time resolved transient absorption spectrum obtained following nanosecond laser excitation of a dye adsorbed on silica powder by monitoring the laser induced reflectance change. It can be seen that the quality of the data obtained using the diffuse reflectance mode is similar to that obtained in transmission mode, compare figures 2 and 4. As far as the analysis of the data in diffuse reflectance mode is concerned, theoretical treatment shows that there are two limiting types of concentration profile below the irradiated surface. In the first case, when there are many more molecules than photons, there is an exponential fall off of transient concentration as a function of the penetration depth below the irradiated surface, in which case the change in reflectance, provided it is less than 10%, is a linear function of the concentration of the transient species. If however, there are many more photons than molecules, the concentration profile is a "plug" type, i.e. there is virtually total conversion of all molecules down to a particular penetration depth when there is a rapid change to a region where no molecules have been excited. In this second case, the data needs to be analysed using the change in the Kubelka-Munk remission function as the measured quantity which is linearly dependent on the concentration of absorbing species, for a detailed discussion of these effects see references [6] and [13].

Picosecond studies have been carried out at the Rutherford Appleton Laboratories using a Spectra Physics picosecond laser system. Figures 5 and 7 show schematic diagrams of the experimental arrangements for picosecond studies in transmission and diffuse reflectance modes respectively together with some typical results in figures 6 and 8. In nanosecond studies, experimental traces are usually obtained from single shots of the laser, however, in these picosecond studies each point on the curves shown in figures 6 and 8 corresponds to the accumulated signal from 100 laser shots and normalisation is carried out to allow for shot to shot variations.
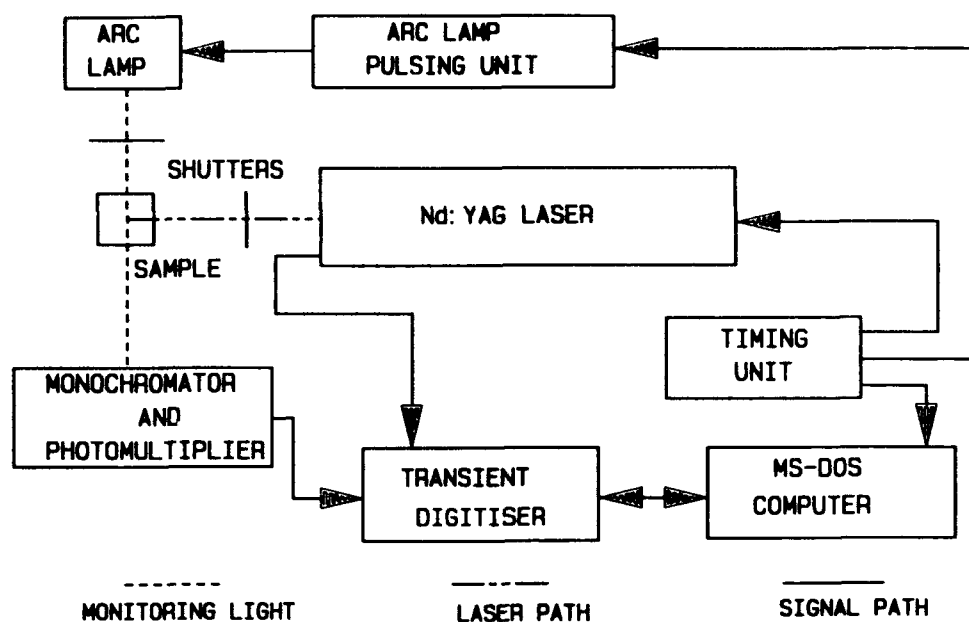
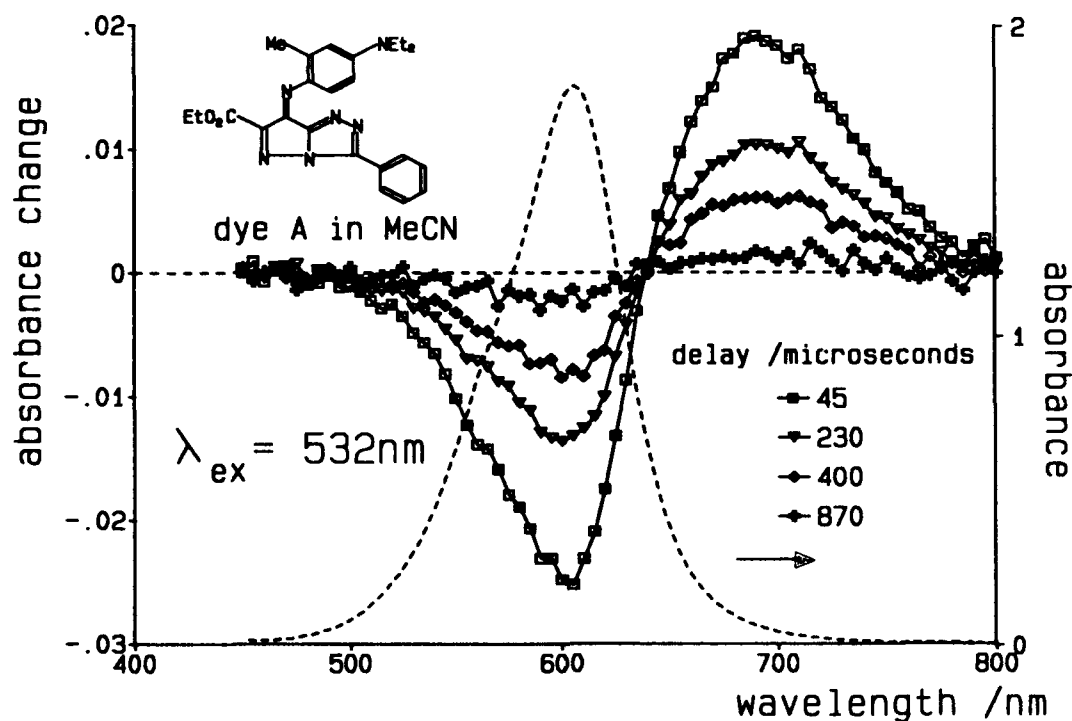**Figure 1 : Nanosecond Transmission Laser Flash Photolysis Apparatus**

Figure 2 : Typical Transient Time–Resolved Spectra

Sample Shutter

Nd: YAG Laser
Lumonics HY200

Trigger Photodiode

Filter Shutter

Arc Lamp

Arc Lamp Pulsing Unit

Timing Unit

Filter

Monochromator and Photomultiplier

Tektronix 7612D Transient Digitiser

MS-DOS Computer

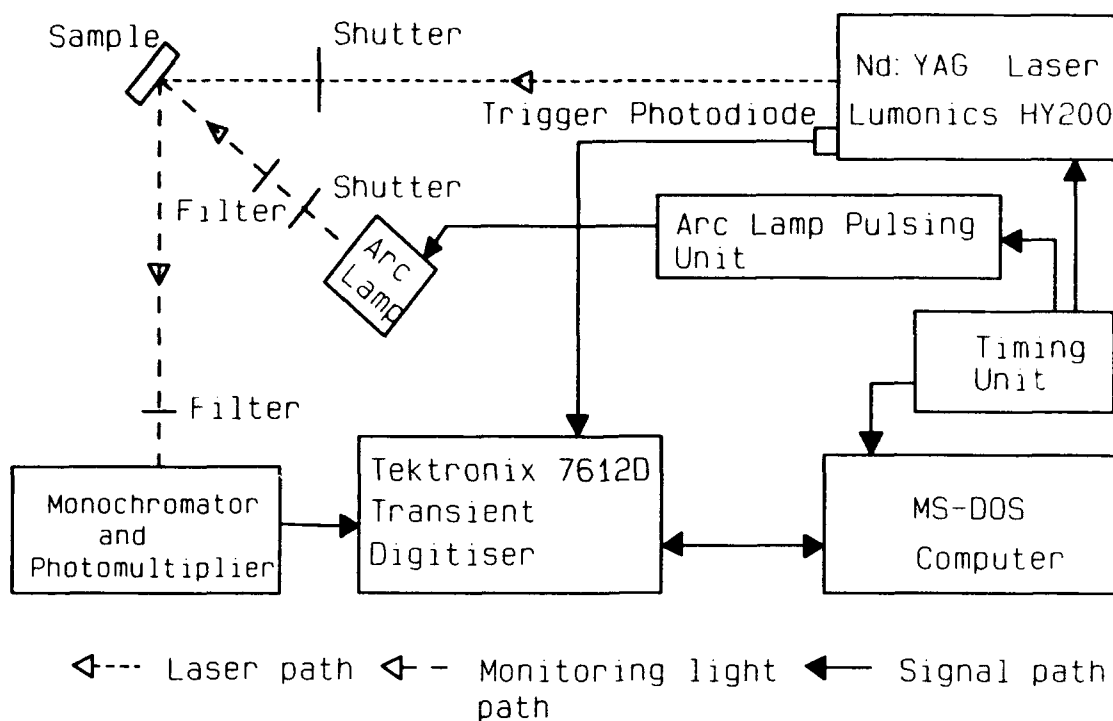◁--- Laser path ◁ - Monitoring light path ◀—— Signal path

Figure 3 : Nanosecond Diffuse Reflectance Laser Flash Photolysis Apparatus

Remission Function $\frac{(1-R)^2}{2R}$

Reflectance Change

λ_{ex} = 532nm

Time from laser pulse /s
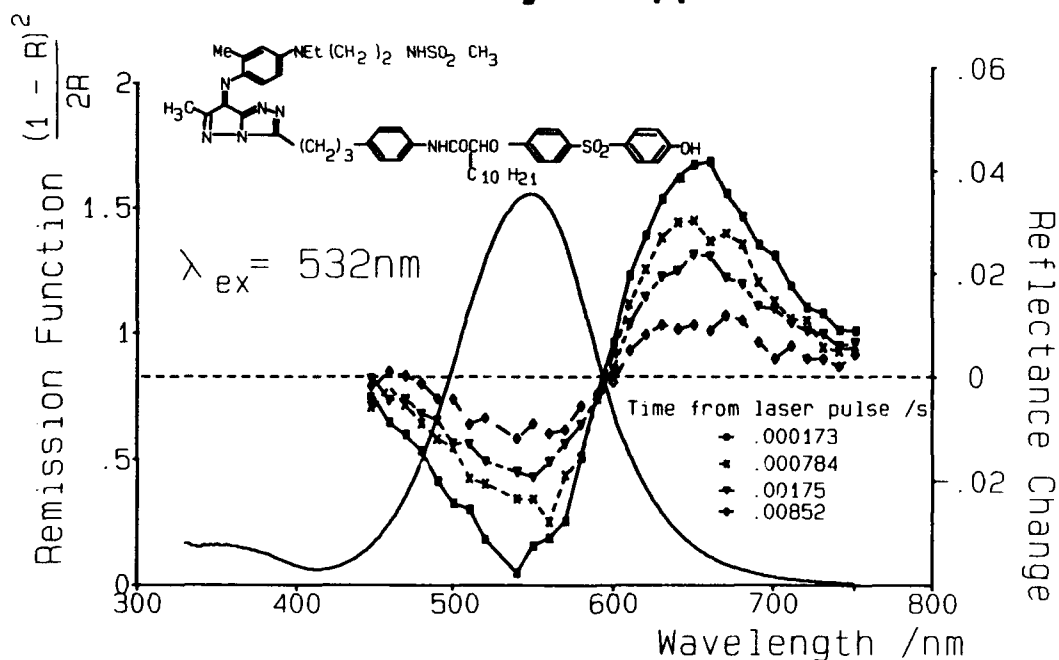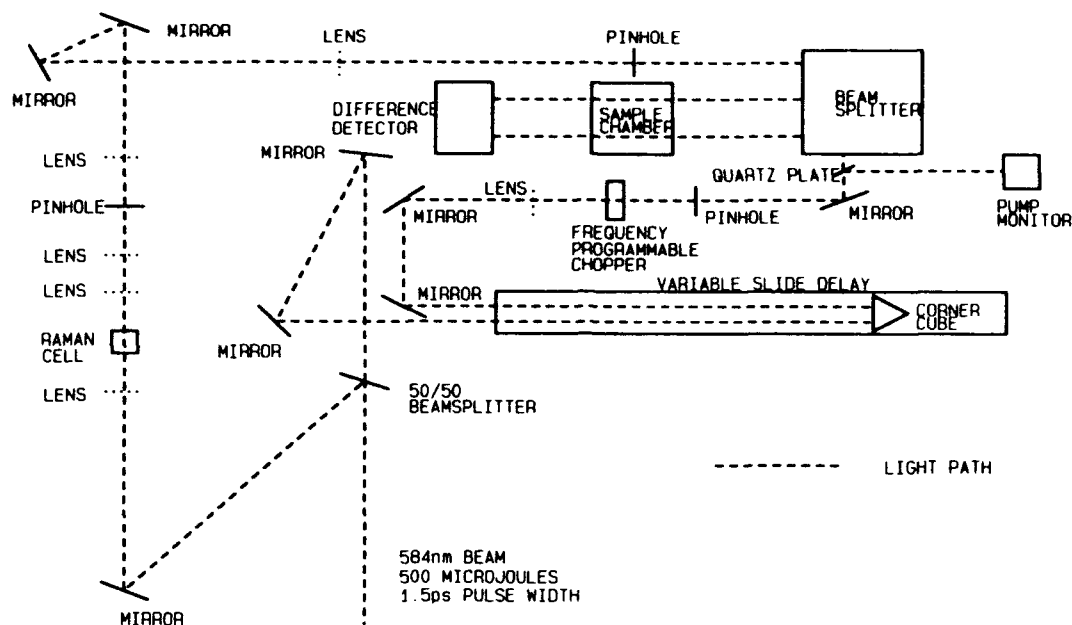.000173
.000784
.00175
.00852

Wavelength /nm

Figure 4 : Time Resolved Transient Spectra of the Dye Shown Adsorbed on Silica

Figure 5 : Picosecond Flash Photolysis Apparatus
(Transmission Mode)
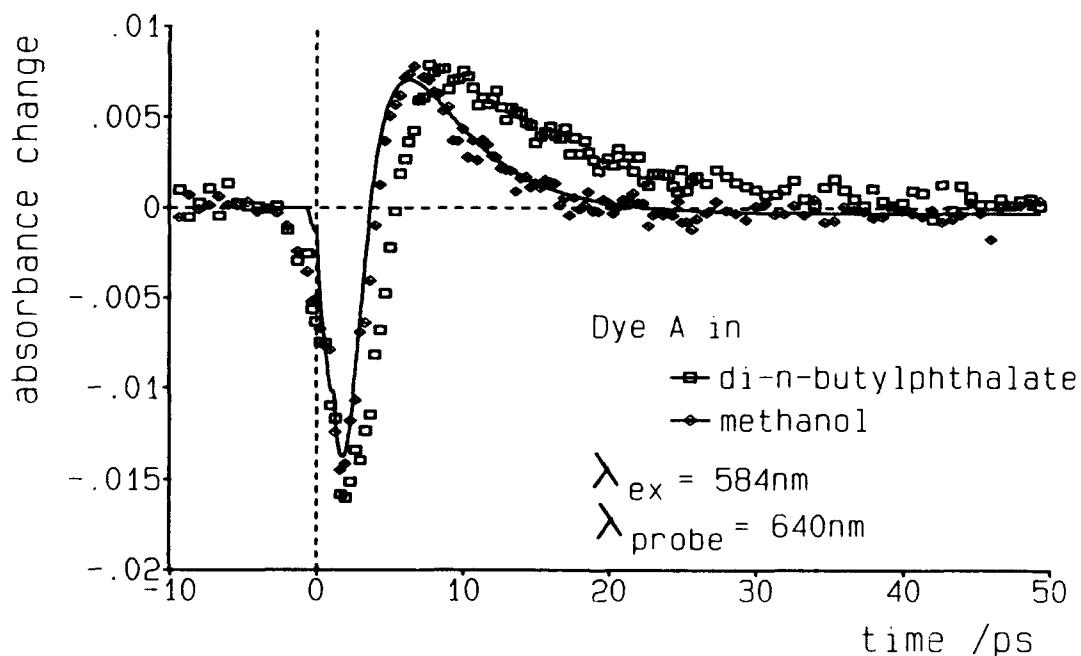
Figure 6 : Picosecond Transient Absorption Data
from Transmission Spectroscopy
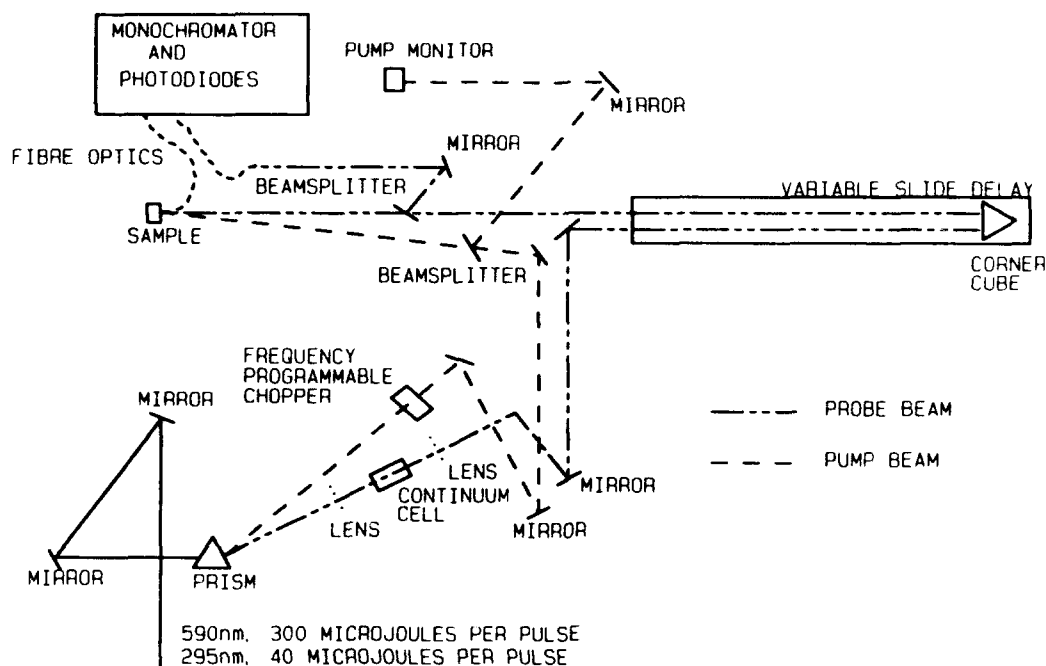
Figure 7 : Picosecond Flash Photolysis Apparatus (Diffuse Reflectance Mode)

λ_{ex}= 295nm

λ_{probe}= 590nm

Figure 8 : Picosecond Diffuse Reflectance Transient Following Excitation of a Powdered Pyrazoline

An important aspect of this work has involved the further development of the laser diffuse reflectance flash photolysis system by incorporating an EG&G Princeton Applied Research gated photodiode array as the detector. Thus the technique of diffuse reflectance laser flash photolysis developed at Loughborough and n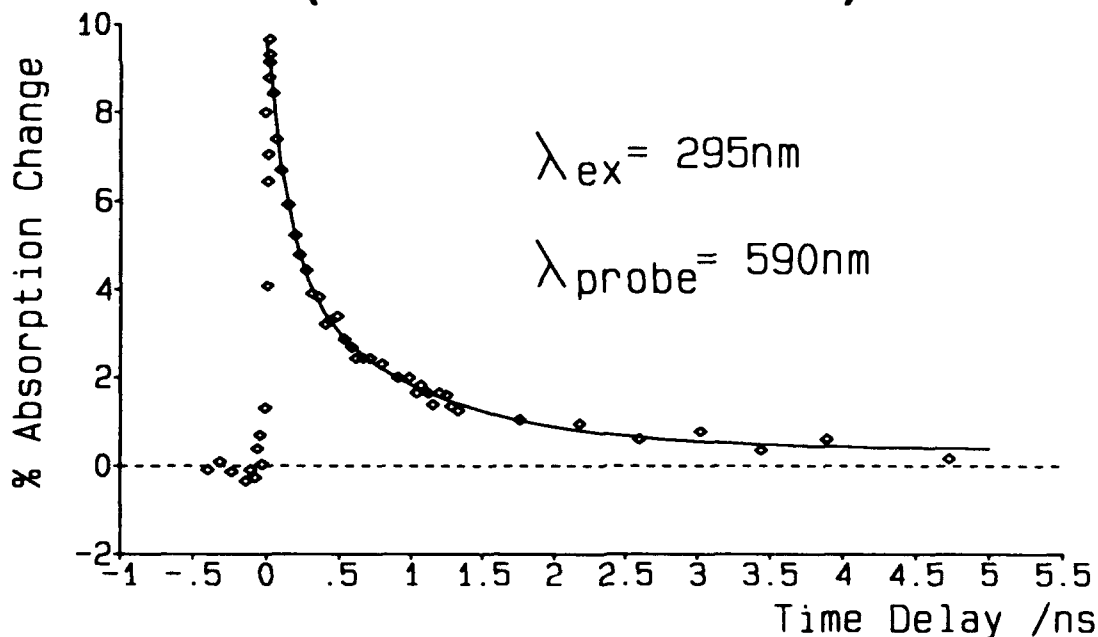ow used in many laboratories worldwide [29-35], has been extended considerably by the development of new hardware and software enabling time resolved transient spectra to be obtained efficiently. This has required a considerable time investment to integrate the new hardware with existing systems for transient detection which hitherto have used only monochromators with attached photomultipliers as detectors, and to develop control software to allow efficient data collection. This system has been installed and is already producing results. More reproducible sample preparation techniques involving purpose-designed glassware have also been employed. The equipment development has already allowed several systems to be studied in greater detail than previously. Now that it is fully developed, this will allow the study of a wider range of systems in the future including those which are sensitive to thermal or photochemical degradation such as many biological samples.

3   RESULTS AND DISCUSSION

3.1   Laser Photolysis of Dyes Adsorbed on Surfaces and Within Dyed Fabrics

3.1.1   *Luminescence Yields - Triplet State Spectra ,Yields and Decay Kinetics*

It is important to be able to understand the photochemical and photophysical behaviour of the compounds employed to colour natural and synthetic fibres, especially from a commercial point of view when they photodegrade. It is possible to obtain useful information from ground state reflectance spectroscopy and from luminescence studies of dyed fabrics as well as time resolved measurements. For example, we have studied cotton fabrics dyed with phthalocyanine and fluorescein derivatives. In both cases, time resolved transient absorption spectra demonstrate ground state depletion and triplet state production. In the case of sulphonated aluminium phthalocyanine the decay follows a first order rate law in water free fabric with a mean lifetime of 0.75 ms in the presence or absence of oxygen. Quenching by oxygen occurs only if the dyed fabric is water saturated. The transient absorption observed when cotton fabrics are dyed with halogenated fluorescein dyes however, show triplet-triplet absorptions which follow non-exponential decays. As in the case of sulphonated aluminium phthalocyanine, water is necessary to observe partial quenching by oxygen of the triplet states of these fluorescein dyes on cotton, see Appendix D [6].

Microcrystalline cellulose of 20 micrometers average particle size forms an ideal solid substrate for studying photochemical and photophysical properties of molecules adsorbed on surfaces. Ground state absorption measurements provide evidence for dimer formation when acridine orange is adsorbed on cellulose and the equilibrium constant for dimerisation was determined as 1.6×10^6 mol^{-1} g, see Appendix E [7]. Steady state emission and time resolved studies following pulsed excitation clearly demonstrate the existence of two emitting species and these were assigned as the monomeric and dimeric forms of acridine orange. Using diffuse reflectance laser flash photolysis, it was possible to probe the triplet state of both these species [7] and thermally activated delayed fluorescence from both

monomer and dimer was established as arising thermally via excited triplet states. At higher loadings i.e. greater than 20 micromoles per gram, the fluorescence intensity decreases and is mainly due to the dimer.

Examples of fluorescence emission yields determined for compounds adsorbed on powdered substrates, or from opaque materials in general, are rather rare in the literature. We have developed a simple method (Appendix G [9]) to determine the fluorescence yield of dyes adsorbed on microcrystalline cellulose. The method is based on corrected fluorescence emission spectra and can easily be applied provided the energy profile of excitation is accurately determined. The quantum yield of fluorescence of rhodamine 101, a rigid molecule is unity and this was used as a standard to determine the values for rhodamine 6G and auramine O adsorbed on cellulose. The fluorescence quantum yields obtained for which were 1.02 ± 0.03 and 0.14 ± 0.01 respectively. At higher loadings on this surface, strong aggregation was detected for the two rhodamine dyes but in contrast auramine O does not aggregate until loadings are much higher than 10 micromoles per gram. In this work [9] we were able to demonstrate that quantum yields of luminescence can be obtained from opaque samples with an accuracy of $\pm 3\%$.

Diffusion coefficient of molecules adsorbed on metal oxide surfaces are scarcely known but a knowledge of the translational mobility of adsorbates is essential for understanding bimolecular surface reactions. When triplet states decay as a result of triplet-triplet annihilation or energy transfer (see later) one can use the kinetic analysis of triplet state decays obtained by transient diffuse reflectance spectroscopy to learn more about activation barriers for lateral diffusion on surfaces. When acridine is adsorbed on silica surfaces, the main adsorbed species is hydrogen bonded acridine which upon excitation gives a strong triplet-triplet absorption at 435 nm. For samples with a high coverage and low pretreatment temperatures, the triplet decay is second order and delayed fluorescence is observed due to the reactions

$$^3A^* + {}^3A^* \rightarrow A + {}^1A^* \qquad \text{triplet-triplet annihilation}$$
$$^1A^* \rightarrow A + h\nu \qquad \text{delayed fluorescence.}$$

By evaluating the half-life of the triplet absorption decay as a function of surface concentration in the range of surface coverage from 1-7% we were able to show that under these conditions bimolecular annihilation was the predominant decay pathway. Calculations suggest that there is a high percentage conversion of ground state to triplet state for these samples, and assuming total conversion, a two dimensional bimolecular rate constant of 2×10^{14} dm^2 mol^{-1}s^{-1} is obtained for triplet-triplet annihilation on silica surfaces pretreated at temperatures less than 300°C. Higher temperature pretreatment of the surface reduces the lateral motion of triplet acridine and when the pretreatment temperature exceeds 600°C no migration on the surface is observed, Appendix I [11].

The ground state diffuse reflectance spectrum of a pyrazolotriazole azomethine dye adsorbed on silica is shown in Figure 4. The spectrum has a similar λ_{max} to that observed in alcoholic solution. No fluorescence emission can be detected from this sample, in accordance with results obtained in solution (Appendix B) [4].
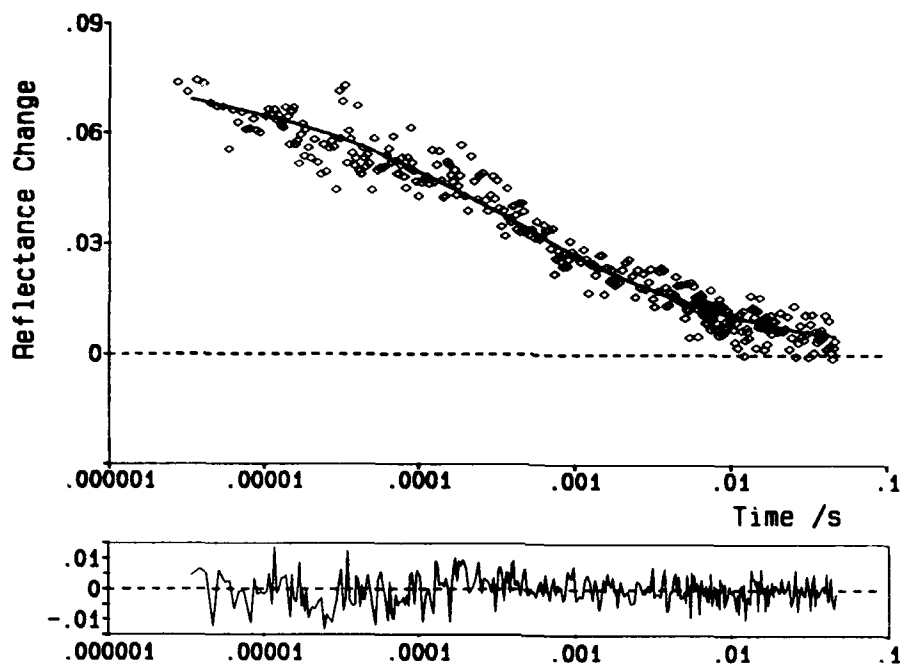
12.

Figure 9: Logarithmic representation of kinetic decay data
for the anti- isomer of a pyrazolotriazole azomethine
dye adsorbed on silica analysing at 640nm

Following pulsed excitation in fluid solution, a non-equilibrium population of isomers is produced. The less stable anti-isomer relaxes thermally via first order kinetics back to the syn-form. The anti-isomer is characterised by a bathochromically shifted absorption spectrum relative to the syn-form. Following pulsed excitation of the silica sample at 532 nm, a transient difference spectrum very similar to that obtained in polar solvents is obtained. Modelling of the diffuse reflectance change so produced by the method described in Appendix K [13] reveals an isomerisation quantum yield of some 0.007, similar to that in fluid solution. This analysis also reveals that the fall-off of concentration with increasing sample depth is exponential, which following Lin and Kan [36] and Kessler et al [37] means that in this instance the observed reflectance change ΔR is proportional to the transient concentration, i.e. to the concentration of the anti-isomer. In these samples, no transients other than that attributable to the anti-isomer could be detected using nanosecond flash photolysis. The kinetics of decay of the anti-isomer are complex, a feature common to many phenomena in heterogeneous systems [38-41], the relaxation times being spread over several decades see figure 9. Hence in attempting to characterise the relaxation kinetics, a rational model is required. Given the size of the adsorbed molecules and the availability of heteroatoms to facilitate hydrogen bonding, it is felt that mobility on the surface will not play a major role in the relaxation mechanism. Hence a model whereby the non-exponential nature of the decay arises from a range of adsorption sites on the silica surface has been employed. The particular model chosen was that of Albery et al [42], which proposes a gaussian distribution of activation energies and consequently a log gaussian distribution of deactivation rate constants. Such a scheme predicts that the decay of concentration C of a species from its initial concentration C_0 should follow equation (1).

13.

$$\frac{C}{C_0} = \frac{\int_{-\infty}^{+\infty} \exp(-x^2)\, \exp[-\tau \exp(\gamma x)]\, dx}{\int_{-\infty}^{+\infty} \exp(-x^2)\, dx} \qquad (1)$$

where

$$\tau = \langle k \rangle t$$

Here, $\langle k \rangle$ is the mean rate constant for deactivation, and γ is a parameter describing the spread of the gaussian distribution. Data was collected over several digitising rates, from 40 ns per point to 200 ms per point, and was globally fitted with equation (1) using a modified sequential simplex optimisation routine. This yielded $\gamma = 4.04$ and $k = 1730\ \text{s}^{-1}$ (giving a mean lifetime of 580 µs). The fitted curve is shown as a solid line in Figure 9, being presented on a logarithmic time axis for clarity. Residuals for this data, also plotted on a log time axis, are also shown.

3.1.2   *Energy Transfer and Photosensitized Reactions on Surfaces*

Triplet-triplet energy transfer has been studied for several systems. Using benzophenone as a triplet sensitizer, a quantitative analysis of the efficiency of energy transfer from triplet benzophenone to an oxazine dye adsorbed on microcrystalline cellulose has been made. In this study it was possible to measure both the quenching of the intensity of the benzophenone phosphorescence and the sensitized production of transient absorption by the triplet oxazine. The mechanism of transfer was shown to be static energy transfer in which each oxazine molecule is capable of accepting energy with unit efficiency from a pool containing 2-3 benzophenone molecules, Appendix H [10]. We have also studied energy transfer from triplet eosin to anthracene when both molecules are adsorbed on porous silica, Appendix J [12]. Excitation of eosin adsorbed on silica at 532 nm yields a long lived transient absorbing with a maximum at 600 nm which is assigned to the triplet state of eosin. When eosin and anthracene are coadsorbed on silica, the lifetime of the triplet state of eosin decreases with increasing anthracene concentration due to the process

$$^3\text{Eosin}^* + \text{Anthracene} \rightarrow {}^3\text{Anthracene}^* + \text{Eosin}$$
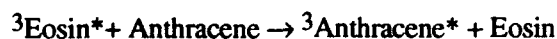
On short timescales the growth in sensitised triplet anthracene production is detectable and can be measured. From the quenching of triplet eosin by anthracene and the kinetics of the growth in absorption by triplet anthracene it is possible to obtain a two dimensional rate constant for this energy transfer process of $6 \pm 2 \times 10^{13}\ \text{dm}^2\ \text{mol}^{-1}\ \text{s}^{-1}$ for triplet energy transfer on a silica surface. This value is close to the value we obtained for a triplet-triplet annihilation of acridine on silica [11] , see above.

Samples of an azomethine dye and anthracene co-adsorbed on silica have also been prepared and subjected to diffuse reflectance laser flash photolysis. Excitation of these samples at 532 nm yields results identical to those observed with the azomethine dye alone. Excitation at 355 nm yields the anticipated anthracene triplet state spectrum, along with some production of the azomethine dye anti isomer. This production of anti isomer is prompt, and is greater than is anticipated from direct

excitation of the azomethine dye at 355nm, indicative of triplet-triplet energy transfer via static quenching of the anthracene triplet state since the quantum yield of isomerisation from the triplet state is considerably larger than from direct excitation (Appendix B [4]). In the samples of anthracene and azomethine dye on silica, the ratio of anthracene cation radical to triplet state absorption is considerably larger than in the absence of the azomethine dye. This may in part be attributed to static quenching of the triplet state, but there is also evidence from the ground state spectra that the azomethine dye undergoes a reaction with the anthracene and this may also be responsible for some additional radical production. Radical production from direct excitation is a unimolecular process arising from either T_2 or S_1, but radical production from reaction with the azomethine dye may come from T_1 and as a consequence it is difficult to correlate production of azomethine dye anti isomer with quenching of the anthracene triplet state. More studies of this system are planned.

3.2   Other Studies using Diffuse Reflectance Laser Flash Photolysis

3.2.1   *Bimolecular Radical Recombination Reactions on Silica and within Zeolites*

In Appendix F [8] we discuss our studies on radical reactions on silica surfaces and using two zeolites, silicalite and NaX as solid supports. Silica gel is a porous surface, with in our case, an average pore size of 6 nm and a surface area of 480 m^2 per gram. Both silica gel and silicalite contain only silicon and oxygen although the latter is hydrophobic whereas the former has a large amount of physically adsorbed water on the surface. The structure of the alumina silicate NaX zeolite comprises a three dimensional network of relatively large cavities or supercages approximately 1.2 nm in diameter connected by pores or channels with a diameter of about 0.75 nm. The silica aluminium ratio is approximately 1.5 which results in a large proportion of exchangeable cations, in our case sodium, and a strong hydrophilic zeolite. We have used the photochemical α-cleavage of 1,1,3,3-tetraphenyl acetone as a source of diphenylmethyl radicals. The production of the second diphenylmethyl radical via decarbonilation of the initially produced diphenylacetyl radical occurs rapidly and thus provides an efficient and practically instantaneous source of 2 diphenylmethyl radicals per ketone molecule as shown.

$$Ph_2CHCOCHPh_2 \xrightarrow{h\nu} Ph_2CHCO + Ph_2CH \rightarrow 2Ph_2CH + CO$$

For all three supports diphenylmethyl radicals are produced with a characteristic absorption maximum of 335 nm which decays over varying timescales from nanoseconds to minutes. A full discussion of the kinetics of decay of these radical reactions can be found in reference [39].

3.2.2   *Photochemistry of Bleached Thermomechanical Paper Pulp*

Diffuse reflectance laser flash photolysis studies of bleached black spruce mechanical pulp exciting at 355 nm reveals a transient absorption with a maximum at 450 nm, Appendix K [13]. The transient was assigned as the electronically excited triplet state of the aryl ketyl group in lignin. Oxygen and phenolic hydroxy groups in lignin reduced the detected amount of transient by static quenching and

15.

the intensity of the transient spectra also decreased in pulps reduced with sodium borohydride. The decay of the transient is quite long and was not described by either simple first order or higher order kinetics. Studies with the lignin model compound, 3,4-dimethoxyacetophenone, in benzene solution (Appendix M [15]) demonstrate that triplet states of carbonyl groups alpha to an aromatic ring are quenched efficiently by phenolic hydroxyl groups $k_q = 6.3 \times 10^9$ l mol^{-1} s^{-1} and can also be quenched by methoxy moieties, $k_q = 2.6 \times 10^6$ l mol^{-1} s^{-1} for methoxybenzene, present in the lignin structure. On the grounds of such comparative studies, both aromatic carbonyls and phenolic hydroxyl groups are confirmed as being important in the mechanism of photoyellowing of paper pulp.

3.2.3 *Picosecond Studies of Triaryl-2-pyrazolines*

In Appendix L [14], we report the first ever application of diffuse reflectance laser flash photolysis to observe the decay of a subnanosecond transient absorption within a microcrystalline sample, see figure 8. The microcrystalline samples were various triaryl-2-pyrazolines which were studied by pump-probe laser flash photolysis in diffuse reflectance mode and in the case of 1,5-diphenyl, 3-styryl-2-pyrazoline biexponential decays with lifetimes of 1.6×10^{-10} and 1.3×10^{-9} seconds were obtained. These lifetimes were compared with decay kinetics obtained using transmission pump-probe laser flash photolysis experiments conducted with a polycarbonate film containing the same compound where the lifetimes were 5.5×10^{-12} and 1.7×10^{-11} seconds respectively, indicating a much slower decay in the crystals. In addition the quenching of the pyrazoline excited states in a polycarbonate matrix by disulphone magenta was shown to take place by a Förster-type long range energy transfer with a critical transfer distance of 25 Å.

3.3 QUENCHING OF EXCITED STATES BY MOLECULAR OXYGEN

3.3.1 *Factors Which Determine the Efficiency of Singlet Oxygen Production*

Laser flash photolysis studies on nanosecond timescales have been carried out in order to demonstrate the importance of charge transfer interactions during quenching of excited states by molecular oxygen. An inverse correlation between the rate constants for oxygen quenching of the triplet states of naphthalene and several of its derivatives and the efficiency of singlet state generation has been established for a range of substituted naphthalenes containing electron donating and electron withdrawing substituents in several solvents, (Appendix C [5]). The only property which varies significantly with the substituent is the oxidation potential of the naphthalene derivative and we have established correlations between the singlet oxygen yields and the triplet quenching rate constants with the free energy change for charge transfer, thereby demonstrating the participation of charge-transfer interactions in the quenching mechanism. Singlet oxygen yields vary from 0.34 to 0.75 and triplet quenching rate constants from 5×10^9 to 1.2×10^9 l. mol^{-1} s^{-1}. for 1-methoxynaphthalene and 1-cyanonaphthalene respectively in benzene solutions. In reference [18] Appendix P we have shown that these effects vary with changes in solvent polarity as a result of the importance of charge transfer interactions in determining the efficiency of oxygen quenching. These results are in contrast to those we have recently obtained for anthracene derivatives where singlet oxygen is produced as a result of oxygen quenching of both singlet and triplet states, (Appendix N [16]). For all of the

anthracene derivatives in cyclohexane the efficiency of singlet oxygen production from the triplet state, f_Δ^T, were found to be unity. In contrast however, the efficiency of singlet oxygen production from the first excited singlet state, f_Δ^S, varies from zero for anthracene to unity for 9,10-dicyanoanthracene. It has been established that the magnitude of f_Δ^S is determined by the same factors which govern intersystem crossing yields for anthracene derivatives, i.e., the activation energy for intersystem crossing to higher triplet states. In addition it was confirmed that oxygen quenching of the excited singlet states of four anthracene derivatives in cyclohexane proceeds exclusively via enhanced intersystem crossing yielding triplet states.

3.3.2   *Picosecond Studies Following Direct Excitation into Charge Transfer Bands of Oxygenated Hydrocarbon Solutions*

Pump-probe picosecond studies in which direct excitation was into the charge transfer bands of oxygenated hydrocarbon solutions have been carried out for the first time, Appendix A [3]. Exciting into the charge transfer bands of oxygenated solutions of 1-ethylnaphthalene, we observed a rapidly formed long-lived absorption which was attributed to the triplet state. The efficiency of production of the triplet state from the excited charge-transfer complex exhibits a marked solvent dependence, for example, in acetonitrile the yield is only 0.4 while in cyclohexane it is 0.8. We have also measured the yield of singlet oxygen following excitation into 1-ethylnaphthalene-oxygen charge transfer complexes, relative to the singlet oxygen yields when the triplet state is produced following sensitisation with the triplet state of an aromatic ketone. The yields of singlet oxygen observed following charge transfer absorption are greater than that which would be expected on the basis of the measured triplet yields. A mechanism is suggested to explain these findings in Appendix O [17].

4.   CONFERENCES ATTENDED AND LECTURES GIVEN

International recognition of the importance of our work is demonstrated by the fact that the principal investigator, Professor F. Wilkinson, has been invited to give plenary lectures on these topics at the Gordon Conference on Energetic Materials, held in New Hampshire, USA 1992 where he gave a lecture entitled 'Ultra fast spectroscopic and kinetic studies in opaque materials' and at the ACS meeting, San Francisco, USA in 1992 where he lectured on 'Diffuse Reflectance Laser Flash Photolysis of Thermomechanical Pulp'. He has given plenary lectures at the Solar Energy Conferences held in Cairo, Egypt in 1991 on 'Diffuse Reflectance Laser Flash Photolysis of Adsorbed Molecules' and in 1993 on 'Factors Which Determine the Efficiency of Sensitized Singlet Oxygen Production'. He has given plenary lectures at the 5th Congress of the European Society of Photobiology in Marburg, Germany on 'Diffuse Reflectance Laser Photolysis Studies of Light Induced Reactions in Heterogeneous Systems', at the XVI th International Conference on Photochemistry, Vancouver, Canada and at the 2nd Conference on Lasers in Chemistry in Trieste, Italy in 1993 where he talked about 'Nanosecond and Picosecond Laser Photolysis studies of Charge Transfer Interactions in the Mechanism of Quenching by Molecular Oxygen'. He was also invited to talk on this topic at the Congreso de Fotoquimica by the Spanish Photochemical Society in Poblet in 1993. He gave a plenary lecture at a conference organised by the Swiss Photochemists on Environmental Photochemistry in Adelboden in 1993 on 'Time Resolved Diffuse Reflectance

Spectroscopy Involving Molecules Adsorbed on Oxide Minerals' and has participated in the 15th International Conference on Photochemistry, chairing sessions and presenting work in 1991 in Paris, France and .n 1992 at the 14th IUPAC International Symposium on Photochemistry in Leuven Belgium. He also has lectured at the Inter American Photochemical Society meeting in 1991 in Florida USA and at the joint Japanese/British Laser Meeting held in 1992 at the Rutherford Appleton Laboratories in the UK.

Professor Wilkinson has lectured at many academic establishments during the three year period including the Max Planck Institut for Strahlenchemie in Germany, at the Universities of Basel and Berne, Switzerland, at the University of Notre Dame, USA, at the Universities of Leeds,of Keele, of Paisley, and of Nottingham and at Imperial College, London, UK. Other overseas venues at which he has accepted invitations to give lectures include the Universities of Strasbourg, France, of Tubingen, Germany and he has also lectured to several industrial firms including Ciba Geigy, Unilever and Pilkington Research. He also gave a lecture at the Association for Science Education Annual meeting held in 1993 at Loughborough University and at Oakham School, Leicestershire.

5.   CONCLUSIONS

The aims and objectives of the original application which was to apply the technique of diffuse reflectance laser flash photolysis to determine absorption spectra and decay kinetics of laser produced transient intermediates in heterogeneous environments including interfaces, zeolites cavities, within polymers and on dyed fabrics has been substantially met. The results obtained have been published in many publications given as Appendixes to this report. The main achievements are further development of the technique of diffuse reflectance laser flash photolysis and its application to dyes adsorbed at interfaces and within fabrics. It is well known that photodegradation of dyes in heterogeneous and homogeneous environments including biological systems often involves photooxidation and one of the most important intermediates is singlet oxygen. Our recent studies, which help unravel the factors which determine the efficiency of sensitized singlet oxygen production, constitute a substantial advancement of knowledge in this area. In several of the photochemical processes investigated, we have been able to obtain results concerning reactive intermediates and mechanisms which cannot be obtained by any other method.

LITERATURE CITED

1. R.W. Kessler and F. Wilkinson, *J. Chem. Soc., Faraday Trans I*, 1981, **77**, 309 .

2. F. Wilkinson, C.J. Willsher, P.A. Leicester, J.R.M. Barr and M.J.C. Smith,
    J. Chem. Soc., Chem. Commun., 1986, 1216 .

3. D.J. McGarvey, F. Wilkinson, D.R. Worrall, J. Hobley and W. Shaikh,
    Chem. Phys. Lett., 1993, **202**, 528.

4. F. Wilkinson, D.R. Worrall, D.J. McGarvey and A. Goodwin,
    J. Chem. Soc. Faraday Trans., 1993, **89**(14), 2385.

5. D.J. McGarvey, P.G. Szekeres and F. Wilkinson, *Chem. Phys. Lett.*, 1992, **199**, 314.

6. F. Wilkinson, D.J. McGarvey and D.R. Worrall,
    Proc. Indian Acad. Sci. (Chem. Sci.), 1992, **104**, 739.

7. F. Wilkinson and D.R. Worrall, *Spectrochemica Acta*, 1992, **48A**, 135.

8. F. Wilkinson and D.R. Worrall, *Proc. Indian Acad. Sci. (Chem. Sci.)*, 1992, **104**, 287.

9. L.F.V. Ferreira, M.R. Freixo and A.R. Garcia and F. Wilkinson,
    J. Chem. Soc. Faraday Trans, 1992, **88**(1), 15.

10. F. Wilkinson, P.A. Leicester, L.F.V. Ferreira and V.M.M.R. Freires,
    Photochem. Photobiol., 1991, **54**, 599.

11. F. Wilkinson, *Proc. Indian Acad. Sci. (Chem. Sci.)*, 1991, **103**, 305.

12. F. Wilkinson and R. Beer, Photochemical Processes in Organized Molecular Systems
    Ed. K. Honda *Elsevier*, 1991, 377.

13. J.A. Schmidt, C. Heitner, G.P. Kelly, P.A. Leicester and F. Wilkinson,
    J. Photochem. Photobiol, 1991, **57**, 111

14. G.P. Kelly, P.A. Leicester, F. Wilkinson and D.R. Worrall,
    Spectrochemica Acta, 1990, **46A**, 975.

15. F.Wilkinson, A.Goodwin and D.R. Worrall, Photochemistry of Lignocellulosic Materials,
    Eds C. Heitner & J.C. Scaiano, *ACS Symp. 531*, 1993, 86.

16. F. Wilkinson, D.J. McGarvey and A.F. Olea, *Accepted by Amer. Chem. Soc..*, 1993.

17. F. Wilkinson, D.J. McGarvey and A.F. Olea,
    Accepted by Proc. Indian Acad. Sci (Chem. Sci.), 1993.

18. D.J. McGarvey, A.F. Olea and F. Wilkinson, *Submitted to J. Chem. Phys.*

19. F. Wilkinson, *2nd Conference on Lasers in Chemistry*, Trieste, 1993.

20. F. Wilkinson, *Congreso de Fotoquimica*, Poblet, Spain, 1993, p3.

21. F. Wilkinson, *Proc. Conf. Environmental Photochem.*, Adelboden, Switzerland, 1993, p21.

22. F. Wilkinson and D.J. McGarvey,
    Proc. Int. Conf. Photochem., Vancouver, Canada, 1993, 110.

23. F. Wilkinson and D.J. McGarvey,
    Presented at 2nd Int. Conf. Solar Energy and Ap. Photochem., Cairo, Egypt, 1993.

24. F. Wilkinson, *Proc. Fifth Cong. Euro. Soc. Photobiology*, Marburg, Germany, 1993, 225.

25. F. Wilkinson, L.F.V. Ferreira and D.R. Worrall,
    Proc. IUPAC Symp. Photochem., Leuven, Belgium, 1992, 546.

26. D.J. McGarvey and F. Wilkinson,
    Proc. IUPAC Symp. Photochem., Leuven, Belgium, 1992, 328.

27. D.J. McGarvey, S. McHugh and F. Wilkinson,
    Proc. XVth Int. Conf. Photochem., Paris, France, 1991, III-41.

28. F. Wilkinson, D.R. Worrall and L.F.V. Ferreira,
    Proc. XVth Int. Conf. Photochem., Paris, France, 1991, III-7.

29. L.J. Johnston, J.C. Scaiano, J.L. Shi, W. Siebrand and F. Zerbetto,
    J. Phys. Chem., 1991, **95**, 10018.

30. N.J. Turro, M.B. Zimmit, I.R. Gould and W. Mahler, *J. Chem. Soc.*, 1986, **107**, 5826.

31. P.P. Levin, L.F.V. Ferreira and S.M.B. Costa, *Amer. Chem. Soc.*, 1993, **9**, 1001.

32. G. Beck and J.K. Thomas, *Chem. Phys. Lett.*, 1993, **94**, 533.

33. R.B. Draper and M.A. Fox, *J. Phys. Chem.*, 1990, **94**, 4628.

34. N. Ikeda, M. Kashioku, H. Masuhara and K. Yoshihara, *Chem. Phys. Lett.*, 1988, **150**, 452.

35. D. Oelkrug, S. Reich, F. Wilkinson and P.A. Leicester, *J. Phys. Chem.*, 1991, **95**, 269.

36. T. Lin and H.K.A. Kan, *J. Opt. Soc. Am.*, 1970, **60**, 1252.

37. R.W. Kessler, G. Krabichler, S. Uhl, D. Oelkrug, W.P. Hagan, J. Hyslop and F. Wilkinson,
    Opt. Acta, 1983, **30**, 1090.

38. D. Oelkrug, S. Uhl, C.J. Willsher and F. Wilkinson, *J. Phys. Chem.*, 1989, **93**, 4551.

39. G.P. Kelly, C.J. Willsher F. Wilkinson, J.C.N. Netto-Ferreira, A. Olea, D. Weir,
    L.J. Johnston and J.C. Scaiano, *Can. J. Chem.*, 1991, **68**, 812.

40. J.K. Thomas, *Chem. Rev.*, 1993, **93**(1), 301.

41. H. Bogaert, P. Douglas and P. Vandermeeren,
    J. Chem. Soc. Faraday Trans., 1992, **88**(23), 3467.

42. W.J. Albery, P.N. Bartlet, C.P. Wilde and J.R. Darwent,
    J. Am. Chem. Soc., 1985, **107**, 1854.

Picosecond absorption studies on the role of charge transfer interactions in the mechanism of quenching of triplet states by molecular oxygen

D.J. McGarvey [a], F. Wilkinson [a], D.R. Worrall [a], J. Hobley [a] and W. Shaikh [b]

[a] *Chemistry Department, University of Technology, Loughborough, Leicestershire LE11 3TU, UK*
[b] *Rutherford Appleton Laboratory, Chilton, Didcot, Oxon OX11 0QX, UK*

The first picosecond pump–probe measurements from oxygenated hydrocarbon solutions exciting directly and exclusively into the charge transfer (CT) absorption bands is described. Upon excitation at 353 nm, which precludes population of the lowest excited singlet state of 1-ethylnaphthalene (EN), its triplet state is produced rapidly in < 10 ps in both oxygenated acetonitrile and cyclohexane solutions. The efficiency of this triplet state production exhibits a pronounced sensitivity to the solvent, being high in cyclohexane ($\approx 80\%$) but considerably less in acetonitrile ($\approx 40\%$). Measurements of the efficiency of singlet oxygen production following CT excitation demonstrate that dynamic quenching of the triplet state is not the sole route to singlet oxygen. We suggest, that following absorption at 353 nm a proportion of the excited complexes, which are formed either by internal conversion from the initially excited CT state or by direct absorption to give a doubly excited complex state, dissociates to give both $^3EN^*$ and $O_2^*(^1\Delta_g)$.

1. Introduction

The mechanism of excited state quenching by oxygen remains poorly understood despite intense research over the last thirty years (see ref. [1], and references therein). The quenching mechanism is believed to proceed via weakly bound excited state complexes which may be represented as $(M...O_2)^*$, where M represents an organic molecule. In this Letter, we aim to further elucidate factors which determine the quenching rate constants (k_q) and the efficiency of production of singlet oxygen (O_2^*, $^1\Delta_g$). The relatively high oxygen quenching constant, observed for quenching of the triplet states of certain aromatic ketones and amines, in comparison with those of aromatic hydrocarbons were interpreted by one of us [2] as being due to the presence of low-lying charge transfer states (CT) which facilitate quenching through enhanced intersystem crossing. Supporting evidence for this suggestion has come from several recent publications [3–5]. The extent of CT within the excited state complexes is thought to have a profound influence on the quenching rate

constants and also on the decay channel distribution. Recently we have published some preliminary results [6] of an investigation on oxygen quenching of triplet excited states which establishes an inverse correlation between the bimolecular rate constants for oxygen quenching (k_q^T) and the efficiency of singlet oxygen produced thereby (S_Δ) for a series of substituted naphthalenes in benzene. In addition we demonstrated that both k_q^T and S_Δ correlate with the oxidation potential of the substituted naphthalene which is evidence for the participation of charge transfer interactions within excited state/oxygen complexes formed during the quenching process. Our objective here is to characterise, by direct and indirect means, the properties of these excited state complexes and thus to account for the wide variation in oxygen quenching rates and singlet oxygen yields observed for organic molecules in homogeneous solution. In this Letter, we exploit the optical absorption properties of oxygen/organic molecule contact complexes to directly populate excited state complexes which may be involved in the dynamic quenching of excited states by oxygen.

The perturbing effect of dissolved oxygen on the UV/VIS absorption spectra of organic molecules is a well known phenomenon first studied in detail by Evans [7] and subsequently discussed by Tsubomura and Mulliken [8] and others [9]. The additional absorption bands observed include the lowest-energy transition which corresponds to the $S_0 \rightarrow T_1$ transition of the organic molecule in intimate contact with an oxygen molecule. More intense absorption is observed at shorter wavelengths and is often attributed to CT transitions within $^3(M...O_2)$ contact complexes,

$$M + {}^3O_2 \rightleftharpoons {}^3(M...O_2) \xrightarrow{h\nu} {}^3(M^+...O_2^-)^* . \qquad (1)$$
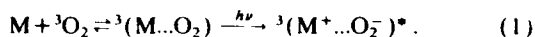
This assignment is supported by the broad structureless appearance of the bands.

In the investigations reported here 1-ethylnaphthalene (EN) was used since it is a liquid at room temperature and concentrated solutions (1.5 M) required to observe CT absorption in the presence of oxygen at a pressure of up to 4 atm are not limited by solubility considerations.

Except for a recent communication by Logunov and Rodgers [10] there are no reports in the literature concerning picosecond absorption measurements of organic molecule–molecular oxygen complexes. Logunov and Rodgers [10] carried out picosecond time-resolved absorption measurements on O_2-saturated solutions of naphthalene (7 mM) in cyclohexane using 25 ps, 266 nm excitation. They observed a biexponential growth (200 ps and 4 ns respectively) of the naphthalene triplet state from the first excited singlet state. The explanation given for this observation was that a small proportion of the excitation light is absorbed by naphthalene–O_2 contact complexes to form a naphthalene–O_2 exciplex state which decays in ≈ 200 ps to yield the naphthalene triplet state. The 4 ns component of the observed growth was attributed to diffusional quenching of the naphthalene singlet state by O_2.

The measurements presented in this Letter differ from those of Logunov and Rodgers in that we are exclusively exciting into the cooperative EN–O_2 charge transfer absorption band at a wavelength (353 nm) which precludes population of the lowest excited singlet state of the naphthalene derivative. In addition the pulse durations we use are considerably

shorter (< 8 ps). However we do not have the advantage of spectral resolution and are limited to only a few probe wavelengths. The two sets of data are therefore not directly comparable at this stage.

2. Experimental

2.1. Materials

Naphthalene (Aldrich, scintillation grade, > 99%). 1-ethylnaphthalene (Fluka, 99%), benzophenone, BP (Aldrich Gold Label), and p-methoxyacetophenone, PMAP (Aldrich, 99%) were used as received. Acridine (Aldrich) was recrystallised from ethanol. Acetonitrile (Aldrich, spectrophotometric grade) was dried by refluxing over calcium hydride. All other solvents were spectrophotometric grade from Aldrich and were used as received.

2.2. Sample preparation

Solutions of 1.5 M EN in cyclohexane and acetonitrile were degassed using the freeze–pump–thaw technique. The EN solutions were subsequently equilibrated with 2–4 atm of oxygen yielding absorbances of ≈ 0.3 around 355 nm compared with ≈ 0.05 for air-equilibrated solutions. The absorbance due to the EN/O_2 contact complex exhibits a linear dependence on the oxygen concentration under our conditions.

2.3. Picosecond pump–probe measurements

The picosecond time-resolved absorption measurements were carried out at the Rutherford–Appleton Laboratory Laser Support Facility. The picosecond laser system was a frequency-doubled mode-locked Nd:YAG pumping a dye laser operating at 706 nm. The pump and probe wavelengths were obtained by appropriate frequency-doubling to give 353 nm and mixing of 1064 and 706 nm to give 424 nm. The operating conditions were as follows: pump wavelength is 353 nm, pump energy is 4 μJ; probe wavelengths is 424 and 706 nm, pulse duration is ≈ 5 ps, irradiation area is 0.8 mm^2. The probe wavelengths are suitable for detection of the EN triplet state (424 nm) and the EN radical cation (706

nm). We are unaware of a documented spectrum for EN$^+$ but expect that it will have a similar spectrum to N$^+$ which is well documented [11]. The yield of EN triplet state following CT excitation was measured by comparing the triplet state absorption, observed at 424 nm, 400 ps after excitation with that from an identical optically-matched air-equilibrat d solution containing BP or PMAP. Under our conditions ([EN] = 1.5 M) energy transfer is observed to be complete within 300 ps. Both ketones give the same yield of sensitised ^{3}EN* demonstrating that energy transfer from the triplet state of these aromatic ketones proceeds with 100% efficiency giving an effective EN triplet state yield of unity for these solutions. For comparison, absorption traces from air-equilibrated EN solutions containing no ketone were also obtained (see fig. 1).

2.4. Nanosecond flash photolysis and singlet oxygen yield measurements

For nanosecond flash photolysis studies and for the singlet oxygen yield measurements the 355 nm harmonic of a Lumonics HY200 Q-switched Nd:YAG laser (8 ns, 15 mJ pulse^{-1}) was employed as the excitation source. Oxygen quenching rate constants were determined in air-equilibrated samples by sensitising the EN triplet state with an aromatic ketone and measuring the triplet decay in the presence and absence of oxygen. Singlet oxygen was detected by monitoring the 0, 0 vibronic band of the phosphorescence centred at 1270 nm,

$$O_2^*(^1\Delta_g) \rightarrow O_2(^3\Sigma_g^-) + h\nu(1270 \text{ nm}),\qquad(2)$$
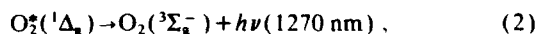
using a Judson germanium photodiode (J16-8SP-R05M, active diameter is 0.5 cm) coupled to a Judson PA100 amplifier.

The phosphorescence was detected at right angles to the exciting beam through a silicon cutoff filter. The laser energies employed did not exceed 0.7 mJ pulse^{-1}. Individual luminescence traces were signal-averaged and fitted using a single exponential function to yield the luminescence intensity I_0 at $t=0$. The I_0 values were plotted against relative laser intensity to obtain plots which were linear below 0.5 mJ pulse^{-1}. Comparison of the slopes of these plots yielded relative singlet oxygen yields. The singlet oxygen yields when excitation, under an elevated pres-
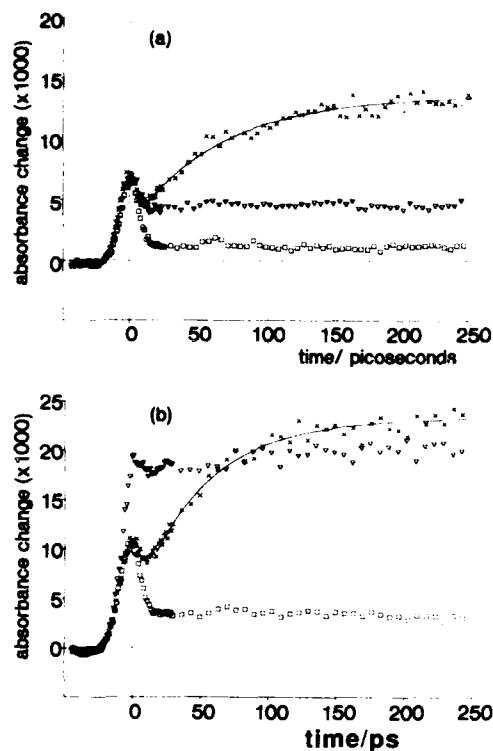

Fig. 1. Picosecond absorption profiles observed for EN samples in (a) acetonitrile, (b) cyclohexane; (□) air-equilibrated 1.5 M EN solutions, (∇) oxygenated (3–4 atm) 1.5 M EN solutions, (×) air-equilibrated 1.5 M EN solutions containing aromatic ketone. The oxygenated and ketone containing samples were optically matched.

sure of oxygen, was directly into the CT state, eq. (1), were compared with the singlet oxygen yield observed via triplet sensitisation from triplet BP (or PMAP), in air-equilibrated 1.5 M EN solutions using optically matched solutions. The singlet oxygen yields from the sensitised samples were assumed to be the same as those measured by us using smaller EN concentrations (≈ 0.05 M). In these measurements the standards used were acridine in acetonitrile, $\Phi_\Delta = 0.82$ [12] and p-methoxyacetophenone/0.1 M naphthalene in cyclohexane, $\Phi_\Delta = 0.92$ [13]. Thus absolute values of the singlet oxygen yields resulting from absorption to CT states of O_2/EN complexes, Φ_Δ^{CT}, were obtained.

3. Results and discussion

Following 355 nm nanosecond flash photolysis of oxygenated 1.5 M EN solutions, i.e. exciting into the charge transfer absorption band, we observed a rapidly decaying transient ($\tau \approx 10$–20 ns) with the characteristic triplet–triplet absorption spectrum of EN. Using 353 nm picosecond excitation of the same solutions a "prompt" increase in absorption at 424 nm was observed (fig. 1) which does not decay significantly over the time scales investigated (≈ 1 ns). We attribute this absorption also to the EN triplet state produced within a few picoseconds. i.e. within the risetime of our picosecond apparatus. Superimposed upon the rise in triplet state absorption we observe a rapid symmetrical rise and fall in absorption which follows the excitation pulse. This component is present regardless of whether the solution is oxygenated or not and so is not derived from the CT state. Also this rapid component is not observed with neat acetonitrile or cyclohexane but is observed in the case of neat benzene. This feature has been observed previously [14,15] in studies of multiphoton absorption by neat aromatic liquids as a rapid component absorbing around 420 nm and was attributed to electron-aromatic ion production and geminate recombination. We believe a similar process is operating when 1.5 M EN solutions are subjected to 353 nm picosecond excitation. The consequence of this multiphoton absorption is the appearance of a relatively small long lived (> 1 ns) absorption which may be due to the excited singlet or triplet state of EN, or it may be due to the EN radical cation or a combination of these. Since we do not have the facility of spectral resolution with our picosecond measurements we are presently unable to identify this weak background absorption.

Using the picosecond apparatus and probing at 706 nm for the EN radical cation we observed only small "prompt" absorptions ($\approx 10^{-3}$) which were not sensitive to the concentration of oxygen. This agrees with our nanosecond photolysis measurements where we also were unable to detect significant absorption in the 680–720 nm region following excitation into the CT band using either solvent. However these observations contrast with the report by Ogilby and co-workers [5] who detected the 1-methylnaphthalene radical cation in acetonitrile following CT excitation. Unfortunately no details concerning the amounts of radical cation produced are given in ref. [5] so that it is difficult to compare results.

The varying efficiencies of triplet state formation (γ_T) for all samples are illustrated in fig. 1. The triplet yield determinations are derived exclusively from the picosecond pump–probe measurements of optically matched solutions and are given in table 1 together with our measurements for the fraction of triplet states quenched by oxygen which produce singlet oxygen (S_Δ). Also included in table 1 are the bimolecular oxygen quenching rate constants (k_q^T) obtained for EN in both solvents and the value of the product $S_\Delta \gamma_T$. which is equal to the amount of singlet oxygen production which would be expected following excitation to the charge transfer state on the basis of the observed yield of triplet state production. It is immediately apparent that there is a discrepancy, particularly in acetonitrile, between ϕ_Δ^{CT} and $\gamma_T S_\Delta$. Thus more singlet oxygen is produced from the charge

Table 1

Effect of changing solvent from acetonitrile (ACN) to cyclohexane (CHX) on γ_T. the triplet formation efficiency of 1-ethylnaphthalene. on k_q^T. the oxygen quenching rate constant for ^{3}EN*. on S_Δ. the fraction of ^{3}EN* states quenched by oxygen which gives singlet oxygen and on ϕ_Δ^{CT}. the quantum yield of singlet oxygen $O_2^*(^1\Delta_g)$. formed upon excitation exclusively into the charge transfer absorption of EN/O_2 complexes such that the localised lowest excited singlet state of EN is not populated. Errors in the S_Δ. γ_T. ϕ_Δ^{CT} and k_q^T values are $\pm 10\%$

Sample	S_Δ	γ_T	$S_\Delta \gamma_T$	ϕ_Δ^{CT}	$S_\Delta/\phi_\Delta^{CT}$	$S_\Delta/\phi_\Delta^{CT}$ [a]	k_q^T (10^9 ℓ mol^{-1} s^{-1})
EN/O$_2$/ACN	–	0.40	0.20	0.36	1.43	1.52	3.3
EN/BP/ACN/air	0.51	1.0	0.51	–			
EN/O$_2$/CHX	–	0.80	0.69	0.78	1.10	1.00	1.6
EN/BP/CHX/air	0.86	1.0	0.86	–			

[a] These values are for 1-methylnaphthalene obtained by Ogilby and co-workers [5].

transfer state than can be accounted for from the amount of triplet state produced. For instance the singlet oxygen yield in acetonitrile from EN triplet state produced by ketone sensitisation is 0.51 while from the charge transfer state it is 0.36, which is considerably greater than the value of 0.2 expected from the observed triplet yield of 0.4 and the observed value of S_Δ of 0.51. Another interesting feature of the data in table 1 is the large solvent dependence of γ_T. Thus in cyclohexane the triplet state production from the charge transfer state is efficient ($\approx 80\%$) but in acetonitrile it is dramatically reduced to only 40%. This difference is clearly shown in fig. 1.

The most important possible decay channels of the excited complex state are given in scheme 1, which attempts to show relative zeroth-order energies of the various excited states of $(M...O_2)$ complexes, with excitation into the charge transfer state shown n the right-hand side of scheme 1 and via the sensitising

ketone, K, shown on the left. Note that since we see no evidence for the production of separate ions in our experiments these have been omitted in scheme 1. In a previous Letter [6] we used the Rehm–Weller equation, neglecting the Coulombic term, and calculating the free energy of the relaxed charge transfer states, $^{1,3}(M^+...O_2^-)^*$ to be ≈ 30 kJ mol^{-1} below the localised triplet for EN. In acetonitrile, where any Coulombic correction will be small since it has a dielectric constant of 37.5, the excited complexes $^{1,3}(M^+...O_2^-)^*$ are likely to lie below the localised triplet and to be populated following the formation of $^3M^*$ by energy transfer from the triplet ketone sensitizer, as indicated starting on the left-hand side of scheme 1, or following triplet state production following charge transfer absorption as shown on the right-hand side of scheme 1. There is a large difference between the S_Δ and k_q^T values given in table 1 for EN in the two solvents. In cyclohexane the values
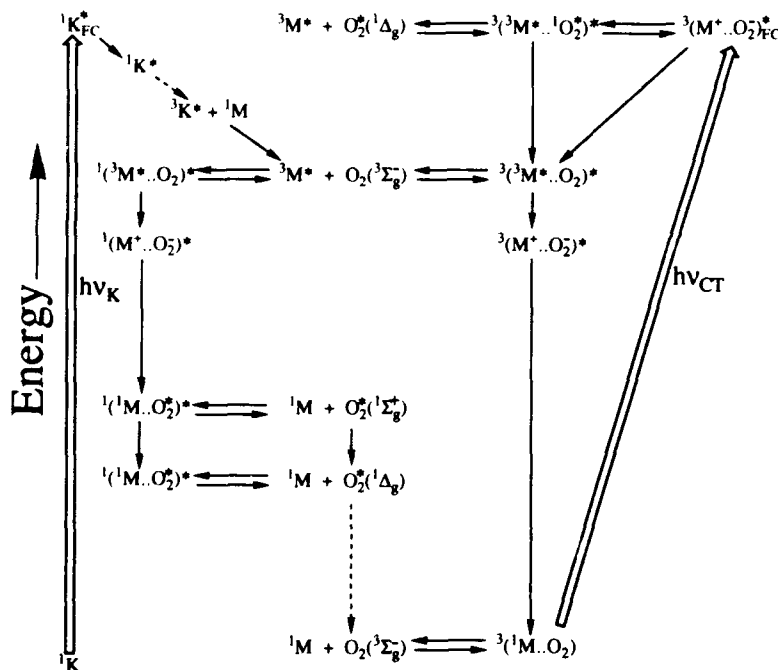

Scheme 1

Scheme 1. Schematic energy level diagram showing radiative transition, $\Rightarrow$, to form the Franck–Condon excited sensitising ketone ($^1K_{FC}^*$) and the Franck–Condon excited CT state $^3(M^+...O_2^-)_{FC}^*$ and likely decay pathways, spin allowed, $\rightarrow$, spin forbidden, $----\rightarrow$. N.B. For clarity neither intersystem crossings between singlet and triplet state complexes nor the $^5(^3M^*...O_2)^*$ complex which is formed from $\frac{1}{9}$ of the collisions between $^3M^*$ and O_2 are shown.

532

of S_Δ and k_q^T are 0.86 and 1.6×10^9 ℓ mol^{-1} s^{-1}, respectively, while for acetonitrile the values are 0.51 and 3.3×10^9 ℓ mol^{-1} s^{-1}. These numbers indicate that the catalysed intersystem crossing via the triplet channel, which as shown in scheme 1 does not produce singlet oxygen, is more important in acetonitrile than in cyclohexane due to the more favourable CT interactions in the more polar solvent. In cyclohexane, which has a dielectric constant of 2.02, it is quite likely that the relaxed charge transfer states, $^{1,3}(M^+...O_2^-)^*$, lie above the localised triplet, not below as shown in scheme 1, and in the absence of CT mediated quenching the triplet channel is impeded relative to the singlet channel because of poor Franck–Condon factors [16]. Thus we would expect that deactivation of the initially prepared excited state complex to give ground state products would be faster in acetonitrile than in cyclohexane. This means that separation of $^3(^3M^*...O_2)^*$ to yield the triplet state would be more important in cyclohexane as observed.

Since the triplet energies of naphthalene and 1-methylnaphthalene are 255 and 249 kJ mol^{-1}, respectively [17], it is likely that the energy of $^3(^3M^*...^1O_2^*)^*$, i.e. the complex formed by association of the triplet state of EN and singlet oxygen, will be ≈ 343 kJ mol^{-1}, which is slightly higher than the excitation energy used in these experiments, which is 338 kJ mol^{-1}. In fact Dijkgraaf and Hoijtink [18] have reported a broad shoulder around 350 nm in oxygenated naphthalene solutions which they attribute to the simultaneous transition described by

$$^1M + {}^3O_2 \rightleftharpoons {}^3(^1M...O_2) \xrightarrow{h\nu} {}^3(^3M^*...^1O_2^*)^* . \quad (3)$$
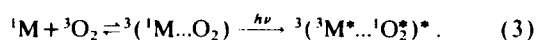
Thus the simplest explanation for the fact that Φ_Δ^{CT} is higher than $S_\Delta \gamma_T$ is that excitation at 353 and 355 nm gives both $^3M^*$ and singlet oxygen following dissociation of $^3(^3M^*...^1O_2^*)^*$ formed either as a result of direct absorption to this doubly excited complex or following internal conversion from the initially formed Franck–Condon charge transfer complex $^3(M^+...O_2^-)_{FC}^*$. In the case of acetonitrile and cyclohexane respectively th.'s would require a quantum yield of 0.16 and 0.08 for this process in these two solvents. The fact that several organic compounds, which have energy gaps between their lowest singlet and triplet states greater than 94 kJ

mol^{-1}, give singlet oxygen yields greater than one [1,19,20] when excited into their lowest singlet excited states, demonstrates that this doubly excited state dissociates to give both the triplet state and singlet oxygen when it is populated in the case of many other compounds. The only other possible explanation consistent with our data for the production of more singlet oxygen than expected from the measured amounts of $^3M^*$ is that enhanced intersystem crossing from $^3(M^+...O_2^-)_{FC}^*$ to $^1(M^+...O_2^-)_{FC}^*$ takes place before relaxation by internal conversion to the thermally relaxed CT complexes. This seems unlikely. We therefore suggest dissociation of the doubly excited state is the most likely explanation of the higher than expected yield of singlet oxygen detected in this work following CT absorption.

4. Conclusions

This Letter describes picosecond absorption measurements of events following excitation of hydrocarbon–molecular oxygen contact complexes for the first time. We have demonstrated that the excited state complex produced upon 353 nm excitation of oxygenated 1-ethylnaphthalene has a lifetime which is less than 10 ps in acetonitrile and in cyclohexane. We have also shown that the decay channel distribution is markedly different in the two solvents studied, leading to different triplet state yields. Measurements of singlet oxygen yields strongly indicate that upon excitation in the CT region some excited state complexes dissociate to give both triplet 1-ethylnaphthalene and singlet oxygen.

References

[1] J. Saltiel and B.W. Atwater, Advan. Photochem. 14 (1988) 1.

[2] A. Garner and F. Wilkinson, Chem. Phys. Letters 45 (1977) 432.

[3] S.K. Chattopadhyay, C.V. Kumar and P.K. Das, J. Photochem. 30 (1985) 81.

[4] R.W. Redmond and S.E. Braslavsky, Chem. Phys. Letters 148 (1988) 523.

[5] M. Kristiansen, R.D. Scurlock, K.-K. Iu and P.R. Ogilby, J. Phys. Chem. 95 (1991) 5190.

[6] D.J. McGarvey, P.G. Szekeres and F. Wilkinson, Chem. Phys. Letters 199 (1992) 314.

[7] D.F. Evans, J. Chem. Soc. (1957) 1351.

[8] H. Tsubomura and R.S. Mulliken, J. Am. Chem. Soc. 82 (1960) 5966.

[9] J.B. Birks, Photophysics of aromatic molecules (Wiley-Interscience, New York, 1970) ch. 10 and references therein, p. 492.

[10] S.L. Logunov and M.A.J. Rodgers, J. Phys. Chem. 96 (1992) 2915.

[11] A. Liu, M.C. Sauer Jr., D.M. Loffredo and A.D. Trifunac, J. Photochem. Photobiol. A 67 (1992) 197.

[12] R.W. Redmond and S.E. Braslavsky, in: Photosensitisation, NATO ASI Series, Vol. H15, eds. G. Moreno, R.H. Pottier and T.G. Truscott (Springer, Berlin, 1988) p. 93.

[13] A.A. Gorman, A.A. Krasnovsky and M.A.J. Rodgers, J. Phys. Chem. 95 (1991) 598.

[14] H. Masuhara, H. Miyasaka, N. Ikeda and N. Mataga, Chem. Phys. Letters 82 (1981) 59.

[15] H. Miyasaka, H. Masuhara and N. Mataga, J. Phys. Chem. 89 (1985) 1631.

[16] O.L.J. Gijzeman, F. Kaufman and G. Porter, J. Chem. Soc. Faraday Trans. II 69 (1973) 708.

[17] S.L. Murov, Handbook of photochemistry (Marcel Dekker, New York, 1973).

[18] C. Dijkgraaf and G.J. Hoijtink, Tetrahedron 19, Suppl. 2 (1963) 179.

[19] A.J. McLean, D.J. McGarvey, T.G. Truscott, C. Lambert and E.J. Land, J. Chem. Soc. Faraday Trans. 86 (1990) 3075.

[20] R.C. Kanner and C.S. Foote, J. Am. Chem. Soc. 114 (1992) 678.

Kinetic Spectroscopy of Pyrazolotriazole Azomethine Dyes

Francis Wilkinson,* David Worrall, David McGarvey and Andrew Goodwin
Department of Chemistry, University of Technology, Loughborough, Leicestershire, UK LE11 3TU
Andrew Langley
Laser Support Facility, Rutherford-Appleton Laboratory, Chilton, Didcot, Oxfordshire, UK

The photophysical properties of pyrazolotriazole azomethine dyes have been investigated using both picosecond and nanosecond flash photolysis. On nanosecond timescales, prompt formation of a photoisomer is observed, the rate of decay of which shows a solvent dependence. In the presence of a triplet sensitiser a triplet pathway to the photoisomer has been established, the yield of isomer from the triplet state being considerably higher than from direct excitation. On picosecond timescales, two transients are observed; the first has a very short, solvent-independent lifetime, while the second has a longer solvent-dependent lifetime. These two transients are assigned as states formed during the relaxation of the molecules along the first excited singlet and the ground-state potential-energy surfaces, respectively. Similar kinetic behaviour is observed in a high concentration, high viscosity environment designed to mimic the photographic emulsion, indicating that the photophysical relaxation pathways are still very rapid even in this type of environment.

Pyrazolone and pyrazolotriazole (PT) azomethine dyes are well known as magenta image formers in the photographic subtractive colour development process. They are formed during development by the oxidative coupling of a *p*-phenylenediamine and the appropriate coupler.[1] They exhibit two maxima in their visible absorption spectra; a high intensity band, typically in the green region, and a lower intensity band in the blue region. Unsymmetrical azomethine dyes can exist as two isomeric configurations about the azomethine linkage, referred to as the *syn-* and *anti-*isomers. It has been demonstrated that this isomerisation can be brought about by electronic excitation.[2] Isomerisation in dyes not symmetrical about the carbon–nitrogen double bond is readily observed as a bathochromic shift in their absorption spectra. The less stable *anti-*isomer so produced relaxes thermally to the *syn-*form on timescales ranging from microseconds to milliseconds depending on temperature, solvent properties and the nature and positions of substituents. Triplet-energy transfer to these dyes also results in production of the isomer, indicating the existence of an isomerisation pathway involving the triplet state. However, the rise of the absorption due to the isomer follows precisely the decay of the sensitiser triplet state irrespective of its lifetime, indicating that the triplet state of the dye must have a lifetime shorter than a few hundred nanoseconds.

Fluorescence quantum yields of these compounds in dilute fluid solution at room temperature are very low,[3] of the order of 10^{-4}. Fluorescence quantum yields and fluorescence lifetimes are observed to increase significantly as the temperature is decreased,[4] although even at liquid nitrogen temperatures no phosphorescence emission can be detected.

Experimental

Solvents were spectrophotometric grade (Aldrich) and were used as received. Dyes were donated by Kodak Ltd. and were used without further purification. The dye structures corresponding to the designations used in the text are shown in Fig. 1. Ultraviolet–visible (UV–VIS) absorption spectra of the dyes in acetonitrile solution are shown in Fig. 2.

The hand coatings are designed to mimic, as far as possible, the photographically formed coatings, but are made with pre-formed dyes and consequently both photographic product dyes and dyes that cannot be formed using the photographic process can be investigated in the product environ-

ment. The formulation of the hand coatings is as follows for a dye with a molecular weight of *ca.* 1000 g mol^{-1} and a molar absorption coefficient of 10^4 dm^3 mol^{-1} cm^{-1}, with which parameters an absorbance of approximately 1.5 is obtained at the dye λ_{max} with a dry coating thickness of about 10 μm. 2.5 g of a 50% gelatin–50% water solid is added to 22.5 g of a 1.39 g dm^{-3} solution of sodium dodecyl sulfate, and the whole heated to dissolve the gelatin. To 20 g of the resulting solution is added a solution of 35 mg of dye and 105 mg of di-*n*-butylphthalate in 2 cm^3 of ethyl acetate, and the whole homogenised using a soniprobe for 5 min. Much of the ethyl acetate evaporates during sonication, and any remaining is removed by additional heating of the mixture prior to proceeding further. The resulting mixture is then spread onto an
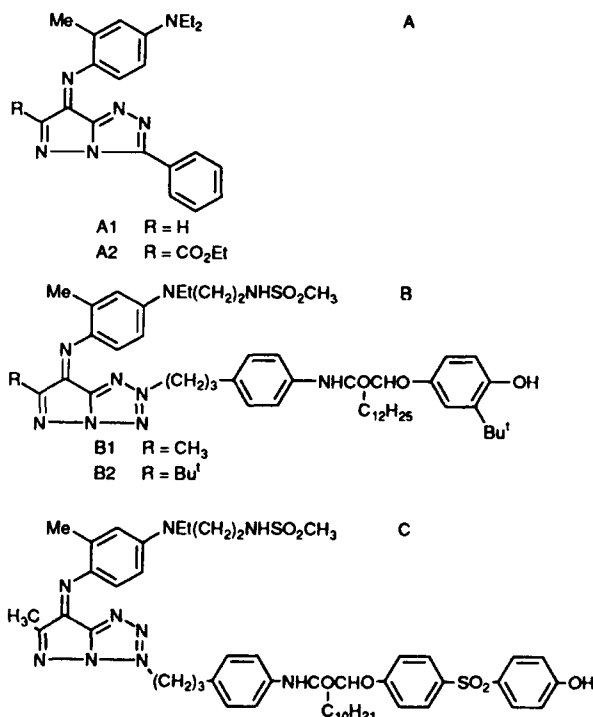

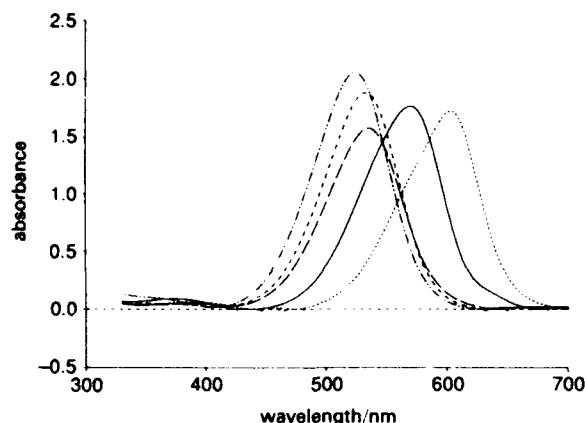Fig. 1 Pyrazolotriazole azomethine dye structures

Fig. 2 UV–VIS absorption spectra of pyrazolotriazole azomethine dyes in acetonitrile solution (concentration 4×10^{-5} mol dm^{-3})

acetate base 'subbed' with gelatin, and dried flat. The mixture is spread at an appropriate thickness given that shrinking of the gelatin causes the dry coating to have a thickness about a tenth that of the wet coating.

Nanosecond laser flash photolysis studies were carried out using an HY200 Nd:YAG laser (Lumonics), frequency doubled to 532 nm for experiments involving direct excitation of the dyes, and frequency tripled to 355 nm for the sensitisation experiments. The analysing source was a 300 W Xenon arc lamp (Optical Radiation Corporation). Detection was with a Hamamatsu R928 photomultiplier tube through an f, 3.4 grating monochromator (Applied Photophysics). Signals from the photomultiplier tube were digitised with a 2432A digital oscilloscope (Tektronix) and the data transferred to an IBM compatible PC via a GPIB interface for analysis. Opening of shutters for the arc lamp and the laser is computer controlled through a DT2808 D/A interface card (Data Translation). The timing of the system is controlled through a home-built analogue delay generator.

All picosecond experiments were carried out with air equilibrated solutions contained within 1 cm × 1 cm quartz cuvettes at room temperature (17–21 °C). Nanosecond experiments involving triplet-energy sensitisation were carried out in solutions degassed by three freeze–pump–thaw cycles. Those involving direct excitation of the dye were carried out in air equilibrated solution as oxygen concentration was found to have no effect on the experiments.

Picosecond laser flash photolysis was carried out at the laser support facility at the Rutherford–Appleton laboratory in Oxfordshire. The system consists of an actively mode-locked Nd:YAG laser (Spectron laser systems) synchronously pumping rhodamine 6G in a model 375 B dye laser (Spectra-Physics). The 585 nm output of the dye laser is amplified at 10 Hz in a three-stage dye amplifier pumped by a DCR-3 Q-switched Nd:YAG laser (Quanta-Ray) to a pulse energy in excess of 400 µJ. The amplified beam is split into two, one half being used to provide the excitation pulses while the other is frequency shifted using either stimulated Raman or continuum generation in a water D$_2$O mixture to provide the probe pulse, the wavelength of interest being isolated using an interference filter. Excitation pulse energy at the sample was 3–10 µJ per pulse in a 1 mm diameter spot.

The detectors used to monitor the pump and probe signals are based on the design of Pollard and Zenith,[5] utilising 1 cm × 1 cm UV sensitive PIN diodes from Hamamatsu (S1723-05). The pump-signal detector is a single diode and amplifier circuit, an integrating sphere being placed in front of the diode to ensure even illumination of the surface. The

probe detector consists of two diodes connected across a differential amplifier circuit, the output from this amplifier being the difference between the two diode outputs, a separate amplification stage providing a signal proportional to the sum of the signals from the two diodes to allow normalisation to probe intensity. The output from each diode is maintained below 250 mV to preserve linearity by the use of appropriate neutral density filters in the probe beam.

The signals from each diode–amplifier combination are fed into SR250 gated integrators (Stanford Research Ltd), which integrate the signals in a gate typically 300 ns wide. The integrated output is then fed to an SR 245 analogue to digital–digital to analogue (A/D D/A) converter and computer interface, and the data fed to a microcomputer via a GPIB interface.

Processing of Pump–Probe Data

The analytical parameter required from these experiments is the change in transmission induced by the pumping pulse at a particular time after its arrival. The normalised probe intensity change induced by the pumping pulse at a time delay t after arrival of the pump pulse of energy P is

$$\left(\frac{\Delta I(P)}{I}\right)_{t,u} = \frac{\bar{D}_{on} - \bar{D}_{off}}{\bar{N} - \bar{N}_{baseline}}$$

where N and D are proportional to the sum and difference signals, respectively, $\bar{D}_{on}$ is the mean difference signal with the pump, $\bar{D}_{off}$ is the mean difference signal with no pump (background signal), $\bar{N}_{baseline}$ and $\bar{N}$ are the mean sum signal in the absence and presence of incident probe respectively and the subscript u indicates that the value of $\Delta I(P)/I$ is uncorrected and at this stage only proportional to percentage transmission change. No correction for emission is necessary with the samples investigated here since the emission quantum yield at ambient temperatures is too low to be detected. The value of $\Delta I(P)/I$ is then normalised to pump intensity using

$$\left(\frac{\Delta I}{I}\right)_{t,u} = \frac{\left(\frac{\Delta I(P)}{I}\right)_{t,u}}{\bar{P} - \bar{P}_{baseline}} \bar{P}_{series}$$

where $\bar{P}_{series}$ is the mean pump intensity for the whole kinetic run. This value of $\Delta I/I$ thus obtained is then corrected to actual percentage transmission change by multiplication by a factor f, obtained from a measurement of the difference signal obtained when an 8% reflecting glass slide is placed in the sample beam. The factor f is then calculated as

$$f = \frac{0.08(\bar{N} - \bar{N}_{baseline})}{(\bar{D}_{in} - \bar{D}_{out})}$$

where $\bar{D}_{in}$ and $\bar{D}_{out}$ relate to the difference signal with the glass slide in and out of the beam, respectively. The analytical parameter most useful in the interpretation of such data, i.e. the absorbance change, is calculated from

$$\Delta A = -\log\left[1 - \left(\frac{\Delta I}{I}\right)_t f\right]$$

Results and Discussion

Nanosecond Flash Photolysis

Following flash excitation, population of the anti-isomeric form of the dye is observed as a bathochromic shift in the dye absorption spectrum; this shift gives rise to a time-resolved transient difference spectrum as shown in Fig. 3. It is clear
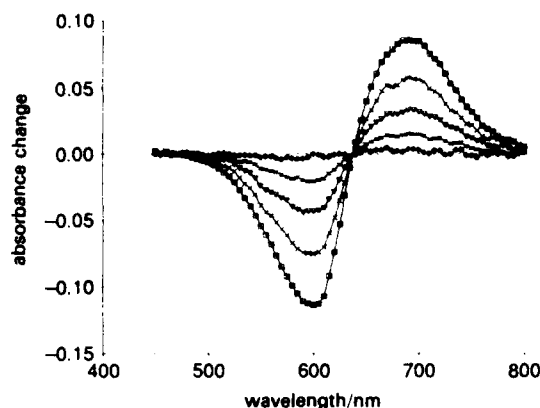
Fig. 3 Transient difference spectrum following pulsed excitation of a 1.68×10^{-5} mol dm^{-3} solution of dye A2 in acetonitrile. Excitation wavelength 532 nm. Time from laser pulse ($\square$) 0.00066, ($\times$) 0.00442, (∇) 0.00924, ($+$) 0.0166 and ($\diamond$) 0.0319 s.

that the decay kinetics are the same across the entire spectrum.

Quantum Yields of Isomerisation from Singlet and Triplet States

In order to convert the measured photoinduced absorption change due to population of the *anti*-isomer into the quantum yield of isomer production, it is necessary to determine the difference in molar absorption coefficients between the two forms. Assuming no absorption by the *anti*-isomeric form in the short wavelength edge of the *syn*-isomer absorption band the calculated yield is independent of analysis wavelength, and hence the quantum yields presented have been calculated on this basis. The quantum yields of isomer production from direct excitation and from triplet sensitisation are given in Table 1. The triplet-sensitised isomerisation yields are calculated on the basis of a calculated proportion of a known population of sensitising triplet state being quenched by the azomethine dye under investigation, assuming all quenching is by energy transfer.

The same transient difference spectrum is obtained from both triplet-energy sensitisation experiments and as a consequence of direct excitation; this demonstrates that the same product is arrived at by both routes. However, the quantum yield of production of the isomer as a result of direct excitation is substantially less than the yield of isomer from the sensitised triplet state.

Anti-*Isomer Relaxation Rates*

Once the *anti*-isomer has been populated, either as a result of direct excitation of the dye or by triplet-energy transfer from a suitable donor, it relaxes thermally to the stable *syn*-

Table 1 Isomerisation efficiencies of some pyrazolotriazole azomethine dyes

dye[a]	sensitiser	solvent	anti-isomer quantum yield mean (std. dev.)	
A2	none	benzene	0.011	(0.001)
	none	acetonitrile	0.075	(0.006)
	2'-acetonaphthone	benzene	0.4	(0.1)
	benzophenone	benzene	0.4	(0.1)
	benzophenone	acetonitrile	0.35	(0.1)
A1	benzophenone	benzene	0.09	(0.02)
C	benzophenone	benzene	0.45	(0.1)

[a] See Fig. 1.

Table 2 *Anti*-isomer relaxation lifetimes

dye	solvent	τ/ms mean (std. dev.)	
A2	acetonitrile	7.89	(1.33)
	di-*n*-butylphthalate	2.13	(0.20)
	methanol	0.279	(0.032)
	benzene	2.22	(0.42)
A1	methanol	452	(4)
	benzene	590	(25)
	chlorobenzene	424	(3)
C	methanol	3.4	(0.5)
	acetonitrile	8.5	(1.5)

configuration by a unimolecular process. The relaxation time is strongly dependent upon both the solvent and the nature of the substituent in the 6-position of the pyrazolotriazole ring of the azomethine dye. Data for the relaxation of *anti*- to *syn*-isomers for a range of substituents and solvents is given in Table 2. All determinations were performed at 21 ± 1 °C. Concentrations were in the range $(1.5-4) \times 10^{-5}$ mol dm^{-3}, and there was no dependence of lifetimes on concentration over the range employed.

Note that there is no correlation between isomer lifetime and bulk solvent properties such as viscosity or relative permittivity; this is illustrated by the relaxation times of the A2 *anti*-isomer in a range of methanol–glycerol mixtures, as shown in Table 3. It is clear that while there is a trend of increasing isomer lifetime with increasing viscosity, this is not the only factor at work, as illustrated by the fact that even with a glycerol : methanol ratio of 20 : 5, and consequently an appreciable viscosity, the isomer lifetime is still shorter than that observed in pure methanol. In addition, no correlation between the *anti*-isomer lifetime and any of the empirical free energy parameters determined for solvents on the basis of equilibria, kinetics and spectroscopic properties[6] has been found.

The rate of the relaxation process will be determined in part by the free energy of solvation of the transition state through which the interconversion proceeds. Clearly, the group in the *para* position on the aromatic ring attached to the axomethine nitrogen, NEt$_2$, is strongly electron donating and as such would be expected to facilitate a torsional mechanism for isomerisation, involving rotation about the carbon–nitrogen double bond, where the negative charge will be delocalised over the pyrazolotriazole ring system.[9] Therefore a degree of charge separation during the isomerisation process is anticipated to occur, and as such the energy of activation associated with the process may be expected to be lowered in highly polar or polarisable solvents. Inspection of the data of Tables 2 and 3 clearly demonstrates that such a simple relationship between polarity and lifetime does not prevail. However, it is possible that the isomerisation may proceed *via* a biradical intermediate. Indeed, data presented by Douglas and Clarke[10] suggest that A2 may isomerise *via*

Table 3 Dye A2 *anti*-isomer relaxation times in glycerol–methanol mixtures

glycerol : methanol	isomer lifetime/μs mean (std. dev.)		η/cP[a]
pure methanol	279	(32)	0.55
5 : 20	156	(18)	0.88
12 : 13	164	(7)	6.6
20 : 5	174	(12)	133
24 : 1	385	(63)	640

[a] Calculated values from ref. 7 and 8.

such a biradicaloid intermediate, this biradical having triplet character assigned on the basis of the pre-exponential factor determined from Arrhenius plots. It is, however, difficult to rationalise the large solvent effects on the thermal back isomerisation rate in A2 on the basis of such a mechanism alone, and the implication therefore is that other processes must be at work in determining the isomer lifetime. For example, it has been noted that the rate of back isomerisation is increased in protic solvents, as a consequence of protonation of the azomethine nitrogen atom,[11] which may explain the very large difference in isomer lifetime seen when comparing methanol and acetonitrile solutions where many of the physical solvent properties are similar. It is therefore anticipated that there may be other specific solvent–solute interactions such as this at work in determining the stability of the states involved in any given solvent and hence the rates of *anti–syn*-isomerisation. The thermal back isomerisation rates for dyes Al and C are much less sensitive to solvent changes than that for A2, which may suggest that a different isomerisation mechanism is dominant in these compounds, possibly one involving less of a change in charge distribution in the transition state relative to the stable conformations, such as inversion over the azomethine nitrogen.

Picosecond Pump–Probe Laser Flash Photolysis

Representative time-resolved transient absorption data are shown in Fig. 4 and 5; these are typical of many more obtained for a range of dye and solvent systems.

General points to note about the kinetic data are:

(a) For all dye and solvent systems it was established that the magnitude of the observed transient absorption was proportional to the exciting laser pulse energy in the range employed (3 to 10 μJ per pulse).

(b) Experiments where the relative polarisation of the pumping and probing beams was changed demonstrated that while the signal recorded with orthogonal polarisations was approximately 2/3 the size of that with parallel polarisations,
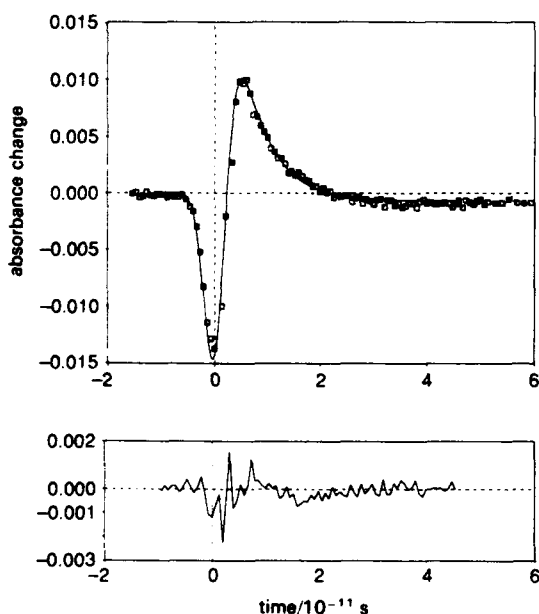

Fig. 4 Picosecond transient absorption trace following excitation of a 7 × 10⁻⁶ mol dm⁻³ solution of dye A2 in ethyl acetate. Excitation wavelength 585 nm; analysing wavelength 630 nm; pulse width (FWHM) 3.3 ps. A plot of residuals for the fitted function is also shown.
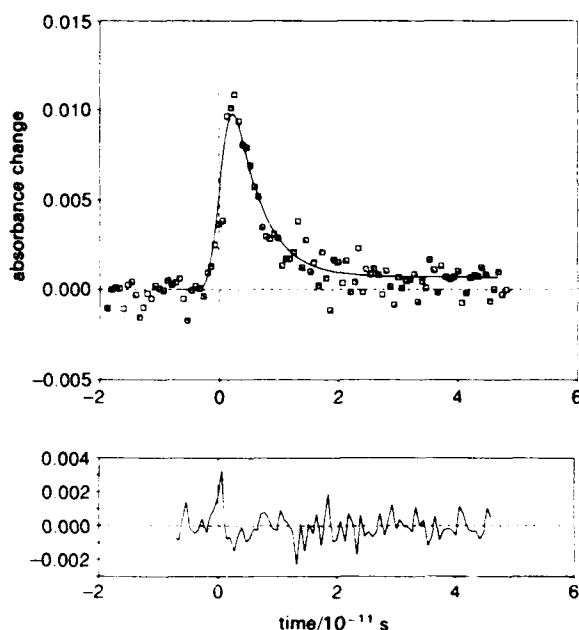

Fig. 5 Picosecond transient absorption trace following excitation of a 4 × 10⁻⁵ mol dm⁻³ solution of dye C in toluene solution. Excitation wavelength 585 nm; analysing wavelength 630 nm; pulse width (FWHM) 2.5 ps. A plot of residuals for the fitted function is also shown.

the normalised traces were superimposable. All data presented were recorded with pumping and probing beams oriented at 54.7° to one another to reduce any effects introduced by rotational diffusion.[12]

(c) Measurements of the absorption spectra of the dyes in solution prior to and following the experiments revealed that no detectable sample degradation had occurred, except in the case of dye A2 in the hand coating. Here it was found that the coating suffered damage from laser irradiation, which is attributed to both photochemical degradation and thermal breakdown of the coating structure. As a consequence, in order to record data traces for A2 in the coating, the sample was changed after every five data points, over which period negligible sample degradation occurred.

The kinetic data may be characterised in terms of a biexponential function convolved with a suitable excitation pulse profile; in this instance a Gaussian profile was employed. In order to extract lifetimes as accurately as possible it is necessary to convolute the resulting profile with another Gaussian function describing the probing pulse. The convolution integral[13] is carried out using Simpson's rule with 13 ordinates. Parameters describing the data can then be extracted and are shown in Table 4. Examples of fits to the data sets are shown in Fig. 4 and 5, with plots of residuals shown for each trace. Some points to note concerning the kinetic data are:

(a) At least two lifetimes are required to fit the data, plus a long-lived component which does not decay on a nanosecond timescale.

(b) The first lifetime is solvent insensitive to within the error of the fitting, the lifetime being 1–3 ps in all solvents. The state associated with this lifetime is not assigned as the Franck–Condon first excited singlet state on the basis of there being no stimulated emission from this state.

(c) The second lifetime shows some solvent dependence, as illustrated in Table 4. However, its lifetime is far too short for it to be assigned as the photoisomer.

Table 4 Best-fit parameters to picosecond data

| dye | solvent | λ/nm | ground state | | FWHM/ps | τ_1/ps | τ_2/ps | ε_1 | ε_2 | ε_{isomer} |
			ε pump	ε probe						
A2	MeOH	600	54500	69000	3.7	1.0	6.0	63000	64000	14000
		610	54500	70000	3.3	1.0	4.4	67000	69000	57000
		640	54500	25000	3.4	1.8	3.7	19300	28700	23500
		650	54500	15000	3.5	1.9	5.3	10000	19000	29000
	benzene	640	73000	12000	4.7	2.1	7.4	10000	13200	25000
		650	73000	7000	3.3	1.2	8.9	6000	9200	49000
	DBP	600	67000	83000	3.5	1.0	6.1	82300	79500	27000
		610	67000	15000	2.3	1.0	5.3	85000	85000	86000
		650	67000	8000	3.8	1.0	7.7	13500	17000	30000
	MeCN	630	40000	25000	3.5	0.7	8.7	17000	27000	24000
		640	40000	30600	3.6	0.5	9.6	8000	16000	15000
		650	40000	17000	3.3	0.6	10.1	2600	11000	10000
	hexane	630	7000	300	1.0	0.9	6.7	750	2700	8000
	EtOAc	630	45000	23500	3.1	1.0	5.8	20000	26000	22500
	coating	640	65000	17000	4.5	5.3	6.3	15000	35000	31000
B1	toluene	650	3500	200	2.3	0.8	2.1	330	1000	9000
B2	toluene	650	3500	200	2.4	1.0	2.6	360	1200	3000
C	toluene	630	7000	725	2.5	0.5	4.7	800	2000	3500
		640	7000	425	2.5	0.9	4.7	800	2000	3500
		650	7000	200	3.0	0.7	3.7	440	500	1000

FWHM pulse full-width-half-maximum, λ probe wavelength, MeOH methanol, MeCN acetonitrile, EtOAc ethyl acetate, DBP di-n-butyl-phthalate, ε values quoted have units of $dm^3\,mol^{-1}\,cm^{-1}$.

(d) The long-lived component necessary to fit the data has identical spectral properties to the photoisomer observed following pulsed excitation on nanosecond timescales. The molar absorption coefficient of this state presented in Table 4 is calculated using isomerisation quantum yields determined from nanosecond flash photolysis experiments. In all cases this component shows no decay on the timescale accessible with the picosecond apparatus, and is consequently assigned as the photoisomer.

Therefore we propose a model for the syn–anti-photoisomerisation process whereby the assignment of the states associated with lifetimes τ_1 and τ_2 are as shown in Fig. 6.

First Short-lived Transient associated with Lifetime τ_1

The kinetic traces obtained for dye A2 probing between 600 and 650 nm in all solvents (except hexane where the syn-isomer absorption spectrum is hypsochromically shifted) show an initial prompt bleaching which recovers in 0.5–3 ps. The data for dyes C, B1, and B2 do not show any initial bleaching by virtue of the very small absorption by the syn-isomer ground state in the probed spectral region. Since there is no evidence for stimulated emission from this state, it is not assigned as the fluorescent singlet state. There then remains the possibility that it is in fact the twisted excited
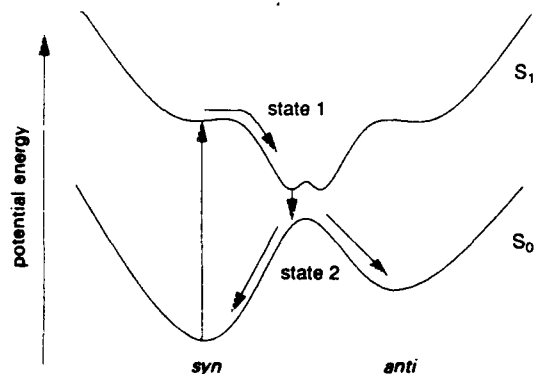

Fig. 6 Schematic potential-energy surface for the pyrazolotrazole azomethine dyes

singlet state at the perpendicular conformation. Within experimental error, the lifetime of this state shows little solvent dependence, although there is evidence that it is slightly longer lived when the environment is that of the dye–di-n-butylphthalate droplet in the hand coating than in fluid di-n-butylphthalate solution. Changes in lifetime with solvent would, however, be very difficult to detect because of the coupling between the lifetime of this state, its molar absorption coefficient and the pulse width. It is proposed therefore that excitation takes place initially to the first excited singlet state of the syn-isomer, and it is this which is the fluorescent singlet state. However, at the temperatures and low viscosities used throughout this work this state is very short-lived and the population immediately evolves toward the perpendicular conformation. As a consequence, the steady-state population of the fluorescent singlet state is very small, explaining the lack of stimulated emission. Hence what is termed here for simplicity as 'state 1' could in fact be thought of as being the excited-state population as it evolves toward the perpendicular conformation, and will therefore have an 'effective absorption coefficient' which varies with time since the absorption coefficient will undoubtedly vary somewhat with position on the excited singlet state surface. Evolution to the perpendicular conformation is therefore postulated as very rapid, the rate-limiting step in reaching the ground-state surface in fluid solution being internal conversion from the perpendicular conformation. This may be relatively insensitive to solvent parameters provided the ground to excited state surface separation does not signficantly change with changing solvent. Such changes may be expected to occur if there were significant charge separation in the perpendicular geometry, and hence the suggestion is tentatively made that this is not the case and that isomerisation proceeds possibly via homolytic fission of the azomethine bond to yield the singlet biradical, followed by torsion about this bond. In the hand coating, the state 1 lifetime is seen to be longer than in fluid solution, and here evolution of the population to the twisted geometry is postulated as rate determining.

Second, Longer-lived Transient associated with Lifetime τ_2

Again taking the example of the data obtained with A2 first, it can be seen from inspection of data in Table 4 that the

Table 5 State 2 lifetime as a function of solvent

solvent	τ/ps mean (std. dev.)
methanol	4.4 (0.9)
di-n-butylphthalate	6.3 (1.1)
benzene	8.1 (1.0)
acetonitrile	9.5 (0.7)

absorption coefficient of this state is somewhat less than that of the syn-isomer ground state at wavelengths shorter than 630 nm, but somewhat greater at longer wavelengths. The lifetime of the state also exhibits some solvent dependence, the mean lifetimes as a function of solvent being shown in Table 5.

Again, there is no correlation between lifetime and either solvent relative permittivity or viscosity. Interestingly, however, the increase of state 2 lifetime with solvent follows the same pattern as that of the lifetime of the anti-isomer (Table 2). This lends weight to the theory which naturally follows from the assignment of state 1 that state 2 is a point (or points) on the ground-state potential surface. The transient seen as state 2 may then be assigned as the evolution of the population along the ground-state surface returning to equilibrium, and again there will be some position dependence of the absorption coefficient on this surface and the transient seen will reflect the population in the ground-state evolving toward the two isomeric forms. The precise reasons why there is no clear correlation between solvent properties and the measured state 2 lifetimes are not known, although several theories have been advanced for the lack of correlation of isomerisation rates in, for example, stilbenes with solvent viscosity.[14] These may be summarised as:

(i) The intramolecular potential surfaces exhibit a solvent dependence (specific solvent–solute interactions).

(ii) Macroscopic solvent viscosity is not an adequate measure of the friction felt by the isomerising molecule, possibly as a consequence of the molecular scale involved in the isomerisation process.

(iii) Other degrees of freedom than the isomerisation coordinate may contribute to the overall relaxation process.

It is felt that, given the complexity of the dyes involved, probably all of the above make some contribution to the overall explanation, although given the small size of the moiety involved in the isomerisation process one may expect the failure of the macroscopic viscosity to describe adequately the prevailing friction to play a major role. The data collected for dyes B1 and B2 in toluene solution demonstrate that these two dyes exhibit identical properties (Table 4). This suggests that steric hindrance in the 6-position is not an important factor in determining the state 2 lifetime.

It should be pointed out at this juncture that there is no direct evidence from the data that state 1 is a precursor of state 2, and there exists the possibility that both states form simultaneously; the data are then simply the superposition of two transients. However, it is simpler to rationalise the observed transients on the basis of a sequential model, so in the absence of evidence to the contrary such a model will be adopted.

Conclusions

The two picosecond transients observed have been assigned as states 1 and 2 which may be represented as in Fig. 6. State 1 is evolution of the excited-state population to the twisted excited-state conformation, which may have a short but finite lifetime; on the basis of the quantum yields of isomer formation (Table 1), a potential minimum on the excited state surface is postulated to be located on the syn-isomer side of the potential barrier between syn- and anti-isomeric forms. This assignment is favoured on account of the lack of stimulated emission observed, which can be explained if the population of the initially formed fluorescent state is vanishingly small. This is suggested to be a consequence of a very small potential barrier from the initially formed state and a very steep potential toward the perpendicular conformation. Such very fast decay times and lack of solvent dependence have been observed for the photoisomerisation of cis-stilbene, and this has also been explained as resulting from the presence of a very small activation barrier in the excited state. However, following internal conversion to the ground-state potential surface the molar absorption coefficient thereof is not observed to change signficantly with time.[15] In the case of the azomethine dyes, state 2 is assigned as the population on the ground-state surface evolving to the two isomeric forms, the absorption coefficient varying with position on the surface. The frequency of the motion on the ground-state surface shows some solvent dependence, and this is the same dependence as seen for the thermal anti—syn-isomerisation following population of the anti-isomer. This picture was suggested by us as a possible explanation in a preliminary publication on this work[16] prior to gathering much of this data. Following this earlier publication, data presented by Douglas et al.[4] have been rationalised in terms of a similar picture. These authors succeeded in detecting the fluorescent singlet state of A2 in a 96 : 4 v/v glycerol : methanol mixture at room temperature from stimulated emission measurements, this state having a lifetime of $\leqslant 2$ ps. However, they could not detect such a state in pure ethanol solution, results which are in agreement with those presented here.

References

1 T. H. James, in *The Theory of the Photographic Process*, Macmillan, London, 4th edn., 1988.
2 W. G. Herkstroeter, *J. Am. Chem. Soc.*, 1976, **95**, 330.
3 P. Douglas, *J. Photogr. Sci.*, 1988, **36**, 83.
4 P. Douglas, S. M. Townsend, R. J. Booth, B. Crystall, J. R. Durrant and D. R. Klug, *J. Chem. Soc., Faraday Trans.*, 1991, **87**, 3479.
5 H. J. Pollard and W. Zenith, *J. Phys. E*, 1985, **18**, 399.
6 C. Reichardt, in *Solvents and Solvent Effects in Organic Chemistry*, VCH, Weinheim, 2nd edn., 1988.
7 *Perry's Chemical Engineers Handbook*, ed. D. W. Green, McGraw-Hill, New York, 6th edn., 1984.
8 *Physical Properties of Binary Systems in Concentrated Solutions*, ed. J. Timmermans, Interscience, New York, 1959, vol. 2.
9 H. Kessler, *Angew. Chem.*, 1970, **82**, 237.
10 P. Douglas and D. Clarke, *J. Chem. Soc., Perkin Trans. 2*, 1991, 1363.
11 C. Couture and P. Douglas, Poster abstract No. II-71, XVth International Conference on Photochemistry, Paris, France, 1991.
12 H. E. Lessing and A. von Jena, *Chem. Phys. Lett.*, 1976, **42**, 213.
13 D. F. Eaton, *Pure Appl. Chem.*, 1990, **62**, 1631.
14 S. K. Kim and G. R. Fleming, *J. Phys. Chem.*, 1988, **92**, 2168.
15 S. Abrash, R. Repinec and R. M. Hochstrasser, *J. Chem. Phys.*, 1990, **93**, 1041.
16 F. Wilkinson, D. R. Worrall and R. S. Chittock, *Chem. Phys. Lett.*, 1990, **174**, 416.

The efficiency of singlet oxygen generation by substituted naphthalenes in benzene. Evidence for the participation of charge-transfer interactions

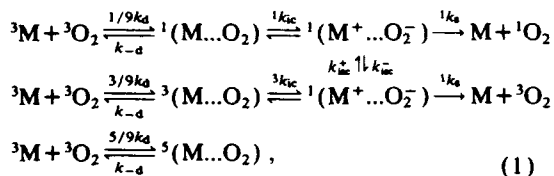D.J. McGarvey, P.G. Szekeres and F. Wilkinson

Department of Chemistry, University of Technology, Loughborough, Leicestershire LE11 3TU, England, UK

An inverse correlation between the rate constant for oxygen quenching of the triplet state (k_q^T) and the efficiency of singlet oxygen generation (S_Δ) is established for a range of substituted naphthalenes in benzene. The participation of charge-transfer interactions are implicated on the basis that the only property which varies significantly with the substituent is the oxidation potential (E_M^{ox}) of the naphthalene derivative. Using published electrochemical data, correlations between S_Δ, k_q^T and the free energy change for charge transfer (ΔG^{CT}) have been found with values of S_Δ and k_q^T ranging from 0.34 to 0.75 and from 5.0×10^9 to 1.2×10^9 M^{-1} s^{-1} for 1-methoxynaphthalene and 1-cyanonaphthalene, respectively.

1. Introduction

In 1977 [1] one of us proposed the involvement of charge transfer (CT) interactions to explain the high oxygen quenching rate constants observed for the triplet states of certain aromatic ketones and amines. It was suggested that a consequence of the participation of CT interactions would be a decrease in the observed singlet oxygen yield [2]. The quenching mechanism which was proposed is reproduced as follows:

$$^3M + {}^3O_2 \underset{k_{-d}}{\overset{1/9k_d}{\rightleftharpoons}} {}^1(M...O_2) \overset{{}^1k_{ic}}{\rightleftharpoons} {}^1(M^+...O_2^-) \overset{{}^1k_e}{\longrightarrow} M + {}^1O_2$$

$$^3M + {}^3O_2 \underset{k_{-d}}{\overset{3/9k_d}{\rightleftharpoons}} {}^3(M...O_2) \overset{{}^3k_{ic}}{\rightleftharpoons} {}^1(M^+...O_2^-) \overset{{}^1k_e}{\longrightarrow} M + {}^3O_2$$

$$^3M + {}^3O_2 \underset{k_{-d}}{\overset{5/9k_d}{\rightleftharpoons}} {}^5(M...O_2), \tag{1}$$

where M represent an organic molecule.

The fraction of sensitiser triplet state-molecular oxygen quenching encounters which yield singlet oxygen (O_2, ${}^1\Delta_g$) is termed S_Δ. In the past fifteen years

Correspondence to: F. Wilkinson, Department of Chemistry, University of Technology, Loughborough, Leicestershire LE11 3TU, England, UK.

or so it has become apparent that S_Δ values do in fact vary over a wide range from near-zero to unity (for tabulated data see refs. [3–5]). The mechanism of triplet state quenching by O_2 is rather complex since the quenching rates and product channel distributions depend on a number of parameters including the triplet state energy (E_T) [6], the nature of the triplet state (nπ^*, $\pi\pi^*$) [7], the oxidation potential of the sensitiser [1,8], the presence of substituent heavy atoms [9] and the solvent [8,10,11]. There has also been a report of a correlation between S_Δ and the sensitiser ionisation potential [12] for a range of aromatic hydrocarbons in benzene. However for the naphthalene derivatives studied here S_Δ varies with ionisation potential in the opposite direction (see later).

For a comprehensive investigation of the interaction between triplet states and molecular oxygen it is desirable to isolate one of these molecular parameters as the only variable. Chattopadhyay et al. [8] have carried out such an investigation on the oxygen quenching of the triplet states of substituted benzophenones and acetophenones in benzene and acetonitrile in which, essentially, the only variable is the sensitiser oxidation potential. They observed a correlation between the electron-donating ability of

the substituent and the oxygen quenching rate constant (k_q^T). However, the wide variation in the k_q^T values was *not* reflected in a similar variation of the S_Δ values (see also ref. [7]). These findings suggest, in the light of the data presented here, that the mechanism for oxygen quenching of aromatic ketone triplet states may be quite different from that involving aromatic hydrocarbon triplets. In fact, Darmanyan and Foote [9] have recently reported a marked difference between $n\pi^*$ and $\pi\pi^*$ triplet states with respect to the sensitivity of S_Δ values to the presence of heavy-atom substituents. They found that the introduction of a heavy atom markedly decreased the value of S_Δ for $n\pi^*$ sensitisers but very little effect was observed with $\pi\pi^*$ sensitisers. A recent paper by McLean and Rodgers [13] involving a variable temperature investigation of oxygen quenching rates provides evidence for the formation of an exciplex between the triplet state of benzophenone and molecular oxygen in toluene. Studies of this type may provide a useful probe for the encounter complexes formed between excited states and molecular oxygen.

This Letter describes the effect of substituent on S_Δ and k_q^T for a range of naphthalene derivatives in benzene. The substituents include both electron-withdrawing and electron-donating groups such that the oxidation potentials cover the range 1.38 to 1.95 V (versus SCE) while other sensitiser properties such as triplet state energies remain essentially constant. We have employed the method used previously by ourselves [2] and by Gorman et al. [10] (eq. (1)) in which the naphthalene (N) triplet state is populated with unit efficiency by energy transfer using aromatic ketones (K) such as benzophenone (BP) which have high triplet energies and triplet quantum yields (Φ_T) equal to one,

$$^1K^* \to {}^3K^*(\Phi_T = 1) \xrightarrow{N} {}^3N^*(100\%) \xrightarrow{O_2} O_2(^1\Delta_g) \, .$$

(2)
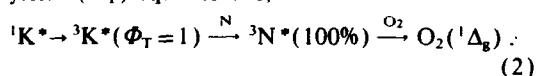
2. Experimental

Benzophenone (Aldrich Gold Label) and *p*-methoxyacetophenone (*p*MAP) (Aldrich, 99%) were used as received. Phenazine (Aldrich) was recrystallised from ethanol. 1-methylnaphthalene was purified by passing through a column containing silica

gel. 2-bromonaphthalene, 1-nitronaphthalene and 2-methoxynaphthalene (Aldrich) were recrystallised from ethanol. 1-ethylnaphthalene (Fluka, 99%) was used as received. Naphthalene was scintillation grade, Gold Label from Aldrich. Benzene was spectrophotometric grade from Aldrich and was used as received. All other materials were from Aldrich and were used without further purification. Kinetic absorption measurements were made using the third harmonic (355 nm) of a JK system 2000 Q-switched Nd:YAG laser (25 ns, 25 mJ pulse^{-1}). The complete laser flash photolysis system is computer-interfaced with a signal-averaging facility for data collection and analysis. For the S_Δ measurements the 355 nm harmonic of a Lumonics HY200 Q-switched Nd:YAG laser (8 ns, 15 mJ pulse^{-1}) was employed as the excitation source. Singlet oxygen (O_2, $^1\Delta_g$ was detected via the 0, 0 phosphorescence band,

$$O_2(^1\Delta_g) \to O_2(^3\Sigma_g^-) + h\nu(1270 \text{ nm}) \, ,$$

(3)
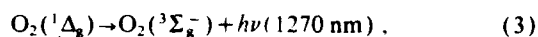
centered at 1270 nm using a Judson germanium photodiode (G-050, active diameter=0.5 cm) coupled to a Judson PA100 preamplifier.

The phosphorescence was detected at right angles to the exciting beam through a silicon cutoff filter. The laser energies employed in the S_Δ measurements did not exceed 0.7 mJ pulse^{-1}. Individual luminescence traces were signal averaged and were fitted using a single exponential function to yield the luminescence intensity I_0 at $t=0$. For each sample I_0 values (at least 24 points) were plotted against relative laser intensity to obtain plots which were linear below 0.5 mJ pulse^{-1}. The slopes of the plots were determined by least squares analysis and comparison of the relative slopes yielded relative S_Δ values.

For both the S_Δ and the k_q^T measurements air-equilibrated solutions in 1 cm×1 cm quartz cells were employed. Substituted naphthalene triplet states were sensitised using BP. In order to ensure complete quenching of the ketone triplet state the substituted naphthalenes were present at concentrations of 0.05–0.06 M (we observed no difference in the S_Δ value for naphthalene when the concentration was increased from 0.05 to 0.1 M). The absorbances of the optically matched solutions were about 0.5 at 355 nm. Under these conditions the BP triplet is exclusively quenched by the substituted naphthalene (we have measured energy transfer rate constants (k_{ET})

for quenching of BP triplet by 1-cyanonaphthalene and 1-ethylnaphthalene to be 7×10^9 M^{-1} s^{-1}). The oxygen concentration in air-equilibrated benzene was taken to be 1.9×10^{-3} M [14].

3. Results

As a standard four our S_Δ measurements we have used the benzophenone/naphthalene system (eq. (2)) employed by Gorman et al. [10]. For this system we believe it is clearly established that the ratio S_Δ^N/S_Δ^{BP} is equal to 1.89 in benzene. However, the absolute S_Δ values for BP and naphthalene are less certain [7,8,10,15]. Chattopadhyay et al. [8] measured S_Δ for BP in benzene to be 0.39 from DPBF bleaching experiments. Gorman et al. [10] combining DPBF bleaching with time-resolved near-IR luminescence measured S_Δ values of 0.29 and 0.55 for BP and naphthalene, respectively. However, Redmond and Braslavsky [7] using time-resolved thermal lensing measured 0.35 as the S_Δ value for BP. This corresponds to an S_Δ value of 0.66 for naphthalene using the ratio of 1.89. In addition Gorman et al. [14] have recently carried out some thermal lensing measurements in which they obtain an S_Δ value of 0.58 for naphthalene. Since the thermal lensing measurements are absolute determinations (i.e. no standard is required) we have decided to take S_Δ for naphthalene in benzene as 0.62 which is the average of 0.58 [15] and 0.66 [7]. We have also included, for comparison, measurements of S_Δ (relative to naphthalene) for the sensitisers phenazine and p-methoxyacetophenone in benzene. Since 1-nitronaphthalene has a strong absorption at 355 nm it was not possible to sensitise the triplet state with BP. Therefore the S_Δ value reported has been calculated using a triplet yield (Φ_T) of 0.63 [16]. We observed no significant increase in the singlet oxygen luminescence when an air-equilibrated 1-nitronaphthalene solution was bubbled with oxygen. Thus we are confident that under our conditions the first excited singlet state of 1-nitronaphthalene is not being intercepted by oxygen.

The results obtained, including S_Δ values, oxygen quenching rate constants and half-wave oxidation potentials (E_M^{ox}) are given in table 1. Where available, literature values of the quenching constants have

been included for comparison. A good estimate for the free energy change to form the solvent-separated ion-pair from neutral molecules in benzene solutions, as shown by Rehm and Weller [22] and by ourselves [1,23], is given by

$$\Delta G^{CT} = F[E_M^{ox} - E_{O_2}^{red}] - E_T, \qquad (4)$$

where F is the Faraday constant, $E_{O_2}^{red}$ is the half-wave reduction potential for O_2 (taken to be -0.78 V versus SCE [24]) and E_T is the triplet state energy of the substituted naphthalene. Values of ΔG^{CT} calculated using eq. (4) are listed in table 1 and are likely to be subject to an uncertainty of ± 10 kJ mol^{-1}.

4. Discussion

It is clear from table 1 that there is a strong inverse correlation between S_Δ and k_q^T. Fig. 1 shows a plot of S_Δ versus k_q^T for all the substituted naphthalenes studied. A general trend is immediately apparent; those naphthalenes which have electron-withdrawing groups (e.g. –CN) exhibit relatively high S_Δ values while those with electron-donating groups (e.g. –OCH$_3$) exhibit relatively low S_Δ values. The opposite trend is observed for the k_q^T values. It is important to stress that the observed variations in k_q^T and S_Δ are almost exclusively determined by differences in the electron-donating/withdrawing properties of the substituents since the triplet state energies of the molecules remain essentially constant (with the exception perhaps of 1-nitronaphthalene).

The electron-donating abilities of the substituted naphthalene triplet states are reflected in the ΔG^{CT} values which span a range of ≈ 70 kJ mol^{-1}. Fig. 2 illustrates the variation of S_Δ and k_q^T with ΔG^{CT} and demonstrates the marked effect of CT interactions on the quenching rate and the amount of singlet oxygen produced. Perhaps the most striking illustration of the effect of CT interactions on S_Δ values is given by comparison of the results for 1-methoxynaphthalene and 2-methoxynaphthalene. Theoretical arguments predict that substitution at the 1-position of naphthalene will have the strongest influence on the oxidation potential [25]. This effect is clearly demonstrated by the difference in the published oxidation potentials (see table 1) and by our S_Δ and k_q^T measurements which show an unambiguous sensi-

Table 1
Photophysical properties of substituted naphthalenes in benzene

Sensitiser	S_Δ [a]	k_q^T [b] $(10^9 \, M^{-1} s^{-1})$	E_T [c] $(kJ \, mol^{-1})$	E_M^{ox} [d] $(V \, versus \, SCE)$	ΔG^{CT} [e] $(kJ \, mol^{-1})$
1-methoxynaphthalene	0.34	5.0	250	1.38	−42
acenaphthene	0.40	4.4	248	1.41	−37
2-methoxynaphthalene	0.50	3.5	−	1.52	−28 [j]
1-methylnaphthalene	0.56	2.6	249	1.54	−25
1-ethylnaphthalene	0.57	2.6	−	−	−
2-methylnaphthalene	0.57	2.5	254	1.52	−32
2-ethylnaphthalene	0.59	2.5	−	−	−
naphthalene	0.62	2.1 (2.2 [17])	255	1.63	−22
2-bromonaphthalene	0.66	1.5	252	1.90	+7
1-fluoronaphthalene	0.68	1.9	251	−	−
1-bromonaphthalene	0.73	1.5	247	1.85	+7
1-chloronaphthalene	0.75	1.6	248	−	−
1-cyanonaphthalene	0.75	1.2	241	1.95 [i]	+22
1-nitronaphthalene	0.83 [f]	1.3	231	1.92	+30
benzophenone	0.33	2.5 (2.3 [8])	287	−	−
pMAP	0.25	6.3 (6.0 [8])	300	−	−
phenazine	0.82 [g]	2.0 (2.0 [7])	186 [h]	−	−

[a] Relative to S_Δ (naphthalene) = 0.62, error ± 10%.

[b] Error ± 15% (values in parentheses are literature values).

[c] From ref. [14] unless stated otherwise.

[d] From ref. [18] unless states otherwise.

[e] Calculated using eq. (4).

[f] Calculated using an intersystem crossing yield of 0.63 [16].

[g] Number refers to Φ_Δ and not S_Δ.

[h] From ref. [7].

[i] Calculated from the ionisation potential [19] using an average value obtained from the equations of Pysh and Yang [20] and Neikam et al. [21].

[j] Calculated assuming $E_T = 250 \, kJ \, mol^{-1}$.
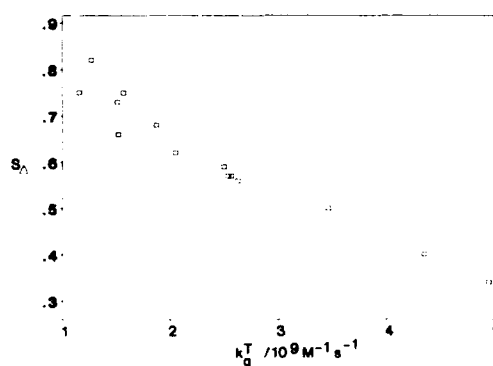
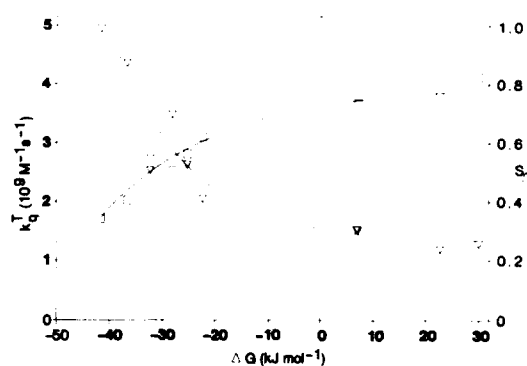Fig. 1. Dependence of S_Δ on k_q^T for substituted naphthalenes in benzene.

Fig. 2. Dependence of k_q^T and S_Δ on ΔG^{CT} for substituted naphthalenes in benzene. Squares refer to S_Δ values.

tivity to the position of the methoxy substituent.

Although the range of our measurements is limited the data in fig. 2 suggest a sigmoidal variation of S_Δ and k_q^T with ΔG^{CT} which is expected because S_Δ and k_q^T will approach limiting values for both positive and negative ΔG^{CT}. At the positive end of the ΔG^{CT} scale both sets of data appear to be approaching limiting values. However, for data on the exoergonic side of the ΔG^{CT} scale there is clear indication that the limits have not been attained.

According to eq. (1) k_q^T should approach a maximum limiting value of $\frac{4}{9}k_d$ (i.e. $\approx 1.3 \times 10^{10}$ M^{-1} s^{-1}) as diffusion becomes rate determining for quenching. For S_Δ, the magnitude of the lower limit is dependent on whether there is any communication between the CT states illustrated in eq. (1). If there is no communication between these states then a limiting value of 0.25 would be expected for S_Δ in the absence of any additional quenching channels.

At the positive end of the ΔG^{CT} scale it is interesting to note that we do not observe an S_Δ value of unity for any of the naphthalenes studied despite the fact that CT interactions for these molecules are energetically unfavourable. This observation implies that quenching via the triplet channel in eq. (1) persists even in the absence of CT interactions. This is most clearly seen in fig. 3 where the net quenching rate constants via the singlet channel ($k_q^1 = S_\Delta(k_q^T)$) and the triplet channel ($k_q^3 = (1 - S_\Delta)k_q^T$) are plotted against ΔG^{CT}. At positive values of ΔG^{CT} where CT interactions are expected to be small k_q^1 exceeds k_q^3 by a factor of three and both rate constants appear to have reached plateau values. However, when ΔG^{CT} is about -42 kJ mol^{-1} the order of the rate constants is reversed and k_q^3 exceeds k_q^1 by almost a factor of two. In the absence of CT-mediated quenching the two quenching rate constants will be controlled by Franck–Condon factors which will inhibit the triplet channel relative to the singlet channel because it is necessary to dissipate more energy non-radiatively via the triplet channel.

It would be interesting to know the maximum limiting values of k_q^1 and k_q^3 since this information may indicate whether communication between the singlet and triplet CT states exists for these molecules. Given the limits of our data we are unable to comment at this stage on the extent of intersystem crossing between the two CT states. In contrast however, Chattopadhyay et al. [8] invoked communication between singlet and triplet quenching channels in order to account for the insensitivity of S_Δ to the nature of the substituent in various aromatic ketones despite large variations in k_q^T. It is abundantly clear from our measurements that the naphthalenes exhibit quite different behaviour compared to that observed for aromatic ketones. We are currently in the process of extending our measurements to include a wider range of naphthalenes (and other aromatic hydrocarbons) in various solvents in order that we may acquire further insight into the role of CT interactions in the quenching of triplet states by oxygen.

5. Conclusions

An inverse correlation between the rate of oxygen quenching and the efficiency of singlet oxygen generation has been demonstrated for the triplet states of a range of substituted naphthalenes in benzene. We believe that this is the first unambiguous confirmation of a relationship between k_q^T and S_Δ. The wide variation in S_Δ and k_q^T values is explained by implicating the participation of CT interactions. This explanation is supported by the dependence of k_q^T and S_Δ on ΔG^{CT}.
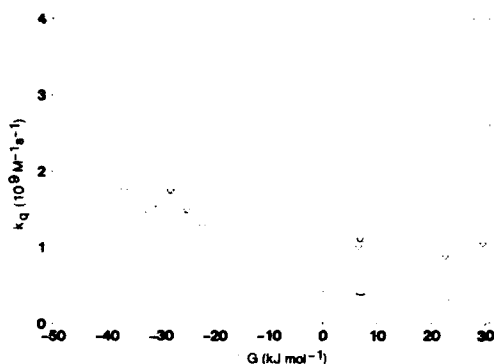
Fig. 3. Dependence of net quenching rate constants (∇) k_q^1 and ($\square$) k_q^3 (see text) on ΔG^{CT} for substituted naphthalenes in benzene.

References

[1] A. Garner and F. Wilkinson, Chem. Phys. Letters 45 (1977) 432.

[2] A. Garner and F. Wilkinson, in: Singlet oxygen, reactions with organic compounds and polymers, eds. B. Ranby and J.F. Rabek (Wiley, New York, 1976) p. 48.

[3] J. Saltiel and B.W. Atwater, Advan. Photochem. 14 (1988) 1.

[4] A.A. Gorman and M.A.J. Rodgers, in: Handbook of organic photochemistry, Vol. 2, ed. J.C. Scaiano (CRC Press, Boca Raton, 1989) p. 229.

[5] F. Wilkinson, W.P. Helman and A.B. Ross, J. Phys. Chem. Ref. Data, to be published.

[6] O.L.J. Gijzeman, F. Kaufman and G. Porter, J. Chem. Soc. Faraday Trans. II 69 (1973) 708.

[7] R.W. Redmond and S.E. Braslavsky, Chem. Phys. Letters 148 (1988) 523.

[8] S.K. Chattopadhyay, C.V. Kumar and P.K. Das, J. Photochem. 30 (1985) 81.

[9] A.P. Darmanyan and C.S. Foote, J. Phys. Chem. 96 (1992) 3723.

[10] A.A. Gorman, I. Hamblett, C. Lambert, A.L. Prescott, M.A.J. Rodgers and H.M. Spence, J. Am. Chem. Soc. 109 (1987) 3091.

[11] M. Kristiansen, R.D. Scurlock, K.-K. Iu and P.R. Ogilby, J. Phys. Chem. 95 (1991) 5190.

[12] A.J. McLean and T.G. Truscott, J. Chem. Soc. Faraday Trans. 86 (1990) 2671.

[13] A.J. McLean and M.A.J. Rodgers, J. Am. Chem. Soc. 114 (1992) 3145.

[14] S.L. Murov, Handbook of photochemistry (Marcel Dekker, New York, 1973).

[15] A.A. Gorman, A.A. Krasnovsky and M.A.J. Rodgers, J. Phys. Chem. 95 (1991) 598.

[16] R. Hurley and A.C. Testa, J. Am. Chem. Soc. 90 (1968) 1949.

[17] G.J. Smith, J. Chem. Soc. Faraday Trans. II 78 (1982) 769.

[18] C.K. Mann and K.K. Barnes, Electrochemical reactions in nonaqueous systems (Marcel Dekker, New York, 1970).

[19] C. Utsunomiya, T. Kobayashi and S. Nagakura, Bull. Chem. Soc. Japan 48 (1975) 1852.

[20] E.S. Pysh and N.C. Yang, J. Am. Chem. Soc. 85 (1963) 2124.

[21] W.C. Neikam, G.R. Dimeler and M.M. Desmond, J. Electrochem. Soc. 111 (1964) 1190.

[22] D. Rehm and A. Weller, Israel J. Chem. 8 (1970) 259.

[23] F. Wilkinson and C. Tsiamis, J. Am. Chem. Soc. 105 (1983) 767.

[24] G.J. Kavarnos and N.J. Turro, Chem. Rev. 86 (1986) 401.

[25] A. Zweig, A.H. Maurer and B.G. Roberts, J. Org. Chem. 32 (1967) 1322.

The application of diffuse reflectance laser photolysis to study photochemistry at interfaces and in dyed fabrics

F WILKINSON*, D J McGARVEY and D R WORRALL

Department of Chemistry, Loughborough University of Technology, Loughborough, Leicestershire, LE11 3TU, England

Abstract. Recently we have extended to heterogeneous, opaque and often highly scattering systems, the application of flash photolysis by using diffuse reflected light instead of transmitted light as the analysing source on timescales extending from several seconds to picoseconds. Laser-induced transient spectra and decay kinetics have been observed from a wide variety of samples including fractions of monolayers of organic molecules adsorbed on catalytic metal oxide surfaces, within inorganic and organic microcrystals, from dyed fabrics and from paper pulp. The potential of the technique to study photochemical reactions at interfaces is demonstrated with particular reference to ion-electron recombination on porous silica surfaces and to photochemical and photophysical processes occurring in dyed fabrics.

Keywords. Diffuse reflectance; laser photolysis; photochemistry: reaction at interfaces; reaction in dyed fabric.

1. Introduction

The technique of flash photolysis has been extensively applied to study rapid homogeneous reactions in the gas phase and in dilute fluid and rigid solutions (Porter and West 1974). Kessler and Wilkinson (1981) demonstrated that the technique can be extended to opaque samples by monitoring changes in the diffuse reflected light from an analysing source following pulsed photo-excitation. In 1984 we reported the first successful diffuse reflectance pulsed radiolysis experiments (Wilkinson *et al* 1984) and more recently (Wilkinson *et al* 1986a) we have demonstrated that diffuse reflectance picosecond laser flash photolysis studies are possible using mode-locked picosecond lasers and pump-probe methods. Photoinduced transient spectra and decay kinetics have already been observed from a wide variety of opaque samples including fractions of monolayers of organic molecules adsorbed on catalytic metal oxide surfaces (Oelkrug *et al* 1988, 1989) and included within zeolites (Kelly *et al* 1990), from semiconductor powders (Wilkinson *et al* 1986b) and doped and undoped porous electrodes (Kossanyi *et al* 1990), from ruthenium(II) complexes within ion exchange resins (Masschelein *et al* 1991), from organic microcrystals (Wilkinson and Willsher 1984), and from organic dyes adsorbed on microcrystalline cellulose (Wilkinson *et al* 1991b, 1992), on fabrics and chemically bound to polymers

---

*For correspondence

(Bourdelande *et al* 1988; Wilkinson *et al* 1990), from paper pulp (Schmidt *et al* 1990) and from photographic emulsions (Wilkinson and Leicester, to be published). Other groups are now increasingly using this method to study the mechanisms of light-induced reactions in heterogeneous environments (Turro *et al* 1986; Ikeda *et al* 1988; Draper and Fox 1990; Levin *et al* 1990).

2. Experimental

The equipment used for laser flash photolysis in diffuse reflectance mode is identical to that used for studies in transmission mode except for the geometry for collecting the analysing light which is diffusely reflected from the excited sample. Full experimental details and more extensive discussions of the analysis of data are given elsewhere (Wilkinson 1986; Oelkrug *et al* 1987). Following the Kubelka–Munk treatment (Kubelka 1948) for diffuse reflectance, two light fluxes are considered travelling in opposite directions perpendicular to the irradiated surface at $x = 0$. The attenuation of the incident flux I depends on the absorption and scattering coefficients K and S respectively and is given by:

$$dI(x) = -I(x)(K + S)dx + J(x)Sdx, \tag{1}$$

and the generated flux, since it passes in the opposite direction, has:

$$dJ(x) = J(x)(K + S)dx - I(x)Sdx. \tag{2}$$

The diffuse reflectance R is given by $R = J_0/I_0$, where I_0 and J_0 are the incident and reflected fluxes at the surface. Equations (1) and (2) can be solved for a layer so thick that any further increase in thickness does not affect R and provided K and S are independent of x this gives:

$$(1 - R)^2/2R = K/S = F(R). \tag{3}$$

The remission function, $F(R)$, is linearly dependent on the number of absorbing chromophores in any sample when S and K are independent of the penetration depth below the surface.

In diffuse reflectance flash photolysis the initially excited chromophores are usually homogeneously distributed. However, photo-excitation produces transient or permanent changes in absorption, preferentially just below the irradiated surface. Theoretical treatments show that there are two limiting types of concentration profile produced, namely an exponential fall-off as a function of penetration depth and a homogeneous (or "plug") profile. The latter case is encountered with large laser fluencies and with low concentrations of ground state absorbers, where there is total conversion from ground state to transient to a certain depth below the irradiated surface. Since a homogeneous concentration of absorbers exists, the Kubelka–Munk theory can be applied. For optically thick samples at analysing wavelengths where only the transient absorbs, the remission function given by (3) is a linear function of the concentration and can be used for kinetic analysis and for plotting absorption spectra. For low percentage conversions the concentration of transients decreases exponentially below the irradiated surface. An analytical solution for the change in
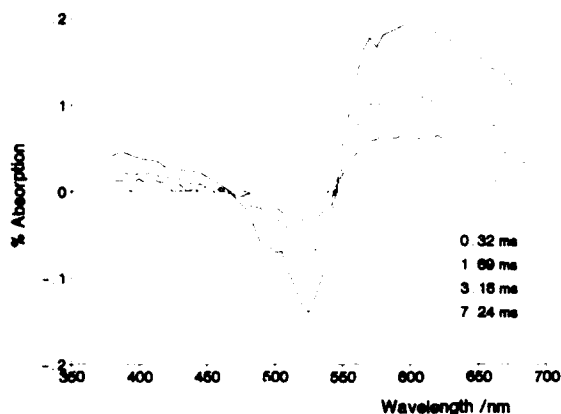
Figure 1. Time-resolved transient difference spectra obtained following diffuse reflectance laser flash photolysis of eosin adsorbed on cotton fabric.

reflectance expected has been obtained by Lin and Kan (1970) and is in the form of a converging series. ΔR, the observable in-diffuse reflectance laser flash photolysis is defined as follows:

$$\Delta R(t) = [R_b - R(t)]/R_b, \tag{4}$$

where R_b and $R(t)$ are the reflectance before and at time t after exposure to laser excitation. For low percentage conversions, the parameter ΔR has been shown to be a linear function of concentration of the transient provided $\Delta R < 0.1$ (Oelkrug *et al* 1987). Often 100 ΔR is referred to as the percentage absorption by the laser induced transient. Full experimental details are given elsewhere (Wilkinson and Kelly 1990).

As in all flash-photolysis experiments one obtains transient difference spectra and decreases in absorption are often observed at wavelengths where the ground state has a stronger absorption coefficient than the transient. Figure 1 gives an example, which shows excellent isosbestic points, obtained by laser excitation at 532 nm of eosin adsorbed on cotton fabric.

If the absorption coefficient K is in excess of $10^4 \, \text{cm}^{-1}$ at the laser excitation wavelength, then the penetration depth is only about 1 μm and dissipation of laser excitation as heat causes considerable temperature rises (Wilkinson *et al* 1986b). This possibility has always to be borne in mind and lower laser fluences, lower concentrations or excitation into weaker bands must be employed to avoid thermal effects on some samples.

3. Results and discussion

3.1 *Radical cation-electron recombination*

Adsorbed radical cations have been detected by the method of diffuse reflectance laser flash photolysis using polycrystalline microporous catalytic metal oxides such as silica and alumina as adsorbents (Oelkrug *et al* 1988). We have studied several diphenylpolyenes adsorbed on alumina. Typical transient absorption spectra obtained
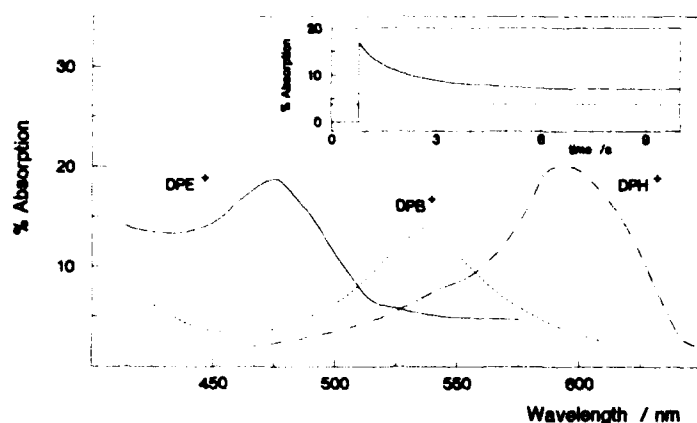
Figure 2. Transient absorption spectra from radical cations on alumina (DPE, DPB and DPH represent diphenyl-ethene,-butadiene and -hexatriene, respectively).

for 1,2-diphenylethene (DPE), 1,4-diphenylbutadiene (DPB) and 1,6-diphenyl-1,3,5-hexatriene (DPH) adsorbed on alumina recorded 1 ms after excitation are shown in figure 2. These transients are long-lived and decay non-exponentially with the first half-life considerably shorter than the second half-life and so on. In the case of DPH on alumina, we also observed (Oelkrug *et al* 1988) a much shorter-lived transient which we have assigned to the adsorbed triplet state of DPH. There is strong evidence that the long-lived transients in DPE, DPB and DPH are radical cations. Thus for DPE adsorbed on Al_2O_3/SiO_2 the radical cation is known to have its stronger absorption band at 480 nm, while for DPB and DPH adsorbed on this catalyst the strongest ground-state absorption bands of the radical cations occur at 542 and 602 nm respectively (Kortu and Schlichenmaier 1966). In solution a short-lived transient ($\tau < 100$ ns, $\lambda_{max} = 478$ nm) is reported after flashing charge-transfer complexes of DPE in the presence of an electron-acceptor such as fumaronitrile (Goodman and Peters 1985). This transient is assigned as the radical cation. We have proved this assignment by measuring the ESR spectra of these adsorbed radical cations at low temperatures (Oelkrug *et al* 1991).

From studies of the dependence of the amounts of radical produced as a function of laser intensity coupled with the computer modelling of the transient concentration profile it is possible to show that the production of the radical cation is a multiphoton process (Oelkrug *et al* 1991) probably involving the consecutive absorption of two photons.

The decay of these transients has been shown to be very dependent on the temperature, on the nature of the adsorbent and on its pre-treatment. Repetitive excitation at room temperature of the same sample area at intervals of a few minutes demonstrates that the intensity of absorption and the decay kinetics of the radical cation are reproducible. Thus the radical cations decay almost exclusively to give back that original molecule. Thus the complex decay is due to radical cation-electron recombination. Variation in surface coverage of adsorbates gives only very small difference in the kinetics observed. This suggests that the process of ionization leaves the radical cation and the electron separated by a small distance (smaller than the nearest distance between adsorbates) and that geminate pair recombination is the

decay mechanism. The decays fit quite well the expression,

$$C_0/C = 1 + \alpha t^{\frac{1}{2}},$$

where C_0 and C represent the concentrations of the radical cations formed initially and remaining after time t. The values of α are strongly dependent on temperature, adsorbent and on the adsorbate (Oelkrug *et al* 1991).

3.2 Triplet–triplet energy transfer

Triplet–triplet energy transfer has been studied between benzophenone and an oxazine dye (2,7-*bis*(diethyl-amino)-phenazonium chloride) co-adsorbed on the surface of microcrystalline cellulose (Wilkinson *et al* 1991b). Ground-state absorption and fluorescence measurements provide evidence for dimer formation of the oxazine dye when adsorbed on cellulose, in contrast to the behaviour in ethanol solution where no dimerisation occurs. The efficiency of energy transfer from triplet benzophenone was studied using both time-resolved absorption and phosphorescence intensity measurements, lifetime measurements indicating that the energy transfer process involves static quenching.

From the sensitised transient difference spectrum (figure 3) of the oxazine dye it has been possible to evaluate the triplet state extinction coefficient relative to that of triplet benzophenone. The ratio of extinction coefficients is found to be identical to that determined in acetonitrile solution (Wilkinson *et al* 1991a).

3.3 Dyed fabrics

It is very important to be able to understand the photochemical and photophysical behaviour of the compounds employed to colour natural and synthetic fibres, especially from a commercial point of view. Although it has been possible to obtain useful information from ground state reflectance spectroscopy and luminescence studies of a dyed fabric, a flash photolysis investigation of the photophysical properties has not been possible hitherto. It was thus necessary to undertake model studies of the dye in solution, simply because transmission flash photolysis cannot be applied to a piece of cloth. The data obtained from model studies had then to be extrapolated
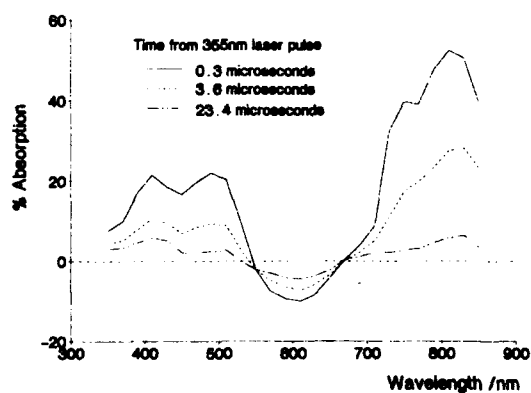

Figure 3. Time-resolved transient difference spectra from 1.8×10^{-4} mol g^{-1} of benzophenone and 2×10^{-5} mol g^{-1} of oxazine coadsorbed on microcrystalline cellulose.

to the environment of a woven fabric, which is quite different from a fluid solution. It is clearly more satisfactory to be able to apply flash photolysis directly to a dyed fabric, and this is now possible using diffuse reflectance laser photolysis. In this section, some results obtained from cotton fabric dyed with phthalocyanine and fluorescein derivatives will be discussed.

3.3a *Cotton fabric dyed with sulphonated aluminium(II) phthalocyanine*: Non-fluorescent woven cotton fabric dyed with sulphonated aluminium phthalocyanine shows both transient absorption and ground state depletion following excitation at 354 nm (intensity = 15 mJ per pulse) (Wilkinson and Willsher 1985). The spectral band observed with λ_{max} around 500 nm indicated that the transient absorption arose from the lowest triplet state. In addition, ground-state depletion is observed around 650 nm. The decay of the absorption follows a first-order rate law in a water-free fabric with $\tau \sim 0.75$ ms, in the presence or absence of oxygen. Quenching by oxygen occurs only if the fabric is water saturated, and even then the overall quenching process is inefficient, since the decay of the absorption cannot be fitted as a pseudo-first-order process. A similar effect is observed if other potential quenchers are present in the fabric. It must be concluded that the rate of diffusion of molecules through the fibres is very much slower than in solution; this is an important factor in determining the rate of reactions which may occur in the fabric between the dye and other molecules such as fluorescent brightening agents or detergents.

3.3b *Cotton fabric dyed with halogenated fluorescein dyes*: The triplet–triplet (T–T) absorption of halogenated fluorescein dyes (eosin, erythrosin and rose bengal) contained in cotton fabric can be readily detected following excitation at either 354 or 532 nm. Figure 1 shows the transient difference spectrum for eosin on non-fluorescent cotton cloth. The positive part of the spectrum from 550 to 680 nm corresponds to absorption from the first triplet state of the dye, while the negative portion represents depletion of the ground state. The decay of the T–T absorption follows a mixed first- and second-order process. Similar spectral and kinetic behaviour is found for rose bengal (Wilkinson *et al* 1985) and erythrosin dyed into cotton. As in the case of sulphonated aluminium phthalocyanine on cotton, water is necessary to observe partial quenching by oxygen of the triplet state of the fluorescein dyes. In the laser-induced emission spectrum of rose bengal in cotton fabric phosphorescence of the dye at 765 nm can be observed since this has the same decay parameters as the T–T absorption (Wilkinson *et al* 1985). A smaller feature at 650 nm disappears more rapidly than the phosphorescence, and occurs at wavelengths where fluorescence from rose bengal would be expected. Its lifetime is too long for this feature to be prompt fluorescence, and it is more likely to be delayed fluorescence which results from T–T annihilation. This process would account for the fact that the early part of the T–T absorption decay is dominated by a second-order process. It is interesting to note that for rose bengal adsorbed onto different substrates the relative sizes of the emission signals at 650 and 765 nm vary. When adsorbed on nylon or polyacryl-amide the emission spectrum is similar to that on cotton fabric but the majority of the decay of the T–T absorption obeys a first-order rate law. With polystyrene as the substrate the delayed fluorescence at 650 nm predominates and virtually no phosphorescence is detected. For this sample the T–T absorption is much shorter lived and decays almost entirely by a second-order rate law. It seems that polystyrene

is a substrate which allows intermolecular T–T energy transfer to take place more readily than the other adsorbents.

Acknowledgements

References

Bourdelande J L, Campa C, Camps J, Font J, de March P, Wilkinson F and Willsher C J 1988 *J. Photochem. Photobiol.* **44** 51

Draper R B and Fox M A 1990 *J. Phys. Chem.* **94** 4628

Goodman J L and Peters K S 1985 *J. Am. Chem. Soc.* **107** 1441

Ikeda N, Kashioku M, Masuhara H and Yoshihara K 1988 *Chem. Phys. Lett.* **150** 452

Kelly G P. Wilkinson F, Willsher C J, Ferreira J C N-, Olea A, Weir D, Johnston L J and Scaiano J C 1990 *Can. J. Chem.* **68** 812

Kessler R W and Wilkinson F 1981 *J. Chem. Soc., Faraday Trans. 1* **77** 309

Kortu G and Schlichenmaier V Z 1966 *Phys. Chem. (Neue Folge)* **48** 267

Kossanyi J, Kouyate D, Pouliquen J, Ronfard-Haret J C, Valet P, Oelkrug D, Mammel U, Kelly G P and Wilkinson F 1990 *J. Luminescence* **46** 17

Kubelka P 1948 *J. Opt. Soc. Am.* **38** 448

Levin P P, Ferreira L F V and Costa S M B 1990 *Chem. Phys. Lett.* **173** 277

Lin T and Kan H K A 1970 *J. Opt. Soc. Am.* **60** 1252

Masschelein A, Mesmaeker A K, Willsher C J and Wilkinson F 1991 *J. Chem. Soc.. Faraday Trans.* **87** 259

Oelkrug D, Honnen W, Wilkinson F and Willsher C J 1987 *J. Chem. Soc., Faraday Trans. II* **83** 2081

Oelkrug D, Krabichler G, Honnen W, Wilkinson F and Willsher C J 1988 *J. Phys. Chem.* **92** 3589

Oelkrug D, Reich S, Wilkinson F and Leicester P A 1991 *J. Phys. Chem.* **95** 269

Oelkrug D, Uhl S, Wilkinson F and Willsher C J 1989 *J. Phys. Chem.* **93** 4551

Porter G and West M A 1974 In *Techniques of organic chemistry* (ed.) A Weisberger (New York: Wiley-Interscience) chap. 10

Schmidt J A, Heitner C, Kelly G P and Wilkinson F 1990 *J. Pulp Paper Sci.* **19** 11

Turro N J, Zimmitt M B, Gould I R and Mahler W 1986 *J. Am. Chem. Soc.* **107** 5826

Wilkinson F 1986 *J. Chem. Soc., Faraday Trans. II* **82** 2073

Wilkinson F and Kelley G P 1990 In *Handbook of organic photochemistry* (ed.) J C Scaiano (Boca Raton, FL: CRC Press) vol. 1, chap. 12

Wilkinson F, Kelly G P, Ferreira L F V, Freire V M M R and Ferreira M I 1991a *J. Chem. Soc., Faraday Trans. II* **87** 547

Wilkinson F, Kelly G P and Mollah M 1990 *J. Textile Inst.* **81** 91

Wilkinson F, Leicester P A, Ferreira L F V and Freire V M M R 1991b *Photochem. Photobiol.* **54** 599

Wilkinson F and Willsher C J 1984 *Appl. Spectrosc.* **38** 897

Wilkinson F and Wilisher C J 1985 *J. Chem. Soc., Chem. Commun.* 142

Wilkinson F, Willsher C J, Leicester P A, Barr J R M and Smith M J C 1986a *J. Chem. Soc., Chem. Commun.* 1216

Wilkinson F, Willsher C J and Pritchard R B 1985 *Eur. Polym. J.* **21** 333

Wilkinson F, Willsher C J, Uhl S, Honnen W and Oelkrug D 1986b *J. Photochem.* **33** 273

Wilkinson F, Willsher C J, Warwick P, Land E J and Rushton F A P 1984 *Nature (London)* **311** 40

Wilkinson F, Worrall D R and Ferreira L F V 1992 *Spectrochim. Acta* **A48** 135

Photochemistry on surfaces: fluorescence emission of monomers and dimers and triplet state absorption of acridine orange adsorbed on microcrystalline cellulose

F. Wilkinson* and D. R. Worrall

Department of Chemistry, Loughborough University of Technology, Loughborough,
Leicestershire LE11 3TU, U.K.

and

L. F. Vieira Ferreira

Centro de Química Física Molecular, Universidade Técnica de Lisboa, Complexo 1,
Instituto Superior Tecnico, Av. Rovisco Pais, 1096 Lisboa Codex, Portugal

Abstract—Prompt fluorescence as well as delayed fluorescence emission of acridine orange was detected at room temperature from samples where this dye is adsorbed on microcrystalline cellulose. Ground state absorption studies provided evidence for dimer formation of the dye when adsorbed on cellulose, and the equilibrium constant for dimerisation was determined as $1.6 \pm 0.1 \times 10^6 \, mol^{-1} \, g$. At low loadings of acridine orange on cellulose ($<1 \, \mu mol \, g^{-1}$) the fluorescence emission is mainly due to the monomer and is similar to that observed in ethanolic solutions where little aggregation occurs, and peaks at 530 nm. A linear dependence of the fluorescence intensity on the amount of light absorbed by the dye was established for these "diluted" samples. However, at higher loadings ($>20 \, \mu mol \, g^{-1}$), the fluorescence intensity decreases, and the emission is broad with its maximum at 620 nm, and is mainly due to the dimer. By assuming that the excited monomer and dimer of acridine orange are the only emitting species, it was possible to determine the fluorescence quantum yields for these two species when adsorbed on microcrystalline cellulose as 0.95 ± 0.05 and 0.40 ± 0.10, respectively. Pulsed emission studies at room temperature in the millisecond time-range also revealed monomer and dimer emissions on this longer time-scale. These are shown to be due to thermally activated delayed fluorescence arising from the triplet states of monomer and dimer acridine orange as confirmed by diffuse reflectance transient absorption studies.

1. Introduction

The study of elementary reactions of dyes on surfaces has recently raised considerable interest due to the very wide chemical applications of such systems. Fluorescence emission studies in front surface geometry and laser flash photolysis in the diffuse reflectance mode are convenient techniques for the study of dyes adsorbed on the surfaces of powdered solid samples. We have published recently several studies describing the behaviour of dyes and other organic and inorganic compounds on a wide variety of substrates (see [1–8] and references therein).

Acridine dyes are cationic dyes that have received considerable interest, not only to enhance understanding of photophysical and photochemical properties [9–13] but also from the point of view of their application as compounds of biological interest [14, 15], as sensitisers in reactions for use in harvesting solar energy by photolysing water [16] and also as laser dyes [17]. Despite the fact that the technological applications are usually in heterogeneous systems, these studies were all performed in homogeneous or micellar solutions.

We present here a study of acridine orange (AO) adsorbed on microcrystalline cellulose using fluorescence emission and flash photolysis as probes for the interaction between the supporting material and this photoactive molecule. Ground state absorption spectra were recorded using diffuse reflectance spectroscopy and these proved invaluable for interpreting the fluorescence signals. In addition, transient diffuse reflectance

---

* Author to whom correspondence should be addressed.
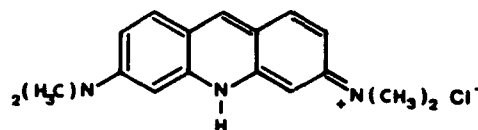
Acridine Orange

Scheme 1. Structure of acridine orange (AO).

techniques were also used to gather information about the organisation and mobility of dye molecules bound to the surface.

2. EXPERIMENTAL

2.1. Materials and sample preparation

Acridine orange (Fluka for microscopy) was purified by recrystallisation in dimethylformamide and its purity checked using UV–vis spectroscopy, as well as by using chromatographic methods. Ethanol (Romil Chemicals, HPLC grade) was used as supplied. Microcrystalline cellulose (Aldrich, 20 μm average particle size) was used as the solid substrate. Sample preparation has been described in detail in a previous publication [1].

2.2. Ground state absorption, steady state fluorescence emission and time-resolved diffuse reflectance emission and absorption equipment

Ground state absorption spectra of acridine orange adsorbed on microcrystalline cellulose were obtained using a Phillips PU8800 UV–vis spectrophotometer with a diffuse reflectance attachment (120 mm diameter integrating sphere). The calibration of the system and data treatment are described in a previous publication [5]. Corrected steady state fluorescence and excitation spectra were obtained by using a home-made fluorimeter described in detail elsewhere [3].

Time-resolved diffuse reflectance laser flash photolysis experiments were carried out by exciting acridine orange at 532 nm in a quartz cell. The laser was a HY hyper YAG 200 from Lumonics, the output from which was frequency doubled to give a 88 mJ pulse with 8 ns width. A 250 W Xenon lamp was used as monitoring source, and a R928 Hamamatsu photomultiplier, sensitive up to 900 nm, was used as a detector. For transient emission and transient absorption, data were acquired into a Tektronix 7612 D transient digitizer interfaced to a microcomputer. Further details of this system and data treatment can be found elsewhere [6, 7].

All these experiments, unless otherwise stated, were performed at room temperature (20 ± 1°C).

3. RESULTS AND DISCUSSIONS

3.1. Ground state absorption spectra of acridine orange adsorbed on cellulose

The absorption spectra of the ground state of AO adsorbed on cellulose at various loadings are shown in Fig. 1a and b. Concentrations are quoted as moles of AO per gram of microcrystalline cellulose. At very low loadings the spectra are similar to those measured using transmission geometry in ethanolic solution [18] apart from the fact that AO adsorbed on cellulose exhibits a ≈10 nm bathochromic shift. Increased loadings of AO adsorbed on microcrystalline cellulose give rise to a new absorption band that peaks at 475 nm, which we assigned to the dimer formed by ground state association. The reasons for this assignment are as follows: if C_0 is the total concentration of dye (mol g^{-1}), and C_M and C_D the monomer and dimer concentrations, respectively, then the remission function $F(R)_{dye}$ can be given in terms of C_0 and C_M as

$$F(R)_{dye} = [C_M(2\varepsilon_M - \varepsilon_D) + \varepsilon_D C_0]/S \qquad (1)$$

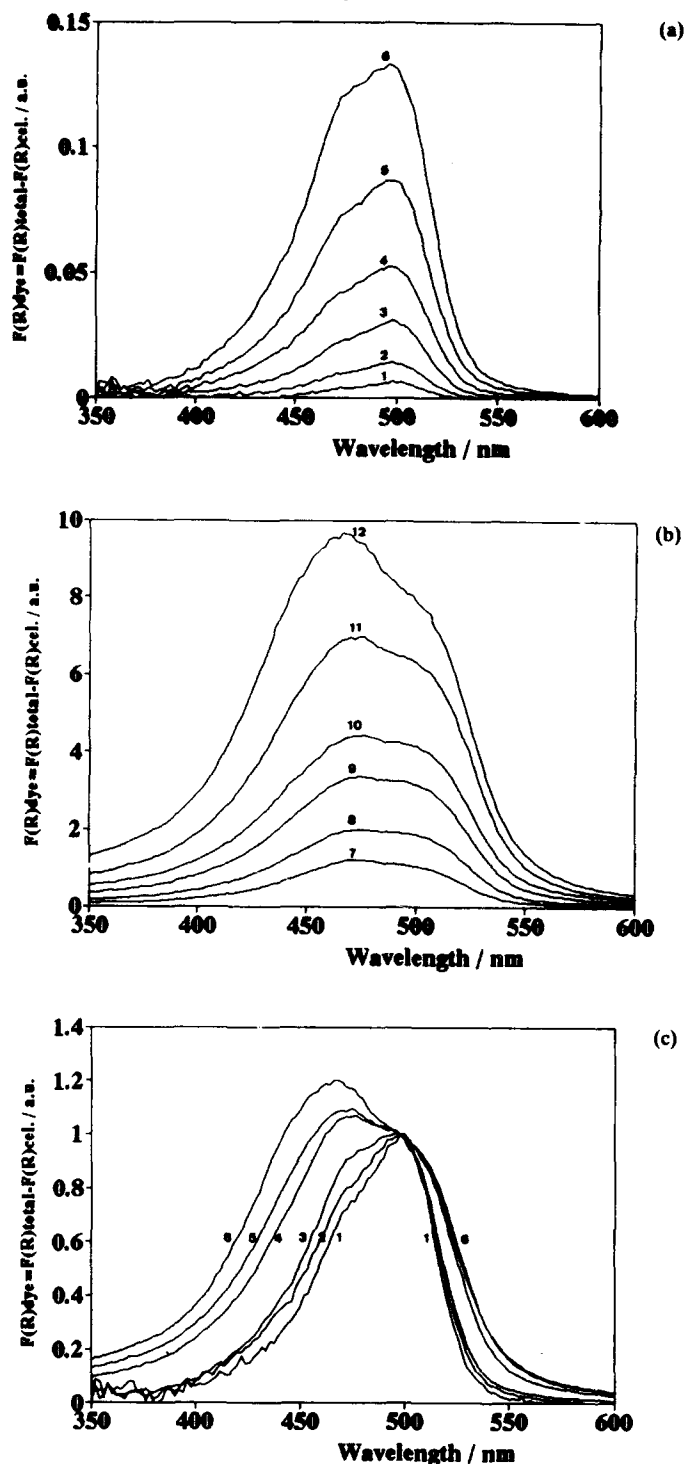Fig. 1. (a) Remission function values for acridine orange adsorbed on microcrystalline cellulose for (1) 5×10^{-8}, (2) 1×10^{-7}, (3) 2.5×10^{-7}, (4) 5×10^{-7}, (5) 1×10^{-6}, (6) 5×10^{-6} moles of dye per gram of the substrate. (b) Remission function values for acridine orange adsorbed on microcrystalline cellulose. The concentrations are (7) 1×10^{-6}, (8) 1.5×10^{-5}, (9) 2×10^{-5}, (10) 3×10^{-5}, (11) 4×10^{-5}, (12) 1×10^{-4} moles of dye per gram of the substrate. (c) Data from (a) and (b) normalised to the maximum value of the remission function for the monomer. The concentrations are (1) 2.5×10^{-7}, (2) 5×10^{-7}, (3) 1.5×10^{-6}, (4) 2.5×10^{-5}, (5) 8×10^{-5}, (6) 1×10^{-4} moles of dye per gram of the substrate.
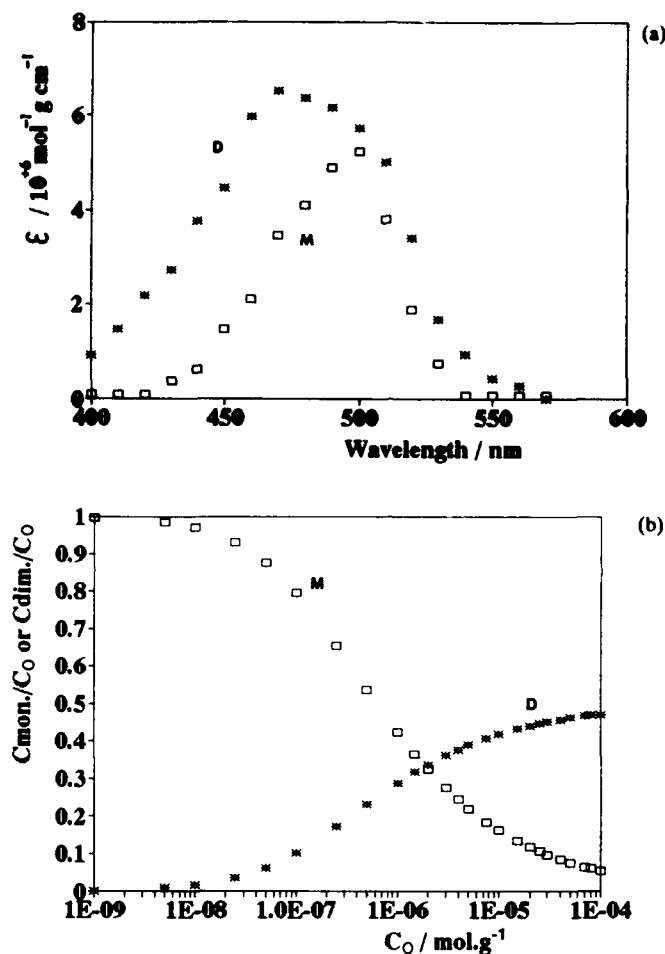
Fig. 2. (a) Ground state absorption spectra for the monomer (M) and dimer (D) of acridine orange adsorbed on microcrystalline cellulose. (b) Ground state monomer (M) and dimer (D) concentrations of acridine orange adsorbed on microcrystalline cellulose plotted as a function of the total concentration C_0.

with

$$C_M = \left(\frac{C_0}{2K_D} + \frac{1}{16K_D^2}\right)^{1/2} - \frac{1}{4K_D}, \tag{2}$$

where K_D is the equilibrium constant for the monomer–dimer equilibrium ($K_D = C_D/C_M^2$ and $C_0 = C_M + 2C_D$), and S is the scattering coefficient of the substrate ($S = 80\ \mathrm{cm}^{-1}$ for microcrystalline cellulose). Equations (1) and (2) were fitted, using a modified sequential simplex optimisation routine [19], to the experimentally determined $F(R)_{dye}$ values as a function of C_0, where $F(R)_{dye}$ are defined as

$$F(R)_{dye} = F(R)_{total} - F(R)_{cellulose}, \tag{3}$$

whereas the equivalent equations for the trimer or tetramer which will be presented in a future publication [20] did not fit the experimental data, giving no evidence for the formation of aggregated species bigger than the dimer. Monomer and dimer ground state absorption spectra are presented in Fig. 2a. The monomer spectrum was experimentally determined at low loadings and the dimer spectrum by fitting of Eqns (1) and (2) to the

experimental data at concentrations ranging from 1 nmol to high loadings (10^{-4} mol) of acridine orange per gram of cellulose. Now using these two spectra, Eqns (1) and (2) and $K_D = 1.6 \times 10^6$ mol^{-1} g it was possible to calculate $F(R)_{dye}$ curves which can be superimposed on experimental data within experimental error in the whole range of concentrations under study.

Figure 2b shows how C_M and C_D vary for the samples under study. In this figure C_M/C_0 and C_D/C_0 are plotted as a function of C_0 showing the ranges where monomer or dimer are the predominant ground state species.

3.2. Fluorescence emission studies

Corrected fluorescence spectra of acridine orange adsorbed on cellulose at various loadings are shown in Fig. 3a and b. At low loadings (from 1×10^{-9} to 1×10^{-6} mol g^{-1}) the intensity of fluorescence I_F shows a linear dependence on the amount of light absorbed by the dye (Fig. 4). This behaviour is expected if we consider that the intensity of the fluorescence emission depends on the amount of light absorbed by the sample, i.e. $I_0^e (1 - R^e)$ where I_0^e is the intensity of the exciting light at the excitation wavelength, and $(1 - R^e)$ is the fraction of the exciting light which is absorbed by both dye and substrate. Since the concentration of the sample C_0, the reflectivity of the sample R and the reflectivity of the background R_b are related by the Kubelka–Munk equation for optically thick samples [21, 22], we may write for this exciting wavelength

$$\frac{(1 - R^e)^2}{2R^e} - \frac{(1 - R_b^e)^2}{2R_b^e} = \frac{2\varepsilon C_0}{S}. \tag{4}$$

An analysis of the I_F dependence on concentration has to consider a wide range of values for C_0 and also include the dependence on the fraction of light absorbed only by the dye in the form of monomer alone or monomer and aggregated forms. These fractions may be determined by the use of ground state diffuse reflectance measurements. The absorption of the substrate at the excitation wavelength has to be taken into account since those photons will not be useful in dye excitation.

Considering all these facts we have to apply Eqn (5):

$$I_F = C\Phi_F I_0^e (1 - R^e)\{\Phi_M F(R^e)_M / F(R^e)_{total} + \sum_i \Phi_{Ai} F(R^e)_{Ai} / F(R^e)_{total}\}, \tag{5}$$

where Φ_M and Φ_{Ai} are the fluorescence quantum yield of the adsorbed monomer or aggregated form of acridine orange, C is a constant which depends on the apparatus geometry, $F(R^e)_{total}$ is the total remission function and $F(R^e)_M$ and $F(R^e)_{Ai}$ are the remission function for the dye in the form of monomer or aggregated forms all measured at the excitation wavelength e.

Obviously Eqn (5) may be written in the form of

$$I_F = C \Phi_F I_0^e (1 - R^e)\{\Phi_M f_M + \Phi_D f_D\} \tag{6}$$

when monomers and dimers are the only fluorescent species, where f_M and f_D are the fraction of the incident light absorbed by the monomer and dimer, respectively. ($f_M = F(R^e)_M / F(R^e)_{total}$ and $f_D = F(R^e)_D / F(R^e)_{total}$.)

The spectra shown in Fig. 3a and b give good evidence for the existence of two emitting species. At low loadings of acridine orange adsorbed on cellulose the emission we see is essentially the fluorescence of the monomer, this being reduced at higher energies by self-absorption due to the overlap of the fluorescence and absorption spectra of the dye. However, the emission spectra shown in Fig. 3b for high loadings of acridine orange (>50 μmol g^{-1}) clearly show dimer emission with a maximum at 620 nm. Figure 3c shows a normalisation of some of the spectra presented in Fig. 3a and b, establishing
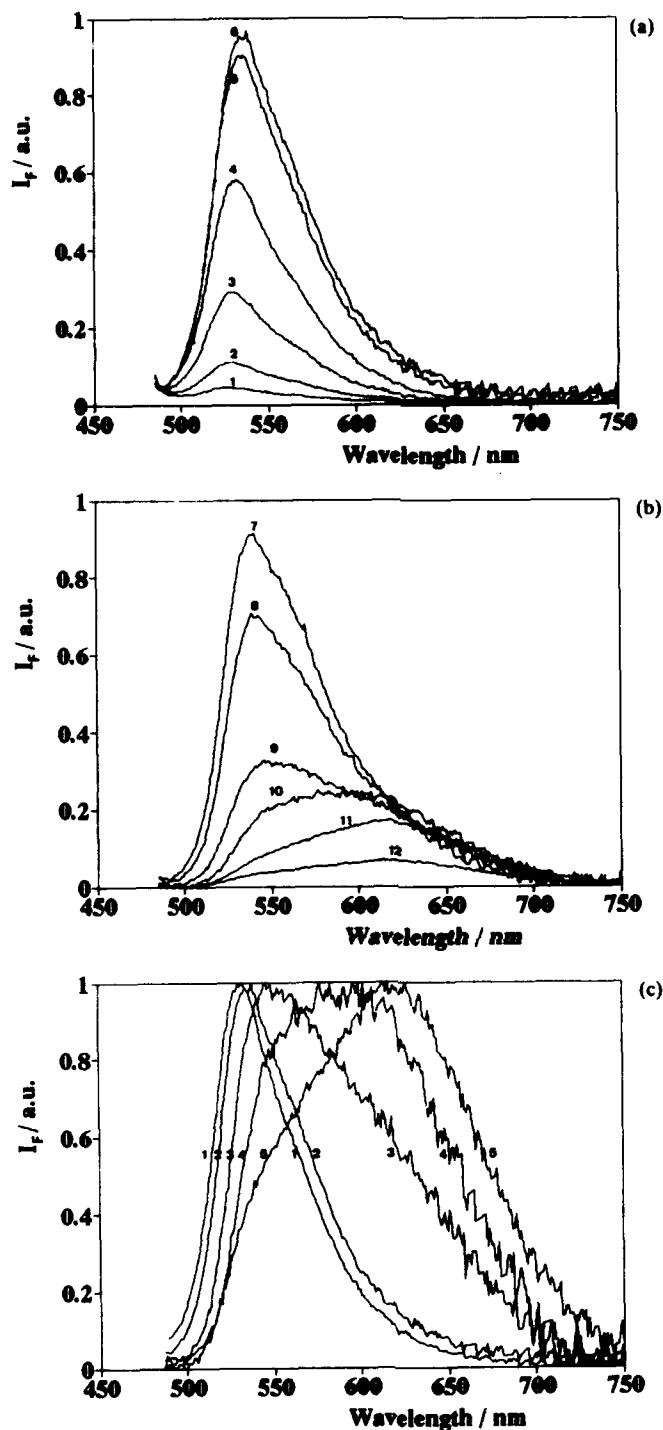
Fig. 3. (a) Corrected fluorescence emission spectra of acridine orange adsorbed on cellulose excited at 475 nm. The concentration of the dye is: curve (1) 1×10^{-8}, (2) 5×10^{-8}, (3) 1×10^{-7}, (4) 2.5×10^{-7}, (5) 1×10^{-6}, (6) 1.5×10^{-6} moles per gram of the substrate. (b) Corrected fluorescence emission spectra of acridine orange adsorbed on cellulose excited at 475 nm. The concentration of the dye is: curve (7) 5×10^{-6}, (8) 7.5×10^{-6}, (9) 2×10^{-5}, (10) 4×10^{-5}, (11) 7×10^{-5}, (12) 1×10^{-4} moles per gram of the substrate. (c) Normalized fluorescence emission spectra of acridine orange adsorbed on cellulose excited at 475 nm. The concentration of the dye is: curve (1) 2.5×10^{-7}, (2) 1.5×10^{-6}, (3) 2×10^{-5}, (4) 4×10^{-5}, (5) 1×10^{-4} moles per gram of the substrate.
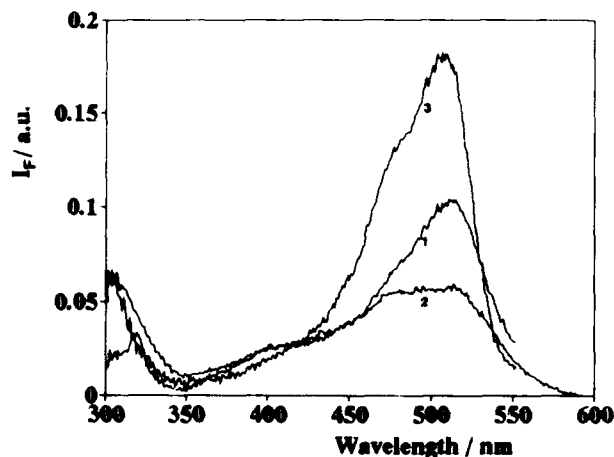
Fig. 4. Corrected fluorescence excitation spectra for acridine orange adsorbed on microcrystalline cellulose (100 μmol g^{-1}) analysed at 570 nm (curve 1) for the monomer emission and at 635 nm for the dimer emission (curve 2). Curve (3) was obtained from a 0.25 μmol g^{-1} sample and analysing at 570 nm.

the difference between monomer emission (curve 1), dimer emission (curve 5) and mixed situations at intermediate concentrations where both emissions are present.

The excitation spectra obtained for the 100 μmol g^{-1} sample presented in Fig. 4 clearly show the existence of the two emitting species of acridine orange which could be obtained by setting the analysing monochromator at a wavelength where the emission is mainly due to the monomer (570 nm) or to the dimer (635 nm). In the same figure the excitation spectra of a sample where only monomers are present (0.25 μmol g^{-1}) is also shown. In this case only the monomer excitation spectrum was obtained.

In Fig. 5 we present the fluorescence intensity of AO adsorbed on microcrystalline cellulose (measured as the integrated area under the corrected emission spectra), excited at 450, 475 and 495 nm. The data are corrected for cellulose absorption and plotted as a function of $(1 - R^e)f_{dye}$. Clearly these curves show that the fluorescence intensity depends on relative amounts of monomer and dimer excited, and suggest that monomer quantum efficiency of fluorescence is bigger than that of the dimer.
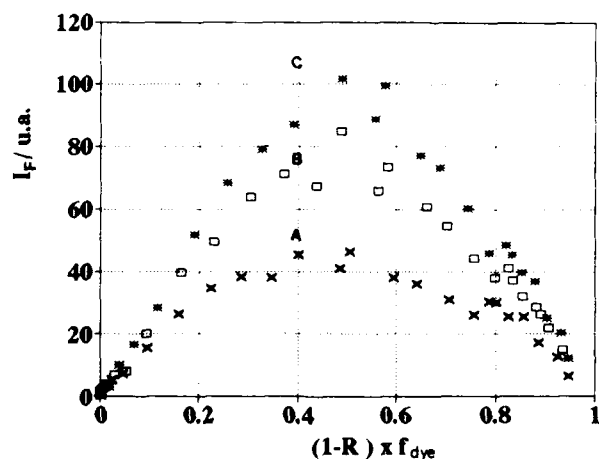

Fig. 5. Fluorescence intensity of acridine orange measured by the integrated area under the corrected emission spectra as a function of $(1 - R^e) \times f$ and corrected for the cellulose absorption. Curve (A) $\lambda_{exc} = 450$ nm; (B) $\lambda_{exc} = 475$ nm; (C) $\lambda_{exc} = 495$ nm.

All these facts support the use of Eqn (6) to analyse the data presented in Fig. 5. The fluorescence quantum yield of the monomer can be obtained by using a standard compound with a known Φ_F according to the method described in detail in a previous publication [5]. Again we used Rhodamine 101 which is a rigid molecule with a well-known fluorescence quantum yield of 1.00 ± 0.02 (see Ref. [5] and papers quoted therein). By the use of this compound (where only monomers emit), Eqn (6) and data from Fig. 5, it was possible to obtain by fitting $\Phi_M = 0.95 \pm 0.05$ and $\Phi_D = 0.40 \pm 0.10$. The errors in this case are larger than those obtained for dyes where monomers are the only fluorescent species, since for AO we are obtaining the best values for two parameters, Φ_M and Φ_D, instead of determining a single parameter Φ_M.

Figure 6 shows the calculated curves for I_M, I_D and $I_F = I_M + I_D$ (by the use of Eqn (6)) superimposed on the experimentally determined fluorescence emission intensities. The agreement is good for $C_0 < 3 \, \mu\text{mol g}^{-1}$, as can be seen in Fig. 6 exciting at 475 nm (the same happens for the three different excitation wavelengths where we vary the relative amount of light absorbed by the monomer and dimer). However, Fig. 6 also shows that there is a marked decrease of fluorescence intensity with increasing acridine orange loading for C_0 greater than $3 \, \mu\text{mol g}^{-1}$. Therefore, in this region we postulate the existence in the excited state of higher, non-fluorescent aggregates, the formation of which is responsible for a concentration quenching effect in this high loading range. Since Eqn (6) does not include this effect, there is a deviation between calculated values and experimental points in this range of very high concentrations of adsorbed dye.

3.3. *Delayed fluorescence emission and transient absorption spectra in the milisecond time-range*

3.3.1. *Time-resolved emission spectra from acridine orange on microcrystalline cellulose.* The emission decay of acridine orange in the low and high loading regimes when adsorbed in microcrystalline cellulose are presented in Figs 7 and 8, exciting at 532 nm in both cases. Figure 7 shows data on a 250 ms time-sweep and Fig. 8 shows the same data on a 20 ms time-sweep. The laser pulse is of negligible duration (8 ns) when compared to the lifetimes of the excited species in both cases. At low loadings, acridine orange emission peaks at about 550 nm and decays initially by a fast process, $t_1 \simeq 5$ ms, leaving a much longer lived component, $t_2 \simeq 100$ ms. However, at higher loadings the emission is different, as can be seen in Fig. 8 for a $60 \, \mu\text{mol g}^{-1}$ sample. The emission is broader and the maximum is now strongly bathochromically shifted to $\simeq 620$ nm. Only a fast decay is detected in this case, with a lifetime of about 5 ms.
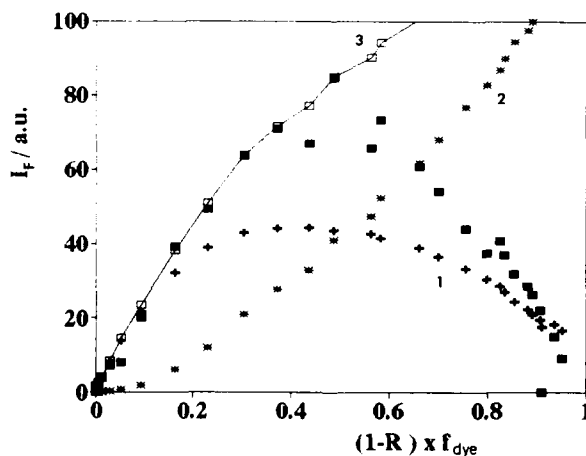

Fig. 6. Calculated I_F curve by the use of Eqn (6) for acridine orange adsorbed on microcrystalline cellulose and excited at 475 nm, superimposed on the experimentally determined I_F values (full symbols). $\Phi_M = 0.95 \pm 0.005$ and $\Phi_D = 0.40 \pm 0.10$. Curve (1) is I_M, (2) is I_D and (3) is $I_F = I_M + I_D$.
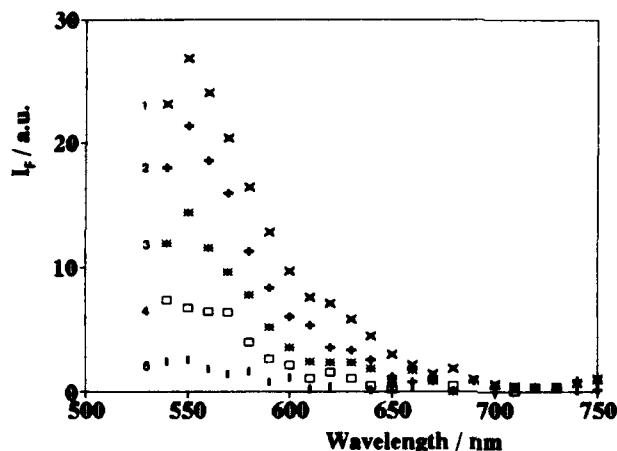
Fig. 7. Time-resolved monomer emission spectra from $0.5 \times 10^{-6}\,\mathrm{mol\,g^{-1}}$ of acridine orange adsorbed on microcrystalline cellulose. Curves (1), (2), (3), (4) and (5) were recorded 0, 13.2, 38.4, 88.1 and 188 ms after the laser pulse.

There is a marked resemblance between the corrected steady state emission spectra in the low and high loading situations and the emission spectra obtained on millisecond time-scales, uncorrected for the instrument response, obtained for the same samples when using pulsed laser excitation. Pulsed excitation of these samples cooled to 77K gave rise to no long-lived emission signal. Also, it was found that the observed emission intensity was linear with laser output energy. These facts indicate that the observed emissions are delayed fluorescence from the triplet monomeric and dimeric species on the cellulose surface, in which case the triplet of the dimeric form must have a much shorter lifetime than the monomer. In addition, there is evidence to suggest that there are short lifetime components in the monomer delayed fluorescence, suggesting a *distribution of absorption sites* on the cellulose surface.

At very high sample loadings, a decrease in delayed fluorescence intensity is observed to take place with increasing concentration, with no decrease in emission lifetime. This
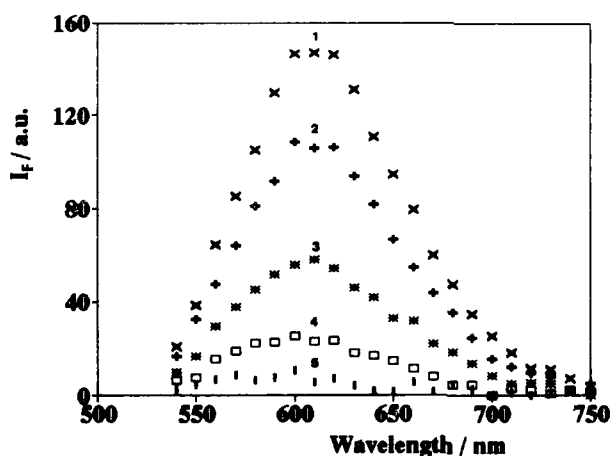

Fig. 8. Time-resolved dimer emission spectrum from $6.0 \times 10^{-5}\,\mathrm{mol\,g^{-1}}$ of acridine orange adsorbed in microcrystalline cellulose. Curves (1), (2), (3), (4) and (5) were recorded 0, 1.1, 3.1, 7.1 and 15.1 ms, respectively, after the laser pulse.
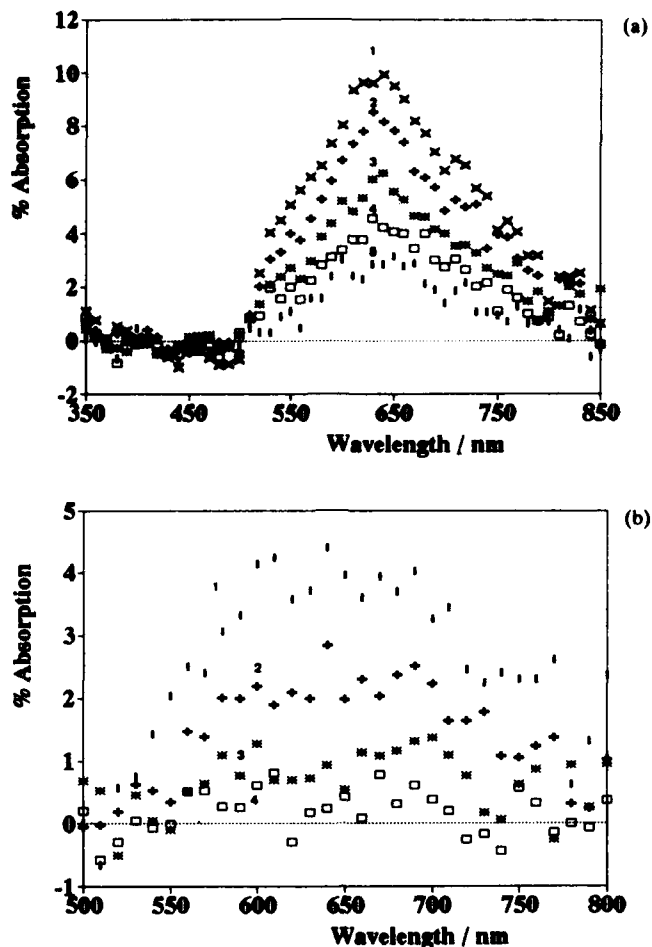
Fig. 9. (a) Time-resolved absorption spectrum from 4.0×10^{-5} mol g^{-1} of acridine orange
adsorbed on microcrystalline cellulose. Curves (1), (2), (3), (4) and (5) were recorded 0, 1.1, 3.1,
7.1 and 15.1 ms, respectively, after the laser pule. (b) Time-resolved absorption spectrum from
4.0×10^{-5} mol g^{-1} of acridine orange adsorbed on microcrystalline cellulose. Curves (1), (2), (3)
(a)   and (4) were recorded 13.2, 38.4, 88.1 and 188 ms, respectively, after the laser pulse. (b)

again points to the existence of non-emitting higher aggregates, here statically quenching
the excited triplet state of dimeric acridine orange.

3.3.2. *Time-resolved transient diffuse reflectance measurements*. Time-resolved tran-
sient absorption spectra obtained for these samples show triplet–triplet absorption
spectra which are consistent with the trend above. Thus for low loadings we see a long-
lived transient, decaying with a lifetime of approximately 100 ms, and as the loading on
the cellulose is increased, an increase is observed in the contribution to the overall decay
kinetics of a short-lived component, having a lifetime similar to that seen in emission.
These fast and slow components are shown to have somewhat different spectra (see
Fig. 9a and b), and are therefore assigned as two distinct species, being the triplet states
of the dimeric and monomeric forms, respectively.

The variations observed in triplet state spectra and lifetimes with loading are in
striking agreement with what is expected if the explanation of the observed thermally
activated delayed fluorescence from both monomer and dimer species is correct. Even
the smaller amount of triplet state absorption observed (compare Fig. 9a and b) at high
loadings is consistent with static quenching of the triplet dimer by higher aggregates, as
expected from the delayed fluorescence studies.

4. CONCLUSIONS

Steady state emission and time-resolved studies following pulsed excitation clearly demonstrate the existence of two emitting species when acridine orange is adsorbed on microcrystalline cellulose, these being assigned as the monomeric and dimeric forms. Following pulsed excitation, thermally activated delayed fluorescence from both monomer and dimer can readily be detected. Using diffuse reflectance laser flash photolysis, it was possible to probe the triplet states of both of these species. A non-linear effect of increasing concentration on fluorescence intensity is observed for high loadings of dye, and is attributed to the formation of non-emitting, higher aggregates of acridine orange. These higher aggregates are also postulated as being responsible for static quenching of delayed fluorescence seen at high sample loadings.

REFERENCES

[1] F. Wilkinson, P. A. Leicester, L. F. Vieira Ferreira and V. M. M. R. Freire, *Photochem. Photobiol.*, **54**, 599 (1991).

[2] F. Wilkinson, G. P. Kelly, L. F. Vieira Ferreira, M. I. Ferreira and V. M. M. R. Freire, *J. Chem. Soc., Faraday Trans. II* **87**, 547 (1991).

[3] L. F. Vieira Ferreira, S. B. Costa and E. J. Pereira, *J. Photochem. Photobiol A: Chem.* **55**, 361 (1991).

[4] L. F. Vieira Ferreira and S. B. Costa, *J. Lumin.* **48 & 49**, 395 (1991).

[5] L. F. Vieira Ferreira, F. Wilkinson, M. R. Freixo and A. R. Garcia, *J. Chem. Soc., Faraday Trans.*, submitted.

[6] F. Wilkinson, *J. Chem. Soc., Faraday Trans II*, **82**, 2073 (1986).

[7] F. Wilkinson and G. P. Kelly, in *Handbook of Organic Photochemistry*, Vol. 1. (edited by J. C. Scaiano), p. 293. CRC Press (1989).

[8] G. P. Kelly, P. A. Leicester, F. Wilkinson, D. R. Worrall, L. F. Vieira Ferreira, R. Chittock and W. Toner, *Spectrochim. Acta* **46A**, 975 (1990).

[9] A. Kellmann, *Photochem. Photobiol.* **20**, 103 (1974); **14**, 85 (1971).

[10] B. Soep, A. Kellmann, M. Martin and L. Lindqvist, *Chem. Phys. Lett.* **13**, 241 (1972).

[11] V. Zanker, *Z. Physic. Chem.* **199**, 225 (1952); **200**, 250 (1952).

[12] J. Fergusson and A. W. H. Mau, *Austr. J. Chem.* **256**, 1617 (1973).

[13] M. G. Newmann and M. H. Gehlen, *J. Colloid. Inter. Sci.* **135**, 209 (1990).

[14] B. M. Sutherland and J. C. Sutherland, *Biophys. J.* **9**, 292 (1969).

[15] C. A. Parker and T. A. Joyce, *Photochem. Photobiol.* **18**, 467 (1973).

[16] M. S. Chan and J. R. Bolton, *Photochem. Photobiol.* **34**, 537 (1981).

[17] K. H. Drexhage, Dye lasers, in *Topics in Applied Physics* (edited by F. P. Shafer), p. 144. Springer, Berlin (1973).

[18] I. B. Berlman, in *Handbook of Fluorescence Spectra of Aromatic Molecules*. Academic Press, London (1965).

[19] J. N. Demas, in *Excited State Lifetime Measurements*. Academic Press, New York (1983).

[20] F. Wilkinson, D. R. Worrall and L. F. Vieira Ferreira, to be published.

[21] P. Kubelka, *J. Opt. Soc. Am.* **38**, 448 (1948).

[22] G. Kortüm, W. Brown and G. Herzog, *Angew. Chem., Inter. Ed.* **2**, 333 (1963).

Diffuse reflectance laser photolysis studies of the mechanisms of light-induced reactions in heterogeneous systems

F WILKINSON* and D R WORRALL

Department of Chemistry, Loughborough University of Technology, Loughborough, Leicestershire, LE11 3TU, UK

Abstract. The technique of diffuse reflectance laser flash photolysis is discussed and examples are given of time resolved spectra showing laser induced changes in diffuse reflectance and of transient decays as a function of time on timescales as short as a few picoseconds. Methods for extracting transient spectra and decay kinetics from raw experimental data are outlined. The application of the technique to the study of various heterogeneous systems including photochemical processes, within organic and inorganic microcrystals, within functionalised polymers and ion exchange resins, and to the laser photolysis of adsorbed species at interfaces and within zeolites are presented.

1. Introduction

Photochemical investigations in heterogeneous systems constitute a great challenge because of the potential such studies have for increased understanding of photobiology and of many technological applications of photochemistry. Heterogeneity makes the analysis of photochemical and photophysical data much more complicated than in homogeneous media but its major importance justifies efforts which are being made to cope with the inherent complexities. Recently we have extended to heterogeneous, opaque and often highly scattering systems the advantages of being able to subject them to flash photolysis investigation by using diffuse reflected light instead of transmitted light as the analysing source on timescales extending from several seconds (Kessler and Wilkinson 1981) to picoseconds (Kelly et al 1990a). Laser induced transient spectra and decay kinetics have been observed for a wide variety of samples including fractions of monolayers of organic molecules adsorbed on catalytic metal oxide surfaces (Oelkrug et al 1987, 1989) and included within zeolites (Kelly et al 1990c) from semiconductor powders (Wilkinson et al 1986c) and porous electrodes doped and undoped (Kossanyi et al 1990, from ruthenium(II) complexes within ion exchange resins (Masschelin et al 1991), from organic microcrystals (Wilkinson and Willsher 1984), and from organic dyes adsorbed on microcrystalline cellulose (Wilkinson et al 1991, 1992), on fabrics and chemically bound to polymers (Bourdelande et al 1988; Kelly et al 1990b), from paper pulp (Schmidt et al 1990), and from photographic emulsions (Wilkinson and Leicester 1992). Other groups are now

---

* For correspondence

increasingly using this method to study the mechanisms of light induced reactions in heterogeneous environments (Turro *et al* 1986; Ikeda *et al* 1988; Draper and Fox 1990; Levin *et al* 1990).

2. Experimental

2.1 Nanosecond diffuse reflectance flash photolysis

The equipment used for nanosecond laser flash photolysis in diffuse reflectance mode is identical to that used for studies in transmission mode except for the geometry for collecting the analysing light which is typically as shown in figure 1. Samples are often held in a powder holder behind a quartz window or in a sealed fluorimeter cell. The observable in diffuse reflectance laser flash photolysis is $\Delta R(t)$ defined as follows:

$$\Delta R(t) = [R_b - R(t)]/R_b, \tag{1}$$

where R_b is the sample reflectance before exposure to the exciting laser pulse and $R(t)$ the reflectance at time t after excitation. ΔR is thus the fractional change in reflectance and $100\,\Delta R$ is often referred to as the percentage absorption by the transient.

Figure 2 shows the four traces which are recorded at each analysing wavelength necessary to obtain a corrected trace of reflectance change $\Delta R(t)$ as a function of time. The four experimental traces are: (1) baseline trace i.e. analysing light reflected from sample in the absence of laser excitation; (2) absorption trace i.e. analysing light reflected from sample before (pretrigger) and after laser excitation. This shows a decrease in reflection due to absorbing transients; (3) emission trace i.e. any emission caused by laser excitation in the absence of analysing light; (4) zero trace i.e. the digitiser is triggered in the absence of either laser excitation or analysing light to establish the zero settings. From these four traces a corrected trace of the reflectance change as a function of time can be obtained at each analysing wavelength. Time resolved spectra are obtained by measuring many such traces at different wavelengths and
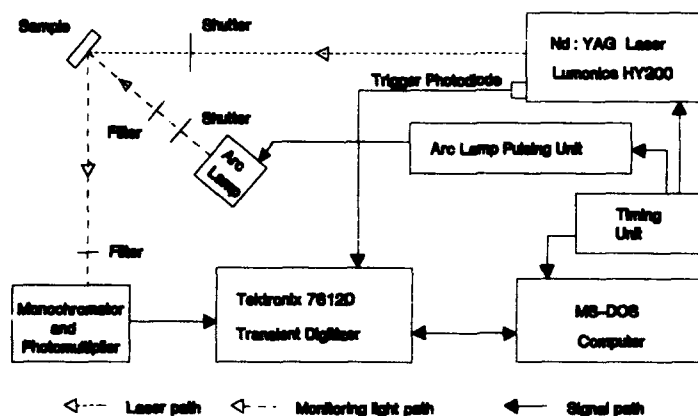

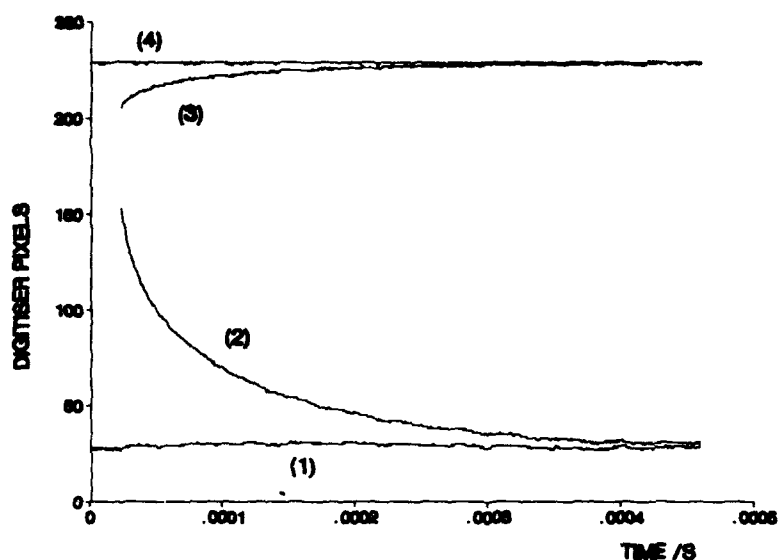Figure 1.   Apparatus for diffuse reflectance laser flash photolysis.

Figure 2. Data traces recorded for microcrystalline benzil exciting at 354 nm and analysing at 510 nm. (1) Baseline (lamp only), (2) transient (lamp and laser), (3) emission (laser only), (4) top line (no light).
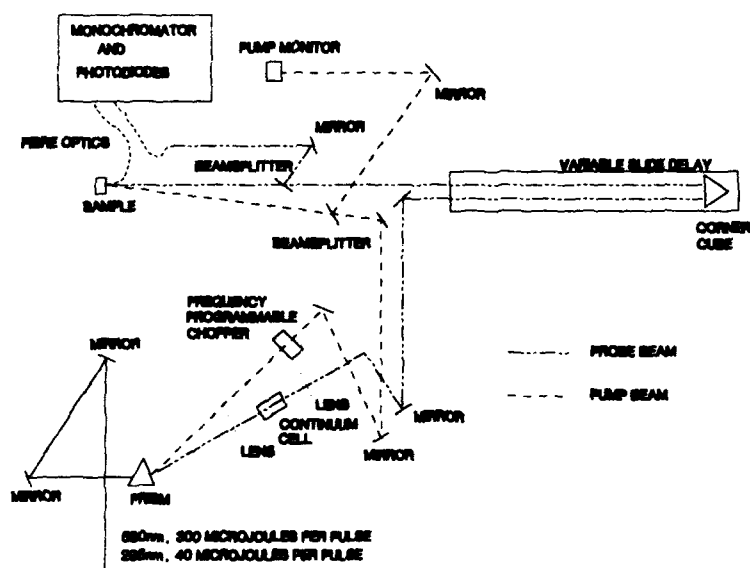

Figure 3. Picosecond diffuse reflectance pump-probe laser photolysis apparatus.

then plotting the magnitude of the reflectance change as a function of wavelength at a known delay (see later). Full experimental details are given in the references (Wilkinson 1986; Wilkinson and Kelly 1990; Wilkinson and Willsher 1990).

2.2 Picosecond diffuse reflectance flash photolysis

Figure 3 illustrates the basic arrangement used to record the first ever transient absorption within an opaque material on picosecond timescales using diffuse reflectance (Wilkinson et al 1986b; Kelly et al 1990). Generation and detection of the transient absorption was effected by pumping the sample at 295 nm (pulse width = 6 ps, energy = 20 μJ) and probing at 590 nm (energy = 1 μJ), using the Spectra-Physics picosecond laser system at The Rutherford Appleton Laboratory. Light diffusely reflected from the sample was detected by a filtered photodiode, and the signal fed to a Boxcar Integrator and thence to a IBM microcomputer. A second photodiode monitored a portion of the probe beam taken before hitting the sample, in order to correct for shot-to-shot variations, in laser intensity.

Samples are usually held in a powder holder behind a quartz window. Nearly co-linear pump and probe beams are incident normal to the quartz window, with the pump beam about 2 mm in diameter and the probe beam located entirely within the excited area of the sample. A portion of the diffusely reflected probe beam was detected by the photodiode. To record transient absorption (which is, strictly speaking, the relative decrease in diffuse reflectance), signals due to the probe beam alone and due to simultaneous pump and probe were obtained. Each run comprised 100 shots, and normalisation for shot-to-shot variation was carried out. Transient absorption following excitation at the pump wavelength reduces the level of the diffusely reflected probe beam to different extents for different delays between the pump and probe beams
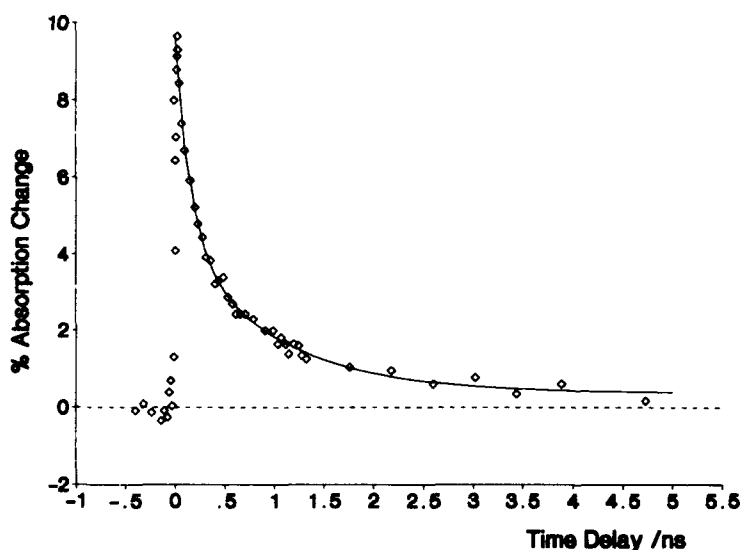

Figure 4. Decay of transient absorption for microcrystalline 1,5-diphenyl-3-styryl-2-pyrazoline (corrected for emission).

incident on the same area of sample. Thus unlike our nanosecond studies we have found it necessary to accumulate at least one hundred pump-probe shots at each delay in order to obtain each point shown on a decay curve. The transient absorption, for microcrystalline 1,5-diphenyl-3-styryl-2-pyrazoline illustrated in figure 4 is assigned to excited singlet states of the pyrazoline (Kelly *et al* 1990). The observed transient decay curve can be fitted using a biexponential model with lifetimes of 1.6×10^{-10} and 1.3×10^{-9} seconds for the faster and the slower decay components respectively. Full experimental details are given elsewhere (Kelly *et al* 1990).

2.3 Data analysis of transient changes in diffuse reflectance

More extensive discussions of the analysis of data are given elsewhere (Kessler *et al* 1983; Oelkrug *et al* 1987). Following the Kubelka–Munk treatment (Kubelka 1948) for diffuse reflectance two light fluxes are considered travelling in opposite directions perpendicular to the irradiated surface at $x = 0$. The attenuation of the incident flux I depends on the absorption and scattering coefficients K and S respectively and is given by

$$dI(x) = -I(x)(K + S)dx + J(x)Sdx, \tag{2}$$

and the generated flux since it passes in the opposite direction has

$$dJ(x) = J(x)(K + S)dx - J(x)Sdx \tag{3}$$

The diffuse reflectance R is given by

$$R = J_0/I_0 \tag{4}$$

where I_0 and J_0 are the incident and reflected fluxes at the surface. Equations (2) and (3) can be solved for a layer so thick that any further increase in thickness does not affect R and provided K and S are independent of x, this gives

$$(1 - R)^2/2R = K/S = F(R). \tag{5}$$

$F(R)$, the emission function is linearly dependent on the number of absorbing chromophores in any sample where S and K are independent of the penetration depth below the surface. In diffuse reflectance flash photolysis the initially excited chromophores are usually homogeneously distributed. However, photo-excitation produces transient or permanent changes in absorption, preferentially just below the irradiated surface. Theoretical treatments (Kessler *et al* 1983; Oelkrug *et al* 1987) show that there are two limiting types of concentration profile produced, namely an exponential fall-off as a function of penetration depth and a homogeneous (or "plug") profile, these are illustrated schematically in figure 5, curves 1 and 4, respectively.

The latter case is encountered with large laser fluences and with low concentrations of ground state absorbers, where there is total conversion from ground state to transient to a certain depth below the irradiated surface. Since a homogeneous concentration of absorbers exists, the Kubelka–Munk theory can be applied (Kubelka 1948). For optically thick samples at analysing wavelengths where only the transient absorbs, the remission function given by (5) is a linear function of the concentration and can be used for kinetic analysis and for plotting absorption spectra. For the low
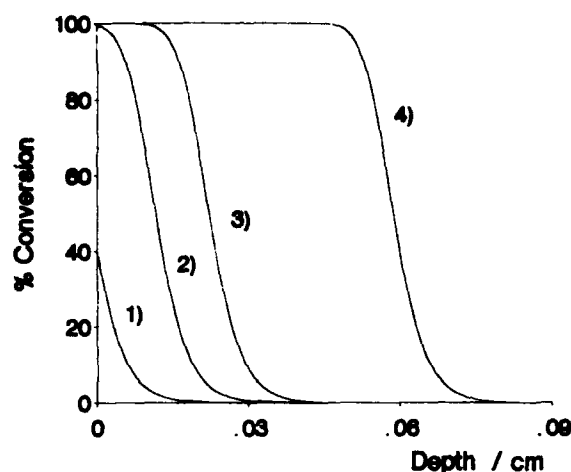
Figure 5. Plot showing percentage conversion of ground state molecules as a function of sample depth with increasing laser intensity.

percentage conversions, the concentration of transients decreases exponentially below the irradiated surface. This occurs when there is a high concentration of ground state absorbers and with low laser fluences. An analytical solution for the change in reflectance expected has been obtained (see Lin and Kan 1970) and is in the form of a converging series which has been shown (Kessler *et al* 1983) to relate ΔR as a linear function of the concentration of transient at values of ΔR less than 0·1. Between these two limiting cases the change in ΔR with concentration depends on the concentration profile below the irradiated surface. In order to establish if either of the two limiting cases pertain, it is necessary to calculate the expected change in transient concentration as a function of distance below the irradiated surface.

2.4 *Calculation of transient concentration profiles*

To extract kinetic information from $\Delta R(t)$ one must first understand the concentration profile. A detailed description of the modelling procedure, including all relevant equations, has been published (Kessler *et al* 1983; Oelkrug *et al* 1987). A brief outline of the algorithm is given below.

(1) The sample is divided into a large number of thin slices i, such that the concentration of the ground-state absorbers stays constant within each individual slice. When the procedure starts (before the sample is subjected to laser excitation) the concentration of ground state absorbers, A, in each of the slices is $A_i = A_0$, the initial concentration of ground-state absorbers. The absorption coefficient at the laser wavelength is given by $K^c_{A,i} = 2\varepsilon^c_A A_i$ where ε^c_A is the extinction coefficient of A at the excitation wavelength. Usually it is assumed that the transient does not absorb significantly at the laser wavelength and that the scattering coefficient S is independent of wavelength.

(2) The laser pulse which excites the sample is divided into portions Δt where Δt is generally 1/100 of the total pulse duration.

(3) The sample is considered as having being irradiated with a portion Δt of the laser pulse. The concentrations of transient species, T_i, formed in each slice because of light absorption are determined, and a new set of ground-state concentrations, A_i, are calculated. In general, after the sample has been exposed to a portion of the laser light, the concentrations A_i are no longer equal, due to the attenuation of the exciting pulse as it passes through the sample. Mass conservation requires that $A_i + T_i = A_0$ in all slices.

(4) Using the new values of A_i, new absorption coefficients $K^e_{A,i}$ are calculated for each slice.

(5) The procedure recycles to step (3), and the next portion of the laser pulse is considered to irradiate the sample.

(6) When all of the laser pulse has irradiated the sample, the concentration of ground state absorbers A_i and the concentration of transient species T_i in each slice are known. Steps (1) through (6) generate the transient concentration profile. To calculate ΔR at an appropriate analysing wavelength the following additional steps are performed.

(7) Estimates of the extinction coefficients at the *analysing* wavelength for the transient species, ε^a_T are used to calculate the absorption coefficients in each slice due to the ground-state absorbers $K^a_{A,i} = 2\varepsilon^a_A A_i$, and transient species, $K^a_{T,i} = 2\varepsilon^a_T T_i$.

(8) The reflectance of each slice, R_i, can now be calculated using the absorption coefficients $K^a_{A,i}$, $K^a_{T,i}$ and the scattering coefficient S.

(9) Finally, the individual reflectances R_i are combined using a recursion formula to give the expected reflectance of the sample.

If the absorption coefficient K is in excess of $10^4\,\text{cm}^{-1}$ at the laser excitation wavelength then the penetration depth is only about $1\,\mu\text{m}$ and dissipation of laser excitation as heat causes considerable temperature rise (see Wilkinson *et al* 1986c). We have not only shown how to predict any temperature rises but have confirmed our calculations by measurements in the case of TiO_2. The possibility of large temperature rises has always to be borne in mind and lower laser fluences, lower concentrations or excitation into weaker bands must be employed where necessary to avoid thermal effects. It is important to stress that when the penetration depth of the exciting light is $>0.1\,\text{mm}$, temperature rises in opaque samples using our nanosecond laser system are negligible i.e. $<1^\circ\text{C}$.

3. Results and discussion

3.1 *Laser photolysis at interfaces and within zeolites*

Kessler and Wilkinson (1981) studied various aromatic hydrocarbons chemisorbed on γ-alumina. The samples were adsorbed at less than monolayer levels, and the transient spectra observed were shown to be due to triplet–triplet absorptions. We have been attempting to make such studies in order to explore the electronic structures, excited state spectra and lifetimes of adsorbates. We are also interested in energy, electron and proton transfer of photoexcited species at interfaces (Wilkinson and Ferreira 1988; Oelkrug *et al* 1991).

We have also studied radical reactions on surfaces, for example, the α-cleavage of 1,1,3-3-tetraphenylacetone (TPA) has been used as a source of diphenylmethyl radicals in our experiments (Kelly *et al* 1990c). The production of the second diphenylmethyl radical via decarbonylation of the intially produced diphenylacetyl radical occurs rapidly and thus, provides an efficient and practically instantaneous source of two diphenylmethyl radicals per ketone molecule as shown below.

$$Ph_2CHCOCHPh_2 \xrightarrow{hv} Ph_2CHCO + Ph_2CH \longrightarrow 2Ph_2CH + CO.$$

The three solid supports used in these experiments differ considerably in their properties. Silica gel is a porous surface with, in our case, an average pore size of 6 nm and a surface area of 480 m^2/g. Both silica gel and Silicalite contain only silicon and oxygen, although the latter is hydrophobic whereas the former has a large amount of physical adsorbed water on the surface. The structure of the aluminosilicate NaX zeolite comprises a three-dimensional network of relatively large cavities or supercages (-1.2 nm) connected by $0.7 - 0.8$ nm pores or channels. The Si/Al ratio of approximately 1.5 results in a large proportion of exchangeable cations (in our case Na) and a strongly hydrophilic zeolite. It should be noted that TPA can easily fit within the pore structure of silica gel and the channel system of NaX. However, the relatively small channels of Silicalite result in adsorption of TPA only on the external surface, although the photoproduced diphenylmethyl radical may migrate into the channels. For all the three supports diphenylmethyl radicals are produced with a characteristic absorption maximum at 335 nm (e.g. see figure 6) which decays over timescales which vary from hundreds of nanoseconds to minutes (for a full discussion see Kelly *et al* 1990c).
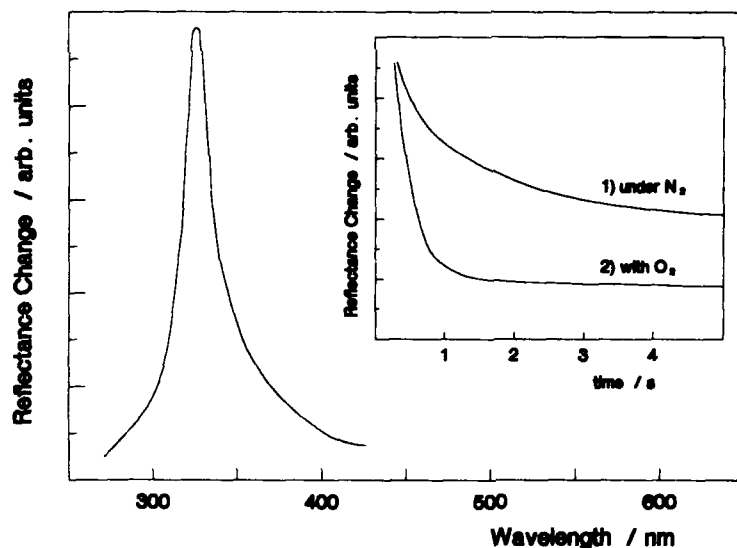

Figure 6. Transient spectrum of diphenylmethyl radicals produced by 266 nm excitation of 3% coverage of tetra-phenylacetone on silica. Inset shows transient decays monitored at 340 nm.

It also is of interest to compare those processes which can occur in both homogeneous and heterogeneous environments. For example, we have studied energy transfer at surfaces (Wilkinson and Ferreira 1988) and in homogeneous solution. Energy transfer on cellulose surfaces shows substantial static quenching which approaches a Perrin-type behaviour which contrasts with the situation in homogeneous solution where dynamic quenching yields Stern–Volmer kinetics (Wilkinson and Ferreira 1988). On silica dynamic quenching is also observed for example between eosin and anthracene due to the process

$$^3\text{eosin}^* + \text{anthracene} \rightarrow {}^3\text{anthracene}^* + \text{eosin},$$
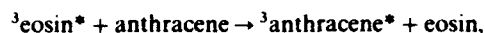
for example, see figure 7 (Wilkinson *et al* 1992).

The nature and mobility of the species present when acridine is adsorbed from high vacuum onto thermally-pretreated alumina and silica have been investigated by ground and excited state spectroscopic techniques (Oelkrug *et al* 1989). For alumina treated at high temperatures ($> 500°C$) σ-bonded acridine is the main species present, while the acridinium cation AH^+ predominates at lower activation temperatures ($100°C$). The triplet–triplet absorption of AH^+ at 480 nm has been directly observed without a triplet sensitiser, and the decay is non-exponential. On silica the main adsorbed species is hydrogen bonded acridine which shows triplet–triplet absorption at 435 nm and which, for samples of low coverage or high pre-treatment temperature, has an exponential decay with a lifetime of about 35 ms. For samples of high coverage or low pre-treatment temperature, the triplet decay is faster and non-exponential, and delayed fluorescence is observed. This arises from triplet–triplet annihilation, a consequence of the mobility of acridine on the silica surface for which the two-dimensional bimolecular rate constant is $8 \times 10^{13} \text{dm}^2 \text{mol}^{-1} \text{s}^{-1}$.

No delayed fluorescence occurs when silica has been pre-treated at high temperatures, conditions which favour dehydroxylation of the surface to form siloxan units. These have a high activation barrier to translational motion and thereby impede the lateral mobility of the adsorbate. For alumina, the nature of the surface permits virtually no mobility of the acridine, and hence no significant bimolecular processes are observed on this adsorbent (see Oelkrug *et al* 1989).

Organic photoreactions on zeolite supports have become an area of increasing interest in the last few years (Casal and Scaiano 1984). A study of the ketone, xanthone, included within the hydrophobic zeolite Silicalite has yielded some very interesting information relating to the host environment (Wilkinson *et al* 1986c). Silicalite is over 99% SiO_2 and consists of a system of near-circular zig-zag channels, cross-linked by elliptical straight channels (Flanagen *et al* 1978). The xanthone transient was assigned as the triplet, showing a characteristic maximum at 605 nm.

It is well-known (Garner and Wilkinson 1976) that the absorption maxima of triplet xanthone is sensitive to the solvent polarity and the value obtained for λ_{max} would be indicative of a polar environment in dilute solution. Since Silicalite is a hydrophobic matrix this is somewhat surprising, however, it may indicate that xanthone is adsorbed on the walls of the channels. Another observation made was that the decay process extends over a considerable timescale from ns to ms. This suggests a variety of lifetimes for this ketone triplet at different surface sites. The growth of this transient on picosecond timescales constituted the first reported example of picosecond diffuse reflectance laser photolysis (Wilkinson *et al* 1986b).
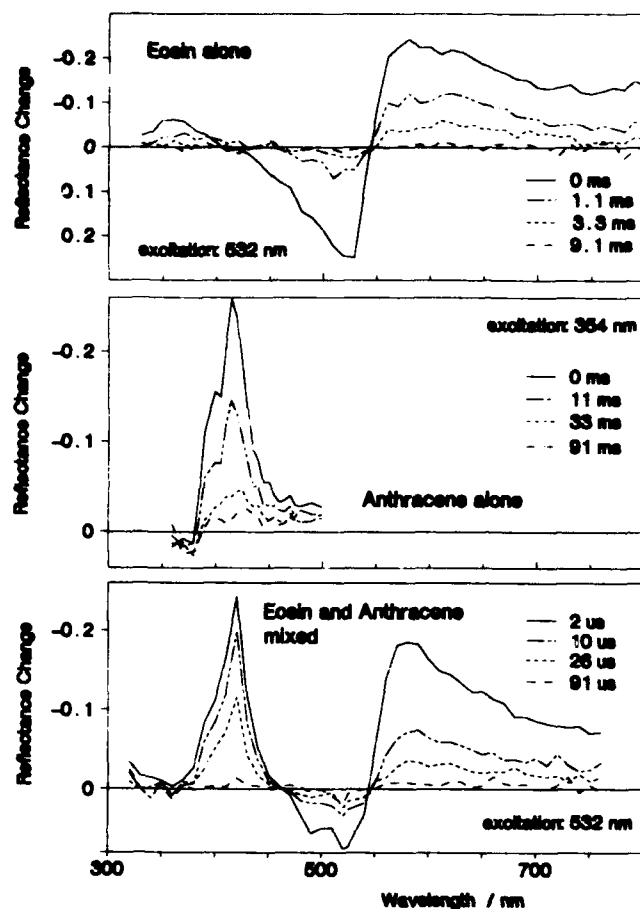
Figure 7. Transient absorption spectra illustrating energy transfer between eosin and anthracene on silica.

3.2 *Functionalised polymers*

The idea of anchoring a photosensitizer to an insoluble polymer support has become widespread. The technique of diffuse reflectance flash photolysis allows one to monitor excited state lifetimes and the production and decay of other transient species. In collaboration with Professor J Font from the Autonomous University of Barcelona, Spain, we have carried out several studies (Wilkinson *et al* 1987; Bourdelande *et al* 1988) to obtain evidence concerning intermolecular and intramolecular energy transfer in insoluble polymeric benzophenone and from ruthenium *tris*(2,2'-bipyridine) bound to insoluble polymers. The transient absorption spectra are similar to those observed for ruthenium *tris*(2,2'-bipyridine) in dilute fluid solution. Experiments using methyl viologen as quencher show that quenching of excited states is forty times slower than in aqueous solution (Bourdelande *et al* 1988).

3.3 Ion-exchange resins

We have also compared the photophysical properties of $Ru(bpy)_3^{2+}$ incorporated into an ion exchange resin sephadex SP C25 with its properties in aqueous solution. Other potential photosensitizers investigated include the three complexes $Ru(bpy)_n(TAP)_{3-n}$ where $n = 0$, 1 and 2 and TAP represents 1,4,5,8-tetraazaphenanthrene.

The partial immobilisation of the complexes in the cavities of the sephadex leads to two opposing effects (i) quenching by the sephadex and (ii) an increase in luminescence lifetimes. The quenching by the sephadex is shown to involve a statistical factor depending on the number of TAP ligands on the complex and on the geometry and size of the cavities in the resin. Full details are given in Masschelein *et al* (1991).

4. Conclusions

In these studies of 'Nanosecond and Picosecond Laser Photolysis of Opaque Heterogeneous Photosensitizers', we have been able to demonstrate the utility of the technique of diffuse reflectance to enable transient spectra and decays to be obtained from many dyes or sensitizers in a variety of heterogeneous environments. Considerable progress has been made in understanding why the technique is so sensitive and computer simulation demonstrates how kinetic parameters can be obtained. Since many heterogeneous systems give a distribution of decay constants it is not usually possible to quote a single decay constant for a heterogeneous system. However, the nature of the distribution of decay constants can be determined.

In several of the photochemical processes investigated, such as photoinduced reactions at interfaces, within zeolites, dyed fabrics and doped semiconductors, we have been able to obtain results concerning intermediates and mechanisms which cannot be obtained by any other method. Many of the studies reported above open up whole new areas for investigation. We also have obtained unique information on the translational mobility, intramolecular and bimolecular photoreactions of adsorbates on metal oxide surfaces.

Acknowledgement

References

Bourdelande J L, Campa C, Camps J, Font J, de March P, Willsher C J and Wilkinson F 1988 *J. Photochem. Photobiol.* **A44** 51
Casal H L and Scaiano J C 1984 *Can. J. Chem.* **62** 628
Draper R B and Fox M A 1990 *J. Phys. Chem.* **94** 4628
Flanagen F M, Bennett J M, Grose R W, Cohen J P, Patton R L, Kirchener R M and Smith J V 1978 *Nature (London)* **271** 512

Garner A and Wilkinson F 1976 *J. Chem. Soc., Faraday Trans. II* **72** 1016

Ikeda N, Kashioku M, Masuhara H and Yoshihara K 1988 *Chem. Phys. Lett.* **150** 452

Kelly G P, Leicester P A, Wilkinson F, Worrall D R, Ferreira L F V, Chittock R and Toner W 1990a *Spectrochim. Acta* **A46** 975

Kelly G P, Mollah M and Wilkinson F 1990b *J. Textile Inst.* **81** 91

Kelly G P, Willsher C J, Wilkinson F, Netto-Ferreira J C N, Opea A, Weir D, Johnson L J and Scaiano J C 1990c *Can. J. Chem.* **68** 812

Kessler R W, Krabichler G, Uhl S, Oelkrug D, Hagan W P, Hyslop J and Wilkinson F 1983 *Opt. Acta* **30** 1090

Kessler R W and Wilkinson F 1981 *J. Chem. Soc., Faraday Trans. I* **77** 309

Kossanyi J, Kouyate D, Pouliqueu J, Ronfard-Haret J C, Valat P, Oelkrug D, Mammel U, Kelly G P and Wilkinson F 1990 *J. Lumin.* **46** 17

Kubelka P 1948 *J. Opt. Soc. Am.* **38** 448

Levin B P, Ferreira L F V and Costa S M B 1990 *Chem. Phys. Lett.* **173** 277

Lin T and Kan H K A 1970 *J. Opt. Soc. Am.* **60** 1252

Masschelein A, Kirsch-De Mesmaeker A, Willsher C J and Wilkinson F 1991 *J. Chem. Soc., Faraday Trans.* **87** 259

Oelkrug D, Honnen W, Wilkinson F and Willsher C J 1987 *J. Chem. Soc., Faraday Trans. II* **83** 2081

Oelkrug D, Krabichler G, Honnen W, Wilkinson F and Willsher C J 1988 *J. Phys. Chem.* **92** 3589

Oelkrug D, Reich S, Wilkinson F and Leicester P A 1991 *J. Phys. Chem.* **94** 267

Oelkrug D, Uhl S, Wilkinson F and Willsher C J 1989 *J. Phys. Chem.* **93** 4551

Schmidt J A, Heitner C, Kelly G P, Leicester P A and Wilkinson F 1990 *J. Pulp Paper Sci.* **19** 111

Turro N J, Zimmit M B, Gould I R and Mahler W 1986 *J. Am. Chem. Soc.* **107** 5826

Wilkinson F 1986 *J. Chem. Soc., Faraday Trans. II* **82** 2073

Wilkinson F, Beer R and Leicester P A (to be published)

Wilkinson F and Ferreira L F V 1988 *J. Lumin.* **40 & 41** 704

Wilkinson F, Ferreira L F V and Worrall D R 1992 (to be published)

Wilkinson F and Kelly G P 1990 *Handbook of organic photochemistry* (ed.) J C Scaino (Boca Raton, FL: CRC Press) vol. 1, chap. 12

Wilkinson F and Leicester P A 1992 (to be published)

Wilkinson F, Leicester P A, Ferreira L F V and Freire V M 1991 *Photochem. Photobiol.* **54** 599

Wilkinson F and Willsher C J 1990 *Lasers in polymer science and technology: Applications* (eds) Foussier and Jan F Rabek (Boca Raton, FL: CRC Press) vol. 2, chap. 9

Wilkinson F and Willsher C J 1984 *Appl. Spectrosc.* **38** 897

Wilkinson F, Willsher C J, Bourdelande J L, Font J and Greuges J 1987 *J. Photochem.* **38** 318

Wilkinson F, Willsher C J, Casal H L, Johnston L J and Scaiano J C 1986a *Can. J. Chem.* **64** 539

Wilkinson F, Willsher C J, Leicester P A, Barr J R M and Smith M J C 1986b *J. Chem. Soc., Chem. Commun.* 1216

Wilkinson F, Willsher C J, Uhl S, Honnen W and Oelkrug D 1986c *J. Photochem.* **33** 273

Photochemistry on Surfaces: Fluorescence Emission Quantum Yield Evaluation of Dyes adsorbed on Microcrystalline Cellulose

Luis F. Vieira Ferreira, * **M. Rosário Freixo and Ana R. Garcia**
Centro de Química Física Molecular, Universidade Técnica de Lisboa—Complexo I—IST. Av. Rovisco Pais, 1096 Lisboa Codex, Portugal

Francis Wilkinson
Department of Chemistry, Loughborough University of Technology, Loughborough, Leicestershire LE11 3TU, UK

A simple method to determine the fluorescence quantum yield (ϕ_F) of dyes adsorbed on microcrystalline cellulose is presented. The method is based on corrected fluorescence emission spectra and can easily be applied provided the energy profile of excitation is accurately determined. The quantitative determination of ϕ_F is based on the ratio of the slopes of curves which correlate the fluorescence intensity and the absorbed light for both standard and unknown samples. The evaluation of the absorbed light is done by determining the reflectance R through the use of an integrating sphere. The remission function can then be determined as a function of wavelength in the two cases.

Rhodamine 101 (R101), a rigid molecule with unitary ϕ_F, was used as a standard compound to determine the ϕ_F values for rhodamine 6G (R6G) and auramine O (AURO), all dyes adsorbed on cellulose, and we obtained 1.02 ± 0.03 and 0.14 ± 0.01, respectively.

Strong aggregation was detected for the two rhodamine dyes in the ground state, which we assign to dimer formation known to influence the fluorescence emission with respect to absorbed intensity. AURO does not aggregate when adsorbed on microcrystalline cellulose for loadings up to 10 µmol g^{-1}. The intensity of the emission depends on concentration in all cases, but no emission was detected from the aggregated forms of the two rhodamines.

The ground-state diffuse reflectance study for R101 and R6G enables us to determine the equilibrium constants for dimer formation of these two rhodamines adsorbed on cellulose which are $K_D = 0.4 \times 10^6$ and 1.3×10^6 mol g^{-1}, respectively.

The results obtained for ϕ_F of these dyes show that the method is sensitive, making it possible to determine emissions from samples ranging from 1 nmol of the dye per gram of cellulose up to 10 µmol g^{-1}. The determination of quantum yields can be obtained with an accuracy >3%.

Fluorescence quantum yield determination of organic compounds in solution is a well established method and detailed discussions have been presented.[1,2] Front surface geometry enables one to obtain fluorescence spectra emitted from samples with high absorbances at the exciting wavelength.[3] Quantitative concentration studies can be made provided a detailed knowledge of the energy profile at excitation wavelengths of the geometry of the system and also an accurate correction curve for sensitivity variations as a function of emission wavelengths are available.[3,4]

Front surface geometry is needed both to study high-absorbance solutions or samples of dyes adsorbed on solids. The determination of the fluorescence quantum yield of dyes adsorbed on powdered solids is more difficult than the equivalent experiments in liquids, since it involves evaluation of the remission function for the dye and also because the dye often aggregates. This affects both the fluorescence emission intensity and shape of spectra, especially in the case where the aggregated forms emit. Self-absorption effects are also important and in many cases different emissions which seem to give evidence for different excited species are only due to this effect.

Examples of fluorescence emission quantum yield determination of compounds adsorbed on powdered substrates are rare in the literature. An absolute determination of quantum yields of powdered samples of inorganic salts mixed with sodium salicylate using a conventional spectrofluorimeter was first presented by Wrighton et al.,[5] but the estimated errors inherent in the method are very large (±25%). More

recently Hurtubise and co-workers[6] presented a determination of quantum yields of fluorescence and phosphorescence at room temperature for organic compounds adsorbed on sodium acetate, polyacrylic acid–NaBr mixtures and filter paper. They also used a spectrofluorimeter equipped, in this case, with a phosphorescence rotary chopper. The relative fluorescence and phosphorescence quantum yields were obtained by the use of a standard, and they also evaluated the reflectance and the remission function for standard and analyte. However, the dependence of the intensity of emission on the relative amount of light absorbed by the adsorbed compound and substrate remained unclear.

We recently reported on oxazine fluorescence emission of the dye adsorbed on microcrystalline cellulose, in the absence and presence of a triplet sensitizer, benzophenone.[7] The data gave evidence for a linear correlation between I_F and the fraction of the exciting radiation absorbed by the dye, but only in a region where dimer formation is negligible. In terms of concentration, we detected a I_F vs. $\sqrt{c}$ dependence.[7] In that paper we did not determine the ϕ_F value for the oxazine adsorbed on microcrystalline cellulose.

In this paper we present a study to evaluate ϕ_F for two dyes, R6G and AURO adsorbed on microcrystalline cellulose using R101 as a reference compound. R101 is a rigid molecule with unitary fluorescence quantum yield ($\phi_F = 1.00 \pm 0.02$),[8,9] which does not vary with temperature and solvent,[9] and was recently recommended as a standard for ϕ_F determinations.[9,10]

rhodamine 101

rhodamine 6 G

auramine O
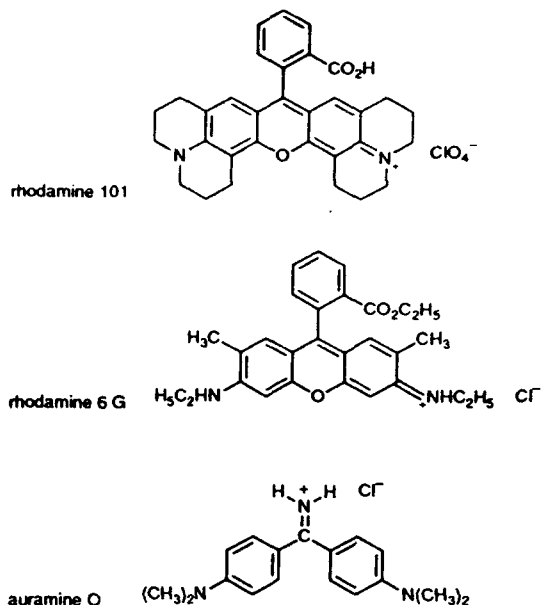
Experimental

Materials and Sample Preparation

R6G chloride was purchased from Merck (Merck, for microscopy), and was recrystallised three times from dimethylformamide. Its purity was checked by chromatographic methods (TLC, one spot on Kieselgel 60 F_{254} Merck) and also by recording UV–VIS spectra. The same procedure was adopted for AURO (Aldrich). R101 was a laser-dye grade product from Exciton and was used as supplied after checking its molar absorption coefficients by measuring UV–VIS absorption spectra. Ethanol was spectroscopic grade (Romil Chemicals).

Microcrystalline cellulose (Aldrich, with 20 µm average particle size) was used as a solid substrate after drying it in a vacuum oven at 70 °C for at least 24 h before sample preparation. A known amount of the dye dissolved in ethanol was added to the previously dried cellulose and the resulting suspension was stirred periodically and allowed to evaporate slowly. The final traces of solvent were removed by placing the samples in a heated vacuum oven at 60 °C for ca. 12 h.

Several samples with low and high loadings of each of the dyes were submitted to a nitrogen atmosphere for 12–24 h before experiments were performed. Fluorescence emission spectra of these samples were compared with those obtained from air-equilibrated samples and no differences were found. All further experiments were of air-equilibrated samples. Similar results, giving evidence for the absence of oxygen quenching on the triplet decay of triplet oxazine and benzophenone adsorbed on cellulose, have been reported previously[7,11] and reflect a large decrease in mobility of oxygen in cellulose.

Steady-state Fluorescence Emission Spectra

Steady-state fluorescence emission studies of powdered samples were performed at room temperature $(20 \pm 1\,^{\circ}\mathrm{C})$ using a home-made fluorimeter specially designed for front surface studies. A detailed description of this apparatus is given in ref. 3. A very accurate energy profile for excitation was determined for the UV, VIS and near-infrared region using appropriate quantum counters for all of these regions.[3] This curve is needed for corrections using the parameter

$I^s_0(\lambda_e)/I^u_0(\lambda_e)$ which is the relative intensity of the exciting light at the excitation wavelength for the standard sample s or for the unknown sample u.[3] The same curve is used to obtain corrected excitation spectra. Details of the method adopted to obtain fully corrected fluorescence spectra irrespective of the apparatus that is being used is also given in ref. 3.

Ground-state Absorption Studies

Ground-state absorption spectra of powdered solid samples were obtained using a Pye Unicam SP8250 with a diffuse reflectance attachment (120 mm diameter integrating sphere, internally coated with a standard white reflectance paint from Kodak). The calibration of the system was performed in the following way: a perfect reflector (100% reflection, $R = 1$) was obtained by the use of barium sulphate (Aldrich 99.999%). As a black standard we used very finely divided carbon black (Cabot 2000), this sample gave 0% reflectance $(R = 0)$. The reflectivity for each sample was obtained by scanning the excitation monochromator from 250 to 900 nm, and the remission function $F(R)$ was obtained by calculating the Kubelka–Munk function for optically thick samples, i.e. those where any further increase of the sample does not affect R:[12-14]

$$F(R) = \frac{(1-R)^2}{2R} = \frac{K}{S} \tag{1}$$

K and S are the absorption and scattering coefficients with dimension $(\text{distance})^{-1}$, and for an ideal diffuser, where the radiation has the same intensity in all directions, $K = 2\varepsilon c$.[14] The remission function is a linear function of the concentration of homogeneous absorbers and it follows that the experimentally determined $F(R)$ is:

$$F(R)_{\text{total}} = \left(\sum_i 2\varepsilon_i c_i + K_{\text{B}}\right)/S \tag{2}$$

where K_{B} is the absorption coefficient of the substrate and the subscript i refers to every absorbing species adsorbed on the substrate.[7] The experimental observable is then:

$$\begin{aligned} F(R)_{\text{dye}} &= [F(R)_{\text{total}} - F(R)_{\text{cellulose}}] \\ &= \sum_i 2\varepsilon_i c_i/S \end{aligned} \tag{3}$$

which predicts a linear relation for the remission function of the dye as a function of concentration (for a constant scattering coefficient) if the dye does not aggregate. The formation of dimers (or higher aggregated forms of the dye) may be studied by the use of eqn. (3), and considering at the same time the excitation of other aggregated forms. Considering only dimer formation, one may easily obtain:[7]

$$F(R)_{\text{dye}} = [c_{\text{M}}(2\varepsilon_{\text{M}} - \varepsilon_{\text{D}}) + \varepsilon_{\text{D}}c_0]/S \tag{4}$$

with

$$c_{\text{M}} = \left(\frac{c_0}{2K_{\text{D}}} + \frac{1}{16K_{\text{D}}^2}\right)^{1/2} - \frac{1}{4K_{\text{D}}} \tag{5}$$

where c_0, c_{M} and c_{D} are the total, monomer and dimer concentrations, respectively, and K_{D} is the equilibrium constant for the monomer–dimer equilibrium $(K_{\text{D}} = c_{\text{D}}/c_{\text{M}}^2)$. Obviously, the total concentration c_0 is related to c_{M} and c_{D} by

$$c_0 = c_{\text{M}} + 2c_{\text{D}} \tag{6}$$

and for very dilute samples $c_0 = c_{\text{M}}$, whereas for very concentrated samples c_{D} approaches $c_0/2$. Equations formally analogous to eqn. (4)–(6) can be used to analyse the possible existence of trimers, tetramers or higher aggregated forms of the dye.

Eqn. (1)–(6) were used in the present work to analyse ground-state absorption data for R101, R6G and AURO adsorbed on microcrystalline cellulose and revealed the existence of dimer formation for R101 and R6G, as will be shown below.

Fluorescence Quantum Yield Determination for Dyes adsorbed on Microcrystalline Cellulose

The intensity of fluorescence, I_F, of a fluorescent compound adsorbed on a solid is related to the concentration of the dye through R^{λ_e}, the reflectance that can be experimentally evaluated at the excitation wavelength λ_e. In fact I_F depends on $I_0^{\lambda_e}(1 - R^{\lambda_e})$ which is the fraction of the exciting light $I_0^{\lambda_e}$ absorbed at the excitation wavelength, and is given by:[7,13,15]

$$I_F = C\phi_F I_0^{\lambda_e}(1 - R^{\lambda_e})f \qquad (7)$$

where C is a constant which depends on the apparatus geometry and ϕ_F is the fluorescence quantum yield of the adsorbed species. f is defined by:

$$f = \frac{F(R^{\lambda_e})_{\text{emitting species}}}{F(R^{\lambda_e})_{\text{total}}} \qquad (8)$$

and is the fraction of the exciting light that is absorbed by the dye in the form of monomer, dimer (or other aggregation form) or all together, meaning total absorption of light by the dye in the latter case. Using the superscripts u and s to refer to the unknown and standard samples and I_F as the integrated area under the corrected emission spectra, we may write

$$\phi_F^u = \phi_F^s \frac{I_F^u}{I_F^s} \frac{(1 - R_s^{\lambda_e})f^s}{(1 - R_u^{\lambda_e})f^u} \frac{I_0^s(\lambda_e)}{I_0^u(\lambda_e)} \qquad (12)$$

where $I_0^s(\lambda_e)/I_0^u(\lambda_e)$ can be easily obtained provided the energy profile of the system is accurately determined.[3] This ratio is reduced to unity if the standard sample and unknown sample are excited at the same wavelength.

Eqn. (12) can easily be applied for the fluorescence quantum yield evaluation for dyes adsorbed on a substrate (microcrystalline cellulose, in the present case) provided a study of the ground-state absorption of the dye is performed, namely the evaluation of the remission function and reflectance for the standard and unknown sample at the excitation wavelengths.

A more careful evaluation of ϕ_F^u can be made using not only one sample for u and one sample for s, but plotting I_F as a function of $(1 - R^{\lambda_e})f$ for both cases. The slope for the unknown compound will be $CI_0^{\lambda_e}(\lambda_e^u)\phi_F^u$ and for the standard $CI_0^{\lambda_e}(\lambda_e^s)\phi_F^s$. It follows that ϕ_F^u will be known provided a value for ϕ_F^s is available. The accuracy for ϕ_F determination will improve since the calculation will be based on a ratio of slopes obtained with several samples and not only on a single sample, as will be seen below.

This method is based on the assumption that R101 has a fluorescence emission quantum yield of 1.00 ± 0.02 when adsorbed on cellulose; this means that we assume that it re-emits absorbed light with the same efficiency as in solution where $\phi_F(R101) = 1.00 \pm 0.02$.[8-10] This assumption is realistic if one considers that usually the non-radiative decay rate of molecules decreases whenever structural or environmental rigidity is imposed on a molecule. Rigid and planar molecular structures usually favour high emission rates. As a consequence, lifetimes and quantum yields of luminescence increase for structurally rigid compounds,[9] or when compounds are adsorbed on rigid substrates.[7] This behaviour is documented experimentally. As an example, R101 in ethanol has $\phi_F = 1.00 \pm 0.02$ independent of temperature and solvent

while rhodamine B (RB) in ethanol only reaches a unitary ϕ_F at low temperatures[8,9] while oxazine triplet has a lifetime of ca. 14.5 µs in acetonitrile and lives for ca. 4.3 ms when adsorbed on cellulose.[7]

Results and Discussion

Ground-state Absorption Spectra of the Dyes adsorbed on Microcrystalline Cellulose

The ground-state absorption spectra of R101 adsorbed on cellulose are shown in Fig. 1(a); all curves are normalised at the maximum absorption at 580 nm. Increasing loadings of the adsorbed dye produce an increase in the 545 nm band due to aggregation. Assuming dimer formation and using eqn. (3)–(6) it was possible to obtain a dimerization equilibrium constant, using $F(R)_{\text{dye}}$ curves for concentrations ranging from 0.015 to 5.8 µmol g^{-1}. K_D in this case is 0.4×10^6 g mol^{-1}. The monomer absorption coefficient was taken as that obtained at low loading of R101, and the final monomer and dimer curves are shown in Fig. 1(b).

Similar results for R6G are presented for $F(R)_{\text{dye}}$ normalised at 530 nm in Fig. 2(a) and for monomer and dimer spectra in Fig. 2(b). The value of K_D in this case is 1.3×10^6 g mol^{-1}.

For AURO, the $F(R)_{\text{dye}}$ curves show no evidence of dimer formation (Fig. 3) since the normalised $F(R)_{\text{dye}}$ curves are
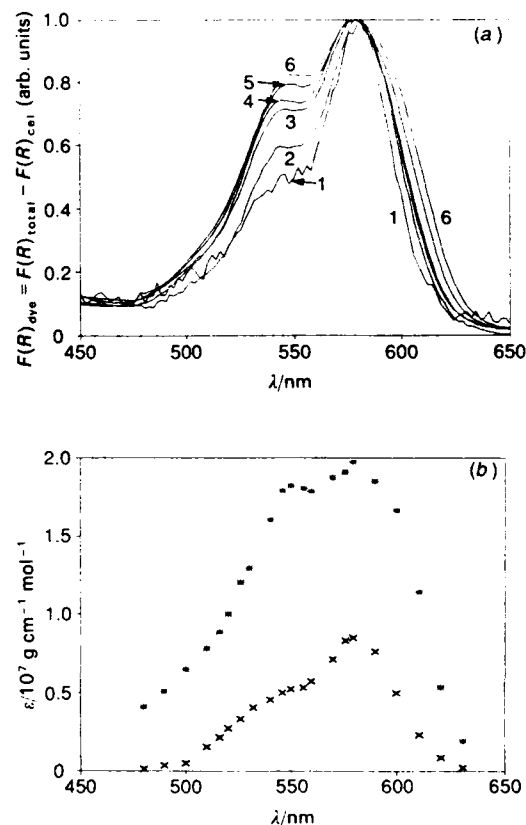

Fig. 1 (a) Remission function values for R101 adsorbed on microcrystalline cellulose for (1) 1.5×10^{-8}, (2) 8.5×10^{-8}, (3) 4.3×10^{-7}, (4) 6.1×10^{-7}, (5) 1.2×10^{-6}, (6) 5.8×10^{-6} mol (dye) g^{-1} of the substrate. The data are normalized to the maximum value of the remission function. (b) Ground-state absorption spectra for the monomer (×) and dimer (•) of R101 adsorbed on microcrystalline cellulose. $K_D = 0.4 \times 10^6$ g mol^{-1}

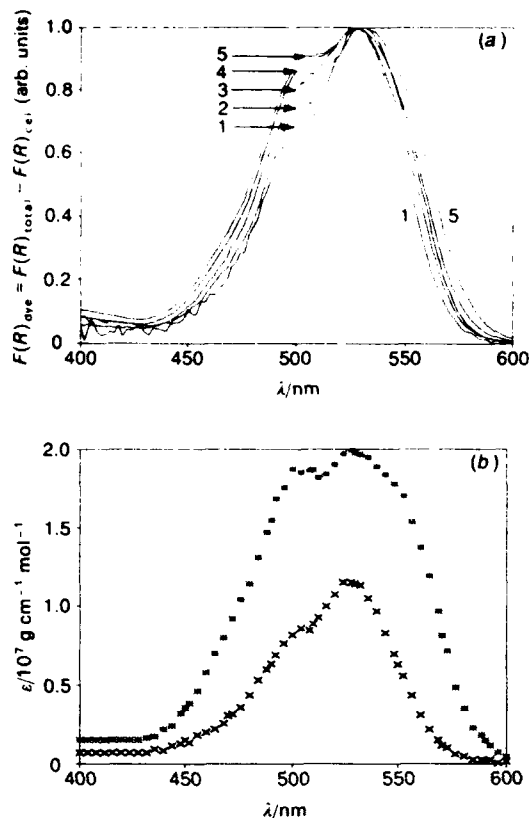**Fig. 2** (a) Remission function values for R6G adsorbed on microcrystalline cellulose. The concentrations of the dye are: (1) 1.0×10^{-7}, (2) 5.1×10^{-7}, (3) 7.3×10^{-7}, (4) 3.6×10^{-6}, (5) 7.3×10^{-6}, mol g^{-1} substrate. The data are normalized to the maximum value of the remission function. (b) Ground-state absorption spectra for the monomer ($\times$) and dimer ($\bullet$) of R6G adsorbed on microcrystalline cellulose. $K_D = 1.3 \times 10^6$ g mol^{-1}

almost superimposed within experimental error in the 0.050–8.2 μmol g^{-1} range. This is certainly connected with the lack of rigidity of the molecule which does not favour association.

Cellulose has a large number of OH groups in the polymer chain and can form hydrogen bonds both within its own structure and also with molecules attached to it;[16] this leads to the creation of a rigid environment for the adsorbed
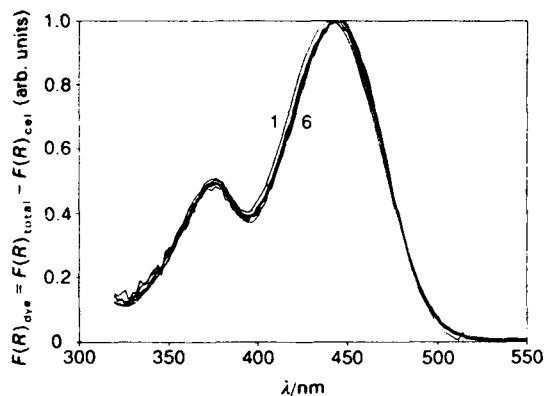

Fig. 3 Remission function values for AURO adsorbed on microcrystalline cellulose for (1) 1.7×10^{-7}, (2) 2.6×10^{-7}, (3) 5.0×10^{-7}, (4) 1.3×10^{-6}, (5) 4.9×10^{-6}, (6) 8.2×10^{-6} mol g^{-1} substrate. The data are normalized to the maximum value of the remission function

species. Cellulose also has a large capacity for fixing molecules that contain substituents capable of localised interactions including the amino groups that exist in R101, R6G and AURO and the carboxyl or carboxylate groups of R101 and R6G.

The extent of aggregation in R101 and R6G depends on dye substrate interactions, but one has to consider also the specific interactions within the natural polymer as well as dye interactions and molecular structure.

R6G aggregates more than R101 as can be seen by the values obtained for the equilibrium constant K_D. This is in accordance with the results obtained for aggregation of R6G and RB in water [K_D(R6G) $= 6.5 \times 10^6$ mol^{-1} g, K_D(RB) $= 1.4 \times 10^6$ mol^{-1} g in water[17,18]]. In ethanol the aggregation still occurs but with a decrease of about three orders of magnitude.[19] RB is identical with R101 from the point of view of the carboxyl group, the only difference being the rigidity of the structures due to the linking of the amino groups to the rest of the molecule. The different aggregation of R101 and R6G is possibly associated with the hydrophobic nature of the methyl groups attached to the chromophoric ring as well as the difference in solvation around the mono- and diethylamino groups as was found for R6G and RB in water.[18]

We can therefore conclude that aggregation of R6G and R101 on microcrystalline cellulose occurs to a degree comparable to that in water, and much higher than in ethanol. Dyes have a general tendency to aggregate in water rather than in organic solvents.[9] Thus cellulose is also a medium which facilitates a high degree of association.

The dimer absorption spectra shown in Fig. 1(b) and 2(b) for R101 and R6G are similar, showing that the low-energy band is the most intense in both cases. A discussion about structures of the aggregates of these and other rhodamines adsorbed on microcrystalline cellulose in terms of exciton theory will be presented in a future publication.

Fluorescence Emission Studies of the Dye adsorbed on Microcrystalline Cellulose

Corrected fluorescence emission spectra of R101, R6G and AURO are presented in Fig. 4–6. There is a strong dependence on the amount of dye adsorbed on microcrystalline cellulose and clearly two different types of behaviour can be detected for the rhodamines, corresponding to parts (a) and (b) of each figure. For low loadings of these dyes I_F increases with concentration until it reaches a maximum. A plateau region is achieved at different loadings, depending on the dye. For the rhodamines the maximum is at ca. 0.5–1 μmol g^{-1} as can be seen in Fig. 4 and 5, but for AURO the fluorescence intensity continues to increase up to ca. 10 μmol g^{-1}.

In each case a strong reabsorption effect is noticeable, causing a bathochromic shift of the maximum. Fig. 4(c), 5(c) and 6(b) show the importance of this effect for the three dyes. Similar results were observed by us[3,4] for solutions of other dyes in ethanol and CH$_2$Cl$_2$, and by other authors[20] for concentrated solutions of oxazine in ethylene glycol and also for oxazine adsorbed on cellulose.[7] As will be discussed later, the effect here can be explained as being due to reabsorption, and no additional fluorescence bands which could be ascribed to the formation of molecular aggregates were found.

Fig. 5(a)–(c) show that the behaviour of R6G as a function of surface loading is very similar to that of R101 and that in this case also no dimer emission is observed. At low loading (from 5×10^{-9} mol g^{-1} to ca. 1×10^{-6} mol g^{-1}) I_F (the total area of the emission spectrum) shows an approximate square root dependence on c_0. This behaviour is expected if we consider that the I_F is dependent on the amount of light adsorbed by the sample, i.e. $I_0'(1 - R^\lambda)f$ as defined above.
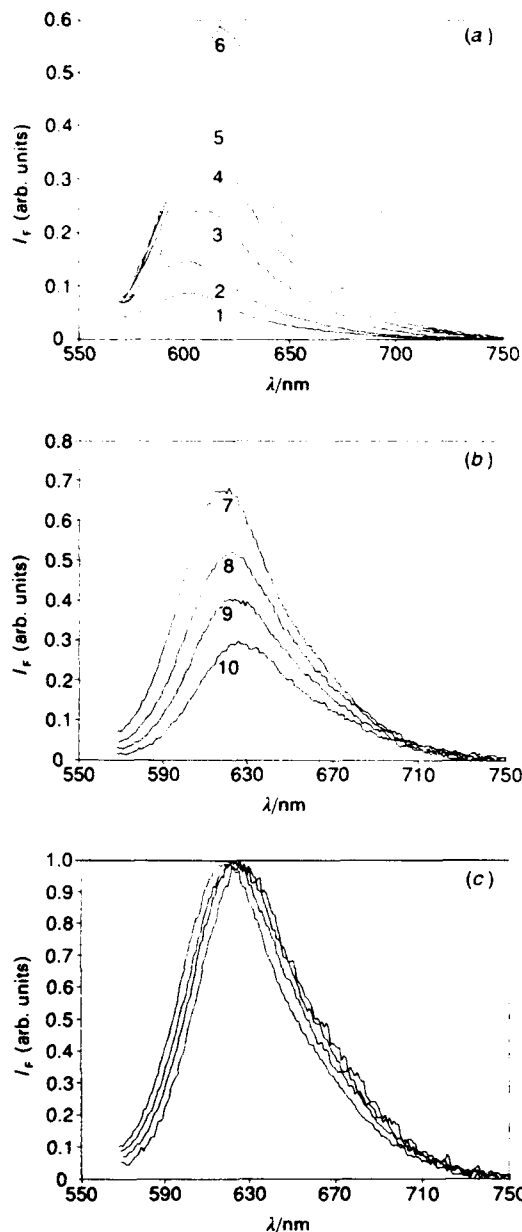
Fig. 4 (a) Corrected fluorescence emission spectra of R101 adsorbed on microcrystalline cellulose and excited at 560 nm. The concentration of the dye is: (1) 8.5×10^{-9}, (2) 1.5×10^{-8}, (3) 4.3×10^{-8}, (4) 8.5×10^{-8}, (5) 1.7×10^{-7}, (6) 4.3×10^{-7} mol g^{-1} substrate. (b) Corrected fluorescence emission spectra of R101 adsorbed on microcrystalline cellulose excited at 560 nm. The concentration of the dye is: (7) 6.0×10^{-7}, (8) 1.2×10^{-6}, (9) 2.7×10^{-6}, (10) 5.5×10^{-6} mol g^{-1} substrate. (c) As for (b), normalized to the maximum emission
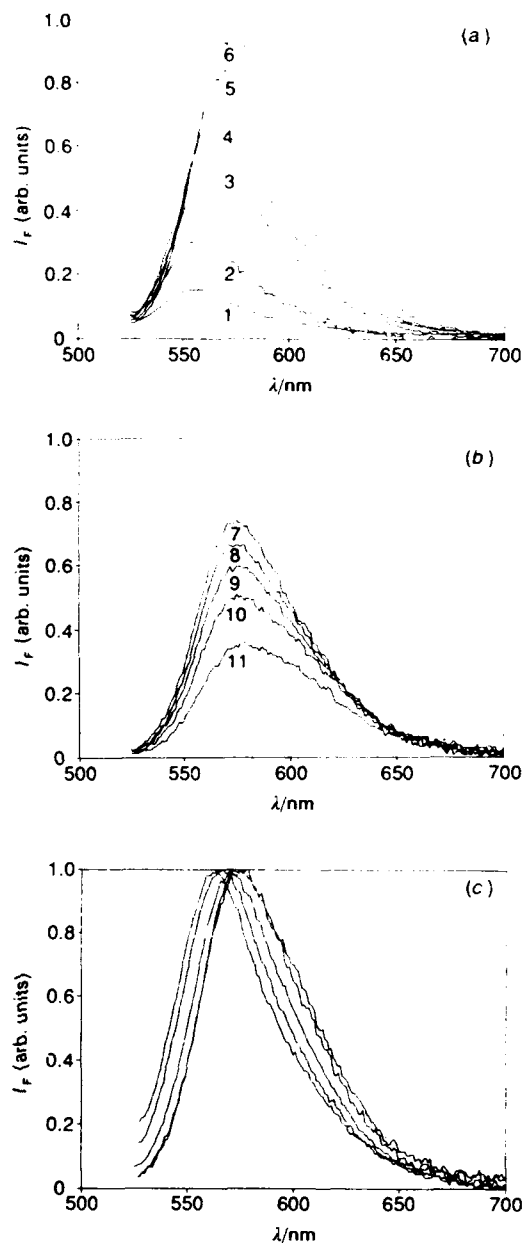
Fig. 5 (a) Corrected fluorescence emission spectra of R6G adsorbed on microcrystalline cellulose and excited at 515 nm. The concentration of the dye is: (1) 1.0×10^{-8}, (2) 2.5×10^{-8}, (3) 1.0×10^{-7}, (4) 2.5×10^{-7}, (5) 5.0×10^{-7}, (6) 7.5×10^{-7} mol g^{-1} substrate. (b) Corrected fluorescence emission spectra of R6G adsorbed on microcrystalline cellulose excited at 515 nm. The concentration of the dye is: (7) 2.0×10^{-6}, (8) 3.0×10^{-6}, (9) 4.0×10^{-6}, (10) 5.0×10^{-6}, (11) 7.5×10^{-6} mol g^{-1} substrate. (c) As for (b), normalized to the maximum emission

Since the concentration of the sample, c_0, the reflectivity of the sample, R, and the reflectivity of the background, R_B, are related by the Kubelka–Munk equation[12,13] for optically thick samples by

$$\frac{(1 - R^{\lambda})^2}{2R^{\lambda}} - \frac{(1 - R_B^{\lambda})^2}{2R_B^{\lambda}} = \frac{2\varepsilon c_0}{S} \qquad (13)$$

and for samples of low concentration $R^{\lambda} \approx 1$, when R_B^{λ} is also close to unity, it follows that

$$I_F^{\lambda}(1 - R^{\lambda})f \propto c_0^{1/2} \qquad (14)$$

Considering also eqn. (7) it follows that I_F shows a linear dependence on $\sqrt{c_0}$ for small values of c_0. This dependence was obtained experimentally for AURO (Fig. 7). The same behaviour was also detected for the two rhodamines.

A more general analysis of the dependence of I_F on the concentration has to include the fact that aggregation occurs to a different extent depending on the dye. Fig. 8–10 present data showing not only the dependence of I_F on f_{dye} [see eqn. (7) and (8)] but also the dependence on the fraction of light absorbed by the monomer, which was assumed to be the only
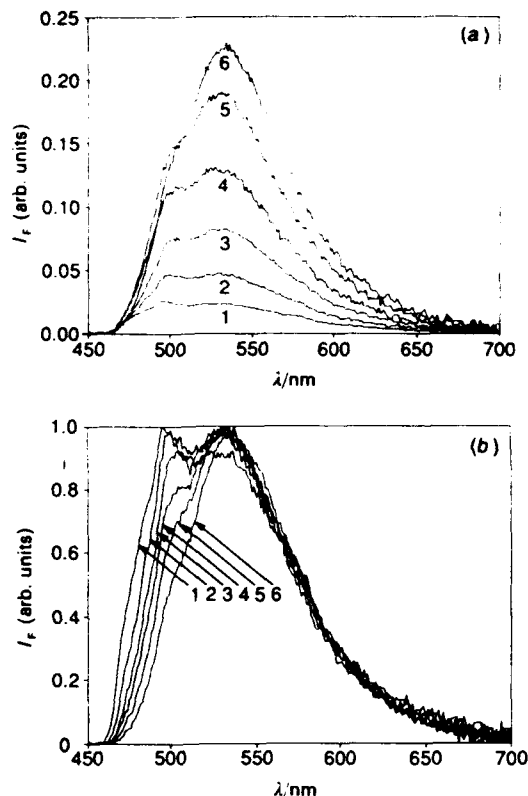
Fig. 6 (a) Corrected fluorescence emission spectra of AURO adsorbed on microcrystalline cellulose and excited at 560 nm. The concentration of the dye is: (1) 2.6×10^{-8}, (2) 7.5×10^{-8}, (3) 1.5×10^{-7}, (4) 1.0×10^{-6}, (5) 2.6×10^{-6}, (6) 8.2×10^{-6} mol g^{-1} substrate. (b) As for (a), normalized to the maximum emission

fluorescent species, i.e. with

$$I_F = C\phi_F I_0^{\lambda}(1 - R^{\lambda_e}) \frac{F(R^{\lambda_e})_{mon}}{F(R^{\lambda_e})_{total}} \tag{15}$$

For the two rhodamines, I_F vs. $(1 - R^{\lambda_e})f_{dye}$ curves clearly show a initial linear dependence on c_0, followed by a plateau region, and finally I_F decreases with the increase of dimer formation. However, if we plot I_F vs. $(1 - R^{\lambda_e})f_{mon}$, then for each dye, all experimental points fall onto a straight line, within experimental error.
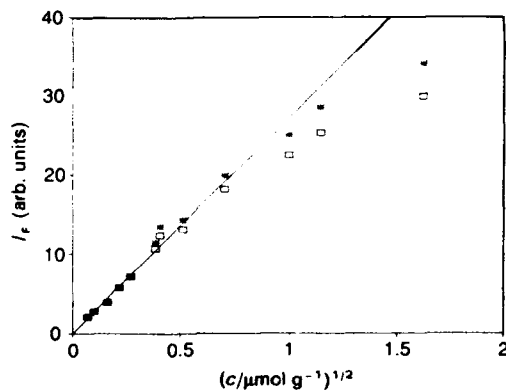

Fig. 7 Intensity of fluorescence of AURO adsorbed on microcrystalline cellulose (measured as the total area under the corrected emission) as a function of the square root of concentration and corrected for the cellulose absorption (□). $\lambda_e = 450$ nm. (•), Corrected data from the reabsorption effect according to eqn. (17)
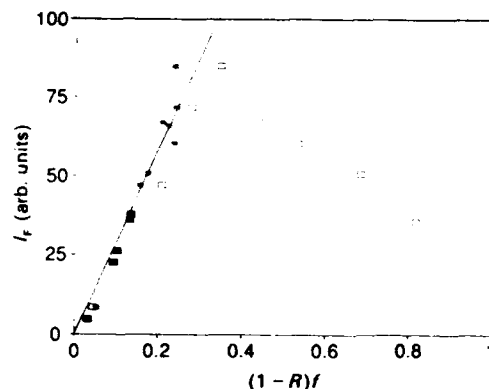

Fig. 8 Intensity of fluorescence of R101 adsorbed on microcrystalline cellulose excited at 560 nm and measured as the total area under the corrected emission as a function of $(1 - R^{\lambda_e})f$ and corrected for the cellulose absorption (□). (•), The same data as a function of $(1 - R^{\lambda_e})f_{mon}$
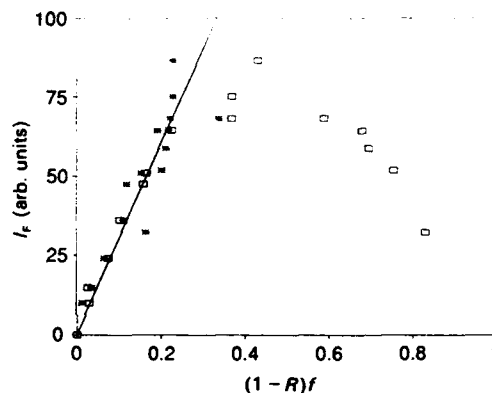

Fig. 9 Intensity of fluorescence of R6G adsorbed on microcrystalline cellulose excited at 515 nm and measured as the total area under the corrected emission as a function of $(1 - R^{\lambda_e})f$ and corrected for the cellulose absorption (□). (•), The same data as a function of $(1 - R^{\lambda_e})f_{mon}$
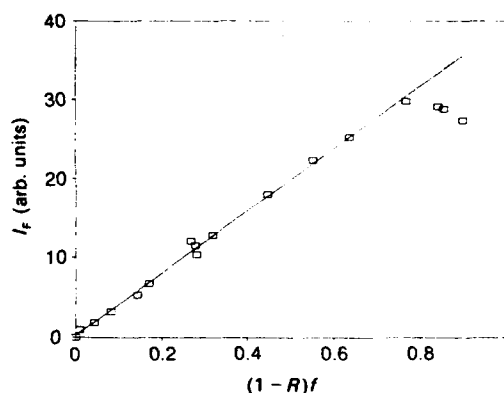

Fig. 10 Intensity of fluorescence of AURO adsorbed on microcrystalline cellulose excited at 450 nm and measured as the total area under the corrected emission as a function of $(1 - R^{\lambda_e})f$ and corrected for the cellulose absorption

For AURO, a plateau is eventually reached, but since no dimer formation occurs the linear dependence as $(1 - R^{\lambda_e})f_{dye}$ is followed up to much higher values of the dye concentration (ca. 10 μmol g^{-1}). The AURO fluorescence spectra presented for samples with high loading [curve 6 of Fig. 6(a)] are

similar to those previously reported for concentrated solutions of this compound in glycerol.[21] However, less concentrated samples of AURO adsorbed on microcrystalline cellulose [curves 1-5 of Fig. 6(a)] give evidence of two distinct bands, which are probably vibrational bands.

As discussed above, we may use the slopes obtained in Fig. 8-10 to determine ϕ_F for R6G and AURO adsorbed on cellulose, assuming ϕ_F to be unity for R101. For R101 the following values were determined:

$$\frac{I_F}{(1 - R^\lambda)f} = C\phi_F = 295 \pm 7 \qquad (16)$$

and for R6G and AURO we obtained 302 ± 10 and 39 ± 1, respectively. Assuming $\phi_F(R101) = 1.00 \pm 0.02$, it follows that $\phi_F(R6G) = 1.02 \pm 0.03$ and $\phi_F(AURO) = 0.13 \pm 0.003$.

R6G chloride has a reported value for ϕ_F of 0.88 in ethanol at room temperature[22] and AURO only presents a significant fluorescence emission in very viscous solvents ($\phi_F = 0.0014$ in glycerol) or when attached to proteins ($\phi_F = 0.022$ to 0.055)[21,23] also at room temperature. Substituted diphenylmethane and triphenylmethane dyes do not fluoresce or fluoresce very slightly except in the cases where the two rings are joined by a bridge as in xanthene dyes.[9,21,24] The restricted rotation of the phenyl groups induced by a viscous solvent (or by an increase of pressure or a decrease of temperature[21]) leads to a decrease in the rate of internal conversion and gives rise to strong fluorescence.

Dried cellulose is a rigid environment for adsorbed dyes and its large capacity for hydrogen bonding stabilises the singlet state, reducing the rate of non-emissive de-excitation. This leads to an increase in the fluorescence emission quantum yield at room temperature, which becomes unitary in the case of R6G chloride and becomes 13% for AURO. In the latter case the increase is 2-3 orders of magnitude when compared with published values for different solvents also at room temperature.[23]

Dissolved molecular oxygen does not give rise to quenching in dried samples, in accordance with previous results for other compounds adsorbed on cellulose.[7,25]

Fig. 4(c), 5(c) and 6(b) clearly show the existence of a re-absorption effect, which can be analysed using an equation derived by Birks[26] that relates the experimentally determined fluorescence emission quantum yield $(\phi_F)_{exp}$ with ϕ_F, using the parameter a, the probability of self-absorption of an emitted photon:

$$(\phi_F)_{exp} = \frac{\phi_F(1 - a)}{1 - a\phi_F} \qquad (17)$$

More elaborate treatments were developed (see ref. 3 and papers quoted there), but for the present discussion the simple treatment is sufficient, i.e. with measured amount of fluorescence $(\phi_F)_{exp}$ as given by eqn. (17).

When considering the case of dyes adsorbed on solids a must also take into account the fact that usually the substrate also absorbs slightly in the emission range of the dye. If $\phi_F = 1$ it follows from eqn. (17) that if the substrate does not absorb then $(\phi_F)_{exp} = \phi_F$. This means that the integrated area under the corrected emission spectrum is a direct evaluation of ϕ_F. The displacement of the emission of R101 and R6G to the red, as shown in Fig. 4(c) and 5(c) (where the emission spectra are normalised to their maximum) can be explained by reabsorption and re-emission effects, but ϕ_F values remain unchanged. For AURO, Fig. 6(b) shows that the decrease of the 495 nm band due to the reabsorption effect is particularly important for loadings > 1 μmol g⁻¹. For this dye and using eqn. (17) and curves from Fig. 6(b) we estimate a correction of ca. 11% due to reabsorption, and finally $\phi_F \approx 0.14 \pm 0.01$.

We felt justified before we made these studies in choosing R101 as a standard for fluorescence yield determinations with ϕ_F equal to unity because it already has a value of 1.00 in fluid media. This choice is now confirmed since we have shown here that the fluorescence yields of R101 and R6G are the same when adsorbed as monomers on microcrystalline cellulose. The most likely explanation for this is that for both compounds in the adsorbed state the quantum yield of fluorescence reaches the limiting value of one, i.e. $\phi_F = 1$.

Conclusions

Using R101 as a standard for fluorescence emission quantum yield determinations, the fluorescence emission quantum yields of R6G and AURO were determined as 1.02 ± 0.03 and 0.14 ± 0.01, when all of the dye was adsorbed on microcrystalline cellulose and the sample was at room temperature. For dried cellulose the results are the same for air-equilibrated or nitrogen-purged samples. The increase in ϕ_F for both dyes when compared with ϕ_F values in solution is due to the restricted movement of the dyes in the adsorbed state, which decreases the rate of radiationless deactivation.

A strong aggregation effect was detected for the two rhodamines in the ground state when adsorbed on microcrystalline cellulose, and this was interpreted as being due to dimer formation. The equilibrium constants for the ground-state equilibrium and the dimer absorption spectra were evaluated in both cases. These dimers were shown to be non-fluorescent. By contrast AURO does not aggregate for concentrations ranging from nanomoles of dye per gram of cellulose up to ca. 10 μmol g⁻¹.

This method for determining the quantum yields of fluorescence of dyes adsorbed on surfaces using a rigid molecule as a standard (R101) has been established here using powdered cellulose as the solid substrate. In addition it can be applied to other solid substrates, provided the remission function is determined for the dye adsorbed on each specific substrate.

References

1 J. B. Birks, J. Res. Natl. Bur. Stand., 1976, **80A**, 389.
2 J. M. Demas and G. A. Crosby, J. Phys. Chem., 1971, **75**, 991.
3 L. F. Vieira Ferreira, S. B. Costa and E. J. Pereira, J. Photochem. Photobiol. A: Chem., 1990, **55**, 361.
4 L. F. Vieira Ferreira and S. B. Costa, J. Lumin., 1991, **48 & 49**, 395.
5 M. S. Wrighton, D. S. Ginley and D. L. Morse, J. Phys. Chem., 1974, **78**, 2229.
6 S. M. Ramasamy, V. P. Senthilnathan and R. J. Hurtubise, Anal. Chem., 1986, **58**, 612; G. J. Burrel and R. J. Hurtubise, Anal. Chem., 1987, **59**, 965.
7 F. Wilkinson, P. A. Leicester, L. F. Vieira Ferreira and V. M. M. R. Freire, Photochem. Photobiol., 1991, **54**, 599. F. Wilkinson, G. P. Kelly, L. F. Vieira Ferreira, V. M. M. R. Freire and M. I. Ferreira, J. Chem. Soc. Faraday Trans., 1991, **87**, 547.
8 T. Kartens and K. Knobs, J. Phys. Chem., 1980, **84**, 1871.
9 K. H. Drexhage, J. Res. Natl. Bur. Stand., 1976, **80A**, 421; K. H. Drexhage, Dye Lasers, ed. F. P. Shafer, Top. Appl. Phys., vol. 1, Springer, Berlin, 1973, p. 144.
10 D. F. Eaton, J. Photochem. Photobiol., B: Biol., 1988, **2**, 523.
11 P. P. Levin, L. F. Vieira Ferreira and Silvia M. B. Costa, Chem. Phys. Lett., 1990, **173**, 227; F. Wilkinson and L. F. Vieira Ferreira, J. Lumin., 1988, **40 & 41**, 704.
12 P. Kubelka, J. Opt. Soc. Am., 1948, **38**, 448.
13 G. Kortum, W. Brown and G. Herzog, Angew. Chem., Int. Ed., Engl., 1963, **2**, 333.

14 F. Wilkinson and G. P. Kelly, in *Handbook of Organic Photo-chemistry*, ed. J. C. Scaiano, CRC Press, Boca Raton, 1989, vol. 1, p. 293.

15 R. W. Kessler, G. Krabichler, S. Uhl, D. Oelkrug, W. P. Hagen, J. Hysslop and F. Wilkinson, *Opt. Acta*, 1983, 30, 1099.

16 P. Wollenweber, in *Thin-layer Chromatography*, ed. E. Stall, Allen & Unwin/Springer-Verlag, 2nd edn., 1969, p. 32.

17 P. R. Ojeda, 1. A. K. Amashja, J. R. Ochoa and I. Lopez Arbeloa, *J. Chem. Soc., Faraday Trans. 2*, 1988, 84, 1.

18 F. Lopez Arbeloa, Y. R. Liebana, E. C. Fernandez and I. Lopez Arbeloa, *Spectrochim. Acta, Part A*, 1988, 45, 253.

19 F. Lopez Arbeloa, P. R. Ojeda and I. Lopez Arbeloa, *Chem. Phys. Lett.*, 1988, 148, 253.

20 U. Kopf and J. Heinze, *Anal. Chem.*, 1984, 16, 1931.

21 G. Oster and Y. Nishijima, *J. Am. Chem. Soc.*, 1956, 78, 1581.

22 J. Olmsted III, *J. Phys. Chem.*, 1979, 83, 2581.

23 R. F. Chen, *Arch. Biochem. Biophys.*, 1977, 179, 672.

24 R. Raue, in *Ullmann's Encyclopedia of Industrial Chemistry*, VCH, New York, 1986, vol. 5, p. 369.

25 J. Murtagh and J. K. Thomas, *Chem. Phys. Lett.*, 1988, 148, 445.

26 J. B. Birks, *Phys Rev.*, 1954, 94, 1567.

PHOTOCHEMISTRY ON SURFACES: TRIPLET–TRIPLET ENERGY TRANSFER ON MICROCRYSTALLINE CELLULOSE STUDIED BY DIFFUSE REFLECTANCE TRANSIENT ABSORPTION AND EMISSION SPECTROSCOPY*

F. Wilkinson[†], P. A. Leicester, L. F. V. Ferreira[‡] and V. M. M. R. Freire[§]
Department of Chemistry, Loughborough University of Technology, Loughborough,
Leicestershire LE11 3TU, England

Abstract—Triplet–triplet energy transfer has been studied between benzophenone and an oxazine dye (2,7-bis(diethyl-amino)-phenazoxonium chloride) co-adsorbed on the surface of microcrystalline cellulose. Ground state absorption and fluorescence measurements provide evidence for dimer formation of the oxazine dye when adsorbed on cellulose in contrast to the behaviour in ethanol solution where no dimerization is observed. The equilibrium constant for dimerization, which is found to be $(1.0 \pm 0.1) \times 10^6$ mol^{-1} $_c$ $(2560 \pm 250$ dm^3 mol$^{-1})$ for oxazine alone on cellulose decreases in the presence of co-adsorbed benzophenone. Fluorescence is detected from excited monomeric but not from excited dimeric oxazine. The absorption spectrum of the triplet state of oxazine adsorbed on cellulose was obtained and its extinction coefficient evaluated relative to that of triplet benzophenone which was used as a sensitizer. The lifetime of adsorbed triplet oxazine is 4.3 ms which is 300 times longer than that in acetonitrile solution.

The efficiency of energy transfer from triplet benzophenone to oxazine on cellulose was studied using both time resolved sensitized absorption and phosphorescence intensity measurements as a function of oxazine concentration. Lifetime measurements show that the energy transfer process involves static quenching since the benzophenone lifetime is independent of oxazine loading at the surface. A mechanism is proposed to explain the results in which one oxazine molecule is suggested as being able to quench phosphorescence from a "pool" consisting of 2 to 3 benzophenone molecules.

INTRODUCTION

The desire to understand primary photochemical processes occurring in heterogeneous environments has led to considerable recent interest in studies of the photophysics and photochemistry of many organic molecules adsorbed on substrates such as silica, alumina, zeolites and semiconductor surfaces. A most convenient technique for studying such systems is diffuse reflectance laser flash photolysis since it can be used to study transient absorption (and emission) in opaque solids (Wilkinson *et al.*, 1990), or at interfaces of powders or microcrystals (Kessler and Wilkinson, 1981; Turro *et al.*, 1985; Kamat and Ford, 1987; Wilkinson and Ferreira, 1988; Levin *et al.*, 1990; Kelly *et al.*, 1990). This enables one to obtain spectroscopic and kinetic information on the excited states of molecules adsorbed at interfaces or within dyed fabrics.

Turro *et al.* (1985) and Wilkinson and Ferreira (1988) have studied triplet energy transfer between molecules co-adsorbed on silica and on cellulose using triplet benzophenone as the donor and naphthalene or one of its derivatives as the energy acceptor. The present study extends this type of investigation to a study of the quenching mechanism of triplet benzophenone by oxazine dyes on the surface of microcrystalline cellulose in order to understand how interactions between the substrate and the dye affect properties such as dye mobility and how the excited state behaviour of these compounds is modified when they are adsorbed on surfaces.

Oxazines are highly fluorescent dyes which are much used as laser dyes (Drexhage, 1973, 1976), as quantum counters in the visible and near IR regions (Kopf and Heinze, 1984) and as dyes in the textile industry (Raue, 1984). They also undergo interesting non-radiative decay processes involving internal conversion in solution associated with the twisting of the amino group (Vogel *et al.*, 1988). In this work we report a study of the excited state properties of the oxazine dye 2,7-bis(diethylamino)-phenazoxonium chloride adsorbed on microcrystalline cellulose as a solid substrate. Cellulose can form hydrogen bonds, both within its own structure and also with other molecules of low molecular weight attached to the polymer by localized interactions

---

(Wollenweber, 1969). Benzophenone co-adsorbed with oxazine on cellulose was used to sensitize the production of considerable amounts of triplet oxazine following triplet–triplet energy transfer.

MATERIALS AND METHODS

Materials and sample preparation. The oxazine dye 2,7-bis(diethylamino)-phenazoxonium chloride was recrystallized three times from dimethylformamide and its purity checked using chromatographic methods as well as IR, UV and visible absorption spectra. Acetonitrile (Aldrich Gold Label, Dorset, England) was used as supplied. Microcrystalline cellulose (Fluka DS-O, Buchs, Switzerland, with 50 μm average particle size) was used as the solid substrate. Microcrystalline cellulose is a mechanically disintegrated cellulose produced by hydrolysing purified cellulose for 15 min in 2.5 M HCl at 105 ± 1°C. The resulting product is a pure form of cellulose free from organic and inorganic contaminants and with a high degree of crystallinity. The microcrystalline aggregates range in diameter from 300Å to about 50 μm and are rod-like or lamellar in shape. The specific internal area of this type of cellulose varies from 10 to 200 m²/g depending on the particle size (Battista, 1965; Krassig, 1986).

Sample preparation was as follows. The microcrystalline cellulose was dried in a vacuum oven at 70°C for at least 24 h prior to use. Since cellulose readily adsorbs considerable amounts of water this treatment was necessary to give reproducible results. The dye and/or benzophenone was dissolved in acetonitrile and a known amount of this solution was added to the previously dried cellulose after suspending it in the solvent. The resulting suspension was stirred periodically and allowed to evaporate slowly. After several hours the removal of the final traces of solvent was effected by placing the sample in a heated vacuum oven at 70°C for about 12 h.

Several samples with low and high loadings of the dye and benzophenone were exposed to an atmosphere of nitrogen gas for times varying from 2 to 24 h before experiments were performed. Data obtained with these samples were compared with those obtained from air-equilibrated samples. Since no differences were found, within experimental error, all further experiments used air equilibrated samples.

Ground state absorption and steady-state emission studies. Ground state absorption spectra of solid samples were obtained using a Pye Unicam SP 8250 or a Shimadzu UV 260 spectrophotometer with a diffuse reflectance attachment. Steady-stage fluorescence and phosphorescence emission studies were performed at room temperature using a home-made fluorimeter. A more detailed description of this apparatus is given elsewhere (Ferreira *et al*., 1991). Corrected emission and excitation spectra could be determined either in the ultra-violet or visible regions.

Time resolved diffuse reflectance transient absorption and emission studies. Time-resolved diffuse reflectance laser flash photolysis experiments were carried out exciting and analysing at the front face of a normal rectangular quartz cell containing the microcrystalline samples. The laser pulse at 354 nm was from a HyperYAG 200 Lumonics laser, the output from which was frequency tripled to give a 22 mJ pulse with a pulse width of 8 ns. The monitoring source was a pulsed 250 W xenon lamp from Applied Photophysics. The detector was a Hamamatsu R928 photomultiplier, which was sensitive up to ~900 nm and the output signal from this was fed into a Tektronix 7612 AD transient digitizer interfaced to a microcomputer in order to acquire and store data. Further details of the system as well as a description of the data treatment have already been given by Wilkinson (1986).

RESULTS AND DISCUSSIONS

Ground-state absorption spectra of oxazines adsorbed on cellulose

A simple and widely adopted approach for describing the interaction of light within a dispersing medium is that due to Kubelka and Munk. In this approach two light fluxes, I and J, moving in opposite directions are considered perpendicular to the irradiated surface at $x=0$ where $I=I_0$ and $J=J_0$ and the diffuse reflectance, $R=J_0/I_0$. If K and S are the absorption and scattering coefficients of the diffuse sample, then the attenuation of the incident flux as it penetrates into the sample is given by

$$dI(x) = -I(x)(K+S)dx + J(x)Sdx \qquad (1)$$

and the generated flux, since it travels in the opposite direction, has the opposite sign, *viz*.

$$dJ(x) = J(x)(K+S)dx - I(x)Sdx \qquad (2)$$

Equations (1) and (2) can be solved (Kubelka, 1948) for a layer so thick that any further increase in thickness of the sample does not affect R, in which case

$$\frac{(1-R)^2}{2R} = \frac{K}{S} = F(R) \qquad (3)$$

$F(R)$ is known as the remission function. An ideal diffuser containing absorbers with Naperian absorption coefficients, ϵ_i, and concentrations C_i, has K = $\Sigma_i 2\epsilon_i C_i$. It follows that when S is independent of wavelength, a plot of $F(R)$ *vs* wavelength yields the absorption spectrum of the diffuse reflector (see Kortüm *et al*., 1963; Kessler *et al*., 1983).

The most convenient units for C_M and C_D are mol g⁻¹, and so we can evaluate K_D in units of mol⁻¹ g. Since the precise surface area per gram for microcrystalline cellulose and also the fractal dimension have not been experimentally determined as yet, we can not give K_D with the two dimensional units of dm² mol⁻¹. However since the density of the powder is 400 g dm⁻³ we can quote the equilibrium constant with the equivalent three dimensional units, dm³ mol⁻¹. In so doing we do not wish to imply a fractal dimension of three.

The absorption spectra of the ground state of oxazine adsorbed on cellulose at various loadings of oxazine C_0, are shown in Fig. 1(a). At low loadings these spectra resemble those measured with transmission geometry in alcoholic solution, except that oxazine adsorbed on cellulose shows a bathochromic shift of ~15 nm, see Fig. 1(b). However, with increased loading of the adsorbed dye on cellulose, the band at 610 nm becomes much more prominent as is shown in Fig. 1(b), where the spectra are normalized at the long wavelength peak at 660 nm.

We conclude that dimers or higher aggregates are present within this range of concentrations.
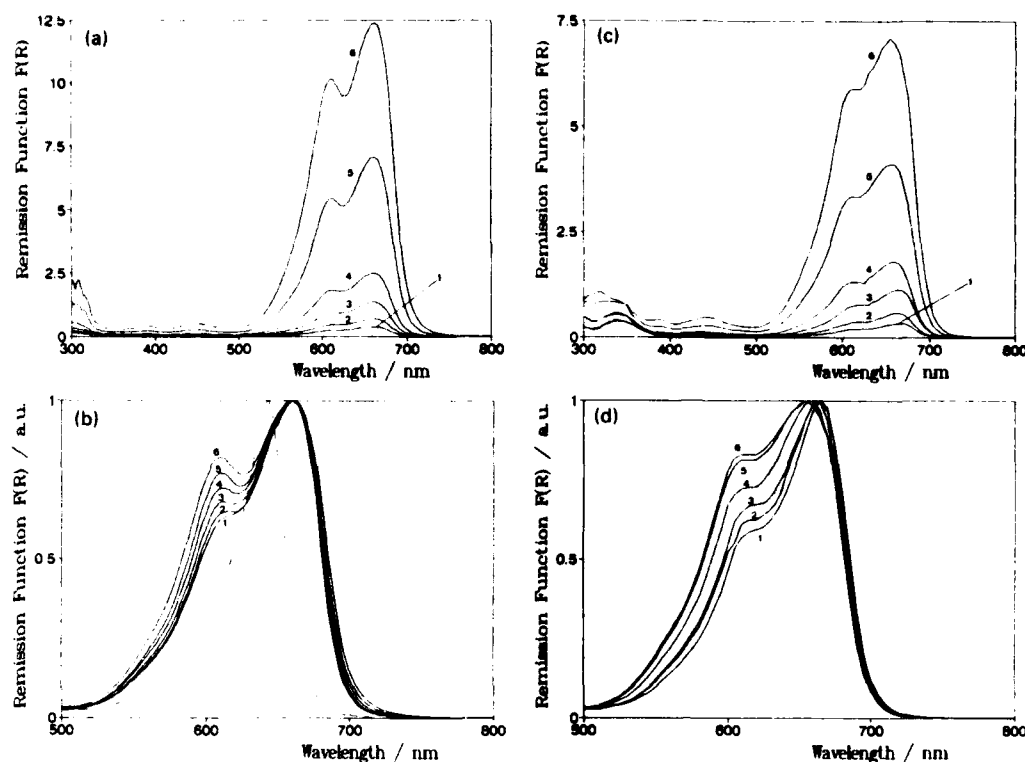
Figure 1(a). Remission function values for oxazine adsorbed on microcrystalline cellulose for (1) 2.5×10^{-7}, (2) 5×10^{-7}, (3) 1×10^{-6}, (4) 2×10^{-6}, (5) 5×10^{-6}, (6) 1×10^{-5} moles of oxazine per gram of the substrate. (b). Same data as in Fig. 1(a) normalized to the maximum value of the remission function. The dashed line is the absorption spectrum of oxazine in ethanol. (c). Remission function values for oxazine and benzophenone coadsorbed on microcrystalline cellulose. The amount of benzophenone is 1.8×10^{-4} mol g^{-1} in all samples. The concentrations of oxazine are (1) 2.5×10^{-7}, (2) 5×10^{-7}, (3) 1×10^{-6}, (4) 2×10^{-6}, (5) 5×10^{-6}, (6) 1×10^{-5} moles per gram of the substrate. (d). Same data as in Fig. 1(c) normalized to the maximum of the remission function.

Assuming only dimer formation, i.e.

$$2M \rightleftharpoons D \qquad (4)$$

with

$$K_D = \frac{C_D}{C_M^2} \qquad (5)$$

where C_M and C_D are the monomer and the dimer concentrations, the remission function is given in terms of C_0 and C_M as

$$F(R) = (C_M (2\epsilon_M - \epsilon_D) + \epsilon_D C_0)/S \qquad (6)$$

and

$$C_M = \left(\frac{C_0}{2K_D} + \frac{1}{16K_D^2}\right)^{\frac{1}{2}} - \frac{1}{4K_D} \qquad (7)$$

Equations (6) and (7) were used to analyse the experimentally determined values of $F(R)$ as a function of the added concentration of oxazine C_0. The scattering coefficient of the cellulose was measured and found to be almost independent of wavelength in the range 500–800 nm with S = 80 cm^{-1}. The monomer spectrum was taken as that obtained at low loadings and this enabled the spectrum of the

dimer to be determined as shown in Fig. 2 with a value of $K_D = (1.0 \pm 0.1) \times 10^6$ mol^{-1} g (2560 $\pm$ 250 mol^{-1} dm^3).

Figures 1(c) and 1(d) show absorption spectra of oxazine in the presence of a fixed concentration of benzophenone. The concentration of benzophenone used was that necessary to produce measurable transient absorption and emission in diffuse reflectance laser photolysis experiments and was much larger than that of oxazine. It is apparent that dimerization still occurs but to a lesser extent. An analysis of the measured values of $F(R)$ in the presence of benzophenone gave $K_D = (3.7 \pm 1.0) \times 10^4$ mol^{-1} g (93 $\pm$ 30 mol^{-1} dm^3) and a dimer spectrum within experimental error equal to that shown in Fig. 2. It is apparent that the high loading of benzophenone on microcrystalline cellulose, which is approaching a monolayer, makes dimer formation by oxazine considerably less likely. Whether this is due to benzophenone–oxazine interactions or simply due to the reduction in the availability of pair sites on the cellulose surface is a topic to which we will return in future studies of ground state interactions of adsorbed dyes. For our purpose here it is suf-
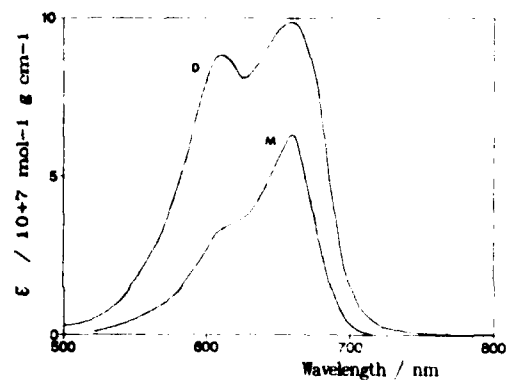
Figure 2. Ground state absorption spectra for the monomer (M) and dimer (D) of oxazine absorbed on microcrystalline cellulose.

ficient to note oxazine dimerization still occurs in the presence of benzophenone but to a lesser extent.

Fluorescence emission studies

Corrected fluorescence spectra from oxazine adsorbed on cellulose at various loadings are shown in Figs. 3(a) and (b). The spectra at low loadings show almost no shift compared with spectra from dilute solutions of oxazine in ethanol. The fluorescence intensity does, however, show a large concentration dependence. At low loadings the intensity of fluorescence, I_F, starts to increase as expected as the fraction of exciting light being absorbed increases according to Eq. (8) (see e.g. Kortüm et al., 1963; Kessler et al., 1983)

$$I_F = G \, \phi_F \, I_o^c (1 - R^c) \, [F(R^c)_{Dye}/F(R^c)_{Total}] \quad (8)$$

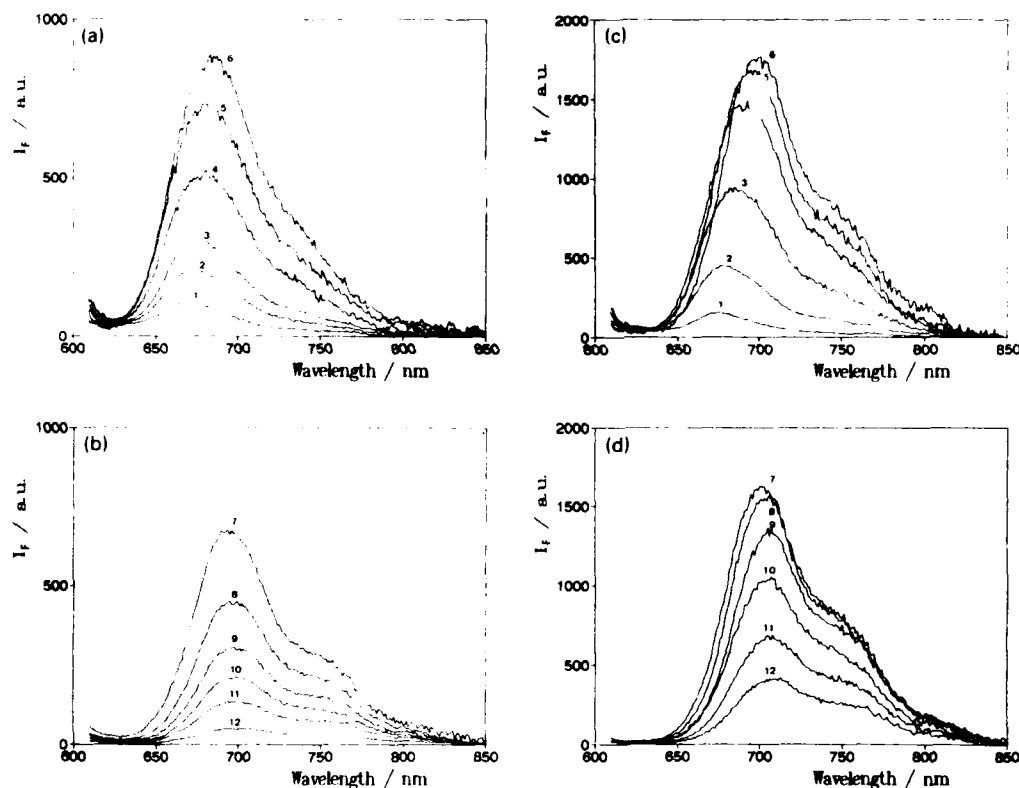
Figure 3(a). Corrected fluorescence emission spectra of oxazine adsorbed on cellulose excited at 600 nm. The concentration of oxazine is: Curve (1) 1 × 10⁻⁹, (2) 5 × 10⁻⁹, (3) 1 × 10⁻⁸, (4) 5 × 10⁻⁸, (5) 1 × 10⁻⁷, (6) 2.5 × 10⁻⁷ moles per gram of the substrate. (b). Corrected fluorescence emission spectra of oxazine adsorbed on cellulose excited at 600 nm. The concentration of oxazine is: Curve (7) 1 × 10⁻⁶, (8) 2 × 10⁻⁶, (9) 3 × 10⁻⁶, (10) 5 × 10⁻⁶, (11) 7.5 × 10⁻⁶, (12) 1 × 10⁻⁵ moles per gram of the substrate. (c). Corrected fluorescence emission spectra of oxazine and benzophenone coadsorbed on cellulose. Excitation is at 600 nm. The concentration of benzophenone is 1.8 × 10⁻⁶ mol g⁻¹ in all samples. The concentration of oxazine is: Curve (1) 1 × 10⁻⁹, (2) 2.5 × 10⁻⁸, (3) 1 × 10⁻⁷, (4) 2.5 × 10⁻⁷, (5) 5 × 10⁻⁷, (6) 1 × 10⁻⁶ moles per gram of the substrate. (d). Corrected fluorescence emission spectra of oxazine and benzophenone coadsorbed on cellulose. Excitation is at 600 nm. The concentration of benzophenone is 1.8 × 10⁻⁶ mol g⁻¹ in all samples. The concentration of oxazine is: Curve (7) 2 × 10⁻⁶, (8) 3 × 10⁻⁶, (9) 4 × 10⁻⁶, (10) 5 × 10⁻⁶, (11) 7.5 × 10⁻⁶, (12) 1 × 10⁻⁵ moles per gram of the substrate.
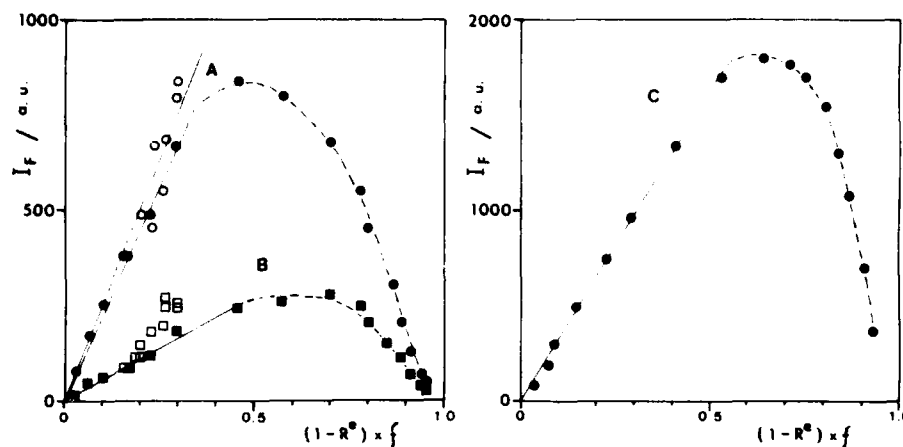
Figure 4. Fluorescence intensity of oxazine measured at (A) 692 nm and (B) 750 nm as a function of $(1-R^c) \times f$ and corrected for the cellulose absorption (solid symbols), and cellulose and dimer absorption (open symbols) using Eq. (8), see text. Curve (C) shows the fluorescence intensity of oxazine, also excited at 600 nm and analysed at 705 nm but in the presence of 1.8×10^{-4} mol g^{-1} of benzophenone coadsorbed on microcrystalline cellulose.

where G is a constant which depends on the apparatus geometry, etc. ϕ_F is the fluorescence quantum yield of the adsorbed oxazine, I_0^c is the incident intensity of the exciting light, $(1-R^c)$ is the fraction of the exciting light which is absorbed and the expression in square brackets in Eq. (8) gives the fraction, f, of the absorbed light which excites the dye.

Plots of I_F vs $(1-R^c) \times f$ show linear increases for low loadings, as shown in Fig. 4 for analysing wavelengths of 692 and 750 nm, but at higher loadings a dramatic decrease in I_F occurs. Examination of Figs. 3(a) and (b) shows that self-reabsorption of fluorescence occurs at shorter analysing wavelengths especially at higher loadings of oxazine, but that the distribution of the fluorescence spectrum at longer wavelengths shows no concentration dependence, indicating that only one species, i.e. the monomer, fluoresces. In which case the dramatic fall off in I_F at higher loadings can be attributed to increased absorption by the dimer which is non-fluorescent. Thus in place of $F(R^c)_{\text{dye}}$ in Eq. (8) we need to use the remission function calculated for monomer only, i.e. $F(\,\cdot\,)_{\text{Monomer}}$ which can be calculated using the equilibrium constant and the monomer and dimer spectra determined above.

When this is done (see Fig. 4) the correction gives a linear relationship for the experimental data collected at 692 nm for all but those samples with very high loadings where experimental errors are very large. However, analysis at 750 nm when "corrected" for dimer absorption shows a positive deviation from a straight line (see Fig. 4). It is obvious from Figs. 1 and 3 that considerable self-absorption of the fluorescence occurs with these samples. If α is the probability of self-absorption of an emitted photon, Birks (1954) has shown that the experimen-

tally measured quantum yield of fluorescence $(\phi_F)_{\text{exp}}$ is given by

$$(\phi_F)_{\text{exp}} = \frac{\phi_F(1-\alpha)}{1-\alpha\phi_F} \qquad (9)$$

Unfortunately, we do not know the fluorescence yield of oxazine adsorbed on cellulose. In ethanol solution the yield is 0.11 at room temperature (Sens and Drexhage, 1981) and in the adsorbed state restricted movement probably leads to a higher fluorescence yield. If the yield were to increase to 0.30, the extent of curvature shown by the data analysed at 750 nm (see Fig. 4) can be explained as due to this effect. This explanation is supported by the linear relationship observed for the data taken at 692 nm also shown in Fig. 4. A close examination of the absorption and emission curves in Figs. 1 and 3 suggests that ignoring re-emission one would expect reabsorption of fluorescence at 692 nm to lead to some downward curvature of the plot. It is apparent that the two effects are almost self-cancelling at this wavelength at low concentrations.

Figures 3(c) and (d) show the corrected fluorescence spectrum of oxazine co-adsorbed with 1.8×10^{-4} mol g^{-1} of benzophenone on cellulose. The dependence of I_F on loading with oxazine is similar to the effect observed in the absence of benzophenone (see Fig. 4) except that the turnover point occurs at a much higher oxazine concentration. Curve C in Fig. 4 can also be explained in terms of absorption of the exciting light by non-fluorescent oxazine dimers.

Benzophenone adsorbed on cellulose. The decay of phosphorescence from 1.8×10^{-4} mol g^{-1} benzophenone when adsorbed on cellulose is a combination of first and second order decays. At early times the second order component is substantial but
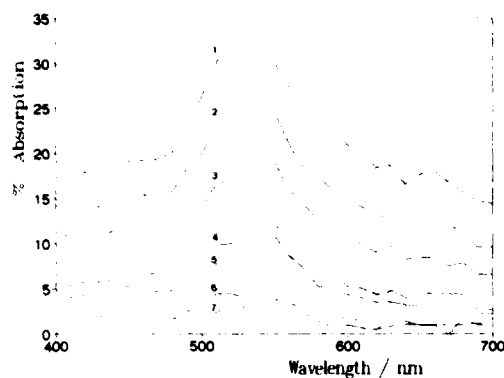
Figure 5. Time resolved spectrum from 1.8×10^{-4} mol g^{-1} of benzophenone adsorbed on microcrystalline cellulose. Curves 1, 2, 3, 4, 5, 6 and 7 were recorded 0, 0.4, 1.2, 4.7, 9.1, 27 and 71 ms after the laser pulse.
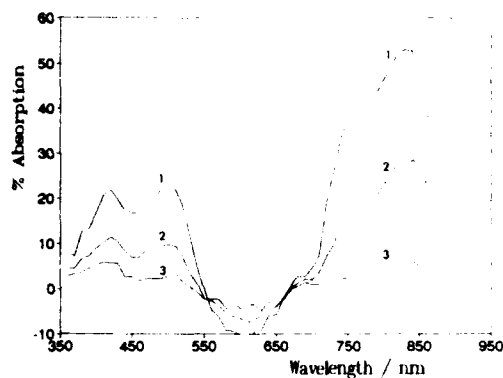
Figure 6. Time resolved spectrum from 1.8×10^{-4} mol g^{-1} of benzophenone and 2.0×10^{-5} mol g^{-1} of oxazine coadsorbed on microcrystalline cellulose. Curves 1, 2 and 3 were recorded 0.3, 3.6 and 23.4 ms after the laser pulse.

after several microseconds the decay becomes first order with a lifetime of 10 µs. This is rather similar to the observed decay of phosphorescence microcrystalline benzophenone (Wilkinson and Willsher, 1984) and from a dilute solution of benzophenone in deaerated acetonitrile (Wilkinson et al., 1991).

The decay of transient triplet–triplet absorption exhi its similar kinetics but as can be seen in Fig. 5, the triplet state absorption decays to reveal the presence of a much longer lived transient which has the characteristic absorption of the ketyl radical (Porter and Wilkinson, 1961). The ketyl radical arises as a result of hydrogen abstraction from the cellulose polymer chain by triplet benzophenone.

Diffuse reflectance laser photolysis of benzophenone in the presence or absence of oxygen has no effect on the triplet decay as measured by either absorption or emission techniques. This reflects the low mobility of oxygen in cellulose as has been reported previously by Murtagh and Thomas (1988).

Oxazine adsorbed on cellulose. When oxazine adsorbed on cellulose is subjected to nanosecond diffuse reflectance laser flash photolysis, no transient absorptions are detected indicating that intersystem crossing of the adsorbed oxazine is negligible as is also the case in dilute solutions (Wilkinson et al., 1991).

Oxazine and benzophenone co-adsorbed on cellulose. Figure 6 shows the time resolved spectrum obtained when benzophenone and oxazine co-adsorbed on microcrystalline cellulose are subjected to diffuse reflectance laser photolysis. We recently showed that benzophenone sensitizes the production of the triplet state of oxazine in acetonitrile solution (Wilkinson et al., 1991) and Fig. 6 demonstrates the sensitized production of adsorbed triplet oxazine which has a characteristic absorption maximum at 830 nm. A similar spectrum obtained with a different sensitizer and less spectral resolution has already been observed from colloidal TiO$_2$

samples by Kamat and Ford (1987), but we present here the first reported spectrum of an oxazine triplet state on a solid surface. The triplet state of oxazine adsorbed on cellulose decays with first order kinetics and a lifetime of 4.3 ± 0.4 ms, which is much longer than that in acetonitrile solution where the lifetime is only 14.5 µs (Wilkinson et al., 1991). This longer lifetime allows us to determine the triplet transient difference spectrum form oxazine absorbed on cellulose in the absence of any absorption from triplet benzophenone which decays on much shorter timescales. A similar result showing that the triplet lifetime of a few organic compounds adsorbed on filter paper is larger than that in solution has been recently reported by utilizing diffuse reflectance transient absorption spectroscopy (Ikeda et al., 1990).

Triplet energy transfer

Phosphorescence quenching. The transfer of energy from triplet benzophenone to oxazine, coadsorbed on microcrystalline cellulose, involves a "static" transfer process since the decay of the phosphorescence of benzophenone is unaffected by the presence of increasing concentration of oxazine. However, the intensity of the phosphorescence decreases markedly with oxazine concentration as shown in Fig. 7. The phosphorescence intensity, I_P, was measured at 450 nm, following laser excitation at 354 nm of a constant concentration of benzophenone $(1.8 \times 10^{-4}$ mol g^{-1} cellulose) as the acceptor concentration was increased from 1 to 50×10^{-6} mol g^{-1} cellulose, relative to I_P^0, the phosphorescence intensity from benzophenone in the absence of oxazine.

Since oxazine absorbs at 354 nm, allowance needs to be made for this. Curve B shows the data from curve A, corrected for absorption by oxazine using the following equation for constant laser intensity
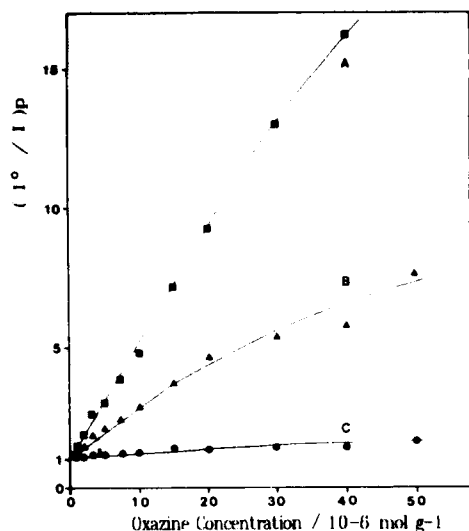
Figure 7. Apparent Stern–Volmer behaviour obtained from room temperature phosphorescence emission data of 1.8×10^{-4} mol g^{-1} of benzophenone and increasing amounts of oxazine as a quencher, both coadsorbed on microcrystalline cellulose. Curve (A), experimental data. Curve (B), corrected for direct absorption of oxazine by the use of Eq. (10). Curve (C), corrected for reabsorption by the substrate and by triplet oxazine using Eqs. (10), (11) and (15).

$$\frac{I_P^0}{I_P} = \left(\frac{I_P^0}{I_P}\right)_{\exp} \frac{(1-R^c)}{(1-R^{c,o})} \frac{f_B^c}{f_B^{c,o}} \tag{10}$$

where the zero superscript indicates the absence of oxazine and f_B^c is the fraction of the absorbed exciting light actually absorbed by benzophenone, i.e.

$$f_B^c = (F(R^c)_B - F(R^c)_{cell})/F(R^c)_{Total} \tag{11}$$

where $F(R^c)_{cell}$, $F(R^c)_B$ and $F(R^c)_{Total}$ are the measured remission functions at the exciting wavelength for cellulose alone, for benzophenone on cellulose, and for oxazine and benzophenone coadsorbed on cellulose respectively.

A second correction is necessary to allow for reabsorption of benzophenone phosphorescence by ground state oxazine and by triplet oxazine produced by energy transfer at the analysing wavelength. Oelkrug and Kortüm (1968) have developed an equation to take account of self-reabsorption of luminescence in powdered samples, i.e.

$$(I_p)_{\exp} = \frac{\Phi_p I_o F(R^c) (1+R^c) (1+R^a)}{(R^c)^{-1} + (R^a)^{-1} - R^c - R^a} \tag{12}$$

where R^c and R^a are the reflectances at the excitation and analysing wavelengths respectively. Since we are dealing with static quenching and since triplet oxazine is formed quickly relative to the phosphorescence decay and, as reported earlier, does not decay at all on microsecond timescales, we used this same equation to correct for reabsorption of

phosphorescence within our samples. This correction applied to curve B yields curve C which we have used to calculate the fraction of quenching due to energy transfer to oxazine. This gives a value of 0.33 ± 0.0^3 for oxazine concentrations above 2×10^{-5} mol g^{-1}.

Sensitized production of triplet oxazine. It is also possible to calculate the fractional triplet energy transfer from benzophenone to oxazine by measuring the amount of triplet oxazine absorption as a function of oxazine concentration. In diffuse reflectance laser flash photolysis one measures $\Delta R(t)$, the change in diffuse reflectance at the analysing wavelength at time t after the laser flash.

$$\Delta R(t) = \frac{R_b - R(t)}{R_b} \tag{13}$$

where R_b is the sample reflectance before exposure to the laser pulse and $R(t)$ is the reflectance at any time t after laser excitation. Under the conditions used here the exciting pulse does not cause any changes to the scattering coefficient so changes in ΔR arise from changes in absorption by these samples and we can refer to $\Delta R \times 100$ as the percentage absorption.

Thus, in Fig. 6 we see increases in absorption due to the production of triplet oxazine at many analysing wavelengths, but a decrease in absorption due to ground state depletion between (560–680 nm), since the extinction coefficient of triplet oxazine in this region is less than that of ground state oxazine. The change in reflectance $\Delta R(t)$ depends on both the decay kinetics of the absorbing transient and the concentration profile of the transient species below the irradiated surface. The concentration profile, with respect to sample penetration depth, can be calculated as described previously by Oelkrug et al. (1987). When the percentage conversion of the absorbing species is small, we have shown that ΔR is directly proportional to the concentration of transient species for $\Delta R < 0.1$, with increasing deviations from a linear dependence as $\Delta R \to 1$ (see Kessler et al., 1983; Oelkrug et al., 1987). Calculations confirm that for the samples investigated here we do not get large fractional conversions of benzophenone or oxazine so $\Delta R(O)$, the initial absorption by triplet oxazine following laser excitation gives a measure of the extent of energy transfer. In the absence of oxazine, benzophenone (1.8×10^{-4} mol per gram of cellulose) gives an initial absorption at 525 nm due to triplet absorption with $\Delta R(O) = 0.33$. In the absence of any absorption of the exciting light by oxazine the fractional transfer to oxazine as a function of oxazine concentration is given by:

$$f_T([OX]) = \frac{\Delta R_{830}^{OX}(O)\ ^3\epsilon_{525}^B}{\Delta R_{525}^B(O)\ ^3\epsilon_{830}^{OX}} \tag{14}$$

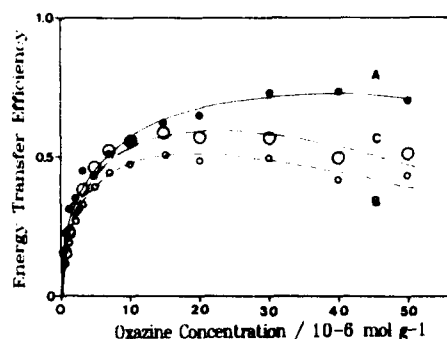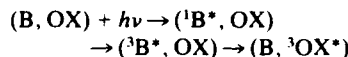where $\Delta R_{830}^{OX}(O)$ is the initial reflectance change due

Figure 8. Energy transfer efficiency (uncorrected for absorption of the exciting light by oxazine) *vs* oxazine concentration obtained from measurements of phosphorescence intensity of benzophenone at 450 nm (curve A), and of absorption by sensitized triplet oxazine at 830 nm, curve (B). Curve (C) is the same data as in curve (B) but corrected using Eq. (14).

to sensitized triplet oxazine at 830 nm and $^3\epsilon^B_{525}$ and $^3\epsilon^{OX}_{830}$ are the extinction coefficients of the triplet states of benzophenone at 525 nm and of oxazine at 830 nm respectively. Equation (14) can be corrected for absorption of exciting light by oxazine using the same correction applied to the phosphorescence data in Eqs. (10) and (11) and compared with the fraction of transfer as measured from phosphorescence quenching measurements. When this is done we get good agreement between the fractions measured by the different methods at low oxazine concentrations using a value of $^3\epsilon^B_{525}/^3\epsilon^{OX}_{830}$ = 2.6, which is the value we measured in acetonitrile solution (Wilkinson *et al.*, 1991). This constitutes the first measurement of the extinction coefficient of an adsorbed triplet state relative to the standard triplet benzophenone. It is worth noting that ground state extinction coefficients of benzophenone and oxazine on cellulose are, within experimental error, the same as in acetonitrile solution and therefore $^3\epsilon^B_{525}$ and $^3\epsilon^{OX}_{830}$ are likely to be the same as in solution, i.e. 7640 dm^3 mol^{-1} cm^{-1} (Carmichael and Hug, 1986) and 2 × 10^4 dm^3 mol^{-1} cm^{-1} (Wilkinson *et al.*, 1991), respectively.
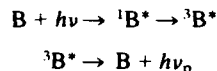
In comparing the energy transfer efficiencies from phosphorescence quenching and sensitized triplet oxazine measurements it is necessary to apply the same corrections to allow for absorption of the exciting light by oxazine since the measurements were made on identical samples. We can minimize the experimental errors by comparing the results of the two different types of measurement without making this correction to either. This is done in Fig. 8 where it can be seen that agreement at oxazine concentrations below 10 × 10^{-6} mol g^{-1} of celluose is satisfactory with the phosphorescence data showing less scatter as they constitute the more accurate data. The two curves start to deviate from each other at higher oxazine concentrations when the dimer of oxazine is formed. If one assumes that

triplet benzophenone also transfers to the oxazine dimer and that the triplet state of the dimer has an extinction coefficient at 830 nm of 9.1 × 10^6 mol^{-1} g cm^{-1} (2.3 × 10^4 dm^3 mol^{-1} cm^{-1}), then the two curves are indistinguishable within experimental error over the whole range of concentrations measured.

To explain static quenching of triplet benzophenone by oxazine we suggest two different types of behaviour by benzophenone molecules depending on whether they have an oxazine molecule as a nearest neighbour represented by (B, OX), or not which we shall represent by B. The fact that the absorption spectra, Fig. 1(d) and fluorescence spectra Fig. 3(c) of oxazine in the presence of benzophenone are different from those in the absence of benzophenone, Figs. 1(b) and 3(a), respectively, suggests the formation of (B, OX). We shall assume absorption of light by (B, OX) leads to triplet oxazine with unit efficiency as shown below

$$(B, OX) + h\nu \rightarrow (^1B^*, OX)$$
$$\rightarrow (^3B^*, OX) \rightarrow (B, \, ^3OX^*)$$

while absorption by B gives

$$B + h\nu \rightarrow \, ^1B^* \rightarrow \, ^3B^*$$

$$^3B^* \rightarrow B + h\nu_p$$

In which case:

$$\frac{I^0_P}{I_P} = \frac{[B_0]}{[B_0] - [OX]} = \frac{1}{1 - [OX]/[B_0]} \approx 1 + [OX]/[B_0]$$

$$(15)$$

where [B$_0$] is the initial constant concentration of benzophenone. According to Eq. (15) the predicted slope of the corrected curve C is 1/[B$_0$] = 5.7 × 10^4 g mol^{-1}. However, the experimental value of K$_{SV}$ from curve C at low oxazine concentrations is 2 × 10^4 g mol^{-1}, which suggests that each oxazine is capable of quenching excitation from a "pool" containing 2 or 3 benzophenone molecules. This is reasonable because of the high loading of benzophenone, making it likely that each oxazine molecule has more than one nearest neighbour. It is also in keeping with the fact that benzophenone affects the dimerization of oxazine on the surface and the fact that the decay of the phosphorescence of benzophenone adsorbed alone on cellulose at these loadings shows a bimolecular component indicating that energy can migrate at these loadings between benzophenone molecules until triplet–triplet annihilation or energy transfer occurs. Unfortunately, it is not possible to reduce the benzophenone loadings much below the value used here without making the collection of data of this type subject to large experimental uncertainties.

CONCLUSIONS

Dimer formation was observed when the oxazine dye, (2,7-bis(diethylamino)-phenazoxonium chlor-

ide) is adsorbed on microcrystalline cellulose using ground-state diffuse reflectance absorption measurements. The equilibrium constant for dimer formation was shown to be $(1.0 \pm 0.1) \times 10^6 \, mol^{-1}$ g $(2650 \pm 250 \, mol \, dm^{-3})$ by the use of a simple analytical treatment which allowed the spectrum of the dimer to be obtained. The equilibrium constant for dimerization on the cellulose surface is reduced to $(3.7 \pm 1.0) \times 10^4 \, mol^{-1}$ g $(93 \pm 30 \, mol \, dm^{-3})$ in the presence of a high load $(1.8 \times 10^{-4} \, mol \, g^{-1})$ of benzophenone.

Fluorescence studies have shown that the excited monomer is the only fluorescent species when this oxazine is absorbed on cellulose. The concentration dependence of the fluorescence intensity of the dye was quantified in the absence and in the presence of benzophenone, confirming that dye aggregation decreases when both species are co-adsorbed on microcrystalline cellulose.

Direct excitation of (2,7-bis(diethylamino)-phenazoxonium chloride) at 354 and 532 nm yields no triplet state absorption. The triplet–triplet absorption spectrum of this oxazine dye on cellulose was obtained using benzophenone as a triplet sensitizer and the extinction coefficient of the triplet state of the adsorbed dye was evaluated relative to that of triplet benzophenone adsorbed on cellulose. The lifetime of adsorbed triplet oxazine was found to be 4.3 ms which is 300 times longer than that in acetonitrile solution.

Using benzophenone as a triplet sensitizer, a quantitative analysis of the efficiency of energy transfer from triplet benzophenone to the oxazine dye adsorbed on microcrystalline cellulose has been made, using measurements of both the quenching of the intensity of benzophenone phosphorescence and the sensitized production of transient absorption by triplet oxazine. A mechanism is presented to explain the static energy transfer process in which each oxazine molecule is capable of accepting energy with unit efficiency from a "pool" containing 2 or 3 benzophenone molecules.

REFERENCES

Battista, O. A. (1965) Microcrystalline cellulose. In *Encyclopedia of Polymer Science and Technology* (Edited by H. F. Mark, N. G. Gaylord and N. M. Bikales) Vol. 3, pp. 285–291. Wiley, New York.

Birks, J. B. (1954) Energy transfer in organic phosphors. *Phys. Rev.* **94**, 1567–1573.

Carmichael, I. and G. L. Hug (1986) Triplet–triplet absorption spectra of organic molecules in condensed phases. *J. Phys. Chem. Ref. Data.* **15**, 1–250.

Drexhage, K. H. (1973) Dye lasers. In *Topics in Applied Physics* (Edited by F. P. Shafer). Springer, Berlin.

Drexhage, K. H. (1977) Fluorescence efficiency of laser dyes. *NBS Spec. Publ.* **466**, 33–40.

Ferreira, L. F. V., S. B. Costa and E. J. Pereira (1991) Fluorescence quantum yield evaluation of strongly absorbing dye solutions as a function of the excitation wavelength. *J. Photochem. Photobiol. A: Chem.* **55**, 361–376.

Ikeda, N., T. Hara and H. Masuhara (1990) Detection of

the triplet state of some organic molecules adsorbed on cellulose substrate by diffuse reflectance laser photolysis method. *Chem. Lett.* 683–686.

Kamat, P. V. and W. E. Ford (1987) Photochemistry on surfaces: triplet–triplet energy transfer on colloidal TiO_2 particles. *Chem. Phys. Lett.* **135**, 421–426.

Kelly, G. P., P. A. Leicester, F. Wilkinson, D. R. Worrall, L. F. V. Ferreira, R. Chittock and W. Toner (1990) Picosecond diffuse reflectance and transmission laser flash photolysis study of various triaryl-2-pyrazolines. *Spectrochim. Acta* **46A**, 975–985.

Kessler, R. W., G. Krabichler, S. Uhl, D. Oelkrug, W. P. Hagen, J. Hyslop and F. Wilkinson (1983) Transient decay following pulse excitation of diffuse scattering samples. *Opt. Acta* **30**, 1099–1111.

Kessler, R. W., D. Oelkrug and F. Wilkinson (1982) Detection of transient spectra within polycrystalline samples using the new technique of diffuse reflectance flash photolysis. *Appl. Spectrosc.* **36**, 673–675.

Kessler, R. W. and F. Wilkinson (1981) Diffuse reflectance triplet–triplet absorption spectroscopy of aromatic hydrocarbons chemisorbed on τ-alumina. *J. Chem. Soc. Farady Trans. 1.* **77**, 309–320.

Kopf, U. and J. Heinze (1984) 2,7-Bis(diethylamino) phenazoxonium chloride as a quantum counter for emission measurements between 240 and 700 nm. *Anal. Chem.* **56**, 1931–1935.

Kortüm, G., W. Brown and G. Herzog (1963) Principles and techniques of diffuse-reflectance spectroscopy. *Angew. Chem. Inter. Ed.* **2**, 333–341.

Krassig, H. (1986) Cellulose. In *Ullmann's Encyclopedia of Industrial Chemistry*, Vol. 5, Chap. 1, pp. 375–418. VCH Verlagsgesellschaft, Weinhein, Germany.

Kubelka, P. (1948) New contribution to the optics of intensely light-scattering materials Part I. *J. Opt. Soc. Am.* **38**, 448–457.

Levin, P. P., L. F. V. Ferreira and S. M. B. Costa (1990) Diffuse reflectance laser photolysis studies of geminate recombination kinetics of triplet radical pairs adsorbed on microcrystalline cellulose. *Chem. Phys. Lett.* **173**, 277–281.

Murtagh, J. and J. K. Thomas (1988) Effect of humidity and temperature on photoinduced reaction in cellulose. *Chem. Phys. Lett.* **148**, 445–451.

Oelkrug, D., W. Honnen, F. Wilkinson and C. J. Willsher (1987) Modelling of transient production and decay following laser excitation of opaque materials. *J. Chem. Soc., Faraday Trans. 2*, **83**, 2081–2095.

Oelkrug, D. and G. Kortüm (1968) Zur Berechnung der Lumineszenzreabsorption bei Pulverformigen Substanzen. *Z. Phys. Chem. N.F.* **58**, 181–188.

Porter, G. and F. Wilkinson (1961) Primary photochemical processes in aromatic molecules. *Trans. Faraday Soc.* **57**, 1686–1691.

Raue, R. (1984) Cationic dyestuffs. *Rev. Prog. Colouration* **14**, 187–203.

Sens, R. and K. H. Drexhage (1981) Fluorescence quantum yield of oxazine and carbazine laser dyes. *J. Lumin.* **24/25**, 709–712.

Turro, N. J., M. B. Zimmit, I. R. Gould and W. Mahler (1985) Triplet energy transfer as a probe of surface diffusion rates: A time-resolved diffuse reflectance transient absorption spectroscopy study. *J. Am. Chem. Soc.* **107**, 5826–5827.

Vogel, M., W. Rettig, U. Fiedeldei and H. Baumgartel (1988) Non-radiative deactivation *via* biradicaloid charge-transfer states in oxazine and thiazine dyes. *Chem. Phys. Lett.* **148**, 347–352.

Wilkinson, F. (1986) Diffuse reflectance flash photolysis. *J. Chem. Soc. Faraday Trans. II* **82**, 2073–2081.

Wilkinson, F. and L. F. V. Ferreira (1988) Diffuse reflectance laser photolysis studies of energy transfer at interfaces. *J. Lumin.* **40/41**, 704–705.

Wilkinson, F., G. P. Kelly, L. F. V. Ferreira, V. M. M. R. Freire and M. I. Ferreira (1991) Benzophenone sensitization of triplet oxazine and of delayed fluorescence by oxazine in acetonitrile solution. *J. Chem. Soc. Faraday Trans. II*, **87**, 547–552.

Wilkinson, F., G. P. Kelly, C. Michael and D. Oelkrug (1990) A study of the photophysical properties of various triaryl-2-pyrazolines in solution and microcrystalline form. *J. Photochem. Photobiol. A: Chem.* **52**, 309–320.

Wilkinson, F. and C. J. Willsher (1984) Detection of triplet–triplet absorption in microcrystalline benzophenone by diffuse reflectance laser flash photolysis. *Chem. Phys. Lett.* **104**, 272–276.

Wollenweber, P. (1969) Organic adsorbents. Cellulose and derivatives. In *Thin-Layer Chromatography*, (Edited by G. Allen and Unwin), 2nd Edn, pp. 32–41. Springer-Verlag, London.

Diffuse reflectance laser flash photolysis of adsorbed molecules

F WILKINSON

Department of Chemistry, Loughborough University of Technology, Loughborough, Leicestershire, LE11 3TU, England

Abstract. Recent progress which allows laser flash photolysis investigation of opaque materials by using diffuse reflectance from analysing sources for the detection of laser induced transient species is described. Experimental details of nanosecond and picosecond diffuse reflectance laser photolysis systems are presented and methods of analysis of data are discussed. The potential of the technique for studying elementary reactions at interfaces is demonstrated with particular reference to bimolecular reactions of (a) the triplet state of acridine adsorbed on various porous silica surfaces and (b) ion-electron recombination following multi-photon ionisation of diphenyl polyenes adsorbed on γ-alumina. The mechanisms of formation and decay of these transient adsorbed species are discussed.

Keywords. Adsorbed molecules; laser photolysis; kinetics; transient spectra.

1. Introduction

Flash photolysis, first developed by Porter (1950), is a most powerful technique which has been extensively applied to study rapid homogeneous reactions in the gas phase and in dilute fluid and rigid solutions. Kessler and Wilkinson (1981) demonstrated that the technique can be extended to opaque samples by monitoring changes in the diffuse reflected light from an analysing source following pulsed photo-excitation. Wilkinson et al (1984) reported the first successful diffuse reflectance pulsed radiolysis experiments and more recently have demonstrated that diffuse reflectance picosecond laser flash photolysis studies are possible using mode locked picosecond laser and pump-probe methods (Wilkinson et al 1986b). Ikeda et al (1987) have already followed up this advance and obtained photoinduced time resolved spectra in the picosecond time domain.

Laser induced transient spectra and decay kinetics have been observed in our laboratory from a wide variety of samples including fractions of monolayers of organic molecules adsorbed on catalytic metal oxide surfaces (Oelkrug et al 1988, 1989) and included within the hydrophobic man-made zeolite silicalite (Wilkinson et al 1986a) from semiconductor powders (Wilkinson et al 1986c) and sintered porous electrodes doped and undoped (Pouliquen et al 1986; Kossanyi et al 1990) from organic and inorganic microcrystals (Wilkinson and Willsher 1984, 1988) and from dyes adsorbed on fabrics and chemically bound to polymers (Wilkinson and Willsher 1985; Wilkinson et al 1987). For recent reviews see Wilkinson (1986), Wilkinson and Kelly (1990) and Wilkinson and Willsher (1990).

2. Experimental

The equipment used for laser flash photolysis in diffuse reflectance mode is identical to that used for studies in transmission mode except for the geometry used for collecting the analysing light (see figure 1) As in all flash photolysis experiments one obtains transient difference spectra and decreases in absorption are often observed at wavelengths where the ground state has a stronger absorption coefficient than the transient. Figure 2 gives an example, which shows excellent isosbestic points, obtained by laser excitation at 532 nm of eosin adsorbed on microcrystalline cellulose. This spectrum, although much broader, bears a close resemblance to the solution triplet spectrum (Kasche and Lindqvist 1985). Analysis of transient changes in diffuse reflectance can follow the Kubelka–Munk treatment (Kubelka 1948) where two light fluxes I and J are considered to be travelling in opposite directions perpendicular to the irradiated surface at $x = 0$. These fluxes depend on the absorption and scattering coefficients K and S respectively, with the attenuation of the incident flux given by

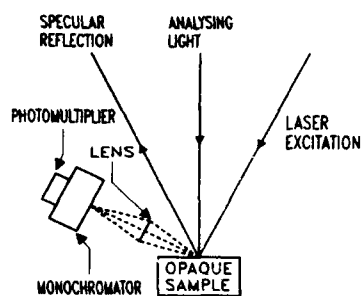$$dI(x) = -I(x)(K + S)dx + J(x)S\,dx. \tag{1}$$

Figure 1. Schematic diagram of the sample geometry used in diffuse reflectance laser flash photolysis.
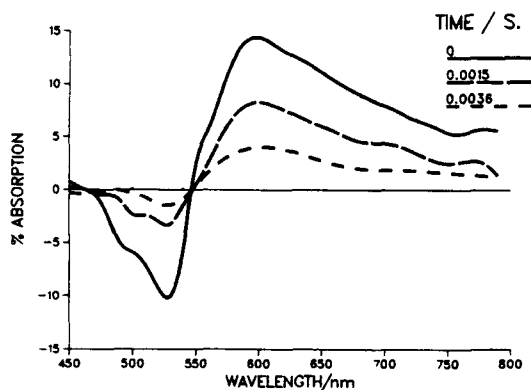

Figure 2. Time resolved transient difference spectra obtained following diffuse reflectance laser flash photolysis of eosin adsorbed on microcrystalline cellulose.

The generated flux J since it is moving in the opposite direction has the opposite sign i.e.

$$dJ(x) = J(x)(K + S)dx - J(x)S dx. \tag{2}$$

The diffuse reflectance $R = J_0/I_0$, where I_0 and J_0 are surface incident and reflected fluxes. Equations (1) and (2) can be solved for a layer so thick that any further increase in thickness does not affect R and provided K and S are independent of x this gives

$$\frac{(1 - R)^2}{2R} = \frac{K}{S} = F(R). \tag{3}$$

$F(R)$, the remission function is linearly dependent on the number of absorbing chromophores in any sample where S and K are independent of the penetration depth below the surface.

In diffuse reflectance flash photolysis the ground state chromophores, which are excited, are usually homogeneously distributed. However, photo-excitation gives transient or permanent changes in absorption, preferentially just below the irradiated surface. Theoretical treatments show that there are two limiting types of concentration profile produced, namely an exponential fall off as a function of penetration depth and a homogeneous (or "plug") profile. The latter case is encountered with large laser fluences and with low concentrations of ground state absorbers, where there is total conversion from ground state to transient to a certain depth below the irradiated surface. Since a homogeneous concentration of absorbers exists the Kubelka–Munk theory can be applied. For optically thick samples at analysing wavelengths where only the transient absorbs the remission function given by (3) is a linear function of the concentration and can be used for kinetic analysis and for plotting absorption spectra. For the low percentage conversions the concentration of transients decreases exponentially below the irradiated surface. Under these conditions $(1 - R_t^a)$, where R_t^a is the relative transient reflectance at the analysing wavelength, is a linear function of the concentration of the transient species at values of $(1 - R_t^a)$ less than 0·1 (Oelkrug *et al* 1987).

If the absorption coefficient K is in excess of 10^4cm^{-1} at the laser excitation wavelength then the penetration depth is only $\sim 1 \, \mu J$ and dissipation of laser excitation as heat causes considerable temperature rises (Wilkinson *et al* 1986c). This possibility has always to be borne in mind, and lower laser fluences and/or lower concentrations and/or excitation into weaker bands must be employed to avoid thermal effects for some samples.

2.1 Picosecond diffuse reflectance laser photolysis

Figure 3 illustrates the basic arrangement used to record the first ever transient absorption within an opaque material on picosecond timescales using diffuse reflectance. Generation and detection of the transient absorption was effected by pumping the sample at 295 nm (pulse width = 6 ps, energy = 20 μJ) and probing at 590 nm (energy = 1 μJ), using the Spectra-Physics picosecond laser system at the Rutherford Appleton Laboratory. Light diffusely reflected from the sample was detected by a filtered photodiode, and the signal fed to a Boxcar Integrator and thence to a IBM microcomputer. A second photodiode monitored a portion of the probe beam taken before hitting the sample, in order to correct for shot-to-shot variations in laser intensity.
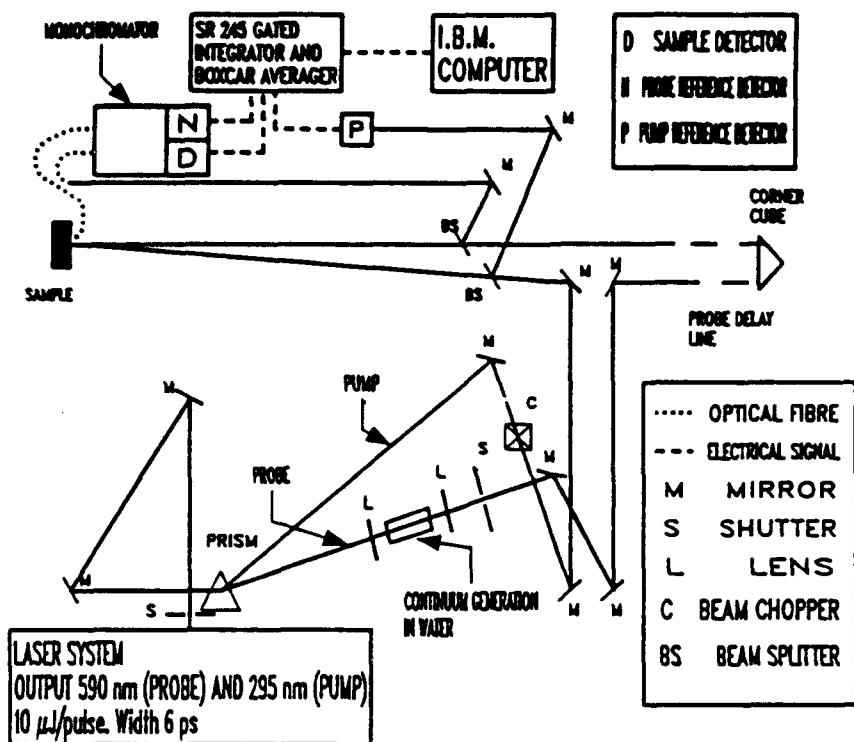
Figure 3. Schematic diagram of the optics and detection system employed in picosecond diffuse reflectance laser photolysis.
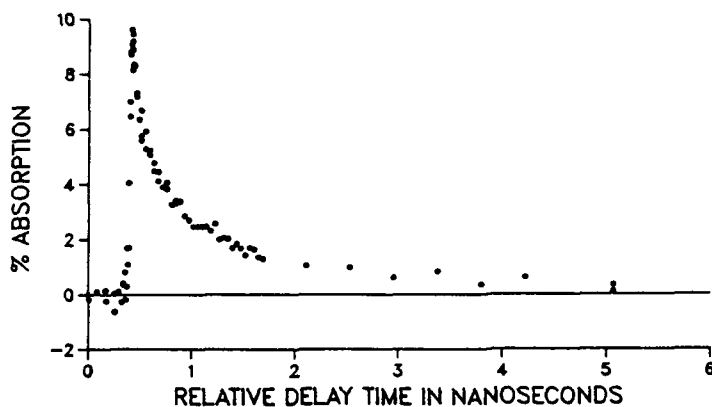
Figure 4. Transient absorption decay from a microcrystalline sample of 1,5-diphenyl-3-styryl-2-pyrazoline, using pump and probe wavelengths of 295 and 590 nm, respectively.

Samples are ususlly held in a powder holder behind a quartz window. Nearly collinear pump and probe beams were incident normal to the quartz window, with the pump beam about 2 mm in diameter and the probe beam located entirely within

the excited area of the sample. A portion of the diffusely reflected probe beam was detected by the photodiode. To record transient absorption (which is, strictly speaking, the relative decrease in diffuse reflectance), signals due to the probe beam alone and due to simultaneous pump and probe were obtained. Each run comprised 100 shots, and normalisation for shot-to-shot variation was carried out. Transient absorption following excitation at the pump wavelength reduces the level of the diffusely reflected probe beam to different extents for different delays between the pump and probe beams incident on the same area of sample. Experimental details are given elsewhere (Wilkinson *et al* 1986b). The transient absorption, illustrated in figure 4 for microcrystalline 1,5-diphenyl-3-styryl-2-pyrazoline, is assigned to the excited singlet of the pyrazoline (Wilkinson 1986).

3. Results and discussion

3.1 *Bimolecular reaction of adsorbed triplet acridine on silica surfaces*

The nature and mobility of species present when acridine is adsorbed from high vacuum and dry solutions onto thermally pretreated silica and alumina have been investigated by ground and excited state spectroscopic techniques (Oelkrug *et al* 1989). On silica the main adsorbed species is hydrogen bonded acridine which upon excitation gives strong triplet–triplet absorption at 435 nm. The triplet state absorption for samples with very low coverage or high pre-treatment temperature has an exponential decay with a mean life-time of $\sim$ 35 ms and these samples show no delayed fluorescence. Mean lifetimes which approach this value are found only in perdeuterated acridine in organic host lattices (Kellman 1977) and the decay in fluid solutions is faster by about 2 orders of magnitude (De Mayo 1982). The high intensity of the transient signals in diffuse reflectance suggests that the triplet yield of the excited adsorbate and the extinction coefficient of the adsorbed triplet are similar to the solution values of 0·5 and 2×10^4 dm^3 mol^{-1} cm^{-1}, respectively. However, for samples of higher coverage or lower pre-treatment temperature the triplet decay is faster and non-exponential and delayed fluorescence is observed due to

$$A^*(T_1) + A^*(T_1) \rightarrow A(S_0) + A^*(S_1) \rightarrow 2A(S_0) + h\nu_F.$$
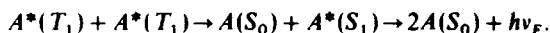
The mechanism of elementary bimolecular interactions at interfaces is by no means fully understood. It can be a consequence of two-dimensional surface migration (diffusion) and bimolecular collisions or alternatively a three-dimensional interaction assuming an adsorption = desorption equilibrium. In order to clarify this problem we have studied a series of silica powders with particle sizes of about 100 μm but with very different pore-diameters ranging from 6–100 nm. We have also varied the surface loading between 0·075 mg and 1 mg of acridine per g of silica. The effect of surface coverage on the rate of triplet decay when the surface has been preheated to $< 300^\circ$C is shown in figure 5. For such non-exponential decays we have evaluated the first half-life, i.e. the time taken for the absorption to reach 50% of the initial amount. These values show no correlation with volume concentration, there is however a clear correlation of the inverse of the lifetime with coverage.

A linear Stern–Volmer plot is obtained (see figure 6) when the inverse of the first half-life is plotted against surface coverage in the range from 1–7% suggesting that
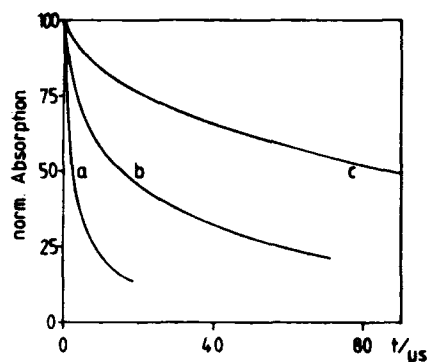
Figure 5. Normalised decay curves of triplet acridine on SiO_2 fractosil 1000. N_2 BET – surface area $20 \, m^2 \, g$. $T_4 = 100 \, C$. (a) $23^o{}_o$, (b) $7^o{}_o$ and (c) $1.7^o{}_o$ of a monolayer.
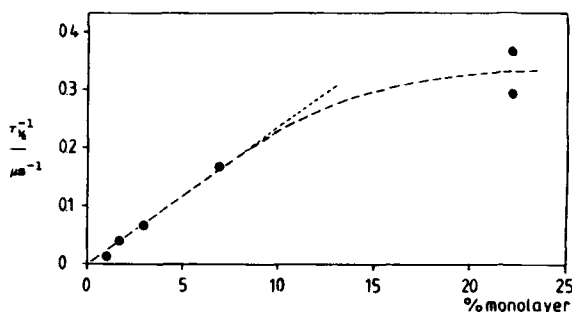
Figure 6. Dependence of the inverse of the first half-life for the decay of triplet acridine adsorbed on silica on surface coverage.

under these conditions bimolecular annihilation resulting from surface diffusion of triplet states is the predominant decay pathway. Calculations suggest that there is a high percentage conversion of ground state to triplet states for these samples. Assuming total conversion a two-dimensional bimolecular rate constant of $2 \times 10^{14} \, dm^2 \, mol^{-1} \, s^{-1}$ is obtained for triplet-triplet annihilation on silica pretreated at $T_A < 300°C$. Higher preheating of the surface reduces the lateral mobility of triplet acridine and when $T_A > 600°C$ no migration is observed.

3.2 Radical ion-electron recombination following multiphoton ionisation of diphenyl-polyenes on alumina

When excited at 354 nm physisorbed diphenylhexatriene, diphenyl butadiene, and chemisorbed stilbene give strong long-lived adsorptions at 570, 540 and 480 nm respectively which deactivate on a time scale extending over more than 6 orders of magnitude with an extremely non-exponential decay. These transients are assigned as radial cations of the adsorbed diphenyl polyenes which decay by radical cation-electron recombination (Oelkrug *et al* 1988).

The ionisation potential of the diphenyl polyenes are such that the consecutive absorption of (at least) two photons at 354 nm is required to form these radical cations

and the dependence of the amount of transient on laser fluence confirms that more than one photon is required to produce the radical cations. The decay is explained as the temperature dependent recombination of the originally produced radical cation-electron pair.

4. Conclusions

Diffuse reflectance laser flash photolysis has been shown to be a powerful method for studying photoinduced reactions at interfaces and within highly scattering samples. In this work we were able to measure a two-dimensional rate constant and to measure ion-electron recombination rates. It needs to be stressed that this technique can be applied to reactions in all types of heterogeneous systems as well as at gas/solid interfaces as discussed here. The ability to rapidly control the switching on of every type of elementary reaction of adsorbed species with pulsed lasers at interfaces and in other heterogeneous environments and to follow the resulting reactions is considerably enhancing the understanding of heterogeneous elementary reactions.

Acknowledgements

References

Ikeda N, Immagi K, Masuhara H, Nakashima N and Yoshihara K 1987 *Chem. Phys. Lett.* **140** 281
Kasche V and Lindqvist L 1965 *Photochem. Photobiol.* **4** 923
Kellmann A 1977 *J. Chem. Phys.* **81** 1195
Kessler R W and Wilkinson F 1981 *J. Chem. Soc., Faraday Trans. 1* **77** 309
Kossanyi J, Kouyte D, Pouliquen J, Ronfard-Haret J C, Valat P, Oelkrug D, Mammel U, Kelly G P and
 Wilkinson F 1990 *J. Luminesc.* **46** 17
Kubelka P 1948 *J. Opt. Soc. Am.* **38** 448
De Mayo P 1982 *Pure Appl. Chem.* **54** 1623
Oelkrug D, Honnen W, Wilkinson F and Willsher C J 1987 *J. Chem. Soc. Faraday Trans. II* **83** 2081
Oelkrug D, Krabichler G, Honnen W, Wilkinson F and Willsher C J 1988 *J. Phys. Chem.* **92** 3589
Oelkrug D, Uhl S, Willsher C J and Wilkinson F 1989 *J. Phys. Chem.* **93** 4551
Pouliquen J, Fichou D, Valat P, Kossanyi J, Wilkinson F and Willsher C J 1986 *J. Photochem.* **35** 381
Porter G 1950 *Proc. R. Soc.* **A200** 284
Wilkinson F 1986 *J. Chem. Soc. Faraday Trans. II* **82** 1073
Wilkinson F and Kelly G P 1990 in *Handbook of organic photochemistry* (ed.) J C Scaiano (Boca Raton,
 FL: CRC Press) vol. 1, ch. 12
Wilkinson F and Willsher C J 1984 *Chem. Phys. Lett.* **104** 272
Wilkinson F and Willsher C J 1985 *J. Chem. Soc., Chem. Commun.* 142
Wilkinson F and Willsher C J 1988 *J. Luminesc.* **33** 187
Wilkinson F and Willsher C J 1990 in *Lasers in polymer science and technology: application* (eds) Foussier
 and F Jan Rabek (Boca Raton, FL: CRC Press) vol. 2, ch. 9
Wilkinson F, Willsher C J, Bourdelande J L, Font J and Greuges J 1987 *J. Photochem.* **38** 381
Wilkinson F, Willsher C J, Casal M L, Johnston L J and Scaiano J C 1986a *Can. J. Chem.* **64** 539
Wilkinson F, Willsher C J, Leicester P A, Barr J R M and Smith M J C 1986b *J. Chem. Soc., Chem.*
 Commun. 1216
Wilkinson F, Willsher C J, Uhl S, Honnen W and Oelkrug D 1986c *J. Photochem.* **33** 273
Wilkinson F, Willsher C J, Warwick P, Land E J and Rushton F A P 1984 *Nature (London)* **311** 40

DIFFUSE REFLECTANCE LASER PHOTOLYSIS OF ADSORBED MOLECULES

Frank WILKINSON and Robert BEER

Department of Chemistry, Loughborough University of Technology, Loughborough, Leicestershire, LE11 3TU, U.K.

Recently we have extended to heterogeneous, opaque and often highly scattering systems the advantages of being able to subject them to flash photolysis investigation by using diffuse reflected light instead of transmitted light as the analysing source on timescales extending from several seconds to picoseconds. Laser induced transient spectra and decay kinetics have been observed from a wide variety of samples including fractions of monolayers of organic molecules adsorbed on catalytic metal oxide surfaces, and included within the hydrophobic man-made zeolite 'Silicalite'. Experimental details are reviewed in brief as are some experimental results concerning a variety of bimolecular reactions which we have studied recently. The potential of the technique to study elementary reactions at interfaces is demonstrated with particular reference to four bimolecular surface reactions : (1) triplet-triplet annihilation in the case of acridine adsorbed on various porous silica surfaces, (2) bimolecular combination of diphenylmethyl radicals on silica gel and included in NaX and 'Silicalite' zeolites, (3) electron - radical cation recombination following multiphoton ionisation of diphenylpolyenes on metal oxide surfaces and (4) triplet energy transfer between eosin and anthracene on silica surfaces.

1. INTRODUCTION

Recently we have developed the technique of diffuse reflectance laser flash photolysis which has the advantage of being able to subject heterogeneous, opaque and often highly scattering samples to flash photolysis investigation by using diffuse reflected light instead of transmitted light as the analysing source on timescales extending from several seconds[1] to picoseconds[2]. Laser induced transient spectra and decay kinetics have been observed from a wide variety of samples including fractions of monolayers of organic molecules adsorbed on catalytic metal oxide surfaces[3,4], and included within zeolites[5], from semiconductor powders[6] and porous electrodes doped and undoped[7,8], from organic and inorganic microcrystals[9,10], and from dyes[11,12] adsorbed on fabrics and chemically bound to polymers. For recent reviews see references 13, 14 and 15.
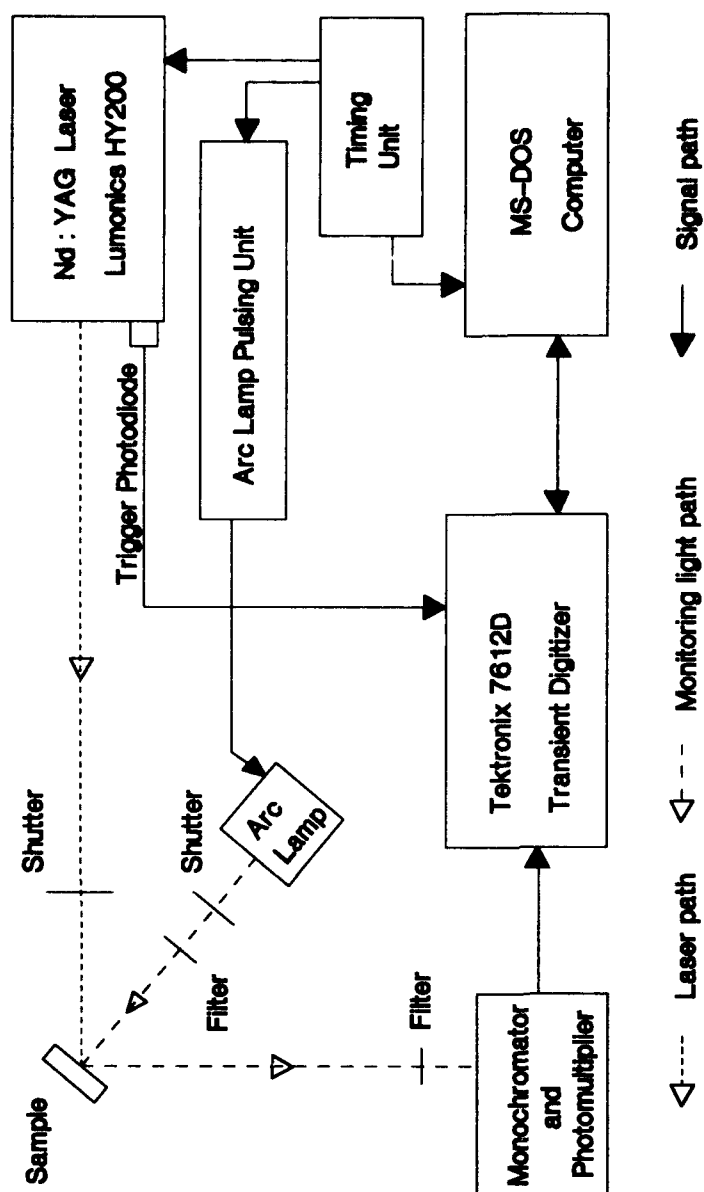
FIGURE 1. SCHEMATIC DIAGRAM SHOWING AN APPARATUS USED IN NANOSECOND DIFFUSE REFLECTANCE LASER FLASH PHOTOLYSIS STUDIES.
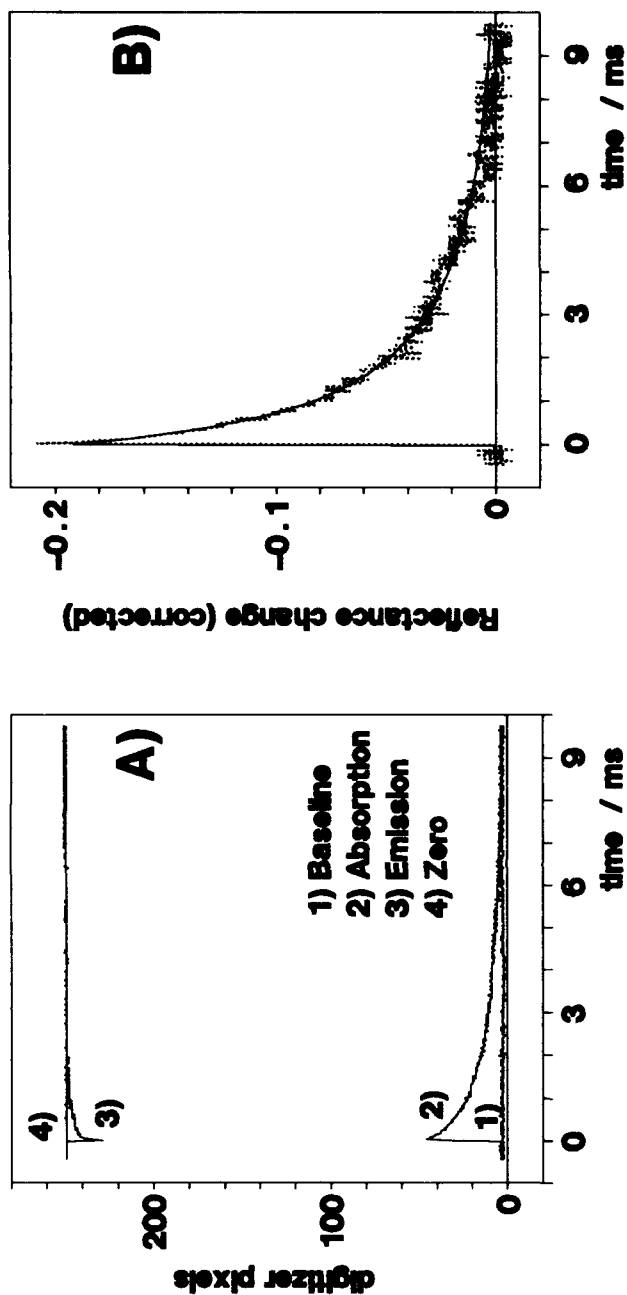
FIGURE 2. DIFFUSE REFLECTANCE LASER FLASH PHOTOLYSIS OF 0.15 μMOL OF ADSORBED EOSIN PER GRAM OF SILICA POWDER, EXCITED AT 532 NM WITH A 8 NS LASER PULSE. A) SEPARATE DIGITIZER TRACES. B) CORRECTED REFLECTANCE CHANGE.

2. EXPERIMENTAL

The equipment used for nanosecond laser flash photolysis in diffuse reflectance mode is identical to that used for studies in transmission mode except for the geometry for collecting the analysing light which is typically as shown in Figure 1. Samples are often held in a powder holder behind a quartz window or in a sealed fluorimeter cell. The observable in diffuse reflectance laser flash photolysis is ΔR(t) defined as follows:

$$\Delta R(t) = \frac{R_b - R(t)}{R_b} \tag{1}$$

where R_b is the sample reflectance before exposure to the exciting laser pulse and R(t) the reflectance at time t after excitation. ΔR is thus the fractional change in reflectance and ΔR x 100 is often referred to as the percentage absorption by the transient.

Figure 2A shows the four traces which are recorded at each analysing wavelength necessary to obtain a corrected trace of reflectance change ΔR(t) as a function of time. The four experimental traces are: 1) Baseline trace i.e. analysing light reflected ιrom sample in the absence of laser excitation. 2) Absorption trace i.e. analysing light reflected from sample before (pretrigger) and after laser excitation. This shows a decrease in reflection due to absorbing transients. 3) Emission trace i.e. any emission caused by laser excitation in the absence of analysing light. 4) Zero trace i.e. the digitizer is fired in absence of either laser excitation or analysing light to establisn the zero settings. From these four traces a corrected trace of the reflectance change as a function of time can be obtained (see Figure 2B) at each analysing wavelength. Time resolved spectra are obtained by measuring many such traces at different wavelengths and then plotting the magnitude of the reflectance change as a function of wavelength at a known delay. Full experimental details are given in references 13 - 15.

2.1. Data Analysis of Transient Changes in Diffuse Reflectance

More extensive discussions of the analysis of data are given elsewhere.[16,17] Following the Kubelka-Munk treatment[18] for diffuse reflectance two light fluxes are considered travelling in opposite directions (see Figure 3A) perpendicular to the
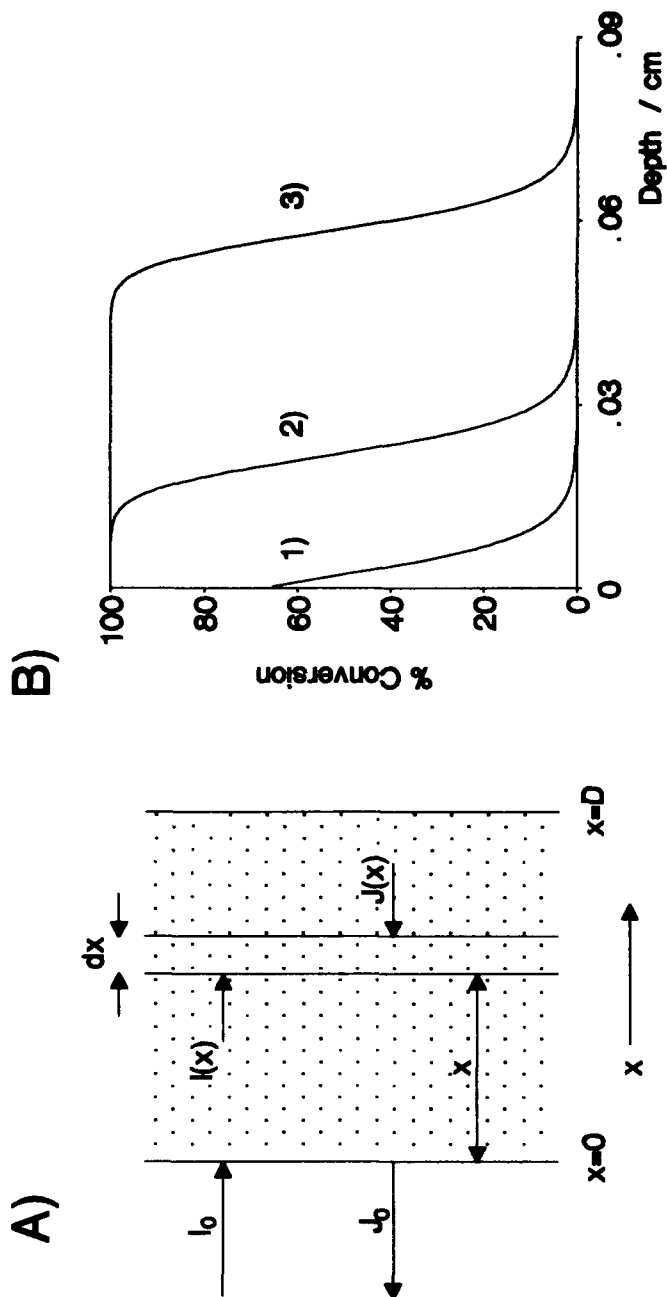
FIGURE 3. A) SCHEMATIC DIAGRAM OF INCIDENT, I AND REFLECTED, J LIGHT PASSING THROUGH A DIFFUSE MEDIUM. B) PLOT SHOWING % CONVERSION OF GROUND-STATE EOSIN TO THE DEPTHS SHOWN BELOW AN IRRADIATED SURFACE FOR 1) 1.0, 2) 10 AND 3) 50 MJ LASER PULSES AT 532 NM.

irradiated surface at x = 0 The attenuation of the incident flux
I depends on the absorption and scattering coefficients K and S
respectively and is given by

$$dI(x) = -I(x) (K+S) dx + J(x)Sdx \qquad (2)$$

and the generated flux since it passes in the opposite direction

has $$dJ(x) = J(x) (K+S) dx - I(x)Sdx. \qquad (3)$$

The diffuse reflectance R is given by

$$R = \frac{J_o}{I_o} \qquad (4)$$

where I_o and J_o are the incident and reflected fluxes at the
surface. Equations (2) and (3) can be solved for a layer so
thick that any further increase in thickness does not affect R
and provided K and S are independent of x this gives

$$\frac{(1-R)^2}{2R} = \frac{K}{S} = F(R) \qquad (5)$$

F(R), the remission function is linearly dependent on the number
of absorbing chromophores in any sample where S and K are
independent of the penetration depth below the surface.

  In diffuse reflectance flash photolysis the initially excited
chromophores are usually homogeneously distributed. However,
photo-excitation produces transient or permanent changes in
absorption, preferentially just below the irradiated surface.
Theoretical treatments[16,17] show that there are two limiting
types of concentration profile produced, namely an exponential
fall off as a function of penetration depth and a homogeneous (or
"plug") profile these are illustrated schematically in Figure 3B
curves 1) and 3) respectively. The latter case is encountered
with large laser fluencies and with low concentrations of ground
state absorbers, where there is total conversion from ground
state to transient to a certain depth below the irradiated
surface. Since a homogeneous concentration of absorbers exists
the Kubelka-Munk theory can be applied [18]. For optically thick
samples at analysing wavelengths where only the transient absorbs
the remission function given by equation (5) is a linear function

of the concentration and can be used for kinetic analysis and for plotting absorption spectra. For the low percentage conversions the concentration of transients decreases exponentially below the irradiated surface. This occurs when there is a high concentration of ground state absorbers and with low laser fluencies. An analytical solution for the change in reflectance expected has been obtained by Lin and Kan [19] and is in the form of a converging series which has been shown[16] to relate ΔR as a linear function of the concentration of transient at values of ΔR less than 0.1.

Between these two limiting cases the change in ΔR with concentration depends on the concentration profile below the irradiated surface. In order to establish if either of the two limiting cases pertain it is necessary to calculate the expected change in transient concentration as a function of distance below the irradiated surface.

2.2 Calculation of Transient Concentration Profiles

To extract kinetic information from $\Delta R(t)$ one must first understand the concentration profile. A detailed description of the modelling procedure, including all relevant equations, has been published[16,17]. A brief outline of the algorithm is given below.

1) The sample is divided into a large number of thin slices *i*, such that the concentration of the ground-state absorbers stays constant within each individual slice. When the procedure starts (before the sample is subjected to laser excitation) the concentration of ground state absorbers, A in each of the slices is $A_i = A_o$, the initial concentration of ground-state absorbers. The absorption coefficient at the laser wavelength is given by $K^e_{A,i} = 2\epsilon^e_A A_i$ where ϵ^e_A is the extinction coefficient of A at the excitation wavelength. Usually it is assumed that the transient does not absorb significantly at the laser wavelength and that the scattering coefficient S is independent of wavelength.

2) The laser pulse which excites the sample is divided into portions Δt where Δt is generally 1/100 of the total pulse duration.

3) The sample is considered as having being irradiated with a portion Δt of the laser pulse. The concentrations of transient species T_i formed in each slice because of light absorption are

determined, and a new set of ground-state concentrations A_i are calculated. In general, after the sample has been exposed to a portion of the laser light, the concentrations A_i are no longer equal, due to the attenuation of the exciting pulse as it passes through the sample. Mass conservation requires that $A_i + T_i = A_o$ in all slices.

4) Using the new values A_i, new absorption coefficients $K^e_{A,i}$ are calculated for each slice.

5) The procedure recycles to step 3), and the next portion of the laser pulse is considered to irradiate the sample.

6) When all of the laser pulse has irradiated the sample, the concentration of ground state absorbers A_i and the concentration of transient species T_i in each slice are known.
Steps 1) through 6) generate the transient concentration profile. To calculate ΔR at an appropriate analysing wavelength the following additional steps are performed.

7) Estimates of the extinction coefficients at the *analysing* wavelength for the transient species, ϵ^a_A are used to calculate the absorption coefficients in each slice due to the ground-state absorbers $K^a_{A,i} = 2\epsilon^a_A A_i$, and transient species, $K^a_{T,i} = 2\epsilon^a_T T_i$.

8) The reflectance of each slice, R_i, can now be calculated using the absorption coefficients $K^a_{A,i}$, $K^a_{T,i}$ and the scattering coefficient S.

9) Finally, the individual reflectances R_i are combined using a recursion formula to give the expected reflectance of the sample.

If the absorption coefficient K is in excess of 10^4 cm^{-1} at the laser excitation wavelength then the penetration depth is only about 1μm and dissipation of laser excitation as heat causes considerable temperature rises (see reference 20). We have not only shown how to predict any temperature rises but have confirmed our calculations by measurements in the case of TiO_2. The possibility of large temperature rises has always to borne in mind and lower laser fluences, lower concentrations or excitation into weaker bands must be employed where necessary to avoid thermal effects. It is important to stress that when the penetration depth of the exciting light is > 0.1 mm, temperature rises in opaque samples using our nanosecond laser system are negligible i.e. < 1°C.
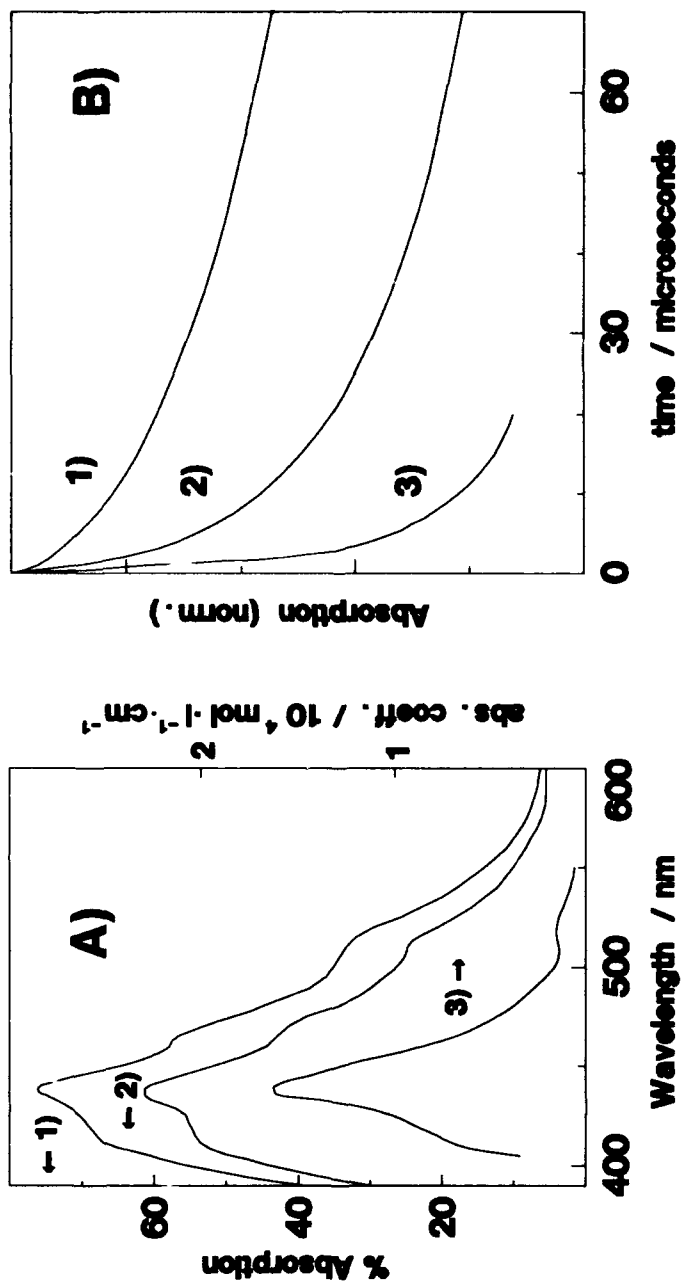
FIGURE 4. A) TRIPLET-TRIPLET ABSORPTION SPECTRA OF ACRIDINE (3% COVERAGE) ON SILICA 1) 0.5 MS, 2) 2 MS, AFTER LASER EXCITATION AND 3) IN BASIC ETHANOL SOLUTION. B) DECAY OF TRIPLET ACRIDINE ON SILICA FOR COVERAGES OF 1) 1%, 2) 3%, AND 3) 23% OF A MONOLAYER.

3. RESULTS AND DISCUSSION

3.1. Triplet-triplet Annihilation on Surfaces

The nature and mobility of species present when acridine is adsorbed from high vacuum and from dry solutions onto thermally pretreated silica have been investigated by ground and excited state spectroscopic techniques[4]. The main adsorbed species is nydrogen bonded acridine which shows strong triplet-triplet absorption at 493 nm (see Figure 4) which for samples of low coverage or high pre-treatment temperature has an exponential decay with a lifetime of 35 ± 2 ms. Such samples do not show delayed fluorescence. However, for samples of higher coverage or lower pre-treatment temperature the triplet decay is faster and non-exponential (see Figure 4) and delayed fluorescence is observed due to the following reaction

$$A^*(T_1) + A^*(T_1) \longrightarrow A(S_0) + A^*(S_1) \longrightarrow 2A(S_0) + h\nu_F \qquad (6)$$

The mechanism of elementary bimolecular interactions at interfaces is by no means fully understood. It can be a consequence of two-dimensional surface migration (diffusion) and bimolecular collisions or alternatively a three-dimensional interaction assuming that the adsorption = desorption equilibrium inside a pore is not completely shifted to the left. In order to clarify this problem we have studied a series of silica powders (particle size - $100\mu m$) with very different pore-diameter ranging from 6 - 100 nm. We have also varied the surface loading on high surface area silicas between 0.075 mg to 1 mg of acridine per g of silica.

The effect of surface coverage on the rate of triplet decay is shown in Figure 4. At very low loading (< 0.1%) we obtain a strictly first order decay with a mean lifetime for the triplet state of 35 ms which is the largest ever reported for acridine at room temperature. At loadings greater than or equal to 1% triplet decay is enhanced and the decay becomes strongly non-exponential. For such non-exponential decays we have evaluated the first half-life as a function of the volume and surface concentration assuming statistical adsorption and using the apparent density of the silica. No correlation is found with volume concentration however, the decay times correlate well with

the surface concentration. This is consistent with a two-dimensional triplet-triplet annihilation mechanism via surface diffusion and rules out a three-dimensional mechanism via volume diffusion. Detailed examination of the triplet absorption decay curves as well as of decay curves for the delayed fluorescence which is observed at higher fractional coverages yield a two-dimensional bimolecular rate constant for triplet-triplet annihilation of 8×10^{13} dm^2 mol^{-1} s^{-1}.

3.2 Combination of Diphenylmethyl Radicals on Surfaces

Organic photoreactions on zeolite supports has become an area of increasing interest in the last few years[21]. A diffuse reflectance nanosecond laser photolysis study of the ketone, xanthone included within the hydrophobic zeolite Silicalite has yielded some very interesting information relating to the host environment[5]. Silicalite is over 99% SiO$_2$ and consists of a system of near-circular zig-zag channels, cross linked by elliptical straight channels[22]. The xanthone transient was assigned as the triplet since it has a characteristic maximum at 605 nm. Another observation made was that the decay process extends over a considerable timescale from nano- to micro-seconds. This suggests a variety of lifetimes for this ketone triplet at different surface sites. The growth of this transient on picosecond timescales constituted the first reported example of picosecond diffuse reflectance laser flash photolysis[2].

The α-cleavage of 1,1,3,3-tetraphenylacetone (TPA), reaction (7) has been used as a source of diphenylmethyl radicals in our experiments[23]. The production of the second diphenylmethyl radical via decarbonylation of the initially produced diphenylacetyl radical occurs rapidly[24] ($k = 1.3 \times 10^8$ s^{-1}) and reaction (7) is, thus, an efficient and practically instantaneous source of two diphenylmethyl radicals per ketone molecule.

$$Ph_2CHCOCHPh_2 \xrightarrow{h\nu} Ph_2CHCO + Ph_2CH \longrightarrow 2Ph_2CH + CO \qquad (7)$$
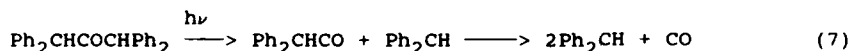
The three solid supports used in these experiments differ considerably in their properties. Silica gel is a porous surface with, in our case, an average pore size of 6 nm and a surface area of 480 m^2/g. Both silica gel and Silicalite contain only silicon and oxygen, although the latter is hydrophobic whereas
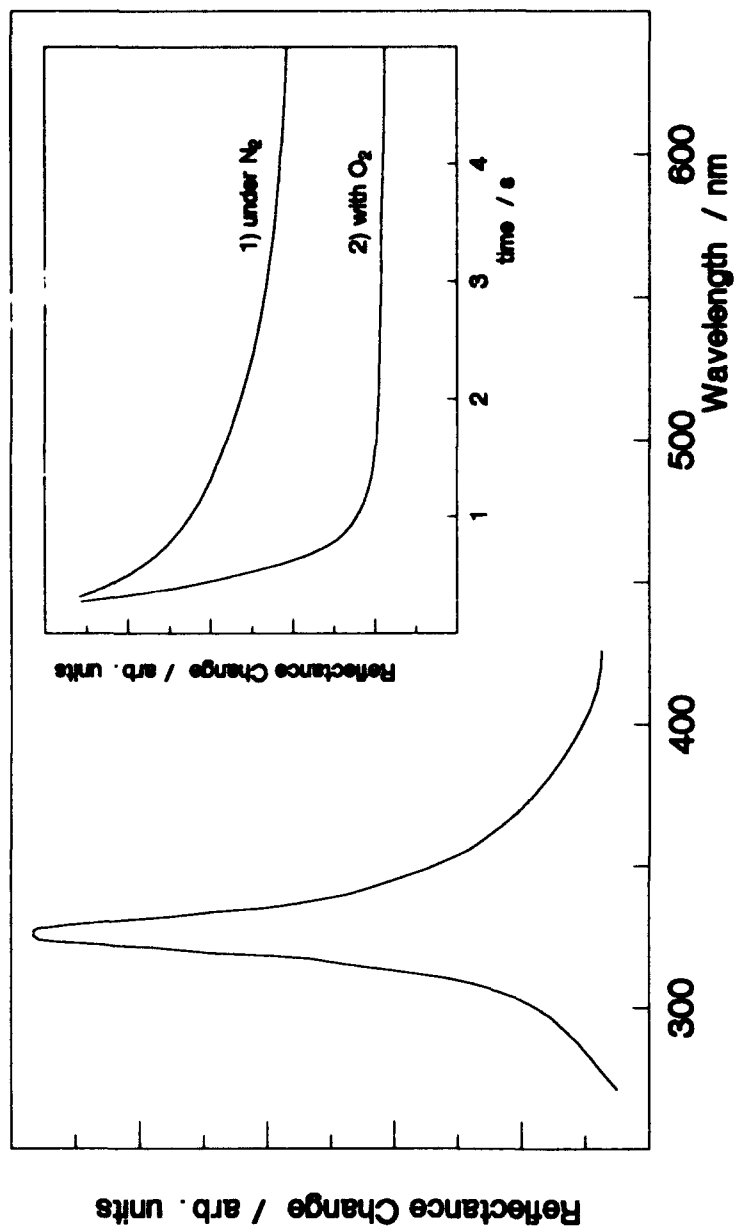
FIGURE 5. TRANSIENT SPECTRUM OF DIPHENYLMETHYL RADICALS PRODUCED BY 266NM EXCITATION OF 3% COVERAGE OF TETRA-PHENYLACETONE ON SILICA. INSET SHOWS TRANSIENT DECAYS MONITORED AT 340 NM.

the former has a large amount of physical adsorbed water on the surface. The structure of the aluminosilicate NaX zeolite is comprised of a three-dimensional network of relatively large cavities or supercages (~1.2 nm) connected by 0.7-0.8 nm pores or channels[24]. The Si/Al ratio of approximately 1.5 results in a large proportion of exchangeable cations (in our case Na) and a strongly hydrophilic zeolite. It should be noted that TPA can easily fit within the pore structure of silica gel and the channel system of Nax. However, the relatively small channels of Silicalite result in adsorption of TPA only on the external surface, although the photoproduced diphenylmethyl radical may migrate into the channels. For all the three supports diphenyl methyl radicals are produced with a characteristic absorption maximum at 335 nm (e.g. see Figure 5) which decays over timescales which vary from hundreds of nanosecond to minutes. The first half-life is much shorter than the second half-life which is shorter than the third half-life etc. These decays can be interpreted[23] in terms of dispersive kinetic analysis[25] to give a distribution of rate constants and a mean value. As can be seen in Figure 5, the radical decay shows oxygen quenching. The efficiency of oxygen quenching increases in going from Silicalite, to NaX, to silica gel, consistent with the greater assessability of oxygen to silica gel pores as opposed to the narrow channels in NaX and very narrow channels in Silicalite.

The above results demonstrate that diphenylmethyl radicals may be readily generated on silica gel, and on the molecular sieves, NaX and Silicalite. The diphenylmethyl radicals show a very wide range of lifetimes on all three supports, as evidenced by the fact that one can obtain lifetimes of anywhere from several microseconds to minutes. Furthermore, for some of the samples there are probably radicals which are decaying on shorter timescales than we can monitor. These results suggest that there are a wide range of possible sites or environments for the radicals. It should be noted that these may reflect largely the distribution of the radicals with respect to each other and the starting ketone rather than particular surface sites on which the radicals are particularly stable. In experiments in which we varied the surface loadings[23], we did not see any evidence for preferential filling of particular sites at low loadings, neither
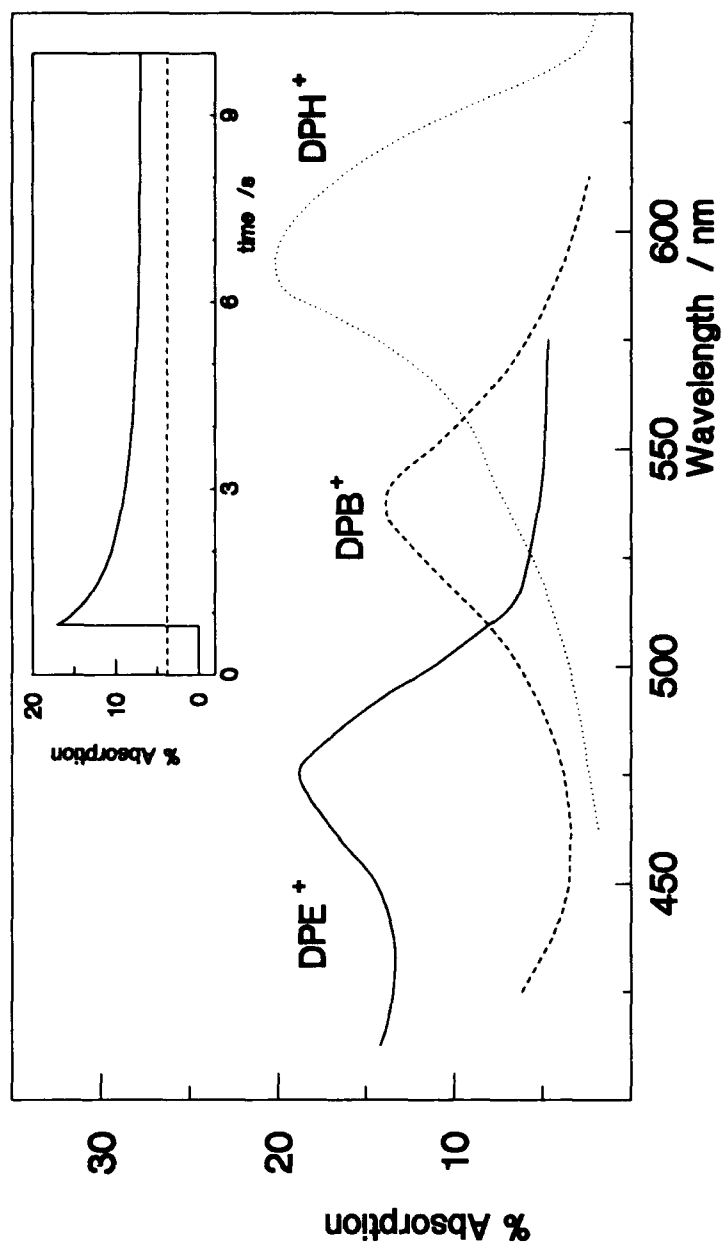
FIGURE 6. TRANSIENT ABSORPTION SPECTRA OF DPE+ ON ALUMINA PRETREATED AT 300°C, AND DPB+ AND DPH+ ON ALUMINA PRETREATED AT 100°C. THE SPECTRA WERE MEASURED 1 MS AFTER THE LASER PULSE. INSET SHOWS LONG-LIVED DECAY.

did we see attenuation effects which could be attributed to the dominance of second order components in the decay of the radicals. A lengthening of the transient lifetimes at low loading would have been expected if radical-radical coupling involving diffusion of both partners was determining the transient lifetime. However, product studies[23] indicate that the radical dimerization accounts for most of the products from laser irradiations. It is likely that a large fraction of the radicals decay very rapidly via dimerization and are invisible in our transient experiments.

3.3 Radical Cation-Electron Recombination

Adsorbed radical cations have been detected by the method of diffuse reflectance laser flash photolysis using polycrystalline microporous catalytic metal oxides such as silica and alumina as adsorbents[3]. We have studied several diphenylpolyenes adsorbed on alumina. Typical transient absorption spectra obtained for 1,2-diphenylethene (DPE), 1,4-diphenylbutadiene (DPB) and 1,6-diphenyl-1,3,5-hexatriene (DPH) adsorbed on alumina recorded 1 ms after excitation are shown in Figure 6. These transients are long-lived and decay with a non-exponential decay with the first half-life considerable shorter than the second half-life and so on. In the case of DPH on alumina, we also observed[3] a much shorter lived transient which we have assigned to the adsorbed triplet state of DPH.

There is evidence that the long lived transients in DPE, DPB and DPH are radical cations. Thus for DPE adsorbed on Al_2O_3/SiO_2 the radical cation is known to have its stronger absorption band at 480 nm, while for DPB ad DPH adsorbed on this catalyst the strongest ground-state absorption bands of the radical cations occur at 542 and 602 nm, respectively[26]. In solution a short-lived transient ($\tau < 100$ ns, $\lambda_{max} = 478$ nm) is reported after flashing charge-transfer complexes of DPE in the presence of an electron acceptor such as fumaronitrile,[27]. This transient is assigned as the radical cation. We therefore assigned the long-lived transient in DPE and DPB and of DPH as radical cations. We have proved this assignment by measuring the ESR spectra of the adsorbed radical cations at low temperature[28].

From studies of the dependence of the amounts of radical produced as a function of laser intensity coupled with the
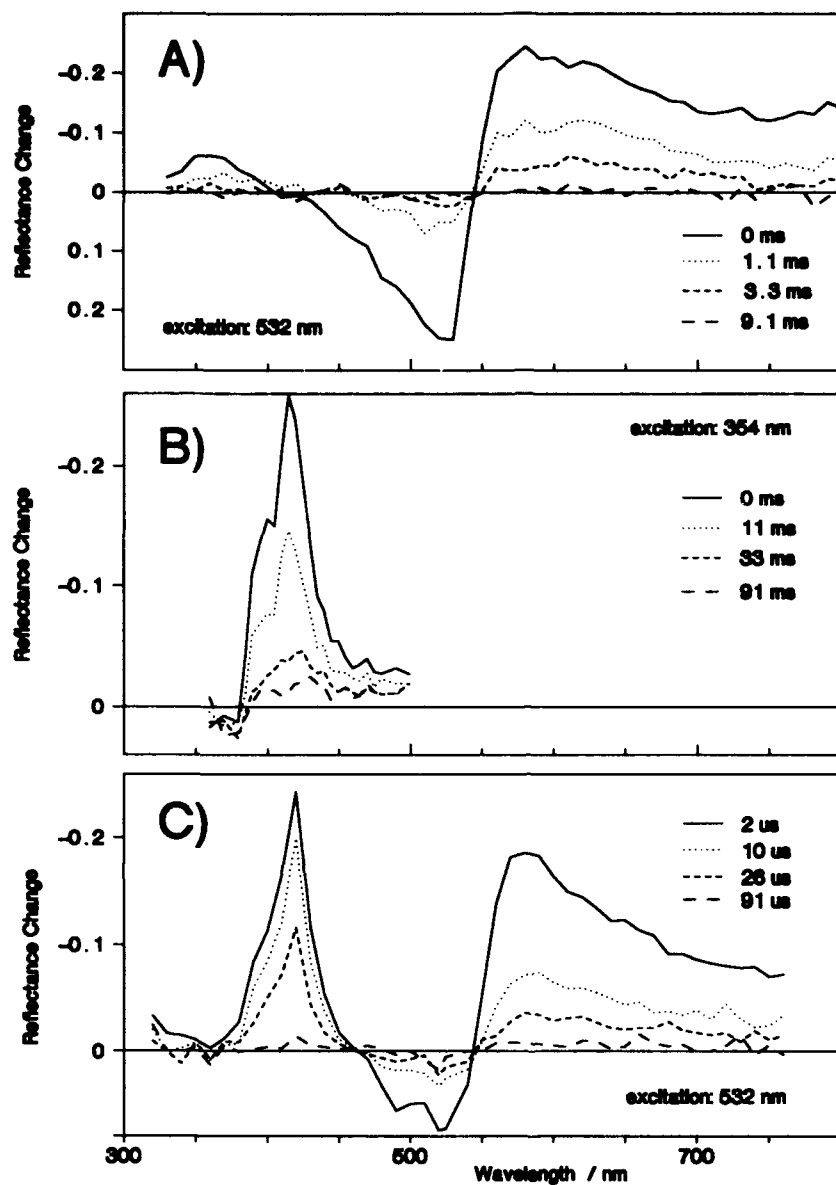
FIGURE 7. TIME RESOLVED TRANSIENT DIFFERENCE DIFFUSE REFLECTANCE SPECTRA FROM SILICA WITH A) 0.12 μMOL EOSIN, B) 6 μMOL ANTHRACENE AND C) 0.12 μMOL EOSIN AND 6 μMOL ANTHRACENE PER GRAM OF SILICA.

computer modelling of the transient concentration profile it is possible to show that the production of the radical cation is a multiphoton process,[28] probably involving the consecutive absorption of two photons.

The decay of these transients has been shown to be very dependent on the temperature, on the nature of adsorbent and on its pre-treatment. Repetitive excitation at room temperature of the same sample area at intervals of a few minutes demonstrates that the intensity of absorption and the decay kinetics of the radical cation are reproducible. Thus the radical cations decay almost exclusively to give back the original molecule. Thus the complex decay is due to radical cation - electron recombination. Variation in surface coverage of adsorbates gives only very small differences in the kinetics observed. This suggests that the process of ionization leaves the radical cation and the electron separated by small distances (smaller than the nearest distance between adsorbates) and that geminate pair recombination is the decay mechanism. The decays fit quite well the expression

$$C_o/C = 1 + \alpha t^{\frac{1}{2}} \tag{8}$$

where C_o and C represent the concentrations of the radical cations formed initially and remaining after time t. The values of α are strongly temperature, adsorbent and adsorbate dependent[28].

3.4 Triplet Energy Transfer on Surfaces

Diffuse reflectance laser flash photolysis has been used by Turro et al[29] and by ourselves[30] to demonstrate triplet energy transfer from triplet benzophenone to naphthalene and some of its derivatives on silica and microcrystalline cellulose via static and dynamic pathways. Recently[31] we have studied energy transfer from triplet eosin to anthracene adsorbed on porous silica and Figure 7 shows some typical results.

Eosin adsorbed on silica exhibits a long lived transient after laser excitation at 532 nm. This we assign to the broad triplet-triplet absorption of eosin with λ_{max} at 600 nm. There is strong laser induced ground state depletion and very good isosbestic points are observed (see Figure 7A). Anthracene adsorbed on silica gives no transient absorption when excited at 532 nm since

it does not absorb at this wavelength but excitation at 354 nm yields the characteristic triplet-triplet spectrum of anthracene with λ_{max} = 420 nm (see Figure 7B). Excitation at 532 nm of eosin coadsorbed with anthracene on silica demonstrates that triplet energy transfer occurs since sensitized production of triplet anthracene results (see Figure 7C). In addition, the lifetime of triplet eosin decreases with increasing anthracene concentration due to the process

$$^3\text{Eosin}^* + \text{Anthracene} \longrightarrow {}^3\text{Anthracene}^* + \text{Eosin} \tag{9}$$

On short timescales the growth in sensitized triplet anthracene is detectable. Later on an equilibrium is established between triplet eosin and triplet anthracene and both triplets then decay with the same apparent lifetime. From the quenching of triplet eosin by anthracene and kinetics of the growth of triplet anthracene, it is possible to obtain a two dimensional rate constant of $6 \pm 2 \times 10^{13}$ dm^2 mol^{-1} s^{-1} for triplet energy transfer on a silica surface. This value is close to the value we obtained for triplet-triplet annihilation of acridine on silica (see earlier) and we consider it may well be the two dimensional diffusion controlled rate constant for silica surfaces pretreated at 100°C. There are very few literature values to compare these values with but Turro et al[29] and De Mayo et al[32] report rate constants for quenching of triplet states on silica surfaces which are two orders of magnitude larger than those reported here. This difference could easily be due to the different pretreatment of the adsorbents.

4. CONCLUSIONS

Diffuse reflectance laser flash photolysis has been shown to be a powerful method for studying photoinduced elementary reactions at interfaces and within highly scattering samples. In this work we were able to measure two-dimensional rate constants for certain heterogeneous systems while in other studies dispersive kinetics were observed. It needs to be stressed that this technique can be applied to reactions in all types of heterogeneous systems as well as at gas/solid interfaces as discussed here. The ability to rapidly control the switching on,

with a pulsed laser, of every type of elementary reaction at interfaces and in other heterogeneous environments and to follow the resulting reactions is enhancing considerably understanding of such systems.

REFERENCES

1) R.W. Kessler and F. Wilkinson, J. Chem. Soc., Faraday Trans I, 77 (1981) 309.

2) F. Wilkinson, C.J. Willsher, P. Leicester, J.R.M. Barr and M.J.C. Smith, J. Chem. Soc., Chem. Commun., (1986) 1216.

3) F. Wilkinson, C.J. Willsher, D. Oelkrug, G. Krabichler and W. Honnen, J. Phys. Chem., 92 (1988) 589.

4) D. Oelkrug, S. Uhl, C.J. Willsher and F. Wilkinson, J. Phys. Chem. 93 (1989) 4551.

5) F. Wilkinson, C.J. Willsher, M.L. Casal, Linda J. Johnston and J.C. Scaiano, Can. J. Chem. 64 (1986) 539.

6) F. Wilkinson, C.J. Willsher, S. Uhl, W. Honnen and D. Oelkrug, J. Photochem. 33 (1986) 273.

7) J. Pouliquen, D Fichou, P. Valat, J. Kossanyi, F. Wilkinson and C.J. Willsher, J. Photochem. 35 (1986) 381.

8) J. Kossanyi, D. Kouyte, J. Pouliquen, J.C. Ronfard-Haret, P. Valat, D. Oelkrug, U. Mammel, G.P. Kelly and F. Wilkinson. J. Lumin. 46 (1989) 17.

9) F. Wilkinson and C.J. Willsher, Chem. Phys. Letts. 104 (1984) 272.

10) F. Wilkinson and C.J. Willsher, J. Lumin. 33 (1988) 187.

11) F. Wilkinson, C.J. Willsher, J.L. Bourdelande, J. Font and J. Greuges, J. Photochem. 38 (1987) 381.

12) F. Wilkinson and C.J. Willsher, J.Chem. Soc., Chem. Comm. (1985) 142.

13) F. Wilkinson, J. Chem Soc., Faraday Trans II, 82 (1986) 2073.

14) F. Wilkinson and G.P. Kelly, Diffuse Reflectance Flash
    Photolysis, in: Handbook of Organic Photochemistry, Vol. 1,
    ed. J.C. Scaiano (CRC Press, Boca Raton, 1990) chap. 12.

15) F. Wilkinson and C.J. Willsher, Diffuse Laser Flash Photolysis
    of Dyed Fabrics and Polymers, in: Lasers in Polymer Science
    and Technology: Applications, Vol II, eds, J.P. Foussier and
    J.F. Rabek (CRC Press, Boca Raton, 1990) chap. 9.

16) R.W. Kessler, G. Krabichler, S. Uhl, D. Oelkrug, W.P. Hagan,
    J. Hyslop and F. Wilkinson, Optical Acta. 30 (1983) 1099.

17) D. Oelkrug, W. Honnen, F. Wilkinson and C.J. Willsher,
    J. Chem. Soc., Faraday Trans II, 83 (1987) 2081.

18) P. Kubelka, J. Opt. Soc. Am. 38 (1948) 448.

19) T. Lin and H.K.A. Kan, J. Opt. Soc. Am. 60 (1970) 1252.

20) F. Wilkinson, C.J. Willsher, S. Uhl, W. Honnen and
    D. Oelkrug, J. Photochem. 33 (1986) 273.

21) H.L. Casal and J.C. Scaiano, Can. J. Chem. 62 (1984) 628.

22) E.M. Flanagen, J.M. Bennett, R.W. Grose, J.P. Cohen, R.L.
    Patton, R.M. Kirchener and J.V. Smith, Nature 271 (1978) 512.

23) G. Kelly, C.J. Willsher, F. Wilkinson, J.C. Netto-Ferreira,
    A. Olea, D. Weir, L.J. Johnston and J.C. Scaiano, Can. J.
    Chem. 68 (1990) 812.

24) I.R. Gould, B.H. Baretz, and N.J. Turro, J. Phys. Chem. 91
    (1987) 925.

25) T. Doba, K.U. Ingold, W. Siebrand and T.A. Wildman, Faraday
    Discuss. Chem. Soc. 78 (1984) 175.

26) G. Kortum and V. Schlichenmaier, Z. Phys. Chem. (Neue Folge)
    48 (1966) 27.

27) J.L. Goodman and K.S. Peters, J. Am. Chem. Soc. 107 (1985)
    1441.

28) D. Oelkrug, S. Reich, F. Wilkinson, P.A. Leicester, J. Phys.
    Chem. in print.

29) N.J. Turro, M.B. Zimmt, I.R. Gould and W. Mahler, J. Am.
    Chem. Soc. 107 (1985) 582.

30) F. Wilkinson and L.P.V. Ferreira, J. Lumin. 49 (1988) 704.

31) F. Wilkinson, R. Beer and P.A. Leicester, in print.

32) P. de Mayo, L.V. Natarajan and W.R. Ware, Chem. Phys. Letts.
    107 (1984) 187.

111

Diffuse-reflectance laser flash photolysis studies of the photochemistry of bleached thermomechanical pulp

John A. Schmidt and Cyril Heitner

Pulp and Paper Research Institute of Canada, 570 Boulevard St. Jean, Pointe Claire, Québec H9R 3J9 (Canada)

Graeme P. Kelly, Phillip A. Leicester and Francis Wilkinson

Department of Chemistry, University of Technology Loughborough, Leicestershire LE11 3TU (U.K.)

(Received September 5, 1990)

Abstract

Diffuse-reflectance laser flash photolysis was used to study the photochemistry of bleached, black spruce mechanical pulp. Following laser excitation of bleached pulp samples at 354 nm, a transient absorption spectrum was observed with $\lambda_{max} = 450$ nm. Oxygen and the phenolic hydroxyl groups in lignin reduced the detected amount of transient by static quenching, and the intensity of the transient spectrum also decreased in pulps reduced with sodium borohydride. The transient was assigned as the electronic triplet state of the aryl ketone group in lignin. Computer simulations indicated that the concentration of the ketone triplet states varied exponentially with depth into the sample, and kinetic analysis was carried out on this basis. The decay of the transient was remarkably long, and was not described by either simple first-order or higher-order kinetics. We interpret this as a manifestation of the heterogeneity of lignin; the aromatic ketone group is distributed over a variety of structurally or chemically distinct sites in the macromolecule.

1. Introduction

Mechanical and ultrahigh yield wood pulps yellow rapidly in daylight, primarily due to the photo-oxidation of lignin [1]. Thus their use is restricted to inexpensive grades of short-life products such as newsprint, and advertising, catalogue and directory papers, even though they can be bleached to high whiteness using hydrogen peroxide. If this whiteness could be stabilized, bleached mechanical pulps could replace significant amounts of more expensive, less environmentally friendly chemical pulps in higher value products. Apart from its commercial importance, the elucidation of the mechanism of light-induced yellowing of wood pulps represents a formidable problem in solid state photochemistry.

Lignin accounts for approximately 30% of the mass of softwoods and 20% of the mass of hardwoods [2]. Biosynthesis of lignin occurs through coupling of propyl-substituted phenoxyl radicals, which are formed by enzymic dehydrogenation of *p*-hydroxycinnamyl alcohols (*e.g.* coniferyl alcohol, Fig. 1). A diverse array of bonding patterns join the phenylpropane building blocks of this complex natural polymer into a rigid, three-dimensional network.

Three structural groups are thought to be important to the photochemical yellowing of wood pulps (Fig. 1): aromatic ketones are the major light-absorbing group in the

112

OH

OCH₃

OH

Coniferyl Alcohol

CH₂OH

O

O-LIGNIN

OCH₃

O-H or LIGNIN

Aromatic Ketone

CH₂OH

LIGNIN or H-O

O-LIGNIN

OCH₃

OH

Phenolic Hydroxyl

O-H or LIGNIN

CH₂OH

CH₂OH

O

O

O-LIGNIN

OCH₃

OCH₃

O-H or LIGNIN

α-Phenoxylacetophenone
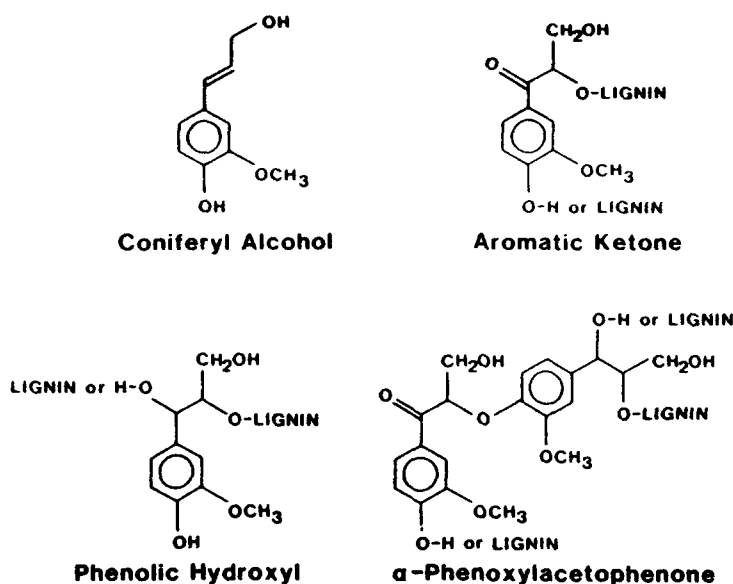
Fig. 1. Some structures in softwood lignin relevant to photochemical yellowing.

300–400 nm region, phenolic groups are a source of easily abstractable hydrogen atoms [3, 4], and α-phenoxylacetophenones undergo rapid photochemical cleavage of the α-C—O bond, yielding phenoxyl and phenacyl radicals [5, 6]. The yellow colour is thought to arise from quinones, which are formed after attack by oxygen at the phenoxyl radicals [7, 8].

Because of the difficulty of working with solid materials, most mechanistic studies have been performed in solution with lignin model compounds, or isolated lignin preparations [3–5, 9–12]. Extrapolation to the behaviour of a solid lignin –cellulose–hemicellulose composite (*i.e.* paper) is difficult. However, the recent extension of many spectroscopic techniques (nuclear magnetic resonance (NMR), Fourier transform IR (FT-IR), UV–visible) to solid materials is providing new insight into this problem. In this paper, we report the observation and preliminary kinetic analysis of short-lived intermediates in bleached, black spruce thermomechanical pulp (TMP) by diffuse-reflectance laser flash photolysis (DRLFP) [13].

2. Experimental details

2.1. General

Black spruce thermomechanical pulp, as a 20% by mass aqueous suspension, was bleached at 60 °C for 2 h with alkaline hydrogen peroxide (4% relative to the mass of oven-dried pulp). The ISO brightness (reflectance at 457 nm) of the bleached pulp was 75. Methylated samples were prepared as previously described [14]. Optically thick samples were prepared either as sheets of basis weight 200 g m⁻², or by grinding the pulp to a powder and placing it in a powder holder (approximately 1 cm in diameter).

Similar results were obtained from both types of sample. Low basis weight, optically thin sheets (10–60 g m^{-2}) were prepared as previously described [15].

Ground state absorption coefficients and scattering coefficients of the pulp were determined by measuring the diffuse reflectance of 10 g m^{-2} sheets over a black, non-reflecting background, and over a white background of known reflectance [15, 16]. Values were obtained at 2 nm resolution over the range 260–500 nm.

The DRLFP system has been described previously [14]: excitation was obtained using the 354 nm line of a Lumonics HY-200 Nd:YAG laser; diffuse reflectance from the sample was detected with a Hamamatsu R928 photomultiplier tube and a Tektronix 7612 digitizer; an IBM XT-286 computer controlled the experiment and stored the data.

The observable in DRLFP is the change in diffuse reflectance at the analysing wavelength at time t after the laser flash, $\Delta R(t)$

$$\Delta R(t) = \frac{R_b - R(t)}{R_b} \tag{1}$$

R_b is the sample reflectance before exposure to an exciting laser pulse and $R(t)$ is the reflectance at time t after the pulse. Transient absorption spectra were plotted as $\Delta R \times 100$ (percentage absorption change) vs. wavelength.

The maximum of the transient absorption spectrum is in the 440–450 nm region; ΔR at 450 nm was used for the determination of the transient concentration profile and for kinetic analysis. For measurements of ΔR as a function of basis weight, the basis weight was varied by stacking 10 g m^{-2} sheets one on top of the other. Alternatively, single sheets with basis weights of 10, 20, 30, 40, 50, 60 and 100 g m^{-2} were used.

Fitting of the kinetic data to a two-exponential function was performed using the Marquardt algorithm for non-linear least-squares analysis [17].

2.2. Modelling the transient concentration profile and ΔR

A detailed description of the modelling procedure, including all relevant equations, has been published [18, 19]. A brief outline of the algorithm is given below.

(1) The sample is divided into a large number of thin slices i, such that the concentration of the ground state absorbers stays constant within each individual slice. The absorption coefficient at the laser wavelength is given by $K_{A,i}^s = 2\epsilon_A^s A_i$. When the procedure starts (before the sample is subjected to laser excitation), the concentration of ground state absorbers in each of the slices is $A_i = A_0$, the initial concentration of ground state absorbers. The scattering coefficient S is assumed to be constant throughout. Also, it is assumed that the transient formed does not absorb significantly at the laser wavelength.

(2) The laser pulse which excites the sample is divided into portions Δt, where Δt is generally 1/100 of the total pulse duration.

(3) The sample is irradiated with a portion Δt of the laser pulse. The concentration of transient species T_i formed in each slice because of light absorption is determined, and a new set of ground state concentrations A_i are calculated. It should be noted that mass conservation requires that $A_i + T_i = A_0$. In general, after the sample has been exposed to a portion of the laser light, the concentrations A_i are no longer equal, due to the attenuation of the exciting pulse as it passes through the sample.

(4) Using the new values A_i, new absorption coefficients $K_{A,i}^s$ are calculated for each slice.

(5) The procedure recycles to step (3), and the next portion of the laser pulse irradiates the sample.

(6) When all of the laser pulse has irradiated the sample, the concentration of ground state absorbers A_i and the concentration of transient species T_i in each slice are known.

Steps (1)–(6) generate the transient concentration profile. To calculate ΔR at an appropriate analysing wavelength, the following additional steps are performed.

(7) Estimates of the extinction coefficients at the analysing wavelength for the transient species (ϵ_T^a) and the ground state absorbers (ϵ_A^a) are required.

(8) These extinction coefficients are used to calculate the absorption coefficients in each slice due to the ground state absorbers $(K_{A_i}^a = 2\epsilon_A^a A_i)$ and the transient species $(K_{T_i}^a = 2\epsilon_T^a T_i)$.

(9) The reflectance of each slice, R_i, can now be calculated using the absorption coefficients $K_{A_i}^a$, $K_{T_i}^a$ and the scattering coefficient S.

(10) Finally, the individual reflectances R_i are summed using a recursion formula to obtain the observed reflectance of the sample.

2.3. Units

In describing the optical properties of scattering materials, the path length of the radiation is customarily given in centimetres. For the modelling procedure, the most convenient units for the optical properties which follow naturally are reciprocal centimetres for K and S, centimetres for the slice thickness, moles per cubic centimetre for concentration, and square centimetres per mole for the extinction coefficient. However, because paper is compressible, an optical path length cannot be defined. Van den Akker [20] has shown that the more precisely defined quantity of basis weight (the mass per unit area) can be substituted for path length in the derivation of the Kubelka–Munk equations, with no loss in rigour. The units which result from this approach are square centimetres per gram for K and S, and grams per square centimetre (i.e. basis weight) for slice thickness. The units of the extinction coefficient must remain the same to be consistent with the units of the laser intensity. This is easily accomplished in the calculation of ϵ_A^e from eqn. (3) (see later) by expressing A_0 in moles per gram.

2.4. Initial choices of values

The scattering coefficient was measured as described above. The background absorption coefficient K_u^e refers to the residual absorption of the support. In mechanical pulp, the absorber is lignin and the support is pure cellulose. The absorption coefficient determined for a sample of pure chromatographic grade cellulose was used for K_u^e.

The maximum output of the laser used for our experiments (Lumonics HY-200 Nd:YAG) was 25 mJ at the excitation wavelength (354 nm). These quantities were used by the program to calculate the number of moles of photons irradiating the sample.

Slice thickness is an adjustable parameter. To obtain satisfactory results, it must be less than 1/100 of the penetration depth of the exciting light. The condition was tested at the beginning of a modelling run.

The napierian extinction coefficient of the ground state at the exciting wavelength (ϵ_A^e) and the concentration of ground state chromophores (A_0) are related by eqn. (3) (see later). The absorption coefficient at 354 nm (K_A^e) was 429 ± 13 cm^2 g^{-1}. Values for ϵ_A^e and A_0 were determined as follows. The aromatic ketone chromophore is the major light absorber in the 300–400 nm region. Studies of softwood milled and dioxane lignins suggest an aromatic ketone content of 0.07 per C_9 unit [21]. Assuming an average molar mass for C_9 units of 180 g mol^{-1}, and that bleached TMP is approximately

30% lignin by mass, gives an aromatic ketone concentration of $0.07 \times (0.3/180) = 1.2 \times 10^{-4}$ mol g^{-1}. This value was assigned to A_0. Thus from eqn. (3), $\epsilon_A^c = 1.8 \times 10^6$ cm^2 mol^{-1}.

3. Results and discussion

3.1. Transient spectra

The transient spectra obtained from bleached TMP under a variety of conditions are shown in Figs. 2 and 3. Under all conditions, the absorption maximum occurs at 440–450 nm and does not shift over the course of the decay. Both oxygen (Fig. 2) and phenolic hydroxyl groups (Fig. 3) reduce the intensity of the transient spectrum, presumably by rapid static quenching. Treatment of the pulp with increasing amounts of sodium borohydride (Fig. 4) reduces the transient intensity by reducing the ground
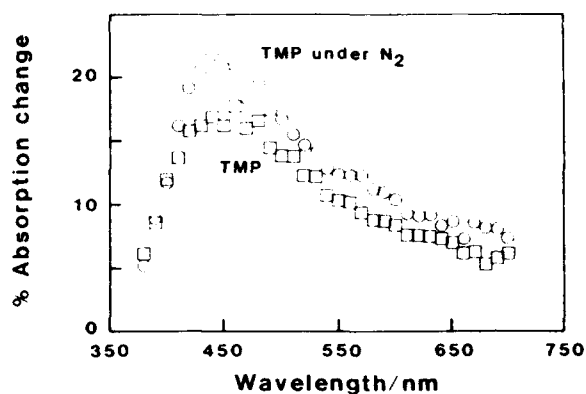

Fig. 2. Transient absorption spectra of bleached, black spruce TMP 0.38 μs after the flash in air and under nitrogen.
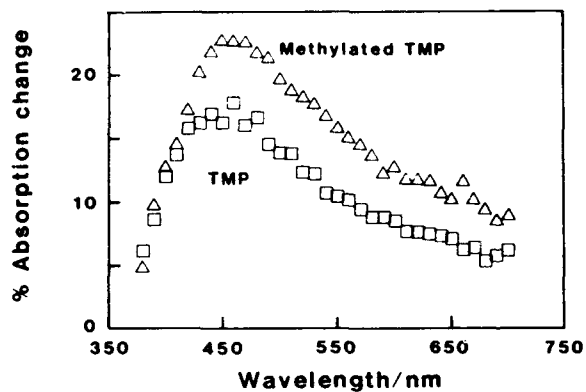

Fig. 3. Transient absorption spectra 0.38 μs after the flash, in air, of bleached, black spruce TMP, and bleached, black spruce TMP treated with phenolic hydroxyl groups (methylated).
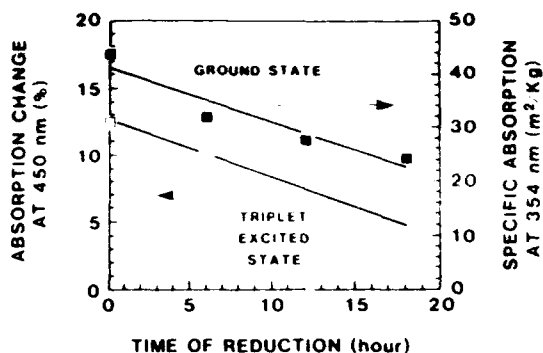
TIME OF REDUCTION (hour)

Fig. 4. Effect of borohydride reduction on the spectral characteristics of bleached TMP. Right axis shows the decrease in ground state absorption at the laser wavelength (354 nm) with increasing time of reduction. Left axis shows the corresponding decrease in the transient absorption change at 450 nm immediately after the laser pulse.

state absorption at the laser wavelength, *i.e.* the light-absorbing group in the pulp is reduced by borohydride.

Aromatic ketones are the only groups known to be present in bleached TMP which have an electronic absorption at 354 nm, and which can be reduced by borohydride. Since both oxygen and phenols quench aromatic ketones efficiently [22], we assign the transient as the lowest triplet state of the aromatic ketone groups in lignin.

Although the quenching behaviour of the transient is consistent with assignment as an aryl ketone triplet state, the absorption maxima are considerably red shifted from those observed for methoxy-substituted acetophenone triplets in solution. For example, the absorption maxima of the triplet states of p-methoxyacetophenone and 3,4-dimethoxyacetophenone are close to 400 nm [11, 23]. In addition, the triplet absorption spectra of these substituted acetophenones do not exhibit the pronounced long-wavelength tail observed for bleached TMP. We attribute these effects to the close packing of chromophores in the solid lignin polymer. An extended long-wavelength absorption, such as that observed here, has also been observed for p-methoxyaceto-phenone adsorbed on the zeolite Silicalite [24], and for poly(p-methoxyacrylophenone) in solution [25].

3.2. Determination of the transient concentration profile

3.2.1. Background

$\Delta R(t)$ depends on the decay of the transient species formed by the laser flash, and on the transient concentration profile. Thus to extract the kinetic information, we must first understand the transient concentration profile. A key relationship in relating concentration to observed reflectance is the Kubelka–Munk remission function $F(R_\infty)$ [26]

$$F(R_\infty) = \frac{K}{S} = \frac{(1-R_\infty)^2}{2R_x} \tag{2}$$

In eqn. (2), K is the absorption coefficient, S is the scattering coefficient and R_∞ is the reflectance of a homogeneous, optically thick sample. An underlying assumption of eqn. (2) is that the concentration of the absorbers is uniform throughout the sample thickness.
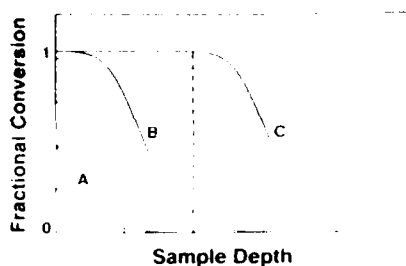
Fig. 5. Schematic representation of the three types of transient concentration profile formed by laser excitation of solid samples: A, exponential profile; B, intermediate profile; C, plug profile. The broken line indicates the penetration depth of the analysing light.

TABLE 1

Initial choices of parameters for generation of transient concentration profile

Scattering coefficient S	291 ± 8 cm^2 g^{-1}
Background absorption coefficient K_u^c	1.47 cm^2 g^{-1}
Laser energy	25 mJ
Laser wavelength	354 nm
Slice thickness	8.5×10^{-6} g cm^{-2}
Number of slices	1000 .
Ground state extinction coefficient ϵ_A^c	1.8×10^6 cm^2 mol^{-1}
Ground state concentration A_0	1.2×10^{-4} mol g^{-1}

After laser excitation, three regimes of transient concentration with respect to sample depth and penetration depth of the analysing light are possible, as depicted in Fig. 5 [19]. Case A arises for samples that have a high absorption coefficient at the laser wavelength, relative to the laser intensity. The exciting pulse is significantly attenuated on passing through each layer of the sample, and the concentration of transient species decreases exponentially with depth into the sample. For these samples, ΔR is directly proportional to the concentration of transient species if $\Delta R \le 0.1$. For ΔR somewhat greater than 0.1 the deviations from linearity are small, but they become quite large as $\Delta R \rightarrow 1$ [18].

Case B occurs at intermediate levels of light absorption. The first few layers of the sample are saturated and form a region of uniform transient concentration, but thereafter the concentration falls off, eventually with an exponential dependence on depth. The analysing light penetrates deeply enough into the sample (broken line in Fig. 5) to probe both of these regions. In this intermediate case, there is no simple quantity directly proportional to the concentration of the transient species. Kinetic analysis is performed by assuming a decay law, and calculating the decay of ΔR from the transient concentration profile. The decay constants are varied until a match between the calculated and experimental decay curves is found.

Case C occurs when the ground state absorption coefficient is low relative to the laser power. Each layer is saturated, and a uniform concentration of transients, a plug, is formed to a depth greater than the penetration of the analysing light. In this situation the Kubelka–Munk relationship applies, and $F(R(t)) - F(R_b)$ is proportional to the concentration of the transient species.

The algorithm used for the determination of a transient concentration profile is summarized in Section 2.2 [19]. The input parameters required for the procedure are the extinction coefficient of the ground state absorber at the exciting wavelength (ϵ_A^c), the concentration of ground state absorbers (A_0) and other parameters listed in Table 1.

3.2.2. Effect of varying ϵ_A^c and A_0 on the transient concentration profile

The parameters in Table 1 give an exponential transient concentration profile. Although the absorption coefficient K

$$K_A^c = 2\epsilon_A^c A_0 \tag{3}$$

can be determined to good precision from diffuse-reflectance measurements, the uncertainties in the individual values of ϵ_A^c and A_0 are large. Therefore, we felt that it was important to establish whether a reasonable variation in these parameters altered the character of the transient concentration profile.

We varied ϵ_A^c and A_0 by an order of magnitude above and below the initial choices in Table 1. If ϵ_A^c was changed by a factor x then A_0 was changed by $1/x$, thus preserving the value of K. The values used are listed in Table 2, and the profiles generated are shown in Fig. 6. The parameter set using the highest value of ϵ_A^c (and therefore the lowest value of A_0) gave an intermediate transient concentration profile, case B of Fig. 5. The other combinations modelled all gave concentration profiles of the exponential type.

These calculations suggest that the transient concentration profile is most likely of the exponential type. However, some uncertainty remains, since the highest value of ϵ_A^c tested generates an intermediate profile. We sought to distinguish between the pairs of ϵ_A^c and A_0 values by calculating $\Delta R(0)$ for the corresponding transient

TABLE 2

Values of ϵ_A^c and A_0 used to generate transient concentration profiles of Fig. 6

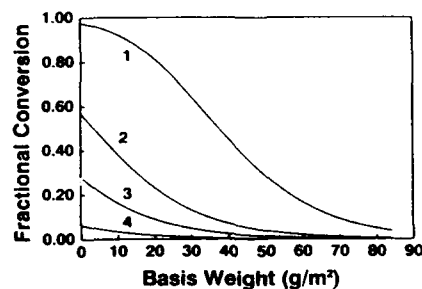| Profile	ϵ_A^c (cm^2 mol^{-1})	A_0 (mol g^{-1})
1	1.8×10^7	1.2×10^{-5}
2	4.5×10^6	4.8×10^{-5}
3	1.8×10^6	1.2×10^{-4}
4	3.6×10^5	6.0×10^{-4}

Fig. 6. Transient concentration profiles corresponding to the values of ϵ_A^c and A_0 in Table 2. All other parameters as listed in Table 1.

concentration profiles (Fig. 6), and comparing them with the experimentally determined values of $\Delta R(0)$.

3.2.3. Calculating ΔR

To calculate a value of ΔR from a transient concentration profile, an additional independent parameter is required: ϵ_T^*, the extinction coefficient of the transient species at the analysing wavelength. Since we assigned the transient observed from bleached TMP as an aromatic ketone triplet, we based our initial estimates on the published extinction coefficient at 450 nm of triplet p-methoxyacetophenone in cyclohexane (10^* cm^2 mol^{-1}) [23]. (Values of ϵ measured in solution are usually given in l mol^{-1} cm^{-1}. Conversion to units of cm^2 mol^{-1} requires multiplication by 1000.) Each profile of Fig. 6 was combined with a range of values of ϵ_T^* above and below the initial estimate, and a value of $\Delta R(0)$ was calculated.

When combined with a value for ϵ_T^* in the range 10^n–10^*, each of the profiles was able to predict the experimentally observed value of $\Delta R(0)$ of an optically thick sample of bleached TMP. Thus this experimental measurement did not resolve which of the two transient concentration profile regimes corresponded to our sample. However, the approach described below was able to distinguish between the two regimes.

Let us consider a bleached TMP sample of basis weight 10 g m^{-2}, such as those used to determine K and S. For any of the transient concentration profiles in Fig. 6, the thickness (basis weight) of this sample is insufficient to absorb all the energy of a 25 mJ laser pulse. (The approximate density of these sheets was 0.2 g cm^{-3}, which gives a thickness of approximately 0.05 cm.) Some of the incident exciting light will pass through the sample, and $\Delta R(0)$ will be less than that of a sample which is optically thick with respect to the exciting light. The dependence of $\Delta R(0)$ on the basis weight of the sample can be calculated for any transient concentration profile. Experimentally, this dependence can be determined in two different ways. Handsheets with a basis weight of 10 g m^{-2} can be stacked together to give samples of varying basis weights. Alternatively, single sheets with basis weights in the range 10–100 g m^{-2} can be prepared.

We performed this experiment for both types of sample. Experimental plots of $\Delta R(0)$ vs. basis weight were compared with the curves predicted by profile 1 of Fig. 6 (the intermediate case B of Fig. 1) and by profile 3 of Fig. 6 (an exponential profile). The comparisons are shown in Figs. 7 and 8 respectively.

The intermediate profile (profile 1), when combined with excited state extinction coefficients of either 2.8×10^6 or 3.0×10^6, gives a fairly good prediction of $\Delta R(0)$ at higher basis weights, where the sample is optically thick with respect to the exciting light (Fig. 7). $\Delta R(0)$ is not predicted very well at lower basis weights. Higher values of the excited state extinction coefficient give better predictions of $\Delta R(0)$ at lower basis weights, but $\Delta R(0)$ values at higher basis weights are then too high.

The exponential profile (profile 3), when combined with values for ϵ_T^* of 1.4×10^6 or 1.5×10^6, gives a good match to the experimental curve for both optically thin and optically thick samples (Fig. 8).

These results favour an exponential profile as the appropriate description of our sample of bleached TMP. Profiles 2 and 4 are also exponential in character, and would also probably give a reasonable prediction of $\Delta R(0)$ vs. basis weight if a different value of the excited state extinction coefficient within the range 10^6 to 10^7 was used. Thus we cannot pinpoint a unique pair of extinction coefficients, ϵ_A^* and ϵ_T^*, which characterize the ground and excited states of the aromatic ketone group in bleached, black spruce TMP. However, on the basis of the analysis above, we feel that we can
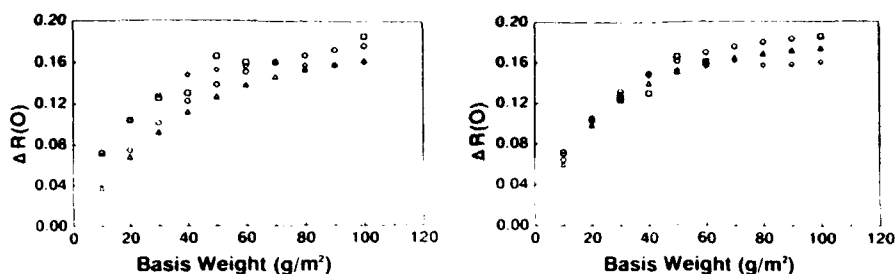
Fig. 7. Comparison of experimental plot of $\Delta R(0)$ vs. basis weight with values calculated assuming an intermediate transient concentration profile (profile 1 of Fig. 6): $\epsilon_A^c = 1.8 \times 10^7$ cm^2 mol^{-1}, $A_0 = 1.2 \times 10^{-3}$ mol g^{-1}. Experimental points: squares represent points where basis weight was controlled using individual sheets of various basis weight; diamonds represent points where basis weight was controlled by piling sheets of basis weight 10 g m^{-2} one on top of another. Calculated points: triangles, $\epsilon_T^c = 2.8 \times 10^6$ cm^2 mol^{-1}; circles, $\epsilon_T^c = 3.0 \times 10^6$ cm^2 mol^{-1}.

Fig. 8. Comparison of experimental plot of $\Delta R(0)$ vs. basis weight with values calculated assuming an exponential transient concentration profile (profile 3 of Fig. 6): $\epsilon_A^c = 1.8 \times 10^6$ cm^2 mol^{-1}, $A_0 = 1.2 \times 10^{-4}$ mol g^{-1}. Experimental points: squares represent points where basis weight was controlled using individual sheets of various basis weight; diamonds represent points where basis weight was controlled by piling sheets of basis weight 10 g m^{-2} one on top of another. Calculated points: triangles, $\epsilon_T^c = 1.4 \times 10^6$ cm^2 mol^{-1}; circles, $\epsilon_T^c = 1.5 \times 10^6$ cm^2 mol^{-1}.

reasonably exclude those values of ϵ_T^c which do not give an exponential transient concentration profile.

3.3. Kinetic analysis

In the previous section, we established that the concentration of transient species formed by the laser pulse falls off exponentially with depth into the sample. For such samples, ΔR is directly proportional to the concentration of the transient species for values of $\Delta R \leqslant 0.1$. Deviations from linearity are small for values of ΔR close to 0.1, but they become severe as $\Delta R \to 1$ [18]. The highest value of ΔR observed for bleached samples is about 0.2; we determined that deviations from linearity were sufficiently small that ΔR could be assumed to be proportional to concentration, and thus it could be used directly for kinetic analysis.

Figure 9 shows the transient signal obtained from bleached, black spruce TMP and 450 nm over two time scales: trace A, 10 μs (20 ns point^{-1} resolution); trace B, 500 μs (1 μs point^{-1} resolution). The signal is remarkably long lived; ΔR is still not zero 500 μs after the laser flash. ΔR returns to zero within about 1 s, i.e. before the laser is triggered again. The initial signal intensity observed at 1 μs point^{-1} is smaller than that observed at 20 ns point^{-1} because the fast information is not captured on long time scales.

Figures 2 and 3 show that the transient is quenched statically by oxygen and by phenolic hydroxyl groups. However, no evidence of dynamic quenching by these groups is observed. On a variety of time scales, the first half-lives of all samples are identical within experimental error.

The absence of dynamic quenching by the phenolic hydroxyl group is easily understood as a consequence of the rigid structure of lignin. Those triplet states which are close to a phenolic group are quenched within the laser flash, but the range of molecular movement within the polymer is too limited to allow dynamic quenching.
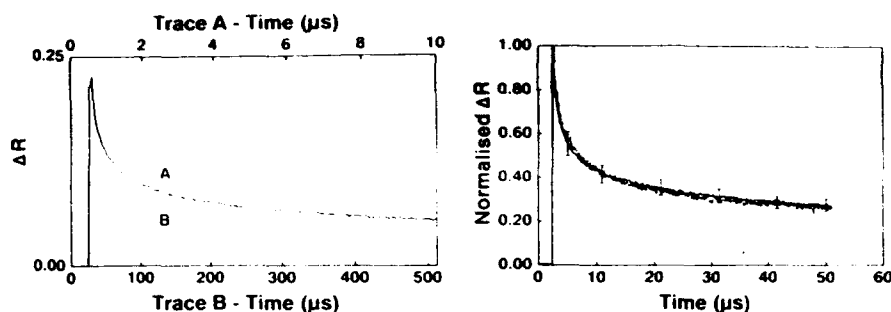
Fig. 9. Decay of transient absorption signal observed at 450 nm in bleached, black spruce TMP after laser excitation at 354 nm: trace A, 20 ns point^{-1} resolution; trace B, 1 μs point^{-1} resolution.

Fig. 10. Transient decays at 450 nm, normalized to the same value of $\Delta R(0)$, for bleached TMP, bleached TMP under nitrogen and bleached TMP with the phenolic hydroxyl groups blocked by methylation. The error bars indicate an uncertainty of $\pm 10\%$.

The absence of a dynamic effect for oxygen quenching is less easily understood; gaseous oxygen should move easily about the macromolecule. Possibly, all the available oxygen is consumed by static quenching, and dynamic quenching becomes limited by the rate of oxygen diffusion into the fibre.

The decay of ΔR cannot be described by simple first-order kinetics; plots of $\ln(\Delta R(t)/\Delta R(0))$ against time are curved. Figure 10 shows plots of ΔR against time, normalized to the same value of $\Delta R(0)$, for bleached TMP, bleached TMP with phenolic hydroxyl groups blocked by treatment with dimethyl sulphate, and bleached TMP under a nitrogen atmosphere. Since the normalized decays of samples corresponding to different values of $\Delta R(0)$ fall on a common curve, the curvature of the first-order plot cannot be attributed to second- or higher-order kinetics [27].

Systems which show the behaviour described above are often analysed as a sum of exponential terms, e.g.

$$\frac{\Delta R(t)}{\Delta R(0)} = A_1 e^{-k_1 t} + A_2 e^{-k_2 t} \tag{4}$$

In such a model, $\Delta R(t)$ represents the absorption of two discrete transient species, each characterized by a unique decay constant. k_1 and k_2 represent the first-order decay constants for species 1 and 2 respectively. The corresponding pre-exponential factors A_1 and A_2 are proportional to the amount of each species present at time zero.

The generally accepted model for the structure of lignin lends at least superficial credence to this idea. Triplet states of methoxyl-substituted α-phenoxylacetophenones (Fig. 1) cleave rapidly ($k \approx 2 \times 10^6$ s^{-1}) at the α-aryl ether bond, giving phenacyl and phenoxyl radicals [6]. Aromatic ketone groups not bearing the α-phenoxyl linkage cannot decay by this pathway, and are expected to decay more slowly. Although aryl ketone triplet groups close to phenolic hydroxyl groups are quenched rapidly by hydrogen abstraction, this occurs within the time of the laser flash, so it does not contribute to the decay of ΔR on nanosecond time scales. As a simple approximation, we divided the aromatic ketone structures in lignin into two discrete groups, those with the α-phenoxyl substitution pattern and those without, and fitted the decay curves in Fig. 9 to eqn. (4).

Each of the decay curves in Fig. 9 gives reasonable values for R^2 and the standard error of the residuals. The values of the parameters recovered for trace A and trace B are shown in Table 3. Although R^2 values and standard errors for the fits are reasonable, the values of the parameters recovered can be assigned little physical significance; in particular, k_1 and k_2 cannot be interpreted as the decay constants of two distinct physical species. Two additional aspects of the data argue against such an interpretation.

First, although the standard error of the residuals appears reasonable, a plot of the residuals (Fig. 11) clearly shows that they are not random. Although radiofrequency interference in the detection circuits may play some role in this, additional chemical processes cannot be ruled out. More importantly, the rate constants recovered from the two different time scales are inconsistent. Clearly, the values of the parameters obtained are dependent on the time over which the transient signal is observed; thus they have limited physical significance.

The long-lived triplet decay and complex kinetic behaviour observed here have also been reported in DRLFP studies of other systems, e.g. p-methoxyacetophenone adsorbed on the zeolite Silicalite [24]. Silicalite offers several types of surface sites for the adsorption of organic molecules, as well as channels where organic molecules of appropriate size can be included. p-Methoxyacetophenone is a reasonable model for the aromatic ketone chromophore in lignin. The long triplet lifetimes observed have been interpreted as the result of a distribution of first-order decays arising from the multiple sites for inclusion or adsorption. An appropriate decay function for this situation has the form

$$\frac{\Delta R(t)}{\Delta R(0)} = \sum_{i=1}^{n} A_i e^{-k_i t} \tag{5}$$

TABLE 3

Parameters from the fitting of $\Delta R(t)/\Delta R(0)$ to a double-exponential function

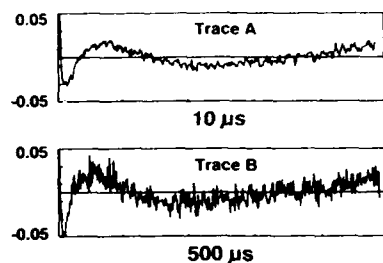| Trace	A_1	k_1 $(10^6\ s^{-1})$	A_2	k_2 $(10^6\ s^{-1})$	R^2
A	0.43	1.9	0.42	0.064	0.99
B	0.47	0.058	0.35	0.0015	0.97

Fig. 11. Plot of the residuals (observed − fitted) for the fitting of traces A and B (Fig. 9) to a two-exponential function (eqn. (4)).

The range of adsorption or inclusion sites gives rise to a range of closely spaced rate constants k_i, which, unfortunately, cannot be resolved by a fitting routine which has both the pre-exponential factors and the rate constants as freely varying parameters. This complex kinetic behaviour is a direct consequence of the inhomogeneity of the system.

The behaviour of the transient signal observed from mechanical pulp is incompatible with the simple picture of two discrete types of aromatic ketone groups in the lignin. Lignin in a pulp fibre wall is an amorphous, inhomogeneous polymer; thus it is reasonable to assume that the aromatic ketone units are distributed among a variety of chemically or structurally non-equivalent sites. The long lifetime and the kinetic complexity of the aromatic ketone triplet state are an indication of this inhomogeneity. A two-exponential function (eqn. (4)) gives a reasonable fit to the data of traces A and B (Fig. 9) largely because of the powerful fitting ability of a function with four freely varying parameters. Although the derived parameters k_1 and k_2 may give crude average rate constants, they give limited insight without a knowledge of the underlying distribution.

That a two-exponential function can give an apparently adequate fit to what must be a more complex set of exponential decays has been previously noted in studies of fluorescence lifetimes in non-homogeneous environments [28]. Extensions to this work have shown that fitting functions of the form of eqn. (5), consisting of 10–15 exponential terms with the rate constants k_i as fixed parameters, can reveal the distribution of rate constants, and can identify cases where the assignment of a discrete species to a particular rate constant is warranted [29].

Albery et al. [27] have described an alternative approach for the kinetic analysis of heterogeneous systems. They assume a gaussian distribution, $\exp(-x^2)$, of activation free energies about some mean value $\Delta \bar{G}^{\ddagger}$

$$\Delta G^{\ddagger} = \Delta \bar{G}^{\ddagger} - \gamma x RT \tag{6}$$

The distribution of the rate constants is then given by

$$k = \bar{k} e^{\gamma x} \tag{7}$$

If this model is valid, two parameters characterize the system. γ, the width of the distribution, is calculated from an experimental decay by

$$\gamma \approx 0.92 \left(\frac{t_{7/8}}{t_{1/2}} - 3 \right)^{1/2} \tag{8}$$

where $t_{1/2}$ is the half-time of the decay and $t_{7/8}$ is the time when the signal has decayed to one-eighth of its initial value. $\bar{k}$, the mean first-order rate constant, is given by $t_{1/e}^{-1}$, where $t_{1/e}$ is the time required for the signal to decay to $1/e$ of its initial value.

Further studies are under way to test this model thoroughly, and to establish whether it gives a better physical insight into the nature of the decay than, for example, eqn. (5).

4. Conclusions

We assign the transient observed after laser excitation of bleached thermomechanical pulp as the triplet state of the aromatic ketone group in lignin, based on the reduction in spectral intensity caused by treatment with sodium borohydride and the static quenching caused by oxygen or phenolic hydroxyl groups.

124

By comparing calculated values of $\Delta R(0)$ as a function of basis weight with experimental observation, we conclude that the concentration of transient species formed by pulsed laser excitation (354 nm, 25 mJ pulse^{-1}) of bleached, black spruce TMP falls off exponentially with depth into the sample. Since the highest values of ΔR are less than 0.2, ΔR is assumed to be directly proportional to the concentration of transient species, and is used for kinetic analysis. The transient decay cannot be explained by a model which assumes the existence of one or two discrete homogeneous chemical species. The remarkably long triplet lifetime and complex kinetics are best explained as a consequence of a distribution of the aromatic ketone groups over a number of structurally or chemically distinct sites in lignin.

Acknowledgments

References

1 L. V. Forman, *Pap. Trade J.*, *111* (1940) 34.
2 E. Sjöström, *Wood Chemistry Fundamentals and Applications*, Academic Press, New York, 1981, p. 68.
3 S. Y. Lin and K. P. Kringstad, *Tappi*, *53* (1970) 658.
4 K. P. Kringstad and S. Y. Lin, *Tappi*, *53* (1970) 2296.
5 J. Gierer and S. Y. Lin, *Sven. Papperstidn.*, *75* (1972) 233.
6 J. C. Netto-Ferreira and J. C. Scaiano, *Tetrahedron Lett.*, *30* (1989) 443.
  J. C. Netto-Ferreira, I. G. J. Avellar and J. C. Scaiano, *J. Org. Chem.*, *55* (1990) 89.
7 G. Leary, *Nature*, *217* (1968) 672.
8 S. E. Lebo, W. F. W. Lonsky, T. J. McDonough, P. J. Medvedcz and D. R. Dimmel, *J. Pulp. Pap. Sci.*, *16* (1990) J139.
9 I. Forsskåhl, *J. Photochem.*, *25* (1984) 197.
10 H. H. Nimz and G. Turznik, *Cellul. Chem. Technol.*, *14* (1980) 727.
11 C. Vanucci, P. Fornier de Violet, H. Bouas-Laurent and A. Castellan, *J. Photochem. Photobiol. A: Chem.*, *41* (1988) 251.
12 M. G. Neumann and A. E. H. Machado, *J. Photochem. Photobiol. B: Biol.*, *3* (1989) 473.
13 G. P. Kelly and F. Wilkinson, in J. C. Scaiano (ed.), *Handbook of Organic Photochemistry*, Vol. II, CRC Press, Boca Raton, 1989, p. 293.
14 J. A. Schmidt, C. Heitner, G. P. Kelly and F. Wilkinson, *J. Pulp Pap. Sci.*, *16* (1990) j111.
15 C. Heitner and Tan Min, *Cellul. Chem. Technol.*, *21* (1987) 289.
16 J. Polčin and W. H. Rapson, *Tappi*, *52* (1969) 1965.
17 P. R. Bevington, *Data Reduction and Error Analysis for the Physical Sciences*, McGraw-Hill, New York, NY, 1969, p. 235.
18 R. W. Kessler, G. Krablichler, S. Uhl, D. Oelkrug, W. P. Hagan, J. Hyslop and F. Wilkinson, *Opt. Acta*, *30* (1983) 1099.
19 D. Oelkrug, W. Honnen, F. Wilkinson and C. J. Willsher, *J. Chem. Soc., Faraday Trans. 2*, *83* (1987) 2081.
20 J. A. Van den Akker, *Tappi*, *32* (1949) 498.

21 E. Adler and J. Marton, *Acta Chem. Scand.*, *13* (1959) 75.
22 P. K. Das, M. V. Encinas and J. C. Scaiano, *J. Am. Chem. Soc.*, *103* (1981) 4184.
23 H. Lutz, E. Bréhéret and L. Lindqvist, *J. Phys. Chem.*, *77* (1973) 1758.
24 F. Wilkinson, C. J. Willsher, H. L. Casal, L. J. Johnston and J. C. Scaiano, *Can. J. Chem.*, *64* (1986) 539.
25 J. C. Selwyn and J. C. Scaiano, *Polymer*, *21* (1980) 1365.
26 G. Kortum, *Reflectance Spectroscopy*, Springer, Berlin, F.R.G., 1969, Chapter 3.
27 W. J. Albery, P. N. Bartlett, C. P. Wilde and J. R. Darwent, *J. Am. Chem. Soc.*, *107* (1985) 1854.
28 D. R. James and W. R. Ware, *Chem. Phys. Lett.*, *120* (1985) 455.
29 A. Siemiarczuk, B. D. Wagner and W. R. Ware, *J. Phys. Chem.*, *94* (1990) 1661.

Picosecond diffuse reflectance and transmission laser flash photolysis study of various triaryl-2-pyrazolines

G. P. Kelly, P. A. Leicester, F. Wilkinson* and D. R. Worrall

Department of Chemistry, Loughborough University of Technology, Leicestershire LE11 3TU, U.K.

L. F. Vieira Ferreira

Centro de Quimica Fisica Molecular, Universidade Tecnica de Lisboa, Complexo 1, Instituto Superior Tecnico, 1096 Lisboa Codex, Portugal

and

R. Chittock and W. Toner

Laser Support Facility, Rutherford Appleton Laboratory, Chilton, Didcot, Oxfordshire OX11 0QX, U.K.

Abstract—In this study the first ever reported application of diffuse reflectance laser flash photolysis for the observation of sub-nanosecond transient absorption decays is presented. The compounds studied are various triaryl-2-pyrazolines, both as microcrytals and contained within polycarbonate films. The microcrystalline samples were studied using pump–probe laser flash photolysis in diffuse reflectance mode and the observed transient absorption decay could be fitted using a biexponential model with, in the case of 1, 5-diphenyl-3-styryl-2-pyrazoline, lifetimes of 1.6×10^{-10} and 1.3×10^{-9} s for the first and second decay components, respectively. This model could also be used to fit the decay kinetics obtained from transmission pump–probe laser flash photolysis experiments conducted upon polycarbonate films containing this same compound, the lifetimes in this instance being 5.5×10^{-12} and 1.7×10^{-10} s for the first and second decay components, respectively. In addition, a study of the quenching of the pyrazoline excited states in a polycarbonate matrix by disulphone magenta was undertaken. In this case it was necessary to modify the second term of the biexponential model with a term to allow for Förster type long range energy transfer, the Förster critical transfer distance being determined as 25 Å. This biexponential model is rationalized as initial excitation being to the S_2 state, the first decay component being relaxation to the S_1 state and the second component decay of the S_1 state to the ground state, by radiative and non-radiative relaxation and, when DSM is present, long range energy transfer to this energy acceptor.

INTRODUCTION

ALTHOUGH most mechanistic photochemical studies have been concerned with homogeneous or at least transparent systems using transmission flash photolysis [1], most commercial applications of photochemistry involve heterogeneous environments [2, 3]. Recently this incompatibility has been overcome with the development of diffuse reflectance laser flash photolysis (DRLFP) [4–6] for examining transient absorptions in opaque and highly scattering materials. In this new mode of flash photolysis the changes in the level of diffusively reflected analysing light are monitored after pulsed excitation of the opaque sample [4, 6]. The technological importance of this development is clearly illustrated by considering the large variety of samples studied, for example microcrystalline solids [7, 8], semiconductor powders [9], species adsorbed on surfaces [10, 11] and dyed fabrics/polymers [9, 12]. Recently the technique has been further developed to study transient absorption in the picosecond time domain. The first results obtained on this time scale were for a sample of xanthone on silica gel and demonstrated the rise in absorption of the triplet state of this ketone [13], the decay of which had previously been studied in the microsecond time domain [10]. More recently IKEDA *et al.* [14] have studied the build up in the absorption due to the triplet state of microcrystalline benzophenone. A number of comprehensive review articles relating to DRLFP are available [15, 16].

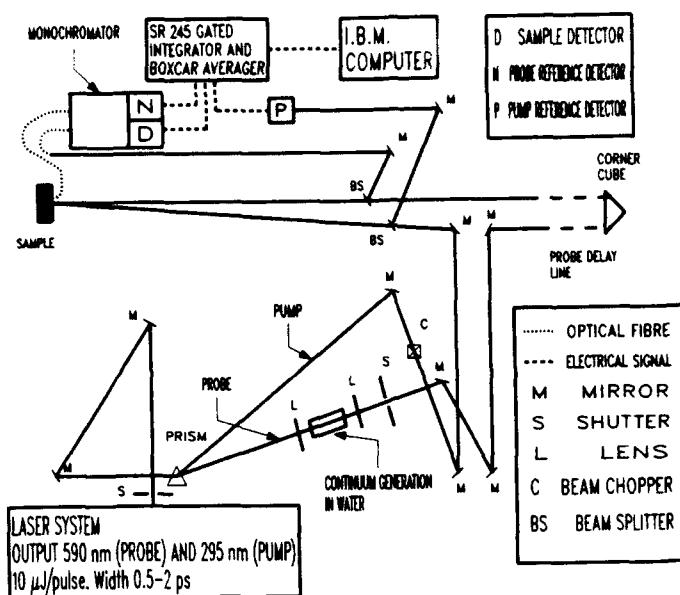* Author to whom correspondence should be addressed.

Fig. 1. Schematic diagram of the optics and detection system employed in picosecond pump–probe diffuse reflectance laser flash photolysis.

In this article full experimental details are presented for the picosecond system together with a series of results obtained from several triaryl-2-pyrazolines as microcrystalline samples and incorporated within polymer films. The pyrazolines were studied because of their interesting properties as optical brightening agents for textiles, paper and plastics [17, 18]. Recently, the photophysical and photochemical properties of such compounds have been surveyed in detail [6], and in addition, a study of the long range quenching of the pyrazoline fluorescence by disulphone magenta (DSM) dye has been undertaken [19].

EXPERIMENTAL

Picosecond pump and probe set-up

The study involves the application of the so-called "pump and probe" method [20] to both transmission and DRLFP in the picosecond time domain. The sample is excited (pumped) at 295 nm and analysed (probed) at 590 nm; it is also possible to focus the 590 nm probe beam into a water cell to produce a continuum to provide a range of probe wavelengths. The laser system, at the Rutherford Appleton Laboratory Laser Support Facility, is based around an actively mode-locked Spectra Physics series 3000 cw Nd/YAG laser, frequency doubled to produce a train of 532 nm pulses with a half width of 120 ps. These pulses are used to synchronously pump a dye laser (Spectra Physics 375B) which is wavelength tunable in the range 560–680 nm. A pulsed dye amplifier, consisting of a frequency doubled Q-switched Nd/YAG laser (Quanta Ray DCR-2) and a three-stage travelling wave dye amplifier chain (Quanta Ray PDA-1), is then employed to amplify these low energy pulses with a typical gain of 5×10^5 at a frequency of 10 Hz. The resultant pulses have a half width of between 0.5 and 2.0 ps and an energy typically of $500 \mu J$ using rhodamine 6G (λ max = 590 nm.) This output is frequency doubled with an efficiency of 7–10% to produce the 295 nm pump beam.

The beam from the laser (i.e. frequency doubled 295 nm pump and residual 590 nm probe) are separated into the two constituent beams using a prism, and are then directed separately through a system of mirrors, diaphragms and quartz lenses on to the sample (see Fig. 1). The pump beam is passed through a Rofin model 7500 frequency programmable chopper, synchronized to the dye amplifier at 35 Hz giving the overall effect of blocking alternate pump pulses. This enables the interleaving of probe only and pump and probe shots (see later for details). The probe beam can

also be focused into a 4 cm pathlength quartz cuvette containing pure water/D$_2$O to generate a picosecond continuum [21]. The 590 nm or continuum probe pulses are then directed on to the sample via an optical delay line, consisting of a corner cube mounted on a computer controlled slide unit, which can introduce a variable delay of the probe beam relative to the pump of up to about 5 ns.

The detection of a transient absorption involves the measurement of three different signals, namely incident pump, incident probe and the diffusely reflected probe off the sample in the case of diffuse reflectance, and incident pump, incident probe and transmitted analysing probe in transmission geometry. Each signal is measured on a detector, based on the design of POLLARD and ZENITH [22], which employs a 1 × 1 cm Hamamatsu u.v. sensitive PIN diode (S1723–05). To preserve the linear response of the detector, the output produced should be less than 250 mV, this limit being adhered to by inserting the appropriate neutral density filters in front of the detectors.

Using diffuse reflectance geometry, a convenient method of collecting the reference and reflected probe beams involves the use of appropriately positioned optical fibres, the signals from which are both passed through the same monochromator. It was found that the two photodiodes could be placed intimately against the exit slit of the monochromator with virtually zero "cross talk" between the two beams. The pump beam intensity was measured by monitoring a reflection of an optical component in the optical path or if this was not appropriate, by using a quartz plate to split off a reference pump beam. A schematic diagram of the pump and probe beams optical paths, plus a schematic representation of the detection system is given in Fig. 1.

In the case of transmission geometry, the pump beam was monitored as above but the reference and analysing beams were directly incident upon two photodiodes on passing through the samples. The two photodiodes were connected as a difference detector using a Wheatstone bridge arrangement, the reference and analysing beam intensities being adjusted to balance the circuit with no transient absorption. Also obtained from this circuit is the sum of the signals from the two photodiodes, allowing normalization for fluctuations in probe intensity.

The electrical signals from the detectors are measured using three model SR250 (Stanford Research Ltd) gated integrators. The SR250 enables integration of the photodiode signal over an adjustable electronic gate, typically of 300 ns width, on receiving an external trigger from the Quanta Ray DCR-2. The integrated signal is held as an analogue voltage between 0 and 10 V and is subsequently read by a model SR245 analogue to digital converter/computer interface (Stanford Research Ltd). The SR245 stores digitized signals in its internal memory before transfer to an IBM-XT microcomputer after one experiment (i.e. a series of 200 laser shots). The computer is also interfaced to the delay line slide stepper motor and controls the shutters.

The data acquisition and processing have been developed to handle the large shot to shot fluctuations which the amplified pulses exhibit. These are caused by pulse pointing instabilities in the first stage in the dye amplifier. The fluctuations observed routinely have a standard deviation of 25%. To effect the measurement of a transient absorption of the monochromatic probe pulse induced by the pump pulses at one delay where the probe pulse has reasonable energy, we have found that at least 100 pump and probe shots are necessary. At wavelengths where the continuum has a low energy, in practice about 100 nm either side of the fundamental, considerably more shots are required. Thus the data acquisition procedure involves collecting all three detector signals over two sets of 200 laser shots, the first set with only the pump shutter open and the second with both pump and probe shutters open. As mentioned above, the pump beam is chopped to allow only alternate shots to reach the sample and consequently the first series of 200 shots enables the measurement of interleaved background (no beams) and emission (pump only) signals, whilst the second series measures interleaved baseline (probe only) and transient (pump and probe) signals.

In order to interrogate different time portions of the transient absorption and build a complete temporal profile of the transient, the above procedure is undertaken at each of a range of optical delays. For typical transients such as discussed below, 50 time delays suffice and the data for a complete transient decay profile can be collected and analysed in 30 min. Alternatively, a spectral profile can be constructed by varying the monochromator wavelength at a fixed delay. However, we have had little success with this method using pyrazoline samples because the continuum intensity rapidly falls off and the emission signal measured at wavelengths shorter than 550 nm becomes larger than the transient absorption itself.

Analysis of data

Diffuse reflectance. The relative change in reflectance from the sample, induced by the pump, is the quantity of interest which needs to be extracted from the raw detector signal D. At a pump intensity, P, this can be represented by Eqn (1):

$$\frac{\Delta R(P)}{R} = \frac{D_{\text{off}} - D_{\text{on}}}{D_{\text{off}}}.$$ (1)

From the first set of interleaved data, the dependence of the signal due to emission from the sample, E, on the intensity of the pump energy, measured by the pump reference signal, P, is established. Normally these quantities have been observed to vary linearly, however for pyrazolines, a non-linear dependence is observed. The two quantities can be mathematically related by a least squares polynomial curve fitting routine to enable a value for the emission intensity, E, to be interpolated for a known pump intensity, P:

$$E(P) = \sum_{i=0}^{n} C_i P^i,$$ (2)

where C_i is the ith coefficient of the calculated polynomial of order n, a value of $n = 3$ is usually sufficient to give a good fit. Also, using the first set of data, the mean background signal on the detectors is calculated and subtracted from the signals measured in the second set.

The second set of interleaved data provides information about the intensity of the reflected probe, D, and the probe reference intensity, N, in the presence and absence of pump beam (signified by the subscripts on or off). In the absence of pump, a linear relationship should exist between N and D_{off}, which can be fitted according to Eqn (3), where α and β are arbitrary constants:

$$D_{\text{off}} = \alpha N + \beta.$$ (3)

Thus, the numerical value of D_{off} to insert into Eqn (1) can be calculated, using Eqn (3), by taking the value of N corresponding to D_{on}. For each pump and probe shot the transient absorption is calculated for the pump energy, P, using the calculated vaue $D_{\text{off}}^{\text{calc}}$ and the calculated emission intensity $E(P)^{\text{calc}}$ as follows:

$$\frac{\Delta R}{R} = \frac{D_{\text{off}}^{\text{calc}} - D_{\text{on}} - E(P)^{\text{calc}}}{D_{\text{off}}^{\text{calc}}}.$$ (4)

The value calculated in Eqn (4) is obtained for each pump on shot in the second set of data. Hence the 100 values obtained are normalized and averaged to a mean pump energy.

Transmission data. In this case, the quantity of interest is the difference in signal between the two photodiodes in the Wheatstone bridge, generated by a difference in intensity between the analysing and reference beams caused by a transient absorption in the sample. At pump intensity P, this can be represented by Eqn (5):

$$\left[\frac{\Delta I(P)}{I}\right]_u = \frac{D_{\text{on}} - \bar{D}_{\text{off}}}{N - \bar{N}_{\text{baseline}}},$$ (5)

where D and N are proportional to the difference and sum signals, respectively, $\bar{N}_{\text{baseline}}$ is the value of the measured sum signal in the absence of probe incident upon the detector, and u indicates that the value of $\Delta I(P)/I$ is uncorrected at this stage and represents a value proportional to percentage absorption. The relative positions of samples and detectors were arranged such that negligible emission reached the detectors, and therefore no correction for emission is necessary in this instance. The value obtained from Eqn (5) is then normalized to pump intensity for each point using Eqn (6):

$$\left[\frac{\Delta I}{I}\right]_{\text{norm}.u} = \frac{(\Delta I/I)u}{P - P_{\text{baseline}}}.$$ (6)

The normalized value of $\Delta I/I$ is then corrected to percentage absorption, using a calibration factor f derived from a glass slide known to give a signal corresponding to 8% absorption. This factor is calculated according to Eqn (7):

$$0.08 = \frac{f(\dot{D}_{on} - \dot{D}_{off})}{(\dot{N} - \dot{N}_{baseline})(\dot{P} - \dot{P}_{baseline})}. \tag{7}$$

In Eqn (7), all data refers to measurements made for the glass slide, which allow the calculation of f. The corrected values of the normalized $\Delta I/I$ can then be converted to absorbance values using Eqn (8):

$$A = -\log_{10}[1 - ((\Delta I/I)f)]. \tag{8}$$

Materials. Four pyrazoline samples were investigated, namely 1,5-diphenyl-3-styryl-2-pyrazoline (PYA), 1-phenyl-5-(thien-2′-yl)-3-[2″-(-thien-2′-yl)vinyl]-2-pyrazoline (PYB), 1-phenyl-5-(thien-3′-yl)-3-[2″-(thien-3′-yl)vinyl]-2-pyrazoline (PYC) and 1-phenyl-2-pyrazoline (PYD). The compounds, supplied by 3M Research Ltd (Harlow, U.K.), were recrystalized three times from petroleum ether to ensure purity. The preparation of these compounds has been detailed fully elsewhere [23]. The disulphone magneta dye (Chemical abstracts registry number 58559-02-7) was supplied purified by 3M Research Ltd. The structures of these compounds are detailed below.

Polycarbonate (Pantite L1 250) films containing the above materials were prepared by dissolving the material in a 10% polymer solution in chloroform (spectrograde: Fisons). The solution was then coated into a transparent polyester base using a number 8 K-bar (manufactured by R-K Print-coat instruments Ltd). The sample was then allowed to dry overnight in an oven at 50 °C.
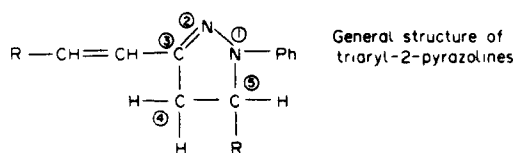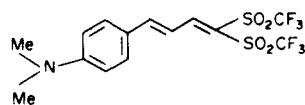
Structure of disulphone magenta (DSM) dye

Structure 1.

RESULTS AND DISCUSSION

Diffuse reflectance

Microcrystalline samples of PYA, PYB, PYC and PYD were investigated using DRLFP in the sub-nanosecond time domain. In all cases, transient absorption was observed at 590 nm with 295 nm excitation. Prior to kinetic analysis of the data, it is important to gain an unde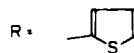rstanding of the nature of the transient concentration profile that exists below the irradiated opaque surface [24]. For this system, an exponentially decreasing concentration of transient as a function of penetration depth is clearly indicated [6] requiring the use of $\Delta R/R_0$ as the term proportional to transient concentration during kinetic analysis. In each of the cases A to C, the observed decay consisted of an initial fast component followed by a slower component and was seen to be fitted by a biexponential model of the type found in Eqn (9):

$$A = a[\exp(-k_1 t)] + b[\exp(-k_2 t)].$$ (9)

The transient absorption decays obtained for microcrystalline samples of PYA and PYB are illustrated in Fig. 2(a) and (b), respectively. Fitting of a biexponential to the observed decays yielded lifetimes for the first and second decay components of $(1.6 \pm 0.2) \times 10^{-10}$ and $(1.3 \pm 0.1) \times 10^{-9}$ s, respectively. There is strong evidence to suggest that the second component of the biexponential decay is due to the first excited singlet state, namely that the lifetime of the fluorescence decay is of the same magnitude as the decay of this state. The nature of the fast component in the decay is a little less conclusive, one possibility is that this component is due to the decay of a directly excited higher singlet which subsequently decays via a non-radiative route either to the ground state or to the first singlet.

Fig. 2. Transient absorption decays from samples of (a) microcrystalline PYA and (b) microcrystalline PYB, with pump and probe wavelengths of 295 and 590 nm, respectively.

Fig. 3. Excitation spectra from microcrystalline samples of PYB and PYD, emission wavelength 500 nm.
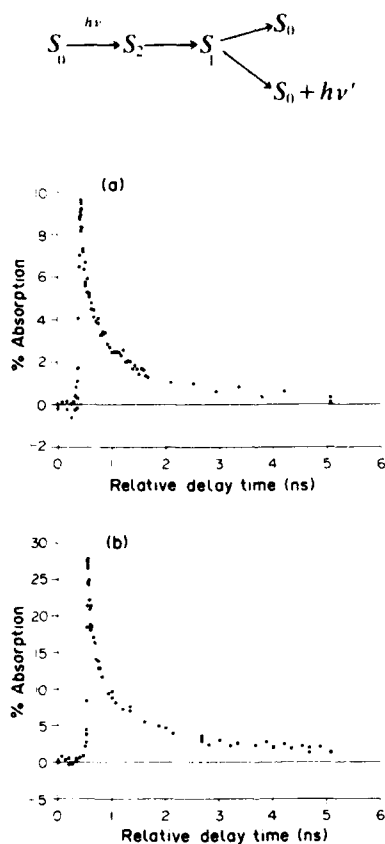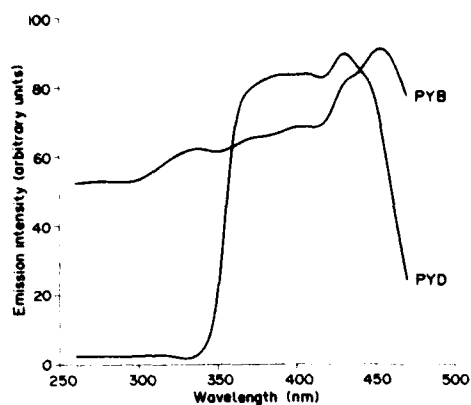
In the case of PYD, the level of transient absorption was seen to be an order of magnitude less than was observed for the other pyrazolines. In addition, microcrystalline PYD exhibits an unusual dependence of its fluorescence quantum yield on exciting wavelengths. It is seen that emission is observed for excitation at wavelengths greater than 350 nm, but this emission rapidly falls to zero following excitation at wavelengths shorter than 350 nm, as illustrated in Fig. 3, where for comparison the excitation spectrum obtained for PYB is also reproduced. Thus, although the PYD sample is completely absorbing at the pumping wavelength, it has a very low fluorescence quantum yield. Excitation at these shorter wavelengths corresponds to promotion to an excited state of higher energy than the first excited state, probably to the S_2 state, and the rapid fall-off in emission intensity is attributed to the presence of a high probability, non-radiative relaxation pathway to the ground state not involving the S_1 state. This hypothesis is supported by the picosecond diffuse reflectance measurements on microcrystalline PYD, where the transient absorption observed decays rapidly to zero with no indication of the second, slower component to the decay observed for the other pyrazolines.

Transmission

Attempts were made to confirm the results obtained in diffuse reflectance using transmittance geometry, with the pyrazolines dissolved within a polycarbonate matrix deposited as a thin film on a polyester base. Again, transient absorptions were observed for samples of PYA, PYB and PYC at 590 nm following excitation at 295 nm. The observed decay kinetics were once more seen to be fitted by a biexponential model, but in this instance the lifetimes of the first and second processes were seen to be $(5.5 \pm 0.6) \times 10^{-12}$ and $(1.7 \pm 0.2) \times 10^{-10}$ s, respectively (i.e. each component is an order of magnitude faster in the polycarbonate film than in the microcrystalline solid).

A similar film to those used above, containing PYA with a trace amount (0.1% by mass) of DSM demonstrated a more rapid transient decay than observed in the absence of DSM. A study was therefore made of the kinetics of the decay of the PYA transient absorption in the presence of a range of concentrations of DSM. It was observed that as the DSM increased, the transient absorption decayed more rapidly, indicating that the DSM quenches the excited state(s) of these compounds. A film containing DSM (0.1% by mass) and polycarbonate only was seen to give no transient adsorption signal when pumped at 295 nm under identical conditions.

The transient absorption decays obtained for the thin films of PYA in the presence of DSM are reproduced in Fig. 4. The unquenched PYA decay is seen to fit, as mentioned earlier, a biexponential model. However, the quenched decays can not be fitted well with such a model. Based on results obtained in solution, it would be expected that quenching

of the PYA singlet by DSM would be via a long range energy transfer mechanism (i.e. Förster type). The Förster radius, R_0, has been determined in dichloromethane solution as being 55 Å [19].

From the Förster equation [25]:

$$\frac{R_0^6}{(cm)} = \left[\frac{9\,K^2\,\ln 10}{128\,\pi^5 N}\right]\left[\frac{\phi_d}{n^4}\right]\frac{J_{da}}{(cm^6\,mol^{-1})},\tag{10}$$

where ϕ_d is the fluorescence quantum yield, n is the refractive index and J_{da} is the spectral overlap integral of donor and acceptor, it can be seen that:

$$R_0^6 \propto \phi_d.\tag{11}$$

It is seen that the unquenched lifetime of the S_1 state is approximately 3×10^{-9} s in solution [6], but is reduced to 1.7×10^{-10} s in polycarbonate film. Since the relationship

$$\frac{\phi_{d\,solution}}{\phi_{d\,film}} = \frac{k_f \tau_{0\,solution}}{k_f \tau_{0\,film}}\tag{12}$$

holds, a decrease in τ_0 will lead to a decrease in the anticipated Förster radius for the polymer film system compared to solution. Also, it is seen that

$$n\,(dichloromethane) = 1.42$$

$$n\,(polycarbonate) = 1.58$$

and, since

$$R_0^6 \propto n^{-4},\tag{13}$$

the increase in refractive index from dichloromethane to polycarbonate will also reduce R_0^6. When both the lifetime and refractive index effect are considered it would be expected that the Förster radius would be reduced in the polycarbonate matrix to the order of 30 Å.

The fitting of the data was performed using a manual iterative method, the initial approach being to take a Förster model in isolation and, using realistic values for the constants involved, to determine the value of R_0 which gave curve shapes best fitting the experimental data with $t > 0.5$ ns. The model expression used in this instance was:
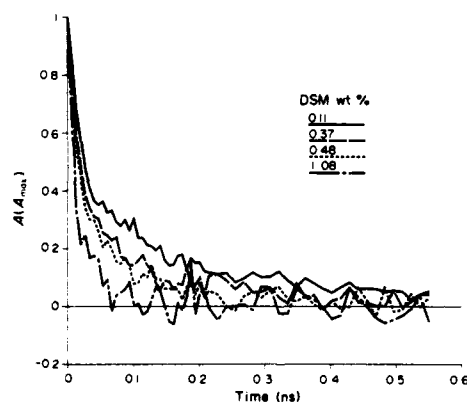
Fig. 4. Decay of PYA transient absorption in a polycarbonate matrix in the presence of varying amounts of DSM, with pump and probe wavelengths of 295 and 590 nm, respectively.

$$(A/A_{max}) = \exp[-t/\tau_0 - (2C/C_0)(t/\tau_0)^{1/2}],\tag{14}$$

where

$$C_0 = \frac{3}{4\pi R_0^3 N}.\tag{15}$$

The value of τ_0 used was that obtained for the second decay component in the unquenched PYA decay, i.e. $\tau_0 = k_2^{-1}$ and it was determined that the curve shapes best fitting the data were obtained using an R_0 value of 25 Å.

Having determined these parameters, the biexponential model used to fit the unquenched data was modified to incorporate the possibility of long range energy transfer. It was observed that the first decay component remains unquenched and so its lifetime is independent of DSM concentration. The second, slower component, however, is quenched and so it is possible to formulate an expression of the type:

$$(A/A_{max}) = a[\exp(-k_1t)] + b[\exp\{-k_2t - (2C/C_0)(k_2t)^{1/2}\}],\tag{16}$$

where the second exponential term used for pyrazoline alone [see Eqn (9)] is modified for samples containing quencher to allow for the Förster transfer. This model can be summarized as describing a mechanism whereby the initial excitation by the 295 nm pulse is to the S_2 state, which decays rapidly to give either the S_1 or S_0 states. The S_1 state then
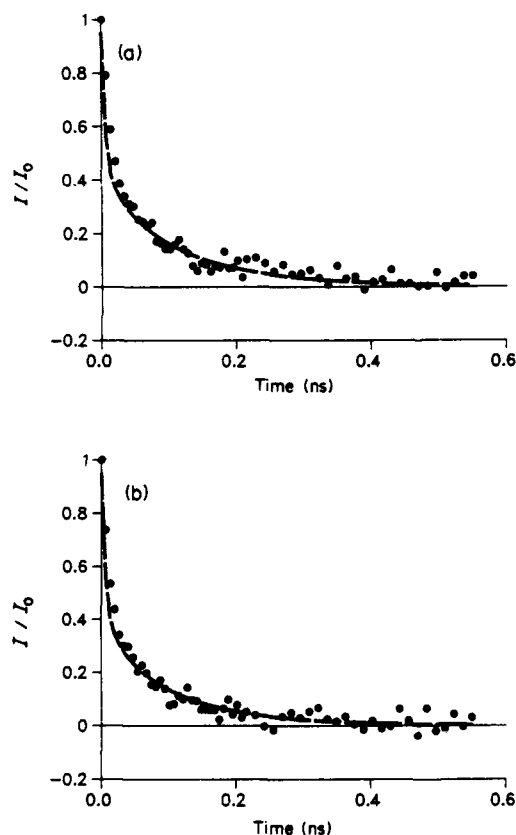
Fig. 5. Comparison of observed and simulated decay data for PYA in a polycarbonate matrix in the presence of (a) 0.37 weight % and (b) 0.48 weight % DSM.

undergoes one of three proceses: radiative and non-radiative relaxation to the ground state; or long range, non-radiative energy transfer to a molecule of DSM.

The above model is seen to give a good global fit to the experimental data, as illustrated in Fig. 5(a) and (b) for DSM concentrations of 0.48 and 0.37 weight %, respectively. The constants employed here are considered realistic based on comparisons with solution work [19] and their use gives a global fit using the proposed model, valid over all concentrations investigated. The above adds further credence to the proposal that the slower component of the biexponential decay in the absence of quencher is indeed due to the decay of the first excited singlet state.

CONCLUSIONS

In this work we have observed a transient absorption, decaying biexponentially in the picosecond time domain, in microcrystalline samples of pyrazolines using diffuse reflectance geometry. This constitutes detection in absorption of the first sub-nanosecond transient within an opaque microcrystalline sample. The slower decaying component is assigned as the lowest excited singlet state S_1 of the pyrazoline. Assignment of the faster component also absorbing at 590 nm is more speculative but is consistent with a much more rapidly decaying higher excited state which we have labelled S_2. These assignments are confirmed using transmission geometry with the pyrazolines incorporated within a polycarbonate matrix, where a similar biexponential decay is seen although the lifetimes of the two states involved are decreased by an order of magnitude relative to those observed in the microcrystals.

Also investigated were the decay kinetics of the PYA incorporated within a polycarbonate matrix in the presence of a range of concentrations of DSM. The mechanism proposed here to explain the observed kinetics involves decay of the initially produced S_2 state to the S_1 state, the rate of which is so rapid as to be unaffected by DSM concentration. This is followed by decay of the S_1 state to the ground state either by radiative and non-radiative relaxation or by long range energy transfer to a molecule of DSM.

REFERENCES

[1] G. Porter and M. A. West, *Techniques of Organic Chemistry* (edited by A. Weissberger), Vol. VIII, Ch. 10. Wiley-Interscience, New York (1974).
[2] M. Formenti and S. J. Teichner, *Catalysis* 2, 87 (1978).
[3] T. Kajiwara, K. Hoshimoto, T. Kawai and T. Sakata, *J. Phys. Chem.* 86, 4516 (1982).
[4] C. J. Willsher, *J. Photochem.* 28, 229 (1985).
[5] F. Wilkinson, *J. Chem. Soc., Faraday Trans II* 82, 2073 (1986).
[6] G. P. Kelly, PhD thesis, University of Loughborough (1987).
[7] F. Wilkinson and C. J. Willsher, *Chem. Phys. Lett.* 104, 272 (1984).
[8] F. Wilkinson and C. J. Willsher, *Appl. Spectrosc.* 38, 897 (1984).
[9] F. Wilkinson and C. J. Willsher, *J. Chem. Soc., Chem. Commun.* 142 (1985).
[10] F. Wilkinson, C. J. Willsher, M. L. Casal, L. J. Johnston and J. C. Scaino, *Can. J. Chem.* 64, 539 (1986).
[11] N. J. Turro, I. R. Gould, M. B. Zimit and C. C. Cheng, *Chem. Phys. Lett.* 119, 484 (1985).
[12] F. Wilkinson, C. J. Willsher and R. B. Pritchard, *Eur. Polym. J.* 21, 333 (1985).
[13] F. Wilkinson, C. J. Willsher, P. A. Leicester, J. R. M. Barr and M. J. C. Smith, *J. Chem. Soc., Chem. Commun.* 1216 (1986).
[14] N. Ikeda, K. Imagi, H. Masuhara, N. Nakashima and K. Yoshihara, *Chem. Phys. Lett.* 140, 281 (1987).
[15] F. Wilkinson and G. P. Kelly, Diffuse reflectance laser flash photolysis, in *Handbook of the Photochemistry of Organic Compounds in Condensed Media* (edited by J. Scaino), p. 293. CRC Press, Florida (1988).
[16] F. Wilkinson and G. P. Kelly, Laser flash photolysis on solid surfaces, in *Photochemistry on Solid Surfaces* (edited by M. Anpo) Elsevier (1988), p. 30.
[17] A. Wagner, C. W. Schelhammer and J. Schroader, *Angew. Chem. Int. Edn. Engl.* 5, 699 (1966).

[18] A. K. Sarkar, *Fluorescent Whitening Agents*. Merrow, Watford, U.K. (1971).

[19] F. Wilkinson, G. P. Kelly and L. F. Vieira Ferreira, *J. Photochem., A: Chemistry* **45**, 223 (1988).

[20] F. E. Lytle, R. M. Parrish and W. T. Barries, *Appl. Spectrosc.* **39**, 444 (1985).

[21] A. Penzkoffer and W. Kaiser, *Opt. Quant. Elect.* **9** 315 (1977).

[22] H. J. Pollard and W. Zenith, *J. Phys. E. Sci. Instrum.* **18**, 399 (1985).

[23] K. Reynolds, PhD thesis, University of East Anglia (1973).

[24] D. Oelkrug, W. Honnen, F. Wilkinson and C. J. Willsher, *J. Chem. Soc., Faraday Trans II* **83**, 2081 (1987).

[25] T. Förster, *Ann. Physik* **2**, 55 (1948).

Chapter 6

Diffuse Reflectance Laser Flash Photolysis of Thermomechanical Pulp

F. Wilkinson, A. Goodwin, and D. R. Worrall

Department of Chemistry, Loughborough University of Technology, Loughborough, Leicestershire LE11 3TU, United Kingdom

A comparative study of the photochemical properties of aromatic α-carbonyl groups found in the lignin part of thermomechanical pulp (TMP) with those of an α-carbonyl lignin model compound 3,4 dimethoxyacetophenone has been undertaken with a view to gaining insight into the photoyellowing mechanisms of TMP. The technique of diffuse reflectance laser flash photolysis has been used to investigate transient reflectance changes observed following pulsed excitation of TMP samples. Chemically modified TMP with reduced phenolic hydroxyl content within the lignin part of the pulp shows a 29% increase in the size of the transient signal upon reducing the phenolic hydroxyl content from 0.128 to 0.0091 phenolic hydroxyl units per C_9 lignin unit. Upon excitation of TMP samples under an atmosphere of oxygen we were able to see dynamic quenching of the transient signal relative to a sample with all oxygen removed. Studies with the lignin model compound 3,4- dimethoxy-acetophenone in benzene solution demonstrate that triplet states of carbonyl groups α to an aromatic ring are quenched efficiently by phenolic hydroxyl groups ($k_Q = 6.3 \times 10^9 \, \text{l.mol.}^{-1} \, \text{s.}^{-1}$) and can also be quenched by methoxyl moieties ($k_Q = 2.6 \times 10^6 \, \text{l.mol.}^{-1} \, \text{s.}^{-1}$ for methoxybenzene) present in the lignin structure.

Mechanistic photochemical investigation in heterogeneous systems such as lignocellulosic materials constitutes a considerable challenge. Heterogeneity makes the analysis of photochemical and photophysical data much more complicated than in homogeneous media but the technological and commercial importance justifies efforts which are made to cope with the inherent complexities. Recently we have extended to heterogeneous opaque and often highly scattering systems, the advantages of being able to subject them to flash photolysis investigation by monitoring changes in diffusely reflected light rather than in transmitted light. This has allowed probing of transient events on timescales extending from several seconds to picoseconds(1, 2).

Laser induced transient spectra and decay kinetics have been observed from a wide variety of samples including fractions of monolayers of organic molecules adsorbed on catalytic metal oxide surfaces(3, 4), and included within zeolites(5), from

semiconductor powders(6), and porous electrodes doped and undoped(7), from ruthenium (II) complexes within ion exchange resins(8), from organic microcrystals(9) and from organic dyes adsorbed on microcrystalline cellulose(10, 11), on fabrics and chemically bound to polymers(12, 13) and from paper pulp(14, 15).

Since the α-carbonyl group is the primary photochemical absorber in the near U.V. part of the electromagnetic spectrum leading to photoyellowing (brightness reversion) of high yield thermomechanical pulp (TMP), we investigate in this paper the excitation of carbonyl groups within lignin using laser flash photolysis in diffuse reflectance mode and compare this with results from an α-carbonyl lignin model compound studied by transmission laser flash photolysis in dilute solution and by diffuse reflectance laser flash photolysis when adsorbed onto microcrystalline cellulose. The effects of methoxylation of phenolic hydroxyl groups within pulp samples, and the presence of moisture and oxygen on both spectral and kinetic observations, were also investigated with regard to the photoyellowing process.

Experimental

Materials. All solvents were spectrophotometric grade (Aldrich) and were used without purification. Microcrystalline cellulose (Aldrich, 20 micron mean particle size) was used as supplied. 3,4-dimethoxyacetophenone (Aldrich) was purified by sublimation under vacuum at a pressure of 5×10^{-4} mBar at 40°C, purity being checked by melting point, UV-Visible and N.M.R. Spectroscopy. Phenol (Aldrich) and methoxybenzene (Aldrich) were used without further purification.

Preparation Of TMP Samples. All experiments with pulp samples were performed using black spruce thermomechanical pulp (TMP) which had been bleached to an ISO brightness of 75% by 4% hydrogen peroxide at 60°C for approximately two hours. With the exception of the data presented in Figure 2 where optically thick pulp sheets were used, all investigations involving TMP were performed using powdered samples. Samples used to investigate the effect of varying phenolic hydroxyl content, the effect of oxygen and the effect of water were ground to a 40 mesh powder in a Wiley mill and packed into quartz cuvettes prior to investigation. Sufficient pathlengths and packing densities were used to ensure that samples were optically thick at both excitation and analysing wavelengths. Pulp samples were dried under a vacuum of 2×10^{-5} mbar for 1 hour prior to introduction of either dry nitrogen or oxygen. Pulp samples used to investigate the effect of water on the observed transient kinetics were saturated with water following packing into the sample cuvette.

Methoxylation of TMP samples was achieved by heating pulp fibres together with appropriate amounts of dimethyl sulphate in an equivolume solvent of water, ethanol and dimethoxyethane(14), methoxyl content of the pulp fibres being controlled by the amount of dimethyl sulphate added (Schmidt, J.A.; Heitner, C. *J. Wood Chem. Chem. Technol.*, In Press). Samples were analysed for methoxyl content by Scharwzkopf Microanalytical Laboratories, Woodside, New York. Analysis of the TMP samples for phenolic hydroxyl content was according to the method of Gellerstedt and Lindfors(16).

All ground state diffuse reflectance spectra were recorded using a Phillips PU8800 UV-Visible spectrophotometer equipped with an integrating sphere, interfaced to an Elonex PC-386SX computer. These ground state diffuse reflectance spectra were measured relative to a $BaSO_4$ white reflectance standard (Eastman Kodak Ltd.).

Preparation Of Samples Adsorbed On Microcrystalline Cellulose. The cellulose powder was dried under vacuum (65 mBar) at 70°C overnight prior to use. A known mass of ca. 2g was weighed into a 100 ml beaker and immediately submerged under the appropriate solvent (in this case benzene) to avoid moisture uptake. To this

mixture was added a solution of 3,4-dimethoxyacetophenone to give a surface concentration of ca. 10^{-6} moles of ketone per gram of cellulose powder. The sample was then magnetically stirred allowing slow solvent evaporation until only residual solvent remained and then dried in a vacuum oven (65 mBar) at 30°C overnight.

Solution Phase Studies. Freshly prepared solutions were used for all experiments. All solution phase studies were carried out using samples which had been thoroughly de-gassed using a minimum of three freeze-pump-thaw cycles for each sample. The final pressure above the sample was in all cases less than 5×10^{-4} mBar. Laser energy densities of less than 2.5 mJ cm^{-2} were used such that sample degradation was kept to a minimum.

The rate constants for quenching of the triplet state of 3,4-dimethoxyacetophenone by methoxybenzene or phenol in benzene solution were determined using samples of 3,4-dimethoxyacetophenone with an absorbance of 0.1 (ca. 2×10^{-3} mol.l.$^{-1}$) at the laser excitation wavelength (354.7 nm) in the presence and absence of the quenchers. Neither phenol nor methoxybenzene absorb at the laser excitation wavelength.

Nanosecond Flash Photolysis. Diffuse reflectance flash photolysis studies were carried out using the apparatus and optical geometry illustrated in Figure 1. The timing of events in the system is controlled by an analogue delay unit, data acquisition being controlled via a microcomputer (Elonex PC286S-10) using software written specifically for the purpose at Loughborough. The excitation source is a Q-switched hyperYAG HY-200 Nd:YAG laser (Lumonics). The analysing source is a 250W xenon arc lamp (Optical Radiation Corporation), which may be pulsed to provide an approximately ten-fold intensity increase for a period of 0.5 ms using an arc lamp pulsing unit (Applied Photophysics). Diffusely reflected light from the sample is collected by a lens system and focussed onto the slit of an f/3.4 grating monochromator (Applied Photophysics). The selected wavelength is detected by an R928 side-window photomultiplier tube (Hamamatsu). The time evolution of the laser induced transient reflectance change is captured by a 2432A digital oscilloscope (Tektronix) and transferred to the microcomputer via an IEEE-488 interface bus. Samples were contained within cylindrical quartz cuvettes of 2 cm diameter and 1 cm pathlength.

The observable parameter in diffuse reflectance laser flash photolysis experiments is the fractional reflectance change $\Delta J(t)/J_0$ defined as in Equation 1.

$$\frac{\Delta J(t)}{J_o} = \frac{R_b - R(t)}{R_b} \tag{1}$$

Here, R_b is the sample reflectance before exposure to the laser pulse and $R(t)$ the reflectance at time t after the laser pulse.

Transmission flash photolysis studies were carried out using a similar system to that used for diffuse reflectance studies. In this case the excitation source was a JK2000 Q-switched Nd:YAG laser (Lumonics), the transient events being captured by a 7612AD transient digitiser with a 7A12 differential plug-in amplifier (Tektronix). For these experiments conventional flash photolysis geometry (ie. perpendicular excitation and analysing beams) was employed. The samples were contained within 1 cm x 1 cm quartz cuvettes.

Results

Effect of Oxygen Concentration on the TMP Transient. Samples of high yield thermomechanical pulp (TMP), when subjected to laser photolysis, show a transient reflectance change which decays by complex kinetics. With these samples substantial fluorescence renders transient absorption measurements unreliable at times less than ~ 150 ns. The difference spectrum of this transient exhibits a peak at approximately 450 nm, the shape of the spectrum being independent of the time delay after the excitation pulse to within experimental error (Figure 2). For dry TMP, the kinetics of the transient decay are seen to be slightly faster in the presence of oxygen than in an atmosphere of pure nitrogen, suggesting some dynamic quenching and thus measurable oxygen mobility in dry pulp (Figures 3a and 3b), although whether this implies penetration of oxygen into the lignin polymer itself or simply interaction with exposed surface groups has not been established. The transient decays in dry pulp are non-exponential and can be characterised by first empirical half lives of 4.5 ± 0.3 and 5.8 ± 0.3 microseconds for oxygen and nitrogen saturated samples, respectively. However, oxygen concentration had no effect on the size of the initial transient reflectance change, suggesting that static quenching of the transient or its precursor by oxygen is not significant in this system.

Following saturation with water, the observed first empirical half life of the transient for a TMP sample which had been bubbled with nitrogen overnight was reduced to 0.90 ± 0.2 microseconds. The first empirical half life for an oxygen saturated wet TMP sample was found to be 0.65 ± 0.2 microseconds. As with dry TMP samples, second and subsequent empirical half lives for water saturated samples were also found to be oxygen sensitive. Given that the first empirical half lives for nitrogen and oxygen saturated **dry** TMP samples were found to be 5.8 ± 0.3 and 4.5 ± 0.3 microseconds, the large decreases in first empirical half lives upon addition of water may be explained by either water quenching the carbonyl triplet states or, water swelling of the pulp fibres allowing for greater mobility of functional groups within the pulp fibres resulting in more rapid triplet carbonyl decay. We interpret the small decrease in first empirical half lives for wet samples with increasing oxygen concentration as being due to greater oxygen mobility resulting in more rapid quenching of the carbonyl triplet states within the lignin.

Treatment of TMP with sodium borohydride reduces the absorption by the pulp sheet in the 330nm region and decreases the size of the laser induced transient reflectance change in proportion (Schmidt, J.A.; Heitner, C. *J. Wood Chem. Chem. Technol.*, In Press). Absorption by the pulp in this spectral region has been attributed to the presence of aromatic carbonyl functionality. This and the fact that the transient signal is seen to be dynamically quenched by oxygen is consistent with the observed transient being assigned as the lowest lying triplet state of the aromatic carbonyl groups present in the pulp(*14,15*).

Effect of Methoxylation of Phenolic Hydroxyl Groups. Methylation of the phenolic hydroxyl groups in the lignin by treatment with dimethyl sulphate has no measurable effect on the ground state diffuse reflectance spectrum of the TMP. Increasing methylation does, however, result in an increase in the size of the transient reflectance change observed upon laser photolysis but does not, to within the error of the experiment, affect the spectral shape thereof (Figure 4). In addition, there is no effect of methoxyl content on the kinetics of decay of the laser induced transient reflectance change.

In going from no methoxylation (0.128 phenolic hydroxyl groups per C_9 unit) to a high proportion of methoxylation (0.0091 phenolic hydroxyl groups per C_9 unit) there is an increase in the size of the transient reflectance change of some 29% (Table I).

Figure 1. Schematic Diagram of the Apparatus and Optical Arrangement used for Diffuse Reflectance Laser Flash Photolysis Experiments.

Figure 2. Transient Difference Spectrum Observed from a Sample of TMP at Two Delays Following the Laser Excitation Pulse.

Figure 3a. Transient Decay Following Laser Excitation Analysing at 450 nm for Dry Samples of TMP under Atmospheres of Oxygen and Nitrogen over a 10 μs Time Sweep.
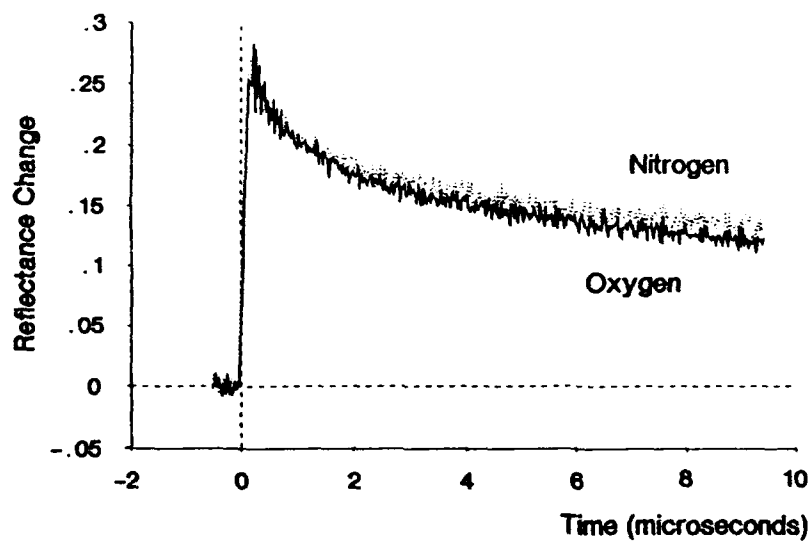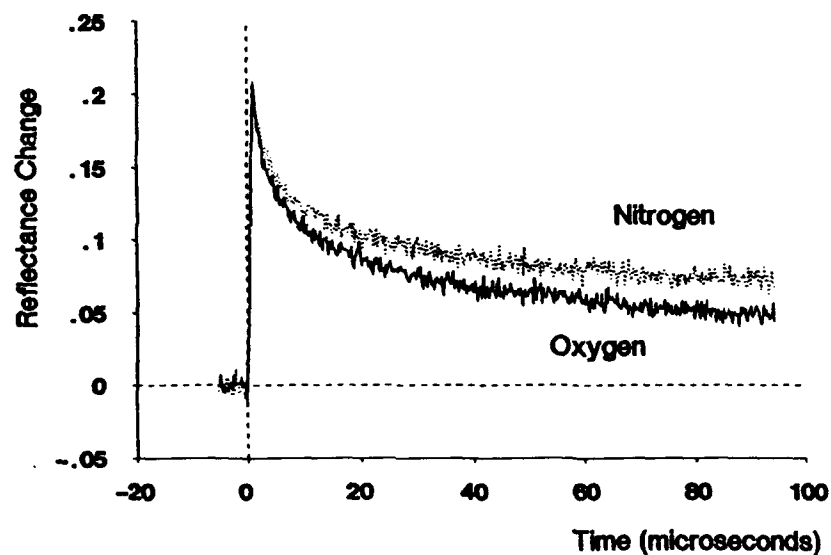

Figure 3b. Transient Decay Following Laser Excitation Analysing at 450 nm for Dry Samples of TMP under Atmospheres of Oxygen and Nitrogen over a 100 μs Time Sweep.
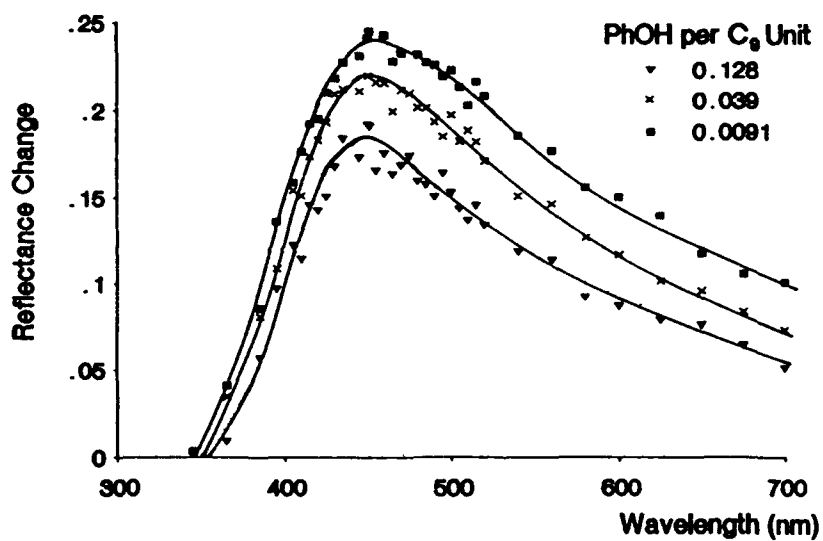
Figure 4. Transient Difference Spectra Recorded 3 µs after the Laser Pulse For TMP Samples with Various Degrees of Methoxylation.

Table I. Relative Transient Reflectance Change ($\Delta J(0)/J_o$) Observed Immediately Following Laser Photolysis (t = 0) For TMP Samples Of Varying Phenolic Hydroxyl Content.

Phenolic Hydroxyl Content per C_9 Lignin Unit	Methoxyl Content (% by Mass)	Relative $\Delta J(0)/J_o$ at 450 nm
0.128	4.4%	1.00
0.039	7.23%	1.19
0.0091	8.13%	1.29

This observation confirms the results obtained in previous studies, where for total methoxylation an increase in signal of 30% was reported(*14*). If the observed transient is due to absorption by the lowest triplet states of the aromatic carbonyl groups within the lignin, then the predominant triplet state deactivation pathway will be intersystem crossing to the ground state. From our measurements, phosphorescence emission as a mode of triplet state deactivation is a minor pathway relative to the intersystem crossing. The increased transient reflectance change from detected triplet carbonyls with increasing methoxylation of the substrate and no change in the observed deactivation kinetics may be explained in two ways;

(i) Reduction in the number of -OH groups leads to less quenching of the precursor of the triplet carbonyls leading to a greater population of the carbonyl triplet state.

(ii) Hydroxyl groups within the lignin structure may quench triplet carbonyls by a static mechanism which is too fast to be detected within the time resolution of our apparatus (< 20 ns). Fewer hydroxyl groups would lead to more triplet carbonyls having a lifetime sufficiently long to be detected.

Given that in TMP which has not had any phenolic hydroxyl groups replaced by methoxyl groups there are approximately 0.07 α-carbonyl groups and 0.128 phenolic hydroxyl groups per C_9 lignin phenylpropane unit(*17*), the magnitude of the increase in transient signal with increasing methoxylation suggests that phenolic hydroxyl groups are not distributed randomly with respect to the carbonyl moieties, perhaps as a result of the biochemical reaction mechanisms leading to lignin formation.

Studies Involving Lignin Model Compounds. Acetophenone derivatives with methoxyl and/or hydroxyl substitution patterns in the 3,4 and 5 positions of the aromatic ring have been suggested as appropriate model compounds for the carbonyl functionality present in the lignin structure(*18*). Consequently, studies involving the lignin model compound 3,4-dimethoxyacetophenone have been conducted to characterise its photochemical and photophysical properties. Upon flash excitation of a solution of 3,4-dimethoxyacetophenone, a transient absorption is seen which displays a solvent dependent λ_{max} and lifetime; these are tabulated in Table II. The transient absorption is assigned as triplet-triplet absorption from the first triplet state on the basis of energy transfer studies to perylene and naphthalene. The triplet yield was determined as unity on the basis of energy transfer studies with naphthalene as the acceptor.

Inspection of the data in Table II reveals a bathochromic shift of the λ_{max} of the triplet-triplet absorption with increasing solvent polarity, with a further bathochromic shift when the compound is adsorbed on microcrystalline cellulose. No phosphorescence emission in solution is seen from this compound at room temperature, indicating that the radiative lifetime of this triplet state is long. This is consistent with the lowest energy excited triplet state having predominantly (π, π^*) character. The shape of the triplet-triplet absorption spectrum also suggests that this is the case(*20*).

Table II Triplet-Triplet Absorption Maxima (λ_{max}), Extinction Coefficient (ϵ_{max}) and Triplet Lieftime (τ_T) for 3,4 dimethoxy-acetophenone in a Variety of Environments

Solvent/Support	Excitation Wavelength/nm	λ_{max}/nm	ϵ_{max} l.mol.$^{-1}$cm.$^{-1}$	Triplet Lifetime τ_T/μs
Benzene	354.7	365	12400[a]	39[b]
Acetonitrile	354.7	385		15[b]
Cellulose	266	400		4000[c]

[a] relative to triplet benzophenone in benzene (ϵ_{max} = 7220 l.mol.$^{-1}$ cm.$^{-1}$)([19])

[b] first order decay (τ_T = 1/k_d)

[c] first empirical half life

The excited triplet state of 3,4-dimethoxyacetophenone is quenched by both phenolic hydroxyl and methoxyl functionalities. The rate constant for decay of the 3,4-dimethoxyacetophenone triplet state k´, in the presence of a quencher Q is related to the rate of triplet state decay in the absence of quencher k_d, the quenching rate constant k_Q and the quencher concentration according to Equation 2.

$$k´ = k_d + k_Q[Q] \tag{2}$$

Hence, a plot of k´ as a function of [Q] will be linear with slope equal to k_Q and intercept k_d. Triplet decay constants k´ were obtained by simultaneously fitting four kinetic traces obtained for each sample with a first order function of the form (Equation 3):

$$A(t) = A(0) \exp -(k´t) + C \tag{3}$$

where A(t) is the laser induced change in absorbance at the analysing wavelength at time t after the laser pulse and A(0) is the change in absorbance at the analysing wavelength immediately following the laser pulse. The term C accounts for a small amount of residual absorbance observed due to formation of the ketyl radical of the 3,4-dimethoxyacetophenone. The yield of the ketyl radical in the presence of phenol is, as anticipated, significantly increased relative to a sample of the ketone alone. In addition, absorption by the phenoxy free radical also contributes to the overall residual absorption following complete triplet state deactivation([21]).

Plots of k´ as a function of quencher are shown in Figures 5a and 5b. The rate constant for quenching by phenol in benzene is determined as 6.3 x 10⁹ l.mol.$^{-1}$ s.$^{-1}$ (Figure 5 a). This is in good agreement with other authors who demonstrated that the quenching of predominantly (π, π^*) character aromatic carbonyl triplet states with phenols is an efficient process([22]). Figure 5b demonstrates that the triplet state of 3,4-dimethoxyacetophenone is also quenched by methoxyl containing moieties, although at a considerably slower rate relative to that observed with phenol as the quencher. The quenching constant for methoxybenzene in benzene was determined as 2.6 x 10⁶ l.mol.$^{-1}$ s.$^{-1}$.

The high value for the quenching of 3,4-dimethoxyacetophenone by phenol suggests that it is probable that within the lignin structure hydroxyl groups are able to quench carbonyls by a static mechanism to yield phenoxy-ketyl radical pairs which decay on a timescales faster than the time resolution of our laser flash photolysis apparatus. Intersystem crossing rate constants for triplet radical pairs in the restricted environments of micelles have been demonstrated to be of the order of 2 -5 x 10⁶ s^{-1} ([23], [24]). However, in the lignin matrix where diffusional processes are likely to be

Figure 5a. A Plot of the Psuedo First Order Rate Constant k′ as a Function of Quencher Concentration [Q] for 3,4-dimethoxyacetophenone in Benzene Quenched by Phenol.

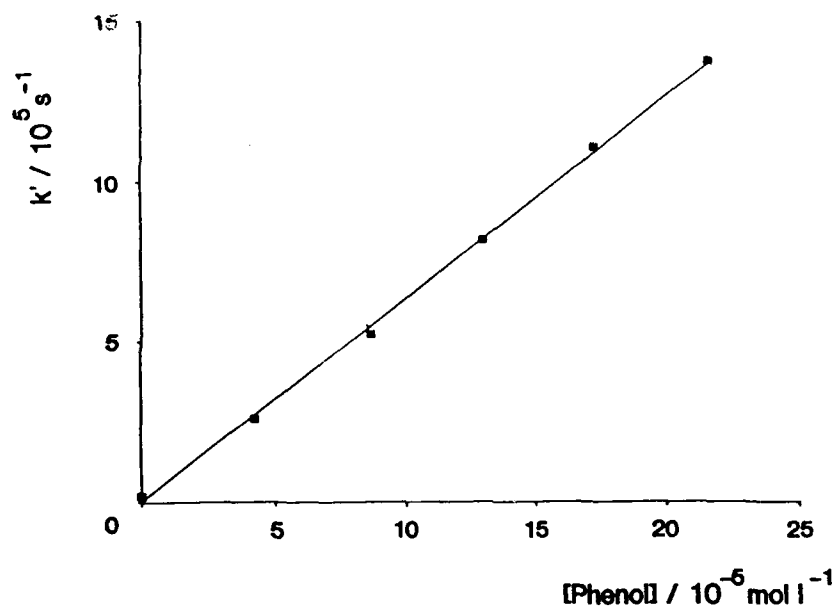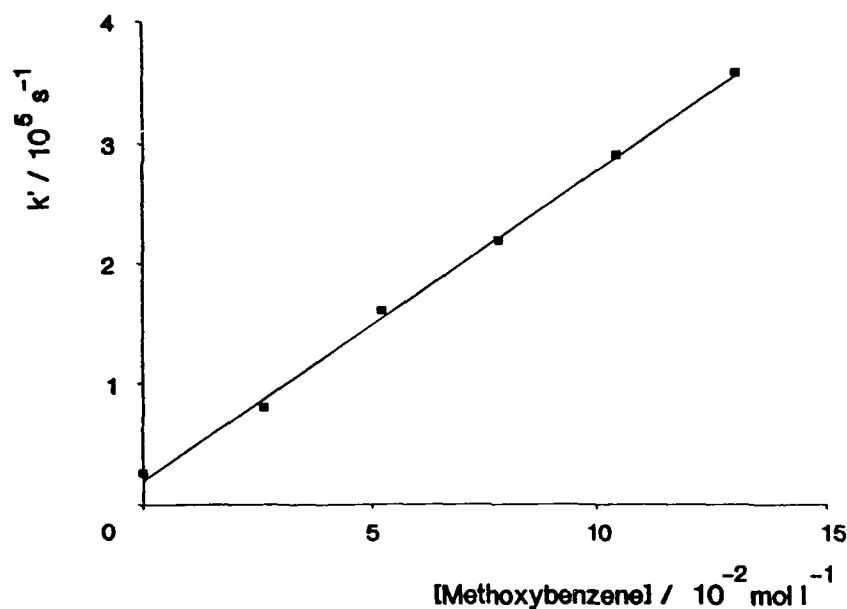

Figure 5b. A Plot of the Psuedo First Order Rate Constant k′ as a Function of Quencher Concentration [Q] for 3,4-dimethoxyacetophenone in Benzene Quenched by Methoxybenzene.
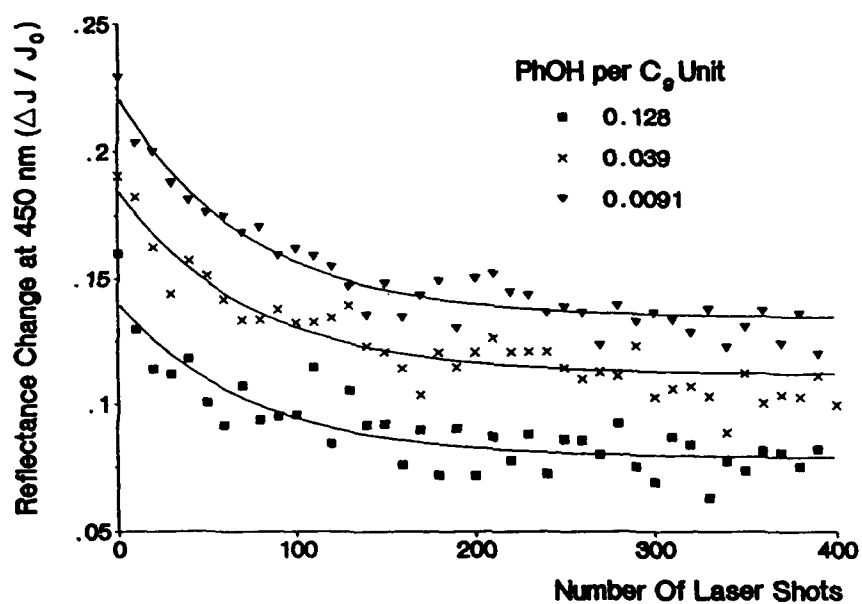
Figure 6. Transient Difference Signal Analysing at 450 nm for Samples of TMP with Varying Degrees of Methoxylation as a Function of Laser Shot Exposure Recorded 4 μs after the Laser Pulse.

even more restricted, rate constants for intersystem crossing of triplet radical pairs are likely to be greater than those observed for micellular environments, leading to much faster radical pair decay which we are unlikely to detect.

Photoyellowing of TMP. The transient absorption signal ($\Delta J(t)/J_0$) observed from TMP at 450 nm is seen to decrease with increasing number of laser shots to which it is exposed as photoyellowing of the sample proceeds (Figure 6). Following exposure to several hundred laser shots, changes in ($\Delta J(t)/J_0$) with further exposure are virtually zero. This may be attributed in the main to consumption of the aromatic carbonyl groups and to the production of products which absorb at 354.7nm, since there is a decrease in ground state reflectance at 354.7 nm of only 3% following irradiation due to lignin photodegradation and product build-up. Assuming that photodegradation products are formed below the surface with the same distribution as the carbonyl moieties within the pulp, the magnitude of this decrease in reflectance at 354.7 nm is not sufficient to explain the above observation as purely an inner filter effect. If the coloured products are generated preferentially at the front surface, perhaps as a consequence of oxygen availability, then filtering of the exciting light by a product would have a greater effect on the observed transient signal than the magnitude of the absorption at 354.7 nm would suggest. However, even allowing for this effect, we calculate some destruction of the carbonyl functionality must also be taking place.

Measurement of the ground state diffuse reflectance spectra of these samples before and after exposure to many laser pulses showed that increasing methoxylation decreases the amount of photoyellowing which occurs, an observation in agreement with those of Schmidt and Heitner (Schmidt, J.A.; Heitner, C. *J. Wood Chem. Chem. Technol.*, In Press) obtained under conditions of steady state irradiation. Additionally, the quantum yield of photoyellowing decreases with increasing irradiation time, which may again be attributed to both an inner filter effect and destruction of the aromatic carbonyl groups. Hence on the grounds of these studies both aromatic carbonyls and phenolic hydroxyl groups are implicated in the photoyellowing mechanism.

Conclusions

We have provided experimental evidence demonstrating the very different behaviour of triplet states of aromatic carbonyls in lignin and in dilute solution. These differences result, we believe, from the very restricted motion within the lignin structure relative to fluid solution. By using oxygen saturated samples rather than air saturated samples, we have been able to establish for the first time that dynamic quenching by oxygen occurs within TMP.

We have also confirmed our previous results on the effect of methoxylation of phenolic hydroxyl groups within lignin. On the basis of our model studies, we suggest that the most likely explanation for this is that triplet carbonyl groups are quenched statically by hydroxyl groups within the lignin structure on timescales less than 20 ns thus reducing the amount of transient detected in our laser photolysis experiments.

Acknowledgements

Literature Cited

(1) Kessler, R.W.; Wilkinson, F. *J. Chem. Soc. Faraday Trans. 1.* **1981**, *77*, 309.
(2) Kelly, G.P.; Leicester, P.A.; Wilkinson, F.; Worrall, D.R.; Ferreira, L.F.V.; Chittock, R.; Toner, W. *Spectrochim. Acta* **1990**, *46A*, 975.

(3) Oelkrug, D.; Honnen, W.; Wilkinson, F.; Willsher, C.J. *J. Chem. Soc. Faraday Trans. 2.* **1987**, *83*, 2081.

(4) Oelkrug, D.; Uhl, S.; Wilkinson, F.; Willsher, C.J. *J. Phys. Chem.* **1989**, *93*, 4551.

(5) Kelly, G.P.; Wilkinson, F.; Willsher, C.J.; Netto-Ferreira, J.C.N.; Opea, A.; Weir, D.; Johnston, L.J.; Scaiano, J.C. *Can. J. Chem.* **1990**, *68*, 812.

(6) Wilkinson, F.; Willsher, C.J.; Uhl, S.; Honnen, W.; Oelkrug, D. *J. Photochem.* **1986**, *33*, 273.

(7) Kossanyi, J.; Kouyate, D.; Pouliqueu, J.; Ronfard-Haret ,J.C.; Valat, P.; Oelkrug, D.; Mammel, U.; Kelly, G.P.; Wilkinson, F. *J. Luminescence* **1990**, *46*, 17.

(8) Masschelein, A.; Kirsch-De Mesmaeker, A.; Willsher, C.J.; Wilkinson, F. *J. Chem.Soc. Faraday Trans.* **1991**, *87*, 259.

(9) Wilkinson, F.; Willsher, C. *J. Appl. Spec.* **1984**, *38*, 897.

(10) Wilkinson, F.; Leicester, P.A.; Ferreira, L.F.V.; Freire, V.M. *Photochem. Photobiol.* **1991**, *54*, 599.

(11) Wilkinson, F.; Ferreira, L.F.V.; Worrall, D.R. *Spectrochim. Acta* **1992**, *48A(2)*, 135.

(12) Kelly, G.P.; Mollah, M.; Wilkinson, F. *J. Textile Institute* **1990**, *81*, 91.

(13) Bourdelande, J.L.; Campa, C.; Camps, J.; Font, J.; de March, P.; Willsher, C.J.; Wilkinson, F. *J. Photochem. Photobiol. A: Chem.* **1988**, *44*, 51.

(14) Schmidt, J.A.; Heitner, C.; Kelly, G.P.; Leicester, P.A.; Wilkinson, F. *J. Pulp Paper Sci.* **1990**, *19*, 111.

(15) Schmidt, J.A.; Heitner, C.; Kelly, G.P.; Leicester, P.A.; Wilkinson, F. *J. Photochem. Photobiol. A: Chem.* **1991**, *57*, 111.

(16) Gellerstedt, G.; and Lindfors, E.L. *Svensk Papperstidning* **1984**, *15*, R115

(17) Alder, E.; Marton, J. *Acta Chem. Scand.* **1959**, *13*, 75.

(18) .Kringstad, K.P.; Lin, S.Y. *Tappi* **1970**, *53*, 2296.

(19) Hurley, J.K.; Sinai, N.; Linschitz, H. *Photochem. Photobiol.* **1983**, *38*, 9.

(20) Lutz, H.; Breheret, E.; Lindqvist, L. *J. Phys. Chem.* **1973**, *77*, 1758.

(21) Das, P.K.; Encinas, M.V.; Steenken, S.; Scaiano, J.C. *J. Am. Chem. Soc.* **1981**, *103*, 4162.

(22) Das, P.K.; Encinas, M.V.; Scaiano, J.C. *J. Am. Chem. Soc.*, **1981**, *103*, 4154.

(23) Gould, I.R.; Zimmt, M.B; Turro, N.J.; Baretz, B.H.; Lehr, G.F. *J. Am. Chem. Soc.* **1985**, *107*, 4607.

(24) Scaiano, J.C.; Abuin, E.B.; Stewart, L.C. *J. Am. Chem. Soc.* **1982**, *104*, 5673.

Factors Governing the Efficiency of Singlet Oxygen Production during Oxygen Quenching of Singlet and Triplet States of Anthracene Derivatives in Cyclohexane Solution

F. Wilkinson,* D. J. McGarvey, and A. F. Olea

Contribution from the Department of Chemistry, Loughborough University of Technology, Loughborough, Leicestershire LE11 3TU, England

Received July 22, 1993

Abstract: The efficiencies of singlet oxygen production from the first excited singlet and triplet states of a range of substituted anthracenes in cyclohexane are reported. For all of the anthracene derivatives in this solvent, the efficiency of singlet oxygen production from the triplet state, f_Δ^T, is found to be unity. In contrast, however, the efficiency of singlet oxygen production from the first excited singlet state, f_Δ^S, varies from zero for anthracene to unity for 9,10-dicyanoanthracene. It is established that the magnitude of f_Δ^S is determined by the same factors which govern intersystem crossing yields for anthracene derivatives, i.e., the activation energy for intersystem crossing to higher triplet states. In addition it is confirmed that oxygen quenching of the excited singlet states of four anthracene derivatives in cyclohexane proceeds exclusively via enhanced intersystem crossing yielding triplet states. Some previously unavailable photophysical data are also reported for these substituted anthracenes, i.e., triplet energies, triplet yields, and rate constants for oxygen quenching of triplet states.

Introduction

There has been considerable recent interest in factors which determine oxygen quenching of excited states and the efficiency of formation thereby of singlet oxygen.[1-13] However, despite intense research over the last 30 years, the mechanism by which oxygen quenches the excited states of organic molecules remains poorly understood.[1-16] It is well-known that singlet oxygen O_2^*-($^1\Delta_g$) is frequently produced as a consequence of these quenching interactions. However, it is abundantly clear that the yield of singlet oxygen and the quenching rate constants vary considerably depending on the nature of the excited state being quenched and on the solvent or microenvironment.[1-16]

The quantum yield of sensitized production of singlet oxygen, ϕ_Δ, is given by the sum of the contributions arising from oxygen quenching of the lowest excited singlet state (S_1) and the lowest excited triplet state (T_1) of the sensitizer, i.e.
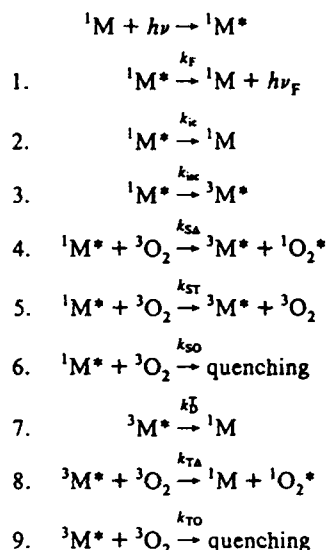
$$\phi_\Delta = \phi_\Delta(S_1) + \phi_\Delta(T_1) \qquad (1)$$

The various competing reactions can be understood by considering

Scheme I (shown below) for a hydrocarbon ^1M excited to singlet and triplet states, $^1M^*$ and $^3M^*$, respectively.

Scheme I

$$^1M + h\nu \rightarrow {}^1M^*$$

$$1. \quad {}^1M^* \xrightarrow{k_F} {}^1M + h\nu_F$$

$$2. \quad {}^1M^* \xrightarrow{k_{ic}} {}^1M$$

$$3. \quad {}^1M^* \xrightarrow{k_{isc}} {}^3M^*$$

$$4. \quad {}^1M^* + {}^3O_2 \xrightarrow{k_{S\Delta}} {}^3M^* + {}^1O_2^*$$

$$5. \quad {}^1M^* + {}^3O_2 \xrightarrow{k_{ST}} {}^3M^* + {}^3O_2$$

$$6. \quad {}^1M^* + {}^3O_2 \xrightarrow{k_{SO}} \text{quenching}$$

$$7. \quad {}^3M^* \xrightarrow{k_T^0} {}^1M$$

$$8. \quad {}^3M^* + {}^3O_2 \xrightarrow{k_{TA}} {}^1M + {}^1O_2^*$$

$$9. \quad {}^3M^* + {}^3O_2 \xrightarrow{k_{TO}} \text{quenching}$$

from which it follows that

$$\phi_F^0 = \frac{k_F}{k_F + k_{ic} + k_{isc}} \quad \text{and} \quad \phi_T^0 = \frac{k_{isc}}{k_F + k_{ic} + k_{isc}} \quad (2)$$

where ϕ_F^0 and ϕ_T^0 are the quantum yields of fluorescence and of triplet state production in the absence of oxygen, respectively. Quencing of the excited singlet state by oxygen leads to a Stern–Volmer relationship between the fluorescence quantum yields in the absence and presence of oxygen as given by eq 3 where F^0 and F represent the fluorescence intensities of the sensitizer in the absence and presence of oxygen, i.e.

$$\frac{\phi_F^0}{\phi_F} = \frac{F^0}{F} = 1 + k_S^{O_2}[O_2]/k_D^S \qquad (3)$$

where $k_S^{O_2} = k_{S\Delta} + k_{ST} + k_{SO}$, $k_D^S = k_F + k_{ic} + k_{isc}$, and we can

* Abstract published in *Advance ACS Abstracts*, Xxxxxxxxx YY, ZZZZ.
(1) Darmanyan, A. P.; Foote, C. S. *J. Phys. Chem.* 1993, *97*, 4573.
(2) Ogilby, P. R.; Sanetra, J. *J. Phys. Chem.* 1993, *97*, 4689.
(3) Kikuchi, K.; Sato, C.; Watase, M.; Ikeda, H.; Takahashi, Y.; Miyashi, T. *J. Am. Chem. Soc.* 1993, *115*, 5180.
(4) Kristiansen, M.; Scurlock, R. G.; Iu, K. K.; Ogilby, P. R. *J. Phys. Chem.* 1991, *95*, 5190.
(5) Kanner, R. C.; Foote, C. S. *J. Am. Chem. Soc.* 1992, *114*, 682. Kanner, R. C.; Foote, C. S. *J. Am. Chem. Soc.* 1992, *114*, 678.
(6) Usui, Y.; Shimizu, N.; Mori, S. *Bull. Chem. Soc. Jpn.* 1992, *65*, 897.
(7) Darmanyan, A. P.; Foote, C. S. *J. Phys. Chem.* 1992, *96*, 3723.
(8) Redmond, R. W.; Braslavsky, S. E. *Chem. Phys. Lett.* 1988, *148*, 523.
(9) Scurlock, R. D.; Ogilby, P. R. *J. Photochem. Photobiol.* 1993, *72*, 1.
(10) Wilkinson, F.; Helman, W. P.; Ross, A. B. *J. Phys. Chem. Ref. Data.* 1993, *22*, 113-262.
(11) McGarvey, D. J.; Szekeres, P. G.; Wilkinson, F. *Chem. Phys. Lett.* 1992, *199*, 314.
(12) McLean, A. J.; McGarvey, D. J.; Truscott, T. G.; Lambert, C. R.; Land, E. J. *J. Chem. Soc., Faraday Trans. II* 1990, *86*, 3075.
(13) McLean, A. J.; Truscott, T. G. *J. Chem. Soc., Faraday Trans.* 1990, *86*, 2671.
(14) Gijzeman, O. L. J.; Kauzman, F.; Porter, G. *J. Chem. Soc., Faraday Trans. II* 1973, *69*, 708.
(15) Wu, K. C.; Trozzolo, A. M. *J. Phys. Chem.* 1979, *83*, 1979. Wu, K. C.; Trozzolo, A. M. *J. Phys. Chem.* 1979, *82*, 2823.
(16) Stevens, B.; Marsh, K. L.; Barltrop, J. A. *J. Phys. Chem.* 1981, *85*, 3079.

define the fraction of singlet states quenched by oxygen as

$$P_S^{O_2} = k_S^{O_2}[O_2]/(k_D^S + k_S^{O_2}[O_2]) = (F^O - F)/F^O \quad (4)$$

The quantum yield of triplet state production in the presence of oxygen ($\phi_T^{O_2}$) is given by eq 5

$$\phi_T^{O_2} = \phi_T^O(1 - P_S^{O_2}) + f_T^{O_2}P_S^{O_2} \quad (5)$$

where $f_T^{O_2}$ is the fraction of singlet states quenched by O_2 which yield triplet states. Note that step 6 in the mechanism represents quenching of the singlet state by oxygen by any route which does not produce either singlet oxygen or triplet state, i.e., other than those shown in steps 4 and 5. Substitution of eqs 4 and 5 into eq 1 gives

$$\phi_\Delta = f_\Delta^S P_S^{O_2} + \phi_T^{O_2}f_\Delta^T P_T^{O_2} \quad (6)$$

where f_Δ^S and f_Δ^T are defined as the fraction of S_1 states and the fraction of T_1 states, respectively, quenched by oxygen which give $O_2^*(^1\Delta_g)$. $P_T^{O_2}$ equals that fraction of the triplet states which are quenched by oxygen thus

$$P_T^{O_2} = \frac{k_T^{O_2}[O_2]}{k_D^T + k_T^{O_2}[O_2]} \quad (7)$$

where $k_T^{O_2} = k_{T\Delta} + k_{TO}$.

Since triplet states are usually quite long lived and oxygen quenching is usually very efficient, $P_T^{O_2}$ in the presence of air is often close to unity. When $P_T^{O_2} = 1$ combining eqs 3–6 gives

$$\phi_\Delta\frac{F^O}{F} = (f_\Delta^S + f_T^{O_2}f_\Delta^T)\left[\frac{F^O}{F} - 1\right] + \phi_T^O f_\Delta^T \quad (8)$$

which can be used to obtain information concerning the determining factors f_Δ^S, f_Δ^T, and $f_T^{O_2}$. However, independent measurements of ϕ_T^O and $f_T^{O_2}$ are required to separately determine f_Δ^S and f_Δ^T.

In a recent compilation we listed over 1400 values of ϕ_Δ in fluid solution together with 357 values for f_Δ^T, but only 28 values for f_Δ^S.[10] We have recently shown that for a series of substituted naphthalenes in benzene the efficiency of singlet oxygen production from triplet states, f_Δ^T, increases with the oxidation potential of the naphthalene derivative.[11] In addition we demonstrated, that $k_T^{O_2}$ shows an inverse correlation with the oxidation potential of the naphthalene derivative being quenched which is evidence for the participation of charge transfer interactions within excited state/oxygen complexes formed during the quenching process. In the present study we report the efficiencies of singlet oxygen generation f_Δ^S and f_Δ^T for a series of anthracene derivatives in cyclohexane.

Experimental Section

Materials. Anthracene, 9,10-dimethylanthracene, and 9,10-diphenylanthracene (Aldrich) and cyclohexane (Aldrich spectrophotometric grade) were used as received; phenazine, 9-chloroanthracene, and 9-phenylanthracene (Aldrich) and 9,10-dichloroanthracene, 9-methylanthracene, and 9-bromoanthracene (Eastman Kodak) were recrystallized from ethanol; 9,10-dibromoanthracene and 9-cyanoanthracene (Aldrich) and 9,10-dicyanoanthracene (Kodak) were recrystallized from benzene; 9-methoxyanthracene was a gift from the late E. J. Bowen which was recrystallized from ethanol.

Apparatus. Absorption spectra were recorded with a Phillips PU8800 spectrophotometer and singlet excited state energies were determined from the position of the 0,0 absorption bands (see Figure 1). Triplet energies were measured using the method developed by Evans[17] in which use is made of the enhancement of singlet–triplet absorption by a high pressure of oxygen, typically 80 atm. Since there is little or no overlap of charge transfer absorption with the enhanced singlet–triplet absorption in the case of anthracene derivatives in the presence of high pressures of

(17) Evans, D. F. *J. Chem. Soc.* **1957**, 1351.
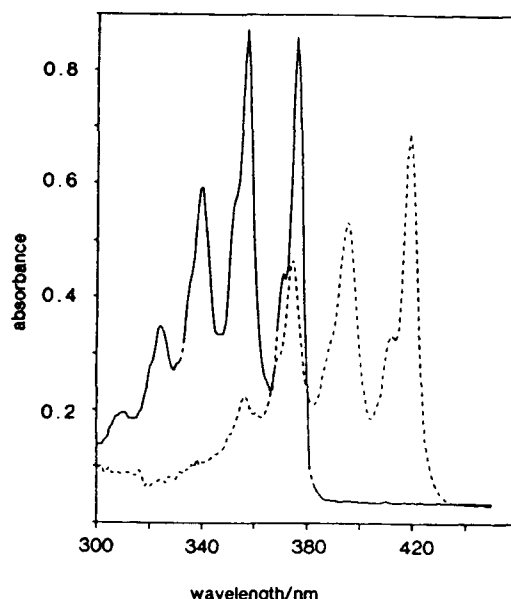
Figure 1. Absorption spectra of anthracene (—) and 9,10-dicyanoanthracene (- - -) in cyclohexane.
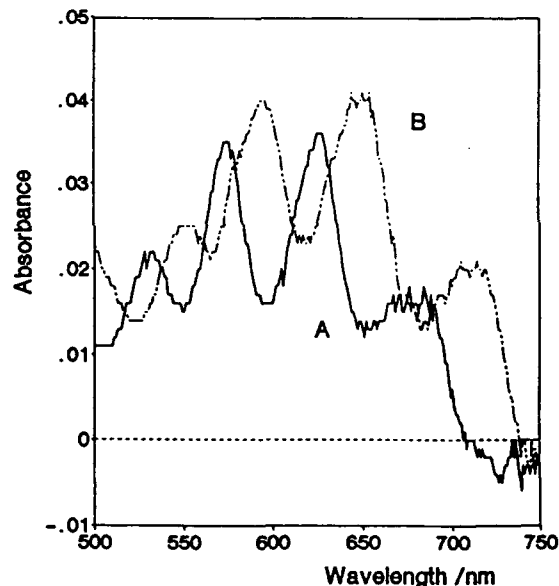
Figure 2. Oxygen-enhanced $S_0 \rightarrow T_1$ absorption spectra in carbon tetrachloride: (A) 9,10-dimethylanthracene and (B) 9-phenylanthracene.

oxygen, triplet energies could simply be determined from the position of the 0,0 bands. Representative spectra are shown in Figure 2. Fluorescence measurements were carried out using a Perkin Elmer LS4 spectrophotofluorimeter.

Transient absorption measurements were obtained using a nanosecond laser flash photolysis system with right angle geometry as described elsewhere.[18] Excitation was with 8-ns pulses (355 nm) from a Lumonics HY200 Q-switched neodymium-YAG laser. Emission from singlet oxygen following laser excitation was detected by time resolved spectroscopy as described previously.[11] For f_Δ^S and f_Δ^T measurements, air was removed from the solutions by 3 freeze–pump–thaw cycles followed by equilibration with pure oxygen at pressures up to 3 atm. For each determination six different concentrations of oxygen were used and for each of these solutions the steady state fluorescence intensity was measured. The intensity of singlet oxygen phosphorescence (P_0) at time $t = 0$ was obtained by fitting the decay curve to a single exponential function. A set of P_0 values were obtained for different laser intensities and plots of P_0 vs relative laser

(18) Wilkinson, F.; Worrall, D.; McGarvey, D. J.; Goodwin, A.; Langley, A. *J. Chem. Soc., Faraday Trans.* **1993**, *89*, 2385.

intensity were linear for pulse energies of up to 0.5 mJ per pulse. The ϕ_Δ values were determined relative to the slope obtained for the plot of P_0 vs relative laser intensity for *p*-methoxyacetophenone/naphthalene in air saturated cyclohexane for which a value of 0.92 has been measured.[19]

Triplet quantum yields of anthracene and 9-methylanthracene were determined using the method of Wilkinson et al.[20] in which the fluorescence quenching and the enhanced triplet–triplet absorption of these hydrocarbons caused by the addition of various amounts of xenon were monitored. Thus solutions degassed by the freeze–pump–thaw method were equilibrated with different amounts of xenon added by freezing from the vacuum line. Triplet–triplet absorption was measured at 430 nm and initial triplet–triplet absorbances were obtained by fitting the decay curve to a monoexponential function. These initial absorbance values were plotted against laser intensity which was varied and linear plots were observed. In the presence of xenon as a heavy atom quencher the following process occurs.

$$10. \quad {}^1M^* + Xe \xrightarrow{k_{T}^{Xe}} {}^3M^* + Xe$$
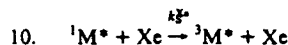
If we consider steps 1–3 in Scheme I together with step 10, it follows that the quantum yield of triplet state production in the presence of xenon, ϕ_T^{Xe}, is given by

$$\phi_T^{Xe} = \phi_T^{0}(1 - P_S^{Xe}) + P_S^{Xe} \tag{9}$$

where P_S^{Xe} is the fraction of singlet states quenched by xenon. The ratio of the triplet yield in the absence and presence of xenon is equal to the ratio of the initial triplet absorbances measured in the absence and presence of xenon, i.e.

$$\frac{\phi_T^0}{\phi_T^{Xe}} = \frac{A_T^0}{A_T^{Xe}} \tag{10}$$

and since P_S^{Xe} can be calculated from the fluorescence intensity ratio for quenching by xenon, i.e.

$$P_S^{Xe} = \frac{F^0 - F}{F^0} \tag{11}$$

rearrangement gives eq 12 (see ref 20).

$$\frac{F^0}{F} - 1 = \phi_T^0\left[\frac{A_T^{Xe}F^0}{A_T^0 F} - 1\right] \tag{12}$$

Values of ϕ_T^0 were determined from the slopes of plots of $(F^0/F) - 1$ against $((F^0/F)(A_T^{Xe}/A_T^0) - 1)$ (see Figure 3).

The rate constants for oxygen quenching of triplet states were determined by fitting the decay curves of triplet–triplet absorption to single exponential functions and using eq 13

$$k_T^{O_2} = (k_a - k_D^T)/[O_2] \tag{13}$$

where k_a and k_D^T are the first-order decay constant under air and under vacuum, respectively, and $[O_2]$ is the oxygen concentration in cyclohexane taken as 2.1×10^{-3} mol dm^{-3} (see ref 21). From the ratio of the triplet absorbances at time $t = 0$, values of $f_T^{O_2}$ were measured using the following equation which is obtained by reorganizing eqs 3–5

$$f_T^{O_2} = \phi_T^0\left(\frac{A_T^{O_2}}{A_T^0} - \frac{F}{F^0}\right)\bigg/\left(1 - \frac{F}{F^0}\right) \tag{14}$$

where $A_T^{O_2}$ and A_T^0 are the triplet absorbances in the presence and absence of oxygen, which are directly proportional to $\phi_T^{O_2}$ and ϕ_T^0, respectively.

Results and Discussion

The photophysical properties of anthracene and its derivatives are collected in Table I. These demonstrate that the energy difference between the lowest singlet and lowest triplet states is

(19) Gorman, A. A.; Krasnovsky, A. P.; Rodgers, M. A. J. *J. Phys. Chem.* 1991, *95*, 598.

(20) Horrocks, A. R.; Kearvell, A.; Tickle, K.; Wilkinson, F. *Trans. Faraday Soc.* 1966, *62*, 3393.

(21) Saltiel, J.; Atwater, B. W. *Adv. Photochem.* 1988, *14*, 1.

(22) Hamanaoue, K.; Tai, S.; Hidaka, T.; Nakayama, T.; Kimoto, M.; Teranashi, H. *J. Phys. Chem.* 1984, *88*, 4380.

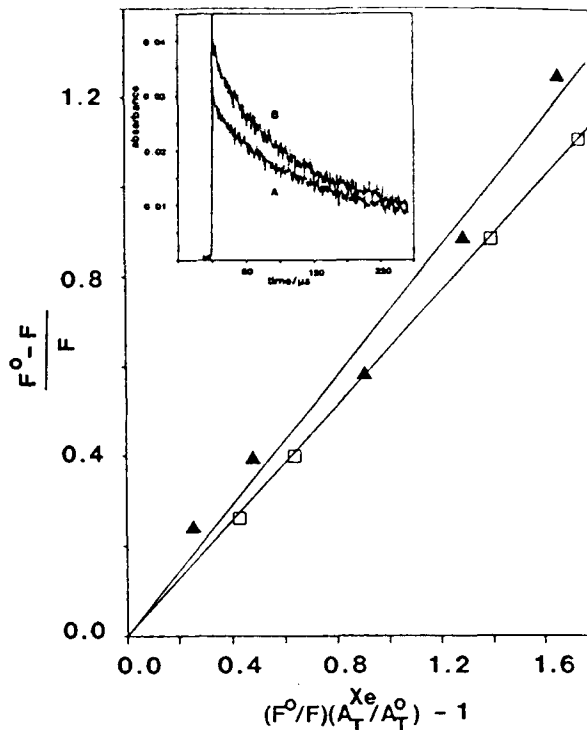(23) Padhye, M. R.; McGlynn, S. P.; Kasha, M. *J. Chem. Phys.* 1956, *24*, 588.

Figure 3. Plots for determination of triplet quantum yields using xenon as a heavy atom quencher of fluorescence. The insert shows T–T absorption of anthracene in cyclohexane at 430 nm in the absence (A) and presence (B) of xenon: (▲) anthracene and (□) 9-methylanthracene.

Table I. Energies of Singlet (E_S) and Triplet (E_T) States, Activation Energies (E_{isc}) for the Intersystem Crossing Process, and Half-Wave Oxidation Potentials (E_{OX}) for Anthracene and Its Derivatives

compd	E_{S_1},[a] kJ mol^{-1}	E_{T_1}, kJ mol^{-1}	E_{isc}, kJ mol^{-1}	E_{T_2},[l] kJ mol^{-1}	E_{OX},[m] eV
anthracene	318	178[b]	4.6[k]	323	1.18
9-bromoanthracene	308	173[c]	12.1[i]	320	1.29
9-chloroanthracene	309		14.1,[k] 12.5[j]	322	
9-cyanoanthracene	299	169[d]	17.1[k]	316	1.57[f]
9-methylanthracene	310	173[b]	11.9[k]	322	0.96
9-methoxyanthracene	309		14.4[j]	323	1.05
9-phenylanthracene	312	176[d]	6.9,[i] 8.9[j]	320	1.13
9,10-dibromoanthracene	297	168[e]	18.7[i]	316	1.45
9,10-dichloroanthracene	298	169[e]	17.2,[k] 18.4[i]	316	
9,10-dicyanoanthracene	266	175[f]	24.9[k]	311	1.89[f]
9,10-diphenylanthracene	305	171[g]	13.5[k]	319	1.52
9,10-dimethylanthracene	301	168[d]	15.9[k]	317	1.67

[a] Determined from the position of the 0–0 band in the absorption spectra. [b] From ref 17. [c] From ref 22. [d] Measured in this work from $S_0 \rightarrow T_1$ oxygen enhanced absorption. [e] From ref 23. [f] From ref 3. [g] From ref 24. [h] From ref 25. [i] From ref 26. [j] Values measured in heptane, ref 27. [k] Calculated from correlation between E_{S_1} vs E_{isc} given in ref 26.[l] $E_{T_2} = E_{S_1} + E_{isc}$. [m] Versus SCE from ref 28 or ref 3 as indicated below.

in all cases greater than 94 kJ mol^{-1} and that therefore it is energetically possible to produce $O_2^*({}^1\Delta_g)$ by oxygen quenching of both singlet and triplet states in the case of these anthracene derivatives. Although substituent effects on the singlet state energies of anthracene derivatives are well documented,[26,27] there have been few systematic measurements for triplet states. However, it is apparent (Table I) that the substituent shifts on T_1 are about one-half as large as those for S_1. It is also apparent

(24) Murov, S. L. *Handbook of Photochemistry*; Marcel Dekker: New York, 1973.

(25) Bowen, E. J.; Sahu, J. *J. Phys. Chem.* 1959, *63*, 4.

(26) Kearvell, A.; Wilkinson, F. *J. Chim. Phys. Phys. Chim. Biol.* 1966, *62*, 3393.

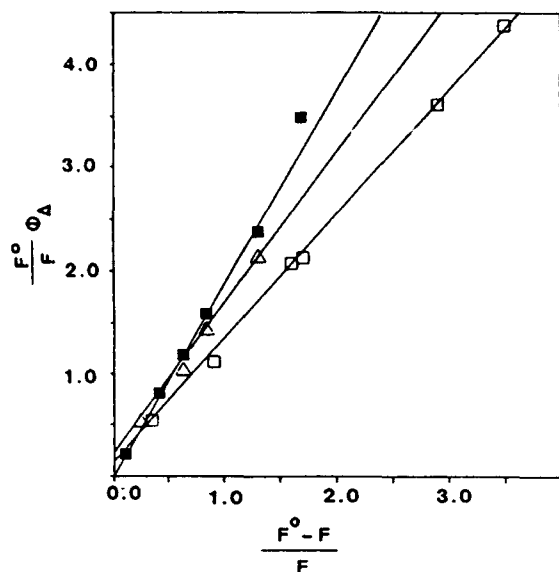(27) Schoof, S.; Gusten, H. *Ber. Bunsenges. Phys. Chem.* 1989, *93*, 864.

Figure 4. Plots to determine f_Δ^S and f_Δ^T according to eq 8: (■) 9,10-dicyanoanthracene, (△) 9-cyanoanthracene, and (□) 9,10-diphenylanthracene.
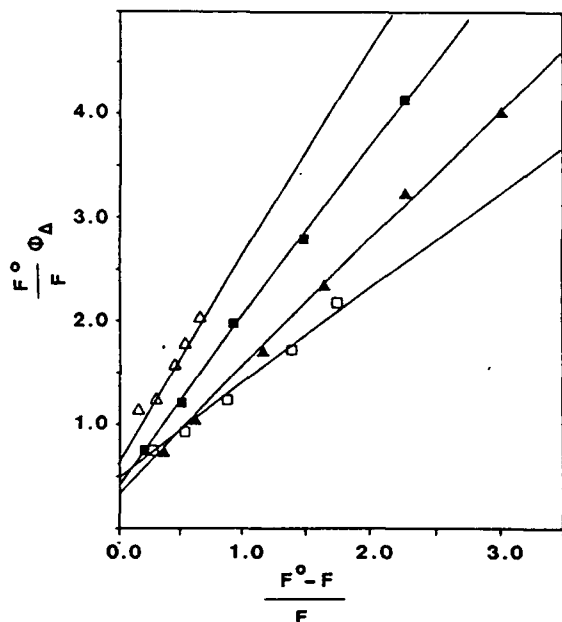

Figure 5. Plots to determine f_Δ^S and f_Δ^T according to eq 8: (■) 9,10-dichloroanthracene, (□) 9-phenylanthracene, (▲) 9-methoxyanthracene, and (△) 9,10-dibromoanthracene.

that the substituent shifts of the dimeso-substituted anthracenes are approximately twice those of the mono-substituted derivatives.

Plots according to eq 8 are shown in Figures 4–6 and the results are collected in Table II. The experimental errors (95% confidence limits) in the slopes of such plots, which equal $(f_\Delta^S + f_\Delta^T f_T^{O_2})$ are $\leq \pm 10\%$. However, the intercepts, which equal $\phi_T^O f_\Delta^T$, have errors

(28) Mann, C. K.; Barnes, K. K. *Electrochemical Reactions in Nonaqueous Systems*; Marcel Dekker: New York, 1970.
(29) Van der Donckt, E.; Barthels, M. R.; Delestinne, A. *J. Photochem.* 1973, *1*, 429.
(30) Medinger, T.; Wilkinson, F. *Trans. Faraday Soc.* 1965, *61*, 620.
(31) Darmayan, A. P. *Chem. Phys. Lett.* 1984, *110*, 89.
(32) Kikuchi, K.; Hoshi, M.; Niwa, T.; Takahashi, Y.; Miyashi, T. *J. Phys. Chem.* 1991, *95*, 38.
(33) Chattopadhyay, S. K.; Kamar, Ch. V.; Das, P. K. *Chem. Phys. Lett.* 1983, *98*, 250.
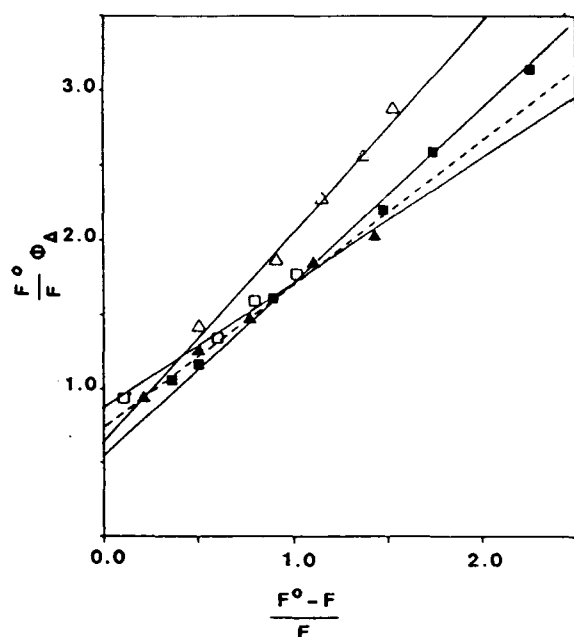(34) Stevens, B.; Algar, B. E. *J. Phys. Chem.* 1968, *72*, 3468.

Figure 6. Plots to determine f_Δ^S and f_Δ^T according to eq 8: (△) 9-chloroanthracene, (□) 9-bromoanthracene, (■) 9-methylanthracene, and (▲) anthracene.

of at least ±10% and are considerably higher in those cases such as 9,10-dicyanoanthracene where the intercept is close to zero. Literature values of triplet quantum yields are given in Table I and where possible those values which were not available were measured (e.g. see Figure 3). Values for ϕ_T^O combined with the intercepts to the plots shown in Figures 4–6 allow values of f_Δ^T to be determined. These f_Δ^T values are found to be unity within experimental error for all of the anthracene derivatives investigated. No value of ϕ_T^O is available for 9-chloroanthracene and therefore a value of $f_\Delta^T = 1$ is assumed in this case.

It is interesting to note that for those compounds with triplet yields in the range 0.26–0.71 where typical intercepts are obtained with 10–20% error, the values of $\phi_T^O f_\Delta^T$ are on average 10% higher than the values of ϕ_T^O. This may indicate that the standard value of ϕ_Δ of 0.92 used for p-methoxyacetophenone/naphthalene in cyclohexane with respect to which these values were measured may be 10% too high. However, Usui et al.,[6] who have measured ϕ_Δ, f_Δ^T, and f_Δ^S values in cyclohexane for three of the derivatives studied here by measuring quantum yields of photooxidation as a function of oxygen concentration, have obtained similar or slightly higher values in their work (see later). For those compounds such as 9-cyanoanthracene, 9,10-dicyanoanthracene, 9,10-diphenylanthracene, and 9,10-dimethylanthracene for which ϕ_T^O is less than 4%, we can only say from the intercepts that f_Δ^T are ≤1. This is of course consistent with these values also being one and there is no reason to assume that this is not the case. In fact in the case of 9,10-dicyanoanthracene one obtains the value $f_\Delta^T = 1$ from the slope of the plot according to eq 8, since the slope $(f_\Delta^S + f_\Delta^T f_T^{O_2})$ equals 2.1 ± 0.1 and this is only consistent with all three values, f_Δ^S, f_Δ^T, and $f_T^{O_2}$, being equal to 1. Other values for $f_T^{O_2}$, the fraction of singlet states quenched by oxygen which produce triplet states, were obtained using eq 14 for anthracene and 9-methyl-, 9-phenyl-, and 9,10-dichloroanthracene. The values obtained were 1.0 ± 0.1 (see Table II). It is interesting to note that Postashnik et al.[35] measured $f_T^{O_2} = 0.95$ and 0.9 for oxygen quenching of singlet anthracene in toluene and acetonitrile, respectively. They studied several hydrocarbons

(35) Postashnik, R.; Goldschmidt, C. R.; Ottolenghi, M. *Chem. Phys. Lett.* 1971, *9*, 404.

Table II. Singlet Oxygen Production from Singlet (f_Δ^S) and Triplet (f_Δ^T) States of Anthracene Derivatives in Cyclohexane,[a] Triplet Quantum Yields (ϕ_T), and the Fractions of Singlet States Quenched by Oxygen That Give Triplet States ($f_T^{O_2}$)

compd	$f_\Delta^S + f_\Delta^T f_T^{O_2}$	$\phi_T f_\Delta^T$	ϕ_T	f_Δ^T	$f_\Delta^{S\,k}$	$f_T^{O_2}$
anthracene	0.91 ± 0.05	0.7ʳ ± 0.05	0.71[b]	1.0 ± 0.1	0.0 ± 0.1	1.0 ± 0.1
9-bromoanthracene	0.96 ± 0.06	0.79 ± 0.04	0.70[c]	1.0 ± 0.1	0.0 ± 0.1	
9-chloroanthracene	1.41 ± 0.08	0.65 ± 0.07		(1.0)	(0.4)	
9-cyanoanthracene	1.51 ± 0.05	0.13 ± 0.04	0.04[d]	1.0	0.5 ± 0.1	
9-methylanthracene	1.12 ± 0.03	0.62 ± 0.05	0.63[b]	1.0 ± 0.1	0.1 ± 0.1	1.0 ± 0.1
9-methoxyanthracene	1.27 ± 0.03	0.25 ± 0.07	0.26[c]	1.0 ± 0.1	0.3 ± 0.1	
9-phenylanthracene	0.97 ± 0.06	0.42 ± 0.07	0.37[f]	1.0 ± 0.1	0.0 ± 0.1	1.0 ± 0.1
9,10-dibromoanthracene	1.76 ± 0.19	0.81 ± 0.08	0.70[g]	1.0 ± 0.1	0.8 ± 0.2	
9,10-dichloroanthracene	1.63 ± 0.03	0.36 ± 0.06	0.29[g]	1.0 ± 0.1	0.6 ± 0.1	1.0 ± 0.1
9,10-dicyanoanthracene	2.08 ± 0.10	0.0 ± 0.13	0.02[f]	1.0 ± 0.1	1.0 ± 0.1	1.0 ± 0.1
9,10-diphenylanthracene	1.22 ± 0.02	0.06 ± 0.04	0.02[i]	1.0	0.2 ± 0.1	
9,10-dimethylanthracene	1.11 ± 0.02	0.07 ± 0.07	0.02[j]	1.0	0.1 ± 0.1	

[a] ϕ_Δ values were obtained relative to ϕ_Δ(p-methoxyacetophenone/naphthalene) = 0.92, ref 19. [b] Obtained by enhancement of intersystem crossing by xenon. [c] Unpublished result. [d] From ref 29. [e] Value measured in heptane, ref 27. [f] From ref 30. [g] Values measured in toluene, ref 31. [h] From ref 32. [i] From ref 33. [j] From ref 34. [k] For any assumptions made see text.

and found $f_T^{O_2}$ close to one in toluene but often considerably less in acetonitrile. Where no value of $f_T^{O_2}$ has been determined it is assumed, in agreement with the measured values, that $f_T^{O_2} = 1$. This allows us to determine the f_Δ^S values and these are given in Table II. These values vary across the whole possible range from 0 to 1, in contrast to the values of f_Δ^T which are all unity.

Estimates of the errors given for f_Δ^S were arrived at as follows. For 9,10-dicyanoanthracene the slope of the plot shown in Figure 4 ($f_\Delta^S + f_\Delta^T f_T^{O_2} = 2.08 \pm 0.10$) is only consistent with all three fractions being equal to 1.0 ± 0.1. Since we have measured f_Δ^T and $f_T^{O_2}$ equal to unity for anthracene, 9-phenylanthracene, 9-methylanthracene, and 9,10-dibromoanthracene, f_Δ^S given in column 6 of Table II can be calculated without any further assumptions. In the case of 9-bromoanthracene, 9-methoxyanthracene, and 9,10-dibromoanthracene where we have shown that $f_\Delta^T = 1.0 \pm 0.1$, we have had to assume that $f_T^{O_2} = 1$ to obtain the values of $f_\Delta^S = 0.0 \pm 0.1$, 0.3, ± 0.1, and 0.8 ± 0.2, respectively. For 9-cyano-, 9,10-diphenyl-, and 9,10-dimethylanthracene for which ϕ_T^O values are less than 0.04, accurate values for f_Δ^T cannot be obtained from the intercepts of lines plotted according to eq 8. We have therefore for these three derivatives assumed both f_Δ^T and $f_T^{O_2}$ equal 1 to calculate the f_Δ^S values. We have made the same assumption in the case of 9-chloroanthracene since no value for ϕ_T^O is available for this derivative.

The fact that anthracene derivatives show no substitution effects on f_Δ^T contrasts with the situation for a series of naphthalene derivatives where even in cyclohexane values of f_Δ^T have been shown to be critically dependent on electron withdrawing and donating substituents.[36] The difference in behavior between anthracene and naphthalene derivatives is attributed to the location of the charge transfer states relative to the lowest triplet states in these two series of compounds. For naphthalene derivatives the charge transfer states are calculated to lie below the lowest locally excited triplet states for most derivatives,[11] whereas for the anthracene derivatives, they are calculated to be above. A good estimate for the energy of the charge transfer state of the complex between the hydrocarbons and oxygen is given by the Rehm–Weller equation[37]

$$E_{CT} = F(E_{ox}^D - E_{red}^A) + \Delta\omega \qquad (15)$$

where E_{ox}^D is the oxidation potential of the donor and E_{red}^A is the reduction potential of the acceptor which has a value in the case of oxygen of –0.78 V versus SCE in acetonitrile.[38] The value of

Table III. Rate Constants, $k_S^{O_2}$ and $k_T^{O_2}$, for Quenching of Singlet and of Triplet States, Respectively, of Anthracene Derivatives by Oxygen in Cyclohexane Solution

compd	$10^{-10}k_S^{O_2}$,[a] dm³ mol⁻¹ s⁻¹	$10^{-9}k_T^{O_2}$, dm³ mol⁻¹ s⁻¹	$k_T^{O_2}/k_S^{O_2}$	$k_T^{O_2}/k_{diff}$[b]
anthracene	2.5	3.4	0.14	0.12
9-bromoanthracene	2.9	3.1	0.11	0.11
9-chloroanthracene	3.1	3.5	0.11	0.13
9-cyanoanthracene	0.67			
9-methylanthracene	3.0	3.3	0.11	0.12
9-methoxyanthracene	2.7	3.2	0.12	0.11
9-phenylanthracene	1.9	3.4	0.18	0.12
9,10-dibromoanthracene	2.4	2.7	0.11	0.10
9,10-dichloroanthracene	2.4	2.7	0.11	0.10
9,10-dicyanoanthracene	0.47			
9,10-diphenylanthracene	1.7			
9,10-dimethylanthracene	2.0	3.5	0.18	0.13

[a] From ref 39. [b] Using $k_{diff} = 2.8 \times 10^{10}$ dm³ mol⁻¹ s⁻¹, from ref 21.

$\Delta\omega$ depends on Coulombic interactions and solvation energies and is difficult to calculate for encounter pairs, but it is likely to be constant for a series of related compounds. Knibbe, Rehm, and Weller[37c] have shown that $\Delta\omega = 0.15 \pm 0.1$ eV for the energy of 60 exciplexes which they studied in hexane.

The rate constants for oxygen quenching of the triplet states of the anthracene derivatives measured here are in the range 3.1 ± 0.4 × 10⁹ dm³ mol⁻¹ s⁻¹. Again there is very little dependence of $k_T^{O_2}$ on substituents for anthracene derivatives in cyclohexane which contrasts with the situation for naphthalene derivatives where both $k_T^{O_2}$ and f_Δ^T vary substantially with substituents.[36] Since the quenching constants $k_S^{O_2}$ for 9-cyanoanthracene and 9,10-dicyanoanthracene are 6.7 and 4.7 × 10⁹ dm³ mol⁻¹ s⁻¹, this clearly demonstrates that oxygen quenching of singlet states is not always diffusion controlled. Values of $k_T^{O_2}/k_S^{O_2}$ which vary from 0.11 to 0.18 are given in Table III. The values obtained for $k_T^{O_2}$ are all approximately equal to or slightly less than $^1/_9 k_{diff}$ where $^1/_9$ is the spin statistical factor expected[14] for quenching by reaction 8, if one assumes that the diffusion controlled rate constant in cyclohexane (k_{diff}) is equal to 2.8 × 10¹⁰ dm³ mol⁻¹ s⁻¹, the average value calculated by Saltiel and Atwater[21] for $k_S^{O_2}$ for a set of aromatic hydrocarbons in cyclohexane (see Table III).

The efficiency of singlet oxygen production from the singlet state, f_Δ^S, varies from 0 to 1. In Figure 7 the zeroth-order energy levels of encounter complexes between anthracene and oxygen on the one hand and 9,10-dibromoanthracene and oxygen on the other are illustrated. In terms of the energy levels in this diagram, the fact that $f_\Delta^S = 0$ for anthracene suggests either a very fast decay through the triplet manifold, i.e., via the complex states labeled $^3(S_1...^3\Sigma) \rightarrow {}^3(T_2...^3\Sigma) \rightarrow {}^3(T_1...^1\Delta) \rightarrow {}^3(T_1...^3\Sigma)$, or alternatively

(36) McGarvey, D. J.; Olea, A. F.; Wilkinson, F. To be submitted for publication.

(37) (a) Rhem, D.; Weller, A. *Z. Phys. Chem.* **1970**, *69*, 183. (b) Weller, A. In *The Exciplex*; Gordon, M., Ware, W. R., Eds.; Academic Press: London, 1975; pp 23–38. (c) Knibbe, H.; Rhem, D.; Weller, A. *Ber. Bunsenges. Phys. Chem.* **1969**, *73*, 839.

(38) Kavarnos, G. J.; Turro, N. J. *Chem. Rev.* **1986**, *86*, 401.

(39) Schoof, S.; Gusten, H.; von Sonntag, C. *Ber. Bunsenges. Phys. Chem.* **1976**, *82*, 1068.
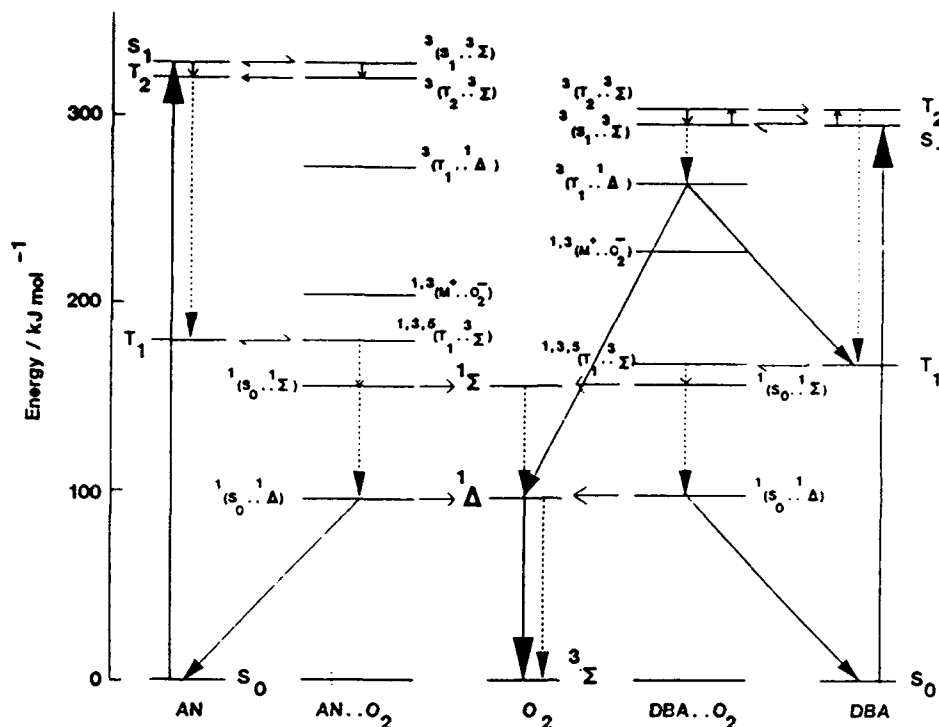
Figure 7. Schematic energy level diagram for anthracene (AN), 9,10-dibromoanthracene (DBA), molecular oxygen (O_2), and encounter complexes (AN...O_2 and DBA...O_2) illustrating major decay pathways.
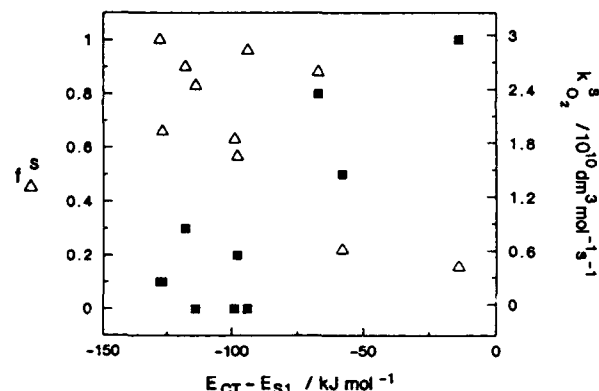

Figure 8. Plot of the fraction (f_Δ^S) of singlet oxygen produced due to oxygen quenching of the singlet state of anthracene derivatives (^{1}M) and of the oxygen quenching constants ($k_S^{O_2}$) against the difference in energy between the lowest singlet states and the (M^+...O_2^-) charge-transfer states ($E_{CT} - E_{S_1}$): (■) f_Δ^S and (△) $k_S^{O_2}$.

the complex labeled ^{3}(S_1...$^3\Sigma$) internally converts to the ^{3}(T_2...$^3\Sigma$) state which then dissociates to give T_2 and O_2($^3\Sigma_g$) with 100% efficiency. In other words the state labeled ^{3}(T_1...$^1\Delta$) either internally converts very rapidly or is not formed at all in the case of anthracene. If we consider the case of 9,10-dicyanoanthracene where f_Δ^S = 1, this requires that the state labeled ^{3}(T_1...$^1\Delta$) is produced with unit efficiency and dissociates also with unit efficiency with no internal conversion to the lower ^{3}(T_1...$^3\Sigma$) state. Other anthracene derivatives, fc ⎯ ⎯mple 9,10-dibromoanthracene (see Figure 7), lie betwee⎯ ⎯ese two extremes, and the different efficiencies could be due to the varying involvement of charge transfer states. Figure 8 shows a plot of f_Δ^S against ΔE = $E_{CT} - E_{S_1}$ calculated using E_{S_1} values given in Table I and eq 15 taking $\Delta\omega$ = 15 kJ mol^{-1} to calculate E_{CT}.[37b] Except in the case of 9,10-dicyanoanthracene, the charge transfer states are calculated to lie well below the S_1 state (58–128 kJ mol^{-1}, see also Figure 7), and internal conversion from the (S_1...$^3\Sigma$) complex

state therefore is probably much more likely to closely lying states such as ^{3}(T_2...$^3\Sigma$) or ^{3}(T_1...$^1\Delta$). Even indirect mixing between the S_1 and charge transfer states, which would be expected[14] to be inversely proportion to ΔE, is not apparent from the scatter of the data shown in Figure 8. In the case of 9,10-dicyanoanthracene, however, where ΔE is calculated to be −14 kJ mol^{-1}, i.e. the energy of the charge transfer state is calculated to be just below that of the S_1 state, it could be argued that the charge transfer assisted internal conversion to the ^{3}(T_1...$^1\Delta$) state is occurring since f_Δ^T is unity in this case. However, the low values of $k_S^{O_2}$ given in Table III show that 9,10-dicyanoanthracene and 9-cyanoanthracene have exceptionally low rate constants for quenching of their singlet states by oxygen which is not consistent with charge transfer assisted quenching. If anything there is an inverse relationship between $k_S^{O_2}$ and $E_{CT} - E_{S_1}$ as shown in Figure 8, but the data show considerable scatter. This demonstrates that in cyclohexane charge transfer interactions are not very significant in determining the efficiency of singlet oxygen production from excited singlet states of anthracene derivatives and we have already shown they do not affect f_Δ^T values. Other workers have shown that charge transfer interactions can be important in the oxygen induced deactivation of excited singlet states of organic molecules in acetonitrile,[3] i.e., w!..en the solvent is polar. However as mentioned earlier, Postashnik et al.[35] have demonstrated that the oxygen catalyzed intersystem crossing efficiency ($f_T^{O_2}$) shows a marked dependence on solvent polarity.

As early as 1968, Stevens and Algar[34] attributed the relative unimportance of the spin allowed production of O_2^*($^1\Delta_g$) during oxygen quenching of singlet states of sensiti⎯ ⎯ in which the singlet–triplet splitting exceeds 94 kJ mol^{-1} ⎯ ⎯h⎯ formation of higher triplet state T_2. See also ref 40. Mor⎯ ⎯cently, Usiu et al.[6] have clearly demonstrated that the contribution to ϕ_Δ arising from singlet state quenching by oxygen depends markedly on the energy of T_2 states in certain compounds. Since $f_T^{O_2}$ = 1 in all of the cases we have measured, it follows that $k_{SA} + k_{ST} \gg k_{SO}$.

(40) Birks, J. B. *Organic Molecular Photophysics*; Wiley: London, 1975; Vol. 2, p 544.
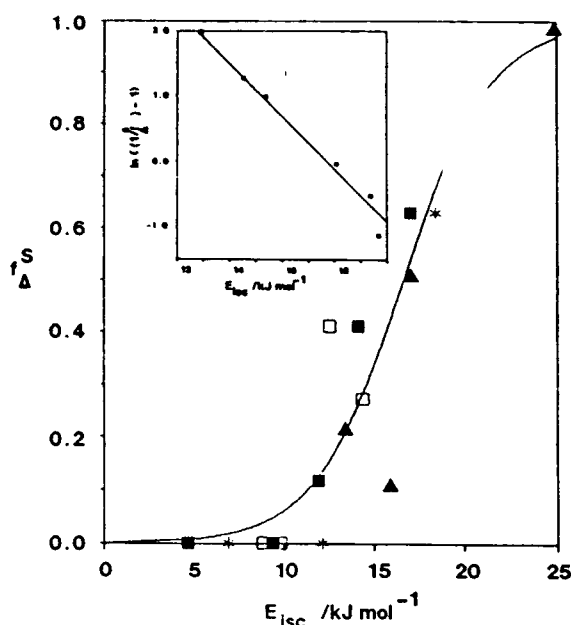
Figure 9. Plot of the fraction (f_Δ^S) of singlet oxygen produced due to oxygen quenching of the singlet state of anthracene derivatives versus the activation energy for intersystem crossing (E_{isc}), according to eq 13: (■) from ref 25, (*) from ref 26, (□) from ref 27, and (▲) extrapolated from the correlation given in ref 26. Insert shows a plot of $\ln\{(1/f_\Delta^S) - 1\}$ against E_{isc}.

and assuming this is the case for all of the anthracene derivatives, analysis of kinetic Scheme I gives

$$f_\Delta^S = \frac{k_4}{k_4 + k_5} = \frac{k_{S\Delta}}{k_{S\Delta} + k_{ST}} \qquad (16)$$

Examination of the energy diagram shown in Figure 7 reveals that reaction 4 must involve dissociation of the $^3(T_1...^1\Delta)$ state. Reaction 5 may involve dissociation of the $^3(T_2...^3\Sigma)$ state or internal conversion to the $^3(T_1...^3\Sigma)$ state. This latter process is ruled out at least for 9,10-dicyanoanthracene in cyclohexane because it does not explain the unit efficiency in this case. This leads us to suggest that the efficiency of production of singlet oxygen depends on competition between internal conversion either to the $^3(T_2...^3\Sigma)$ state or to the $^3(T_1...^1\Delta)$ state both of which dissociate efficiently. It has already been demonstrated[25-27] that intersystem crossings of many meso-substituted anthracene derivatives are temperature dependent with activation energies (E_{isc}) depending on the energy gap between their lowest excited singlet states (S_1) and higher triplet states. The activation energies for intersystem crossing measured from temperature dependence of fluorescence in the absence of oxygen are given in Table I. If f_Δ^S is reduced because of dissociation of the $^3(T_2...^3\Sigma)$ state to give the T_2 state of the hydrocarbon, lying at higher energy than the S_1 state, which then internally converts from the T_2 to the T_1 state without producing singlet oxygen, eq 16 becomes

$$f_\Delta^S = \frac{k_{S\Delta}}{k_{S\Delta} + Ae(-E_{isc}/RT)} \qquad (17)$$

for these meso-substituted anthracenes. Equation 17 rearranges to give

$$\frac{1}{f_\Delta^S} - 1 = \frac{Ae(-E_{isc}/RT)}{k_{S\Delta}} \qquad (18)$$

in which case a plot of $\ln\{1/f_\Delta^S - 1\}$ versus E_{isc} should be linear with a slope of $-1/RT$. Such a plot is shown as an insert in Figure 9, and the linear part of this curve has a slope of -0.41 mol kJ^{-1},

which agrees very well with the expectation value for $1/RT$. Figure 9 shows a plot of f_Δ^S versus E_{isc} according to eq 17 which clearly demonstrates that f_Δ^S increases with increasing E_{isc} and thus quenching of singlet excited states of anthracene derivatives by molecular oxygen therefore involves efficient dissociation from both $^3(T_2...^3\Sigma)$ and $^3(T_1...^1\Delta)$ states when they are formed and the efficiency of singlet oxygen production depends almost completely upon the extent to which these two states are formed.

As mentioned earlier, Usui et al.[6] have recently evaluated f_Δ^S and f_Δ^T values for anthracene, 9,10-dimethylanthracene, and 9,10-dicyanoanthracene in cyclohexane from fluorescence quenching measurements coupled with measurements of the quantum yields of photosensitized oxidation of 1,3-diphenylisobenzofuran as a function of oxygen concentration. These workers assumed $f_T^{O_2} = 1$ and measurements given in this paper would support this assumption. Our values for f_Δ^T which all equal 1 are in agreement with their values. However, our values for f_Δ^S for anthracene and 9,10-dimethylanthracene of 0 and 0.11 respectively do not compare so favorably with their values of 0.3 and 0.2, respectively. In the case of 9,10-dicyanoanthracene our values of $f_\Delta^T = 1$ and $f_\Delta^S + f_T^{O_2}f_\Delta^T = 2.1 \pm 0.1$ agree very well with those of Usui et al.[6] Only in the case of anthracene in cyclohexane is the discrepancy beyond the expected experimental errors. The only other measurement on anthracene derivatives in cyclohexane as solvent which is relevant to this work is the value obtained by Kristiansen et al.[4] for 9,10-dicyanoanthracene in cyclohexane of $f_\Delta^S + f_T^{O_2}f_\Delta^T = 1.9$ obtained as a limiting value at infinite oxygen concentration. This is in good agreement with our value and that of Usui et al.[6] Bearing in mind the dangers of comparing values for singlet oxygen formation efficiencies in different solvents, we feel that it is pertinent to mention that Wu and Trozzolo[15] found the following values for f_Δ^S in *n*-hexane from studies of the sensitized photooxidation of 2,5-dimethylfuran coupled with fluorescence quenching measurements. These authors found $f_\Delta^S \geq 0.19, 0.42, 0.41,$ and 0.48 for 9-methyl-, 9-phenyl-, 9,10-dimethyl-, and 9,10-diphenylanthracene, respectively. Our values in cyclohexane for these same compounds, given in Table II, are 0.1, 0.0, 0.1, and 0.2 for 9-methyl-, 9-phenyl-, 9,10-dimethyl-, and 9,10-diphenylanthracene. Once again it is apparent that the values we have obtained from emission measurements are lower than those obtained using measurements of quantum yields of photooxidation but the different solvent has to be borne in mind. The only other value which has been measured for f_Δ^S of anthracene is that by Stevens et al.,[16] who also use photosensitized oxidation measurements and found $f_\Delta^S = 0.46$ for anthracene in benzene solution. It is worth noting that some photooxidation quantum yields of furans are anomalously high because of the destruction of furans by intermediate endoperoxides[41] which may account for some of the differences between the values presented here and those given in refs 6, 15, and 16. We are currently investigating the influence of the solvent on f_Δ^T and f_Δ^S and since this is considerable, further work is needed before critical evaluation of available data can be made.

Conclusion

Measurements of the yields of singlet oxygen production combined with fluorescence quenching measurements for anthracene and eleven of its meso derivatives have clearly demonstrated that the fraction of triplet states quenched by oxygen which yield $O_2^*(^1\Delta_g)$ is unity in all cases. We have shown that the fraction of triplet states produced following oxygen quenching of singlet states of anthracene and 9-phenyl-, 9,10-dichloro-, and 9,10-dicyanoanthracene in cyclohexane is also unity. However, the fraction of quenching of the excited singlet states of these derivatives by oxygen which yield $O_2^*(^1\Delta_g)$, f_Δ^S, is only unity in the case of 9,10-dicyanoanthracene. Values of f_Δ^S, which vary in

(41) Adam, W. A.; Rodriguez, A. *J. Am. Chem. Soc.* **1980**, *102*, 404–406.

cyclohexane from zero in the case of anthracene, 9-bromoanthracene, and 9-phenylanthracene to one in the case of 9,10-dicyanoanthracene, have been shown to depend on the efficiency of formation of the triplet encounter complex $^3(T_2...^3\Sigma)$, which dissociates to give ground state oxygen and the T_2 state of the separated anthracene derivative, which then dissipates excess energy by internally converting to its T_1 state, without forming singlet oxygen. The efficiency of formation of this $^3(T_2...^3\Sigma)$ state is often temperature dependent for meso derivatives of anthracene and this is shown to determine the value of f_Δ^Σ with dissociation of $^3(T_2...^3\Sigma)$ states being much more likely than internal conversion to the lower complex state, $^3(T_1...^1\Delta)$,

dissociation of which produces singlet oxygen. These processes are both temperature and solvent dependent and consequently a considerably amount of work remains to be done before it is possible to provide a complete description of the interactions between molecular oxygen and the excited state of anthracene derivatives.

PC 2120 pp1-10

SET 2

PROOF TO BE RETURNED TO THE ACADEMY

Factors which determine the efficiency of sensitized singlet oxygen production

copy posted by Air mail

F WILKINSON*, D J McGARVEY and A OLEA

Department of Chemistry, Loughborough University of Technology, Loughborough, Leicestershire, LE11 3TU, UK

Abstract. Nanosecond laser photolysis measurements of sensitized phosphorescence from oxygen have been used to obtain values for singlet oxygen formation efficiencies during oxygen quenching of excited singlet and triplet states of anthracene and naphthalene derivatives. Oxygen quenching of excited singlet states of anthracene and dicyanoanthracene in cyclohexane has been shown to lead to catalysed production of triplet states with unit efficiency in both cases, but concurrent production of singlet oxygen only occurs in the case of 9,10-dicyanoanthracene with efficiency close to unity whereas the efficiency for singlet oxygen production due to direct oxygen quenching of excited singlet anthracene is close to zero. In contrast to these results, oxygen quenching of the triplet states of anthracene and dicyanoanthracene in cyclohexane yields singlet oxygen with unit efficiency whereas the singlet oxygen formation efficiency during oxygen quenching of triplet 1-ethylnaphthalene is only 0·86 in cyclohexane and drops to 0·5? in acetonitrile. This solvent dependence demonstrates the role which charge transfer interactions play in determining singlet oxygen yields. Further information concerning the decay of excited oxygen–aromatic hydrocarbon charge-transfer complexes have been obtained from picosecond laser pump-probe studies where direct excitation is into the charge transfer bands of oxygenated 1-ethylnaphthalene. Following the excitation of the charge-transfer complex, the triplet state of 1-ethylnaphthalene is rapidly produced with an efficiency which shows a marked solvent dependency, being 0·4 and 0·8 in acetonitrile and cyclohexane, respectively. The measured yields of singlet oxygen formation following excitation into 1-ethylnaphthalene-oxygen charge-transfer complexes are 0·36 and 0·78 in these two solvents which is greater than that expected on the basis of the measured triplet yields. Mechanisms of quenching of excited states by oxygen which explain these results are discussed.

Keywords. Singlet oxygen yields; oxygen quenching; charge transfer absorption.

1. Introduction

It is well known that molecular oxygen is a paramagnetic molecule which is ubiquitous and efficiently quenches electronically excited states in dilute fluid solution (Birks 1970). The ground electronic state of molecular oxygen has zero angular momentum about its internuclear axis, contains two unpaired p-electrons and is given the group theoretical symbol $^3\Sigma_g^-$. The two electronically excited states of oxygen which arise from the same electron configuration, both with spin pairing of these two electrons, are the $^1\Delta_g$ and the $^1\Sigma_g^+$ states which lie 94 and 157 kJ mol^{-1} respectively above the
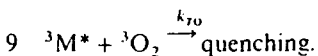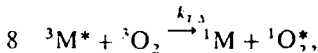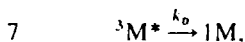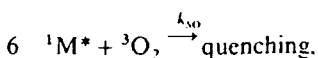
---

* For correspondence
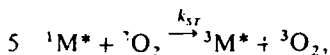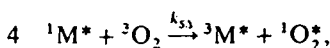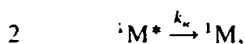
ground state. Oxygen is one of the most efficient quenchers of electronically excited states and it is often assumed that electronic excitation energy is transferred to oxygen with high efficiency when spin statistical factors are taken into account. In a set of classic studies, Porter et al (1973) showed that the rate constants for oxygen quenching of the triplet states of several aromatic hydrocarbons are less than those expected for a diffusion-controlled reaction, being $\leqslant 3 \times 10^9 \, dm^3 \, mol^{-1} s^{-1}$ in benzene solution at room temperature, which is about one ninth of the rate constants observed for oxygen quenching of excited singlet states of aromatic hydrocarbons (Ware 1962). However, the fractions of singlet and triplet states quenched by oxygen which produce singlet oxygen have more recently been shown to vary substantially from one compound to another. (Redmond and Braslavsky 1988a; Saltiel and Atwater 1988; McLean e. al 1990; Wilkinson et al 1993). Quenching of excited singlet states by oxygen may produce singlet oxygen when the gap between the first excited singlet and triplet states of the aromatic hydrocarbon exceeds $94 \, kJ \, mol^{-1}$ and can, in addition, catalyse further production of triplet states (see below). This has to be taken into account when interpreting the quantum yields of singlet oxygen production measured in any experiments where there is oxygen quenching of singlet states.

Tha various competing reactions can be understood by considering the nine steps shown below from which it follows that

$$\phi_F^0 = \frac{k_F}{k_F + k_{ic} + k_{isc}} \quad \text{and} \quad \phi_T^0 = \frac{k_{isc}}{k_F + k_{ic} + k_{isc}}. \tag{1}$$

where ϕ_F^0 and ϕ_T^0 are the quantum yields of fluorescence and of triplet state production in the absence of oxygen, respectively.

Step 1 $^1M^* \xrightarrow{k_F} {}^1M + h\nu_F.$

2    $^1M^* \xrightarrow{k_{ic}} {}^1M.$

3    $^1M^* \xrightarrow{k_{isc}} {}^3M^*.$

4    $^1M^* + {}^3O_2 \xrightarrow{k_{S\Delta}} {}^3M^* + {}^1O_2^*.$

5    $^1M^* + {}^3O_2 \xrightarrow{k_{ST}} {}^3M^* + {}^3O_2.$

6    $^1M^* + {}^3O_2 \xrightarrow{k_{SO}} \text{quenching.}$

7    $^3M^* \xrightarrow{k_D} {}^1M.$

8    $^3M^* + {}^3O_2 \xrightarrow{k_{T\Delta}} {}^1M + {}^1O_2^*.$

9    $^3M^* + {}^3O_2 \xrightarrow{k_{TO}} \text{quenching.}$

We can define the fraction of singlet states quenched by oxygen as

$$P_S^{O_2} = k_{O_2}^S [O_2] / (k_D^S + k_{O_2}^S [O_2]). \tag{2}$$

where

$$k_{O_2}^S = k_{S\Delta} + k_{ST} + k_{SO} \text{ and } k_D^S = k_F + k_{ic} + k_{isc}.$$

The quantum yield of triplet production in the presence of oxygen $\phi_T^{O_2}$ is given by

$$\phi_T^{O_2} = \phi_T^0(1 - P_S^{O_2}) + f_T^{O_2} P_S^{O_2}, \tag{3}$$

where $f_T^{O_2}$ is the fraction of singlet states quenched by O_2 which yield triplet states. Note that step 6 represents quenching of the singlet state by oxygen by any mechanism which does not produce either singlet oxygen or triplet states i.e., other than those shown in steps 4 and 5. The quantum yield of singlet oxygen production by sensitization ϕ_Δ is given by the sum of the contributions due to oxygen quenching of singlet and triplet states i.e.

$$\phi_\Delta = \phi_\Delta(S_1) + \phi_\Delta(T_1) \tag{4}$$

If f_Δ^S and f_Δ^T are defined as the fractions of S_1 and T_1 states respectively quenched by oxygen which give $O_2^*(^1\Delta_g)$ it follows that

$$\phi_\Delta = f_\Delta^S P_S^{O_2} + \phi_T^{O_2} f_\Delta^T P_T^{O_2}, \tag{5}$$

where $P_T^{O_2}$ equals that fraction of the triplet states which are quenched by oxygen, which is often close to unity because of the long lifetimes of many triplet states.

Quenching of the excited singlet state leads to a Stern–Volmer relationship between the fluorescence quantum yields in the absence and presence of oxygen as given by (6) where F^0 and F represent the fluorescent intensity of the sensitizer in the absence and presence of oxygen i.e.

$$\phi_F^0/\phi_F = F^0/F = 1 + k_{O_2}^S[O_2]/k_D^S. \tag{6}$$

When $P_T^{O_2} = 1$, combining (2), (3), (5) and (6) gives

$$\phi_\Delta(F^0/F) = (f_\Delta^S + f_T^{O_2} f_\Delta^T)[(F^0/F) - 1] + \phi_T^0 f_\Delta^T. \tag{7}$$

which can be used to obtain information concerning the crucial factors; however, one needs independent measurements of ϕ_T^0 and $f_T^{O_2}$ to determine f_Δ^S and f_Δ^T.

Alternatively one can produce the triplet states of the sensitizer with unit efficiency by energy transfer using aromatic ketones as triplet energy donors. Then (5) becomes

$$\phi_\Delta = f_\Delta^T P_T^{O_2}. \tag{8}$$

This allows values of f_Δ^T to be determined. We have recently employed this method used previously by ourselves (Garner and Wilkinson 1976) and others (Gorman *et al* 1987) to demonstrate the dependence of f_Δ^T for a series of naphthalene derivatives in benzene on the oxidation potential of the sensitiser (McGarvey *et al* 1992).

The perturbing effects of dissolved oxygen on the uv/vis absorption spectra of organic molecules is a well-known phenomenon which was first studied in detail by Evans (1957) and subsequently discussed by Tsubomura and Mulliken (1960) and Birks (1970). The additional absorption bands observed include the lowest energy transition which corresponds to the $S_0 \to T_1$ transition of the organic molecules in intimate contact with an oxygen molecule. More intense absorption is observed at
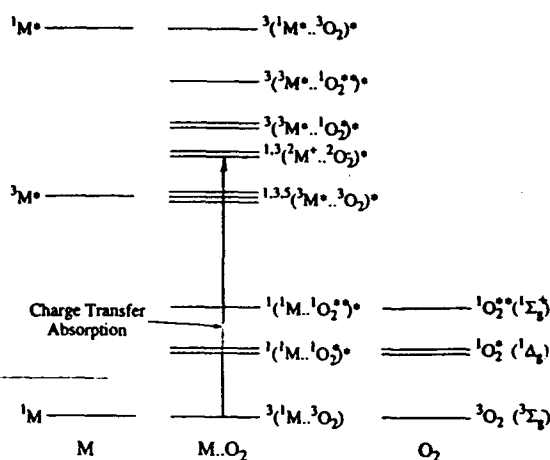
Figure 1. Schematic diagram of the lower energy levels of the M..O$_2$ complex between an aromatic molecule, M, and molecule oxygen, O$_2$.

shorter wavelengths is often attributed to CT transitions within ^{3}(M..O$_2$) contact complexes (see figure 1) and this assignment is supported by the broad structureless appearance of the bands. In this paper, we exploit the optical absorption properties of oxygen/organic molecule contact complexes to directly populate, using both nanosecond and picosecond laser pulses, excited state complexes which may be involved in the dynamic quenching of excited states by oxygen.

2. Experimental

2.1 *Materials*

Anthracene (Aldrich Gold Label), naphthalene (Aldrich, scintillation grade, > 90"$_o$), 1-ethylnaphthalene (Fluka, 99"$_o$), benzophenone (BP) (Aldrich Gold Label) and *p*-methoxyacetophenone (PMAP) (Aldrich, 99"$_o$) were used as received. Acridine (Aldrich) was recrystallised from ethanol and 9,10-dicyanoanthracene (Kodak) was recrystallised from benzene. Acetonitrile (Aldrich, spectrophotometric grade) was dried refluxing over calcium hydride. All other solvents were spectrophotometric grade from Aldrich and were used as received.

2.2 *Picosecond pump-probe measurements*

Solutions of 1·5 M 1-ethylnaphthalene (EN) in cyclohexane and acetonitrile were equilibrated with 2–4 atmospheres of oxygen yielding absorbances of ~ 0·3 around 355 nm compared with ~ 0·05 for air-equilibrated solutions. The absorbance due to the EN O$_2$ contact complex exhibits a linear dependence on oxygen concentration under our conditions. The picosecond time-resolved absorption measurements were carried out at the Rutherford-Appleton Laboratory Laser Support Facility. The picosecond laser system was a frequency-doubled mode-locked Nd/YAG pumping a dye laser operating at 706 nm. The pump and probe wavelengths were obtained by

frequency-doubling to give 353 nm and mixing of 1064 nm and 706 nm to give 424 nm. The operating conditions were as follows: pump wavelength = 353 nm, pump energy = 40μJ; probe wavelengths = 424 nm and 706 nm, pulse duration = ~ 5 ps, irradiation area = 0·8 mm². The probe wavelengths are suitable for detection of the EN triplet state (424 nm) and the EN radical cation (706 nm). We are not aware of a documented spectrum for EN⁺ but expect that it will have a similar spectrum to the naphthalene radical which is well documented (Liu *et al* 1992). The yield of EN triplet state following CT excitation was measured by comparison of the triplet state absorption, observed at 424 nm, 400 ps after excitation with that from an identical optically-matched air-equilibrated solution containing BP or PMAP. Under our conditions ([EN] = 1·5 M) energy transfer is complete within 300 ps. Both ketones give the same yield of sensitised 3EN* demonstrating that energy transfer from the triplet state of these aromatic ketones proceeds with 100% efficiency giving an effective EN triplet state yield of unity for these solutions.

2.3 *Nanosecond flash photolysis and singlet oxygen yield measurements*

For nanosecond flash photolysis studies and for the singlet oxygen yield measurements the 355 nm harmonic of a Lumonics HY200 Q-switched Nd/YAG laser (8 ns, 15 mJ pulse⁻¹) was employed as the excitation source. Oxygen-quenching rate constants were determined by sensitising the EN triplet state with an aromatic ketone and measuring the rate of triplet decay in an air-equilibrated solution. Singlet oxygen was detected by monitoring the 0,0 vibronic band of the phosphorescence centred at 1270 nm (eq 9) using a Judson germanium photodiode (J16-8SP-R05M, active diameter = 0.5 M) coupled to a Judson PA100 amplifier.

$$O_2^*(\Delta_g) \rightarrow O_2(^3\Sigma_g^-) + h\nu(1270\,\text{nm}). \tag{9}$$

The phosphorescence was detected at right angles to the exciting beam through a silicon cut-off filter. The laser energies employed did not exceed 0·7 mJ pulse⁻¹. Individual luminescence traces were signal-averaged and fitted using a single exponential function to yield the luminescence intensity I_0 at $t = 0$. The I_0 values were plotted against relative laser intensity to obtain plots which were linear below 0·5 mJ pulse⁻¹. Comparison of the slopes of these plots yielded relative singlet oxygen yields. The fluorescence measurements with anthracene and dicyanoanthracene were carried out using a Perkin–Elmer 3000 fluorimeter and the oxygen concentrations were in the range 2·4 × 34·6 × 10⁻³ mol dm⁻³.

3. Results and discussion

The singlet–triplet energy map in the case of many aromatic hydrocarbons, e.g. anthracene, naphthalene and their derivatives, is such that it is energetically possible to produce singlet oxygen via oxygen quenching of both excited singlet and triplet states i.e. by reactions (4) and (8) given earlier. According to (7) plots of $\phi_\Delta(F^0/F)$ versus $[(F^0/F) - 1]$ should be linear and figure 2 shows that this applies to the data we obtained for anthracene and dicyanoanthracene in cyclohexane. The slopes and intercepts for these two compounds show very large differences. The slopes of these plots give values for $(f_\Delta^S + f_\Delta^T f_T^{O_2})$ of 0·91 ± 0·05 and 1·95 ± 0·05 respectively for
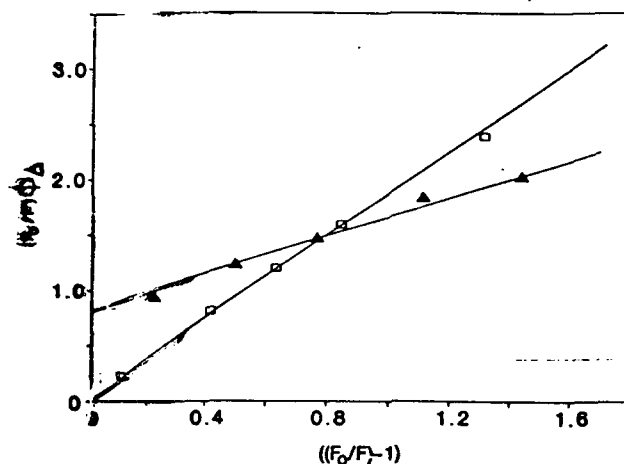
Figure 2. Plots according to (7) (see text) which illustrate the dependence of ϕ_Δ, the singlet oxygen yield, on the extent of fluorescence quenching by oxygen, where F^0 and F represent the fluorescence intensities in the absence and presence of oxygen, for (▲) anthracene and (□) di-cyanoanthracene in cyclohexane.
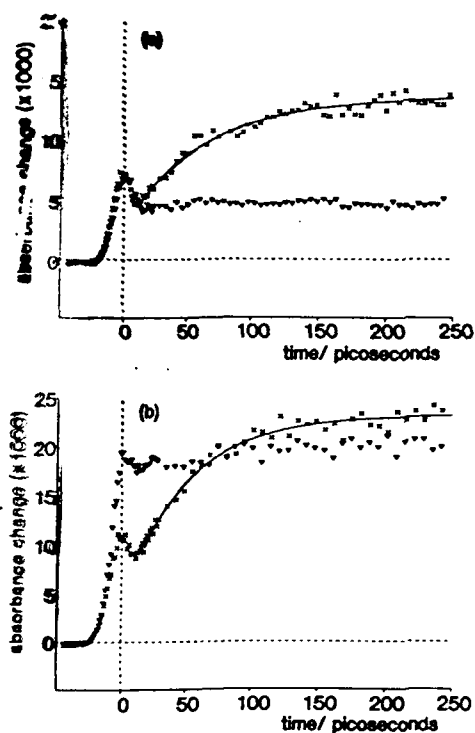
Figure 3. Picosecond absorption profiles observed for $1.5\,mol\,dm^{-3}$ of 1-ethylnaphthalene in (a) acetonitrile and (b) cyclohexane: (▽) oxygenated with 3–4 atmosphere of oxygen, (×) air-equilibrated containing benzophenone. The oxygenated and ketone-containing solutions were optically matched at the excitation wavelength (353 nm).

anthracene and dicyanoanthracene. The value for dicyanoanthracene is close to the maximum value of 2 which arises when $f_\Delta^S = f_\Delta^T = f_T^{O_2} = 1$ i.e. all these fractions are unity which applies when oxygen quenching is exclusively via steps 4 and 8. This is the situation for dicyanoanthracene in this solvent. Note that the intercept of the plot for dicyanoanthracene in figure 3 is 0 ± 0.05 which is consistent with $\phi_T \approx 0$. In the case of anthracene however, the intercept is equal to 0.77 ± 0.05 which equals $(f^T \phi_T^O)$ and since the triplet yield is reported to be 0.72 ± 0.05 (Horrocks and Wilkinson 1968) these values are consistent with $f_\Delta^T = 1.0 \pm 0.05$ Potashnik *et al* (1971) have shown that oxygen quenching of singlet anthracene does lead to enhanced triplet absorption with $f_T^{O_2} = 0.9 \pm 0.1$ in tolene and acetonitrile. It follows that f_Δ^S is close to zero for anthracene. The reasons why f_Δ^S values are so different for anthracene and dicyanoanthracene is likely to be due to the same reason which causes the intersystem crossing yields of these two compounds to be so different, namely the presence or absence of an intermediate triplet state between the S_1 and T_1 states in these anthracene derivatives.

The probabilities of dissociation of collisional complexes of the type shown in figure 1 relative to the probability of internal conversion leading to energy dissipation in these complexes determines the values of f_Δ^S and f_Δ^T. In an attempt to understand such processes we have examined the singlet oxygen yields when excitation, under an elevated pressure of oxygen, was directly into the CT state (see figure 1) in comparison with the singlet oxygen yields observed via triplet sensitisation from triplet BP (or PMAP) in air-equilibrated 1.5 M EN solutions using optically matched solutions. The singlet oxygen yields from the sensitised samples were assumed to be the same as those measured by us using smaller EN concentrations (~ 0.05 M). In these measurements the standards used were acridine in acetonitrile, $\Phi_\Delta = 0.82$ (Redmond and Braslavsky 1988b) and *p*-methoxyacetophenone/0.1 M naphthalene in cyclohexane, $\Phi_\Delta = 0.92$ (Gorman *et al* 1991). Thus values of the singlet oxygen yields resulting from absorption to CT states of O_2/EN complexes, Φ_Δ^{CT}, equal to 0.36 and 0.78 were obtained in acetonitrile and cyclohexane respectively.

Using 353 nm picosecond excitation of the same solutions, a 'prompt' increase in absorption at 424 nm where triplet naphthalene absorbs was observed (figure 3), which does not significantly decay over the timescales investigated (~ 1 ns). Thus the EN triplet state is produced within a few picoseconds i.e. within the risetime of our picosecond apparatus. Superimposed upon the rise in triplet state absorption we observe a rapid symmetrical rise and fall in absorption which follows the excitation pulse. This component is present regardless of whether the solution is oxygenated or not and so is not derived from the CT state. Also this rapid component is not observed with neat acetonitrile or cyclohexane but is observed in the case of neat benzene. This feature has been observed previously (Masuhara *et al* 1981; Miyasaka *et al* 1985) in studies of multiphoton absorption by neat aromatic liquids as a rapid component absorbing around 420 nm and was attributed to electron-aromatic ion production and geminate recombination. We believe a similar process is operating when 1.5 M EN solutions are subjected to 353 nm picosecond excitation. The consequence of this multiphoton absorption is the appearance of a relatively small long-lived (> 1 ns) absorption which may be due to the excited singlet or triplet state of EN or it may be due to the EN radical cation or a combination of these. Since we do not have the facility of spectral resolution with our picosecond measurements we are presently unable to identify this weak background absorption.

Using the picosecond apparatus and probing at 706 nm for the EN radical cation we observed only very small 'prompt' absorptions ($\sim 10^{-3}$) which were not sensitive to the concentration of oxygen. This agrees with our nanosecond photolysis measurements where we also were unable to detect significant absorption in the 680–720 nm region following excitation into the CT band using either solvent. However these observations contrast with the report by Kristiansen *et al* (1991) who detected the 1-methylnaphthalene radical cation in acetonitrile following CT excitation. Unfortunately no details concerning the amounts of radical cation so produced were given. Thus it is difficult to compare results.

The varying efficiencies of triplet state formation (ϕ_T^{CT}) as a function of solvent is apparent from the traces shown in figure 3. The triplet yield determinations derived exclusively from the picosecond pump-probe measurements of optically matched solutions are 0·40 and 0·80 in acetonitrile and cyclohexane respectively. We have determined f_Δ^T for EN in acetonitrile and cyclohexane using triplet ketones as triplet energy donors and the values we obtained were 0·51 and 0·86 respectively. The value of the product $f_\Delta^T \phi_T^{CT}$, which is equal to the amount of singlet oxygen production, which would be expected following excitation to the charge transfer state on the basis of the observed yield of triplet state production equals 0·20 and 0·69 in acetonitrile and cyclohexane respectively which is not equal to our measured values of Φ_Δ^{CT} particularly in acetonitrile. Thus more singlet oxygen is produced from the charge transfer state than can be accounted for from the amount of triplet state produced. Another interesting feature of the data is the large solvent dependence of ϕ_T^{CT}. Thus in cyclohexane the triplet state production from the charge transfer state is very efficient ($\sim 80\%$) but in acetonitrile it is dramatically reduced to only 40%. This difference is clearly shown in figure 3.
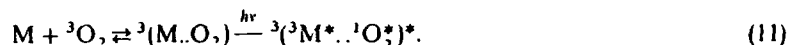
In a previous paper (McGarvey *et al* 1992) we used the Rehm–Weller equation (Rehm and Weller 1970) neglecting the coulombic term, and calculated the free energy of the relaxed charge transfer states, $^{1,3}(M^+..O_2^-)^*$ to be $\sim 30 \text{ kJ mol}^{-1}$ below the localised triplet for EN. In acetonitrile where any coulombic correction will be small since it has a dielectric constant of 37·5 the excited complexes $^{1,3}(M^+..O_2^-)^*$ are very likely to lie below the localised triplet and to be populated followed the formation of $^3M^*$ by energy transfer or following triplet state production following charge transfer absorption. There is a large difference between the f_Δ^T and k_q^T values for EN in the two solvents. In cyclohexane the values of f_Δ^T and k_q^T are 0·86 and $1·6 \times 10^9 \text{ l mol}^{-1}\text{s}^{-1}$ respectively, while for acetonitrile the values are 0·51 and $3·3 \times 10^9 \text{ l mol}^{-1}\text{s}^{-1}$. These numbers indicate that reaction 9 is more important in acetonitrile than in cyclohexane due to the more favourable CT interactions in the more polar solvent. It is likely that this is due to the catalysed intersystem crossing via the triplet channel i.e.

$$^3M^* + {}^3O_2 \rightleftarrows ({}^3M..O_2)^* \rightarrow {}^3(M^+..O_2^-)^* \rightarrow {}^1M + {}^3O_2, \tag{10}$$
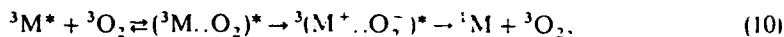
which does not produce singlet oxygen. In cyclohexane which has a dielectric constant of 2·02 it is quite likely that the relaxed charge transfer states. $^{1,3}(M^+..O_2^-)^*$ lie above the localised triplet and in the absence of CT-mediated quenching the triplet channel is impeded relative to the singlet channel because of poor Franck–Condon factors (Gijzeman *et al* 1973). Thus we would expect that deactivation of the initially prepared excited state complex to give ground state products would be faster in acetonitrile than in cyclohexane. This means that separation of $^3(M..O_2)^*$ to yield the triplet state would be more important in cyclohexane as observed.

Since the triplet energies of naphthalene and 1-methylnaphthalene are 255 and 249 kJ mol^{-1} respectively (Murov 1973) it is likely that the energy of $^3(^3M^*..^1O_2^*)^*$ i.e., the complex formed by association of the triplet state of EN and singlet oxygen, will be ~ 343 kJ mol^{-1}, which is slightly higher than the excitation energy used in these experiments (338 kJ mol^{-1}). In fact, Dijkgraaf and Hoijtink (1963) have reported a broad shoulder around 350 nm in oxygenated naphthalene solutions which they attribute to the simultaneous transition described by

$$M + {}^3O_2 \rightleftarrows {}^3(M..O_2) \xrightarrow{h\nu} {}^3(^3M^*..^1O_2^*)^*. \tag{11}$$

Thus the simplest explanation for the fact that Φ_{CT}^Δ is higher than $f_\Delta^T \phi_T^{CT}$ is that excitation at 353 and 355 nm gives both $^3M^*$ and singlet oxygen following dissociation of $^3(^3M^*..^1O_2^*)^2$ formed either as a result of direct absorption to this doubly excited complex or following internal conversion from the initially formed Franck–Condon charge transfer complex $^3(M^+..O_2^-)_{FC}^*$. In the case of acetonitrile and cyclohexane, respectively, this would require a quantum yield of 0·16 and 0·08 for this process in these two solvents. The fact that several organic compounds, which have energy gaps between their lowest singlet and triplet states greater than 94 kJ mol^{-1} give singlet oxygen yields greater than one (Tsubomura and Mulliken 1960; Saltiel and Atwater 1988; Kanner and Foote 1992) when excited into their lowest singlet excited states, demonstrates that this doubly excited state dissociates to give both the triplet state and singlet oxygen when it is populated in the case of many other compounds.

4. Conclusions

We have shown how fluorescence quenching measurements combined with singlet oxygen yield measurements can be used to obtain values of f_Δ^S and f_Δ^T, the fractions of singlet oxygen formed for oxygen quenching of excited singlet and excited triplet states, respectively. The values of f_Δ^S for anthracene and 9,10-dicyanoanthracene are 0 and 0·95 ± 0·05 respectively. Unfortunately there are very few f_Δ^S values in the literature (see Saltiel and Atwater 1988 and Wilkinson *et al* 1993 and references therein). Thus it is difficult at present to speculate on the reasons for observed variations in f_Δ^S. By contrast, many authors have obtained values for f_Δ^T, and recent measurements by ourselves (McGarvey *et al* 1992) have indicated the important role charge transfer interactions play in increasing the probability of quenching by pathways which do not lead to energy transfer. We have used picosecond pump probe techniques following exclusive direct excitation of charge transfer complexes of 1-ethylnaphthalene O_2 complexes to probe the fate of excited charge transfer complexes. We observe a prompt production of the triplet state is less than 5 picoseconds. We have shown that the quantum yields of prompt triplet states produced are 0·4 and 0·8 in acetonitrile and cyclohexane, respectively, i.e. we have shown that the value is strongly dependent on the polarity of the solvent. The quantum yield of singlet oxygen production following charge transfer excitation is also solvent dependent: however, the values obtained for Φ_Δ^{CT} are 0·36 and 0·78 which are greater than one would expect on the basis of the measured triplet yields. We suggest that the excited charge transfer complex can dissociate to give both triplet and singlet oxygens immediately following excitation.

10   *F Wilkinson, D J McGarvey and Olea*   [handwritten: check place of publn.]

References

[handwritten: London]

Birks J B 1970 *Photophysics of aromatic molecules* (~~New York~~: Wiley-Interscience) chap 10, and references
     therein. p. 492
Dijkgraaf C and Hoijtink G J 1963 *Tetrahedron Suppl.* 2 19 179
Evans D F 1957 *J. Chem. Soc.* 1351
Garner A and Wilkinson F 1976 *Singlet oxygen, reactions with organic compounds and polymers* (eds)
     B Ranby and J F Rabek (New York: John Wiley & Sons) p. 48
Gijzeman O L J, Kaufman F and Porter G 1973 *J. Chem. Soc., Faraday Trans.* 2 69 708
Gorman A A, Hamblett I, Lambert C, Prescott A L, Rodgers M A J and Spence H M 1987 *J. Am. Chem.*
     Soc. 109 3091
Gorman A A, Krasnovsky A A and Rodgers M A J 1991 *J. Phys. Chem.* 95 598
Horrocks A R and Wilkinson F 1968 ~~Faraday~~ *Proc. R. Soc.* A306 257
Kanner R C and Foote C S 1992 *J. Am. Chem. Soc.* 114 678
Kristiansen M, Scurlock R D, Iu K-K and Ogilby P R 1991 *J. Phys. Chem.* 95 5190
Liu A, Sauer Jr M C, Loffredo D M and Trifunac A D 1992 *J. Photochem. Photobiol.* A67 197
Masuhara H, Miyasaka H, Ikeda N, and Mataga N 1981 *Chem. Phys. Lett.* 82 59
McGarvey D J, Szekeres P G and Wilkinson F 1992 *Chem. Phys. Lett.* ~~(in press)~~ 199, 314. [handwritten: pl. give compltd details]
McLean A J, McGarvey D J, Truscott T G, Lambert C and Land E J 1990 *J. Chem. Soc., Faraday Trans.*
     86 3075
Miyasaka H, Masuhara H and Mataga N 1985 *J. Phys. Chem.* 89 1631
Murov S L 1973 *Handbook of photochemistry* (New York: Marcel Dekker)
Potashnik et al 1971
Redmond R W and Braslavsky S E 1988a *Chem. Phys. Lett.* 148 523
Redmond R W and Braslavsky S E 1988b *Photosensitisation; NATO ASI Series* (eds) G Moreno, R H Pottier
     and T G Truscott (Heidelberg: Springer-Verlag) vol. H15, p. 93
Saltiel J and Atwater B W 1988 *Adv. Photochem.* 14 1
Tsubomura H and Mulliken R S 1960 *J. Am. Chem. Soc.* 82 5966
Utsunomiya C, Kobayashi T and Nagakura S 1975 *Bull. Chem. Soc. Jpn.* 48 1852
Ware W R 1962 *J. Phys. Chem.* 66 455
Wilkinson F, Helman W P and Ross A B 1993 *J. Phys. Chem. Ref. Data* ~~22 414~~ 22, 113

[handwritten annotations:]

Rehm D and Weller A 1970 Z. Phys. Chem. 69, 183.

~~Foster et al 1973~~

pl. give details incl: name + initials of all authors

Potashnik R, Goldschmidt C.R and Ottolenghi M 1971
                    Chem. Phys. Lett. 9, 404.

Excited Triplet State Interactions with Molecular Oxygen: Influence of Charge Transfer on the Bimolecular Quenching Rate Constants and the Yields of Singlet Oxygen, (O$_2^{*}$,$^1\Delta_g$) for Substituted Naphthalenes in Various Solvents.

D J McGarvey[*], A F Olea[†] and F Wilkinson

Department of Chemistry, Loughborough University of Technology, Loughborough, Leicestershire, LE11 3TU, UK

ABSTRACT

The bimolecular rate constants ,$k_{O_2}^T$, for oxygen (O$_2$($^3\Sigma_g^-$)) quenching and the efficiencies ,f_Δ^T, with which singlet oxygen (O$_2^{*}$($^1\Delta_g$)) is thereby produced are reported for a range of substituted naphthalene triplet states in acetonitrile, benzene and cyclohexane. The magnitudes of $k_{O_2}^T$ and f_Δ^T are inversely correlated and both parameters exhibit pronounced sensitivity to the oxidation potential (E_M^{OX}) of the naphthalene derivative and some dependence on the solvent. Since within the range of naphthalenes studied the triplet state energy (E$_T$) remains largely constant and the molecules are structurally similar the dominant variable is the free energy change (ΔG^{CT}) for charge transfer to molecular oxygen. It is demonstrated that the large variations observed in $k_{O_2}^T$ and f_Δ^T depend on the energy of the substituted naphthalene/molecular oxygen charge transfer (CT) states, ^{1,3}(M^{*+}..O$_2^{*-}$). In acetonitrile, for example, the respective magnitudes of $k_{O_2}^T$ and f_Δ^T are 7.2 x 10^9 dm^3 mol^{-1} s^{-1} and 0.33 for 1-methoxynaphthalene compared with 1.4 x 10^9 dm^3 mol^{-1} s^{-1} and 0.74 for 1-cyanonaphthalene. In the non-polar solvent cyclohexane, the CT state energy levels are raised (by ~14 kJ mol^{-1}) relative to the energy levels in acetonitrile and benzene and this is reflected in decreased oxygen quenching rate constants (1-3 x 10^9 dm^3 mol^{-1} s^{-1}) and increased efficiencies of singlet oxygen production (0.56-1.0), particularly for those naphthalenes which contain electron donating substituents. In all three solvents the $k_{O_2}^T$ and f_Δ^T values for naphthalenes containing strong electron-withdrawing substituents (e.g. - CN, -NO$_2$) remain largely constant. In order to account for the observed data it is necessary to invoke a potential barrier ($\Delta G^\ddagger$) to charge transfer formation or the formation of exciplexes with significant CT character in the quenching step.

*Present Address: Department of Chemistry, University of Keele, Newcastle, Staffordshire, ST5 5BG, UK † On leave from Departamento de Quimica, Facultad de Ciencias, Universidad de Chile, Santiago, Chile

We have recently shown that for a series of substituted naphthalenes in benzene the efficiency of singlet oxygen production during oxygen quenching of triplet states (f_Δ^T) increases with the oxidation potential (E_M^{OX}) of the naphthalene derivative (9). In addition, we demonstrated that $k_{O_2}^T$ exhibits an inverse correlation with the oxidation potential of the naphthalene derivative being quenched which is evidence for the participation of CT interactions within excited state - O_2 complexes formed during the quenching process. We have also measured recently (12) the efficiencies of singlet oxygen production during quenching of both the first excited singlet and triplet states (f_Δ^S and f_Δ^T respectively) of a range of substituted anthracenes in cyclohexane. In contrast to the situation for naphthalene derivatives , anthracene derivatives have efficiencies of singlet oxygen production from the triplet state, f_Δ^T, all equal to unity, while the efficiency of singlet oxygen production from the first excited singlet state, f_Δ^S , varies from zero for anthracene to unity for 9,10-dicyanoanthracene. In that work it was established that the magnitude of f_Δ^S is determined by the same factors which govern intersystem crossing yields for anthracene derivatives, i.e., the activation energy for intersystem crossing to higher triplet states, and does not depend critically on CT interactions.

In contrast to many previous investigations of triplet state quenching by oxygen our recent work (9) is characterised by the selective variation of one molecular parameter (so far as this is possible) in order to determine the influence of that parameter on the magnitudes of $k_{O_2}^T$ and f_Δ^T. In this paper we extend this approach to a range of substituted naphthalenes in acetonitrile, benzene and cyclohexane in an attempt to further enhance understanding of solvent effects on oxygen quenching. The marked variations in $k_{O_2}^T$ and f_Δ^T which we observe are interpreted as being due to variations in the energies of the CT states, $^{1,3}(M^+..O_2^-)$, in these different solvents brought about mainly by varying the nature of the substituents on the naphthalene ring.

EXPERIMENTAL

Materials

Phenazine (Pz), acridine, 2-bromonaphthalene, 1-nitronaphthalene and 2-methoxynaphthalene (Aldrich) were recrystallised from ethanol; biphenyl (Aldrich, 99%) was sublimed; 1-methyl-naphthalene, 1-methoxynaphthalene and 1-bromonaphthalene were purified by repeated vacuum distillation; naphthalene (N) (Aldrich scintillation grade, Gold Label), 1-ethylnaphthalene (Fluka,

99%), benzophenone (BP) (Aldrich, Gold Label) and p-methoxyacetophenone (pMAP) (Aldrich, 99%) were used as received; acenaphthene, 2-methylnaphthalene, 2-ethylnaphthalene, 1-fluoro-naphthalene, 1-chloronaphthalene and i-cyanonaphthalene (Aldrich) were used as received; tetraphenylporphyrin (TPP) was a gift from C. Tanielian. Acetonitrile (Aldrich, spectrophotometric grade) was dried by refluxing over calcium hydride; benzene (Aldrich spectrophotometric grade), cyclohexane (Aldrich spectrophotometric and anhydrous grades) and carbon tetrachloride (Aldrich spectrophotometric grade) were used as received.

Instrumentation

Kinetic absorption measurements were carried out using the third harmonic (355 nm) of a JK system 2000 Q-switched Nd:YAG laser (25 ns, 25 mJ pulse^{-1}) as described elsewhere (24). For singlet oxygen luminescence measurements the third harmonic of a lumonics HY200 Q-switched Nd:YAG laser (8 ns, 15 mJ pulse^{-1}) was employed as the excitation source. Time-resolved singlet oxygen luminescence (1270 nm) was detected using a Judson germanium photodiode (J16-85P-RO5M)-amplifier combination as described previously (10). Steady state absorption measurements were made on a Phillips PU8800 spectrophotometer. Triplet state energies (E_T) were determined by employing the oxygen perturbation method developed by Evans (25). Briefly, a solution of the substituted naphthalene (~0.1 mol dm^{-3}) in carbon tetrachloride was exposed to a high pressure of oxygen (~80 atmospheres) in a stainless steel cell with fused silica windows (path length ~ 5 cm). Following vigorous agitation the absorption spectrum was recorded and the triplet state energy evaluated from the position of the (0,0) band.

Methods

(i)   *Singlet Oxygen Quantum Yield Measurements*

The procedure for determination of singlet oxygen yields was as follows. Air-equilibrated solutions of the substituted naphthalenes (0.05-0.1 mol dm^{-3}) each containing an aromatic ketone sensitiser, were optically matched (± 0.01 absorbance units) at the laser excitation wavelength to a standard reference solution for which the singlet oxygen yield is published (vide infra). Solutions were prepared in 1 cm square quartz cells with absorbances at 355 nm of ~0.5. This procedure eliminates the requirement to apply corrections for differential fractional absorption of the exciting light. The concentrations of the substituted naphthalenes in these solutions are not high enough to significantly

4.

influence the refractive index of the solvent and therefore it was not necessary to apply any refractive index correction factor (20).

The use of aromatic ketones as sensitisers for the substituted naphthalene triplet states derives from the method used previously by ourselves (26) and by Gorman et al (27) in which the naphthalene (N) triplet state is populated with unit efficiency by energy transfer from the aromatic ketone (K) triplet state, viz.,

$$^1K^* \rightarrow {}^3K^* \; (\phi_T = 1) \xrightarrow{N} {}^3N^* \; (100\%) \xrightarrow{O_2} O_2^*(^1\Delta_g) \qquad (1)$$
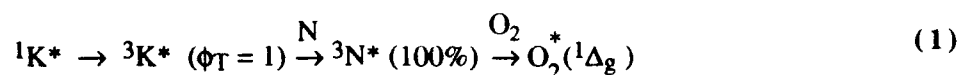
The singlet oxygen yield (ϕ_Δ) arising from triplet state quenching is given by equation (2).

$$\phi_\Delta = \phi_T \, P_T^{O_2} f_\Delta^T \qquad (2)$$

where ϕ_T is the quantum yield of triplet state production of the molecule of interest under the conditions of the experiment, $P_T^{O_2}$ is the fraction of triplet states quenched by oxygen and f_Δ^T is the fraction of these triplet states quenched by oxygen which yield $O_2^*(^1\Delta_g)$. Since the method we employ results in $\phi_T = 1$ (with one exception) and also for all the naphthalene derivatives studied $P_T^{O_2} = 1$, then $\phi_\Delta = f_\Delta^T$. In the case of 1-nitronaphthalene, which absorbs strongly at 355 nm, direct excitation of optically matched solutions was employed which yielded a measurement of ϕ_Δ and not f_Δ^T. Since nitronaphthalenes are non-fluorescent, it is likely that their singlet lifetimes are so short that no excited singlet states are intercepted by oxygen under our experimental conditions. Thus to determine a value of f_Δ^T for 1-nitronaphthalene we used equation (2) (with $P_T^{O_2} = 1$) and the published value (28) of ϕ_T (= 0.63) which we assumed to be solvent independent.

For the other naphthalene derivatives, which were all sensitised using aromatic ketones, we assumed energy transfer from the triplet ketone to be 100% efficient. Support for this assertion is given in references 29a and 29b. To further support this assumption we monitored the triplet absorption of 1-methoxynaphthalene, at 440 nm, in degassed acetonitrile at low laser intensities (< 5 mJ pulse^{-1}) in the following optically matched solutions: (a) benzophenone/0.1 mol dm^{-3} 1-methoxynaphthalene, (b) benzophenone/0.1 mol dm^{-3} biphenyl/10^{-3} mol dm^{-3} 1-methoxy-naphthalene. For these two

solutions plots of 1-methoxynaphthalene triplet absorbance at 440 nm versus laser intensity were constructed and found to have equal slopes to within experimental error (5%). In solution (b) the yield of triplet 1-methoxynaphthalene produced equals the product of the efficiency of energy transfer from the ketone triplet to the triplet state of biphenyl multiplied by the efficiency of energy transfer from triplet biphenyl to the triplet state of 1-methoxynaphthalene. Thus since introducing the biphenyl as an intermediate in the transfer of energy from triplet benzophenone to 1-methoxynaphthalene has no effect on the amount of triplet 1-methoxynaphthalene produced, this strongly suggests the efficiency of energy transfer from the ketone triplet is 100% to both biphenyl and 1-methoxynaphthalene.

In the determination of f_Δ^T values the time resolved 1270 nm luminescence signal was recorded following 355 nm laser excitation of each solution at variable laser intensities. At each laser intensity the recorded luminescence trace was obtained by signal averaging ten single shot traces. For each solution the averaged luminescence traces at different laser intensities were fitted using a single exponential function in order to extract the initial luminescence intensity (I_0) at time t = 0. Plots of I_0 versus laser intensity were observed to be linear up to incident laser intensities of 0.5 mJ pulse^{-1}. Within this laser intensity range 15-20 data points were obtained for each plot. The slopes of the I_0 versus laser intensity plots are proportional to f_Δ^T (or ϕ_Δ in the case of one of the samples) and thus f_Δ^T (or ϕ_Δ) values may be obtained by comparison with the slope obtained for the reference standard. For each compound at least three separate determinations of f_Δ^T were carried out. The mean singlet oxygen lifetimes (τ_Δ) of 80 μs in acetonitrile, 31 μs in benzene, and 24 μs in cyclohexane, which we observed are in good agreement with previous measurements in the literature (20, 30). However, in acetonitrile we noticed that the singlet oxygen lifetime is reduced to ~ 30 μs in the presence of 0.1 mol dm^{-3} 1-methoxynaphthalene. This suggests a rate constant of 2.1 x 10^5 dm^3 mol^{-1} s^{-1} for the quenching of $O_2^*(^1\Delta_g)$ by 1-methoxynaphthalene in acetonitrile. The other naphthalenes are less efficient singlet oxygen quenchers in this solvent since the ability to quench appears to depend on E_M^{OX}. The standards which we have employed for the three solvents used are as follows:- (a) acetonitrile:- acridine in air-equilibriated acetonitrile for which ϕ_Δ = 0.82 (31),

(b) benzene:- naphthalene (0.1 mol dm^{-3}) in air-equilibriated benzene containing benzophenone for which $\phi_\Delta = f_\Delta^T(N)$ = 0.62 (9, 18), and (c) cyclohexane:- naphthalene (0.1 mol dm^{-3}) in air-equilibriated cyclohexane containing p-methoxyacetophenone for which $\phi_\Delta = f_\Delta^T(N)$ = 0.92 (32).

6.

Some comments regarding the choice of these particular standards are given in the 'Results and Discussion' section of this paper.

(ii) Oxygen Quenching Rate Constant $(k_{O_2}^T)$ Measurements

The rate constants $(k_{O_2}^T)$ for oxygen quenching of the triplet states of substituted naphthalenes were determined by kinetic absorption measurements on air-equilibrated solutions. The intrinsic first-order triplet decay rate constant (k_1) is small compared with the pseudo first-order oxygen quenching rate constant $(k_2 = k_{O_2}^T[O_2])$ for the molecules studied and so decay of the triplet states in the presence of oxygen by routes other than by oxygen quenching may be neglected. Ten single-shot kinetic absorption traces were signal-averaged for each measurement and excellent single-exponential fits were obtained for all the triplet state decays in air-equilibriated solvents. The oxygen concentrations in air-equilibriated solvents were taken to be 1.9×10^{-3} mol dm^{-3} in acetonitrile, 1.9×10^{-3} mol dm^{-3} in benzene and 2.4×10^{-3} mol dm^{-3} in cyclohexane (22).

RESULTS AND DISCUSSION

The measured f_Δ^T and $k_{O_2}^T$ values for the substituted naphthalenes in acetonitrile are collected in Table 1 together with the triplet state energies (E_T), the half-wave oxidation potentials (E_M^{OX}) and the free energy change, ΔG^{CT}, for charge transfer from the substituted naphthalene triplet state to $O_2(^3\Sigma_g^-)$. Table 2 lists analogous $k_{O_2}^T$ and f_Δ^T data for benzene and cyclohexane as solvents.

(i) Singlet Oxygen Yield Measurements

We have previously justified the use of $f_\Delta^T = 0.62$ for naphthalene in benzene (9) based on an average of published values. Furthermore, this value is equal to the reference value recommended by one of us in a recent compilation, on the basis of a self consistent fit of all absolute and relative data (33 ratios) concerning f_Δ^T and ϕ_Δ values in benzene published up to the end of 1991 (18). Tables 1 and 2 include for comparison f_Δ^T (or ϕ_Δ) measurements for other frequently employed reference sensitisers in each solvent. The reliability of our data is supported by the excellent agreement between our measurements and literature values for BP (0.35) (19), pMAP (0.27) (21), Pz (0.83) (19) and TPP (0.58) (33) in benzene. Some typical I_0 versus laser intensity plots used to determine f_Δ^T values in benzene are given in Figure 1A.
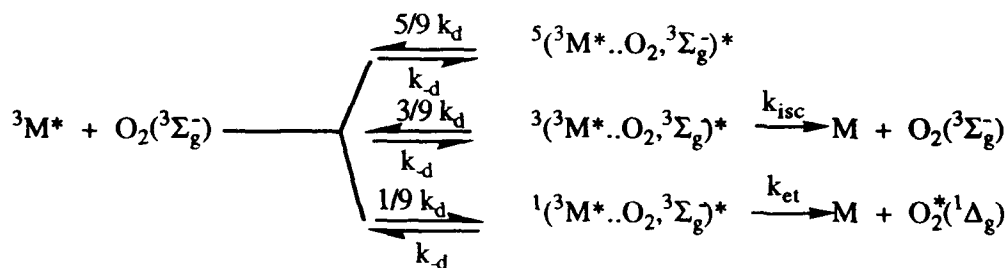
For f_Δ^T measurements in acetonitrile we have used as standard the thermal lensing measurement of ϕ_Δ for acridine ($= 0.82$) by Redmond and Braslavsky (31). Figure 1B shows some representative I_0 versus laser intensity plots for measurements in acetonitrile. Gorman et al (27) previously inferred that $f_\Delta^T = 1$ for naphthalene in acetonitrile which has been restated more recently by Logunov and Rodgers (11). Our data are inconsistent with an f_Δ^T value of unity for naphthalene in acetonitrile since we have measured (see Table 1) f_Δ^T values for six naphthalene derivatives which are substantially larger than that for naphthalene. In addition, our data shows that both phenazine and acridine produce more (>30% more) singlet oxygen in acetonitrile than naphthalene sensitised by an aromatic ketone in the same solvent. Furthermore, our f_Δ^T measurement for BP in acetonitrile of 0.38 is in excellent agreement with the value of 0.37 published by Chattopadhyay et al (21). Recent results by Kristiansen et al (20) who report the singlet oxygen yield of 1-methylnaphthalene in acetonitrile at infinite oxygen concentration (ϕ_Δ^∞) as 0.33 also suggests f_Δ^T is not unity for naphthalene in acetonitrile. However, it is not trivial to make comparisons with Kristiansen et al's data in acetonitrile since it is not known what contribution to ϕ_Δ^∞ derives from excited singlet state quenching (see references (12) and (18)) or what proportion ($f_T^{O_2}$) of 1-methylnaphthalene singlet states when quenched by oxygen yield the triplet state of 1-methylnaphthalene (18). It is important to note that, regardless of the absolute f_Δ^T values, our relative data for acetonitrile as solvent (Table 1) clearly demonstrates that for naphthalene in this solvent $f_\Delta^T < 1$.

In cyclohexane we have used as reference $f_\Delta^T = 0.92$ for naphthalene as determined by Gorman, Krasnovsky and Rodgers (32) using thermal lensing measurements. Some representative I_0 versus laser intensity plots are given in Figure 1C for measurements in cyclohexane. Despite this later measurement of $f_\Delta^T = 0.92$ for naphthalene, Logonov and Rodgers (11) take f_Δ^T for naphthalene in cyclohexane to be unity in accordance with earlier work by Gorman et al (27). Once more our data is inconsistent with this value being unity in that we have measured f_Δ^T values for five naphthalene derivatives in cyclohexane which exceed that for naphthalene. Furthermore, several of our f_Δ^T values based on $f_\Delta^T = 0.92$ for naphthalene slightly exceed unity (Table 2). However our data do suggest a genuine increase in f_Δ^T on changing the solvent from acetonitrile (or benzene) to cyclohexane. In addition if the singlet oxygen yield for phenazine (ϕ_Δ^{Pz}) is solvent independent as suggested recently by Logonov and Rodgers (11), it is clear from our data that f_Δ^T for naphthalene ($f_\Delta^T(N)$) in cyclohexane is greater than in acetonitrile or benzene since $f_\Delta^T(N)$ is very similar to ϕ_Δ^{Pz} in this solvent

8.

where $\phi_\Delta^{Pz}/f_\Delta^T(N) = 1.04$ but is relatively much smaller in both acetonitrile and benzene where $\phi_\Delta^{Pz}/f_\Delta^T(N) = 1.35 \pm 0.04$. If ϕ_Δ^{Pz} is indeed solvent independent then our data suggests that the f_Δ^T value of 0.92 for naphthalene may be a little high which is supported by the fact that some of our f_Δ^T values exceed unity based on this reference value. Using $\phi_\Delta^{Pz} = 0.85$ as a solvent independent value for phenazine results in f_Δ^T for naphthalene in cyclohexane being reduced to 0.81 which is marginally (0.01) outside the error limits quoted by Gorman, Krasnovsky and Rodgers (32) for their measurements. Extending this argument to the other naphthalenes results in the largest f_Δ^T value being 0.92 for 1-bromonaphthalene and the lowest being 0.5 for 1-methoxynaphthalene. In so far as the data are comparable our measurements are consistent with the data of Kristiansen et al (20) who quote a value of $\phi_\Delta^\infty = 0.77$ for 1-methylnaphthalene and 0.73 for biphenyl which compares favourably with our respective measurements (Table 2) of 0.84 (0.74 relative to $\phi_\Delta^{Pz} = 0.85$) and 0.86 (0.76 relative to $\phi_\Delta^{Pz} = 0.85$) assuming that $f_\Delta^S = 0$ and $f_T^{O_2} = 1$. Preliminary measurements by us suggests that these latter assumptions are valid for 1-methylnaphthalene in cyclohexane (34).

(ii) *Influence of CT on $k_{O_2}^T$ and f_Δ^T*

In 1973 Gijzeman, Kaufman and Porter (2, 3) rationalised the rate constants they had determined for oxygen quenching of aromatic triplet states in terms of spin-statistical weighting and restrictive Franck-Condon factors based on the mechanism in Scheme 1:

$$^3M^* + O_2(^3\Sigma_g^-) \underset{k_{-d}}{\overset{5/9\,k_d}{\rightleftharpoons}} \;^5(^3M^*..O_2,^3\Sigma_g^-)^*$$

$$^3M^* + O_2(^3\Sigma_g^-) \underset{k_{-d}}{\overset{3/9\,k_d}{\rightleftharpoons}} \;^3(^3M^*..O_2,^3\Sigma_g^-)^* \xrightarrow{k_{isc}} M + O_2(^3\Sigma_g^-)$$

$$^3M^* + O_2(^3\Sigma_g^-) \underset{k_{-d}}{\overset{1/9\,k_d}{\rightleftharpoons}} \;^1(^3M^*..O_2,^3\Sigma_g^-)^* \xrightarrow{k_{et}} M + O_2^*(^1\Delta_g)$$

Scheme 1

where M represents an aromatic hydrocarbon, k_d is the bimolecular diffusion controlled rate constant for the system, k_{-d} is the unimolecular rate constant for separation of the encounter pairs to original reactants and k_{isc} and k_{et} are the rate constants for catalysed enhanced intersystem crossing and for exchange energy transfer from the encounter complex formed between $^3M^*$ and $O_2(^3\Sigma_g^-)$ respectively.

9.

According to Scheme 1

$$k_{O_2}^T = (k_d/9)[k_{et}/(k_{et} + k_{-d})] + (3k_d/9)[k_{isc}/(k_{isc} + k_{-d})] \tag{3}$$

Gijzeman et al (2, 3) found that for aromatic hydrocarbons with relatively low triplet state energies ($E_T < 200$ kJ mol^{-1}) the observed oxygen quenching rate constants ($k_{O_2}^T$) in benzene, hexane and cyclohexane were approximately equal to $1/9\ k_d$ (cf equation (3)) implying exclusive quenching via the energy transfer channel (with $k_{et} \gg k_{-d}$ and $k_{isc} \ll k_{-d}$) to produce $O_2^*(^1\Delta_g$). Our recent measurements of $k_{O_2}^T$ and f_Δ^T for substituted anthracenes in cyclohexane are consistent with this conclusion (12). However, for aromatic hydrocarbons with high triplet energies the quenching rate constants were found to be less than $1/9\ k_d$ and exhibited an inverse dependence on the triplet energy. In addition, $k_{O_2}^T$ was observed to be sensitive to solvent polarity for aromatic hydrocarbons with high triplet energies which was attributed (2,3) to indirect involvement of CT states of similar energy to the encounter complexes depicted in Scheme 1. These authors (2,3) also stated that the relative importance of CT state participation during the quenching interaction would depend on the ionisation potential of the hydrocarbon (with a particular value of E_T) as well as the solvent polarity since both these parameters affect CT state energy levels. Our recent work is in good agreement with this argument in that we have found for a range of substituted anthracenes (low E_T) in cyclohexane that $k_{O_2}^T$ (and f_Δ^T) are not sensitive to the oxidation potential E_M^{OX} of the hydrocarbon (12) whereas for substituted naphthalenes (high E_T) in benzene (9), cyclohexane and acetonitrile (vide infra) $k_{O_2}^T$ (and f_Δ^T) values are profoundly sensitive to E_M^{OX}.

The effect of varying the nature of the substituent on the naphthalene ring is to influence E_M^{OX} and thereby ΔG^{CT}. A good estimate for the free energy change (ΔG^{CT}) to form ion-pairs from neutral molecules in benzene or acetonitrile, as shown by Rehm and Weller (35) and by ourselves (4, 36), is given by equation (4),

$$\Delta G^{CT} = F[E_M^{OX} - E_{O_2}^{red}] - E_T \tag{4}$$

where F is the Faraday constant and $E_{O_2}^{red}$ is the half-wave reduction potential for $O_2(^3\Sigma_g^-)$ taken to be -0.78 V versus SCE (37).

It is worth mentioning that equation (4) gives the relaxed CT state energy relative to the energy of the hydrocarbon triplet state. Several recent reports (7, 11, 20) refer to CT energy levels for naphthalene derivatives which are well above the energies obtained using equation (4), these estimates being based principally upon the energy of contact CT absorption (equation (5)) in concentrated hydrocarbon solutions containing oxygen. Charge transfer absorption may be represented as

$$M + O_2(^3\Sigma_g^-) \rightleftharpoons {}^3(M..O_2,^3\Sigma_g^-) \xrightarrow{h\nu_{CT}} {}^3(M^+..O_2^-)_{FC} \qquad (5)$$
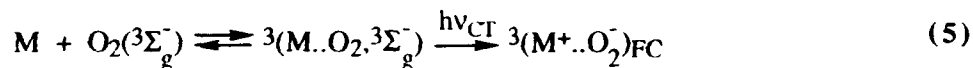
where $^3(M^+..O_2^-)_{FC}$ refers to the charge transfer state which is directly populated by absorption in the charge transfer band and is subject to the operation of the Franck-Condon principle. However, in accordance with Marcus (38) the spectroscopic CT energy ($h\nu^{CT}$) is given by equation (6),

$$h\nu^{CT} = \lambda + \Delta G^O \qquad (6)$$

where $\Delta G^O = E_T + \Delta G^{CT}$.

In order to estimate ΔG^{CT} from equation (4), for cyclohexane as solvent it is necessary to include an additional term, $\Delta\omega$ (39), which depends on Coulombic interactions and solvation energies. The magnitude of $\Delta\omega$ for encounter pairs is difficult to calculate but is likely to be constant for a series of structurally similar compounds. Knibbe, Rehm and Weller (39) have shown that $\Delta\omega = 14.5 \pm 1.5$ kJ mol^{-1} for sixty exciplexes in hexane and therefore we have used this value of $\Delta\omega$ in our estimate of ΔG^{CT} for cyclohexane. Thus the ΔG^{CT} values in Table 1 calculated using equation (4) are appropriate for the solvents benzene and acetonitrile while for cyclohexane the ΔG^{CT} values are more endoergonic by 14 kJ mol^{-1}. This means that for these substituted naphthalenes in the solvents used the magnitude of ΔG^{CT} varies by ~90 kJ mol^{-1} from -43 kJ mol^{-1} in the case of 1-methoxynaphthalene in acetonitrile or benzene to + 44 kJ mol^{-1} for 1-nitronaphthalene in cyclohexane. A schematic energy level diagram illustrating the range of CT state energies existing for the naphthalene deriviatives studied here is shown in Figure 2.

That the arguments of Gijzeman et al (2, 3) mentioned above are clearly borne out is best illustrated by reference to Figure 3 in which our $k_{O_2}^T$ data for substituted naphthalene triplet states in benzene

11.

(Table 2) is superimposed upon the $k_{O_2}^T$ values of Gijzeman et al for aromatic hydrocarbons in benzene. It is abundantly clear from Figure 3 that the participation of CT interactions has a strong influence upon $k_{O_2}^T$ since within the narrow E_T window of our measurements $k_{O_2}^T$ varies by approximately a factor of five from $\sim 10^9$ dm^3 mol^{-1} s^{-1} for naphthalenes with electron-withdrawing substituents and high oxidation potentials (eg -CN) to 5×10^9 dm^3 mol^{-1} s^{-1} ($\sim 2/9$ k_d) for 1-methoxynaphthalene which has the lowest value of E_M^{OX}. This dependence of $k_{O_2}^T$ on the nature of the substituent is also observed in acetonitrile and cyclohexane although in acetonitrile the range of $k_{O_2}^T$ values is larger (~ 1-7×10^9 dm^3 mol^{-1} s^{-1}) while in cyclohexane the range is considerably smaller (~ 1-3×10^9 dm^3 mol^{-1} s^{-1}).

In all three solvents it is apparent that $k_{O_2}^T$ exhibits an inverse dependence on ΔG^{CT}. In addition, it is clear from Tables 1 and 2 that f_Δ^T varies in the opposite manner and that f_Δ^T and $k_{O_2}^T$ are inversely correlated. The dependence of $k_{O_2}^T$ upon ΔG^{CT} is shown in Figure 4A where it can be seen that a non-linear free energy relationship exists which is preserved across the solvent boundaries and which is good evidence for the involvement of CT interactions in the quenching process. It may be argued that plotting data derived from three different solvents together is unjustified since the rate constant for diffusion (k_d) is solvent dependent. However, as shown below, attempts to allow for this makes little difference.

For excited state quenching by molecular oxygen the magnitude of k_d is often assumed to be equivalent to the rate constant for excited singlet state quenching ($k_{O_2}^S$) by $O_2(^3\Sigma_g^-)$. There exists ample evidence which suggests this assumption may be unjustified (see for example Murov et al (22) Kikuchi et al (13) and Olea et al (12)). In any case, the approximately constant value in all three solvents of $k_{O_2}^T$ for those substituted naphthalenes with high oxidation potentials suggests that k_d does not vary very much between these solvents. Darmanyan and Foote (14, 15) have recently quoted estimates of k_d derived from the oxygen quenching data of Ware (40) in various solvents including benzene (3×10^{10} dm^3 mol^{-1} s^{-1}), acetonitrile (3.7×10^{10} dm^3 mol^{-1} s^{-1}) and cyclohexane (3×10^{10} dm^3 mol^{-1} s^{-1}). Using these k_d values we have plotted $k_{O_2}^T/k_d$ against ΔG^{CT} in Figure 4B where it can be seen that the plot is not significantly different from that shown in Figure 4A. The curve passing through the data in figure 4B is an exponential fit according to equation (7):

12.

$$k_{O_2}^{T} \propto \exp - (\alpha \Delta G^{CT}) \tag{7}$$

where $-\alpha$ is the slope of a plot of $\ln k_{O_2}^{T}$ versus ΔG^{CT}. For total electron transfer quenching α would be expected to be equal to $1/RT$. However, for our data we find that α is substantially less then $1/RT$ ($\sim 0.25/RT$) which may be indicative of exciplex formation (37) with substantial but not complete charge transfer. Figure 5 shows the relationship between f_{Δ}^{T} and $k_{O_2}^{T}$ using the complete data from all three solvents. It is obvious from Figure 5 that there is a clear inverse correlation between $k_{O_2}^{T}$ and f_{Δ}^{T} which also is preserved across solvent boundaries.

It is interesting to note that in our recent work on anthracene derivatives in cyclohexane (12) we found $f_{\Delta}^{T} = 1$ and $k_{O_2}^{T}$ to be constant ($3.0 \pm 0.4 \times 10^9$ dm^3 mol^{-1} s^{-1}) for all the anthracene derivatives. A similar behaviour is observed here for those naphthalene derivatives in cyclohexane which have $f_{\Delta}^{T} \sim 1$ since for these compounds $k_{O_2}^{T}$ equals $1.3 \pm 0.2 \times 10^9$ dm^3 mol^{-1} s^{-1} i.e. $k_{O_2}^{T}$ is also constant but a factor of 2.3 smaller, which can be explained in terms of increasingly restrictive Franck-Condon factors for the naphthalene derivatives which have higher triplet energies.

The observed dependence of $k_{O_2}^{T}$ on ΔG^{CT} is entirely consistent with the participation of CT interactions within encounter complexes, $^{1,3}(M..O_2\ ^3\Sigma_g^-)^*$, formed during the quenching process. Whether complete electron transfer to form radical-ion pairs, $^{1,3}(M^+..O_2^-)$, or exciplex formation, $^{1,3}(M^{\delta+}..O_2^{\delta-})^*$, is involved in the quenching mechanism remains to be established and is likely to depend on solvent polarity, the nature of M and perhaps on the quenching channel (Scheme 1). It is clear from Scheme 1 and Figure 2 that energy transfer and electron transfer may operate through the singlet channel (O_2^*, $^1\Delta_g$ production) but for the other principal quenching channel (triplet channel) no possibility exists for electronic energy transfer due to spin conservation restrictions.

The net quenching rate constant ($k_{O_2}^{3}$) for the triplet channel in Scheme 1 is given by equation (8).
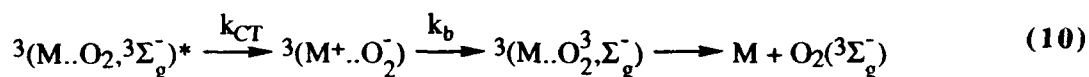
$$k_{O_2}^{3} = k_{O_2}^{T} (1 - f_{\Delta}^{T}) \tag{8}$$

In the limit when $f_{\Delta}^{T} = 1$, $k_{O_2}^{3} = 0$ so that for those molecules where f_{Δ}^{T} approaches unity (for ΔG^{CT} » 0, Table 2) quenching via the enhanced intersystem crossing channel is absent. Thus we may

assume that quenching via the triplet channel depends exlusively upon electron-transfer quenching and that non CT-mediated quenching may, for these molecules, be neglected. From Scheme 1 and equation (3) the following expression for $k_{O_2}^3$ is obtained.

$$k_{O_2}^3 = 3k_d\, k_{isc}/9(k_{-d} + k_{isc}) \qquad (9)$$

The electron transfer quenching may be visualised as proceeding according to equation (10)

$$^3(M..O_2,^3\Sigma_g^-)^* \xrightarrow{k_{CT}} {}^3(M^+..O_2^-) \xrightarrow{k_b} {}^3(M..O_2^3,\Sigma_g^-) \longrightarrow M + O_2(^3\Sigma_g^-) \qquad (10)$$

If the assumption is made that the primary electron-transfer step (k_{CT}) is irreversible and that the subsequent back electron transfer (k_b) to form ground state products is fast relative to k_{CT} then $k_{isc} = k_{CT}$. The rate constant k_{CT} may be expressed according to transition state theory by equation (11).

$$k_{CT} = Z \exp - (\Delta G^{\ddagger}/RT) \qquad (11)$$

where Z is the frequency factor and $\Delta G^{\ddagger}$ is the free energy of activation for electron transfer.

Substitution of equation (11) into (9) gives

$$k_{O_2}^3 = [\frac{3k_d}{k_dZ} \exp (\Delta G^{\ddagger}/RT) + \frac{9}{3k_d}]^{-1} \qquad (12)$$

which gives a limiting value of $k_{O_2}^3 = \frac{3}{9} k_d = 10^{10}$ dm^3 mol^{-1} s^{-1} when $k_{CT} = Ze\text{-}(\frac{\Delta G^{\ddagger}}{RT}) \gg k_{-d}$.

Various methods for estimation of $\Delta G^{\ddagger}$ exist of which the most widely used are by Marcus (41), see equation (13) and by Rehm and Weller (35). Due to the limited range of ΔG^{CT} values available in

$$\Delta G^{\ddagger} = \lambda/4(1 + \Delta G^{CT}/\lambda)^2 \qquad (13)$$

14.

this study we find that our data is satisfactorily described by any of the commonly used models for electron transfer. The dependence of $k_{O_2}^3$ on ΔG^{CT} predicted from equation (12) using the Marcus equation (equation (13)) to estimate $\Delta G^{\ddagger}$ with the solvent reorganisation energy term $(\lambda) = 78$ kJ mol^{-1}, and taking $Z = 10^{11}$ s^{-1} and $k_{-d}/k_d = 1$ mol dm^{-3} is shown as the curve passing through the data in Figure 6.

Our data suggest that changing the solvent from polar (acetonitrile) or polarisable (benzene) to non-polar (cyclohexane) influences ΔG^{CT} for each of the substituted naphthalenes studied by 14.5 kJ mol^{-1} since this adjustment makes the quenching rates observed in cyclohexane at a particular ΔG^{CT} equivalent to the quenching rates observed in benzene and acetonitrile at the same ΔG^{CT} (see Figure 4).

The main effect of the participation of charge transfer interactions is to render the catalytic enhanced intersystem crossing channel of scheme 1 more competitive resulting, for these molecules, in an increase in $k_{O_2}^T$ and a decrease in f_{Δ}^T. This result contrasts with our recent study (12) of $O_2^*(^1\Delta_g)$ formation from the triplet states of anthracene derivatives (low E_T) in cyclohexane for which we found f_{Δ}^T, and $k_{O_2}^T$ to be independent of ΔG^{CT}. However, in the case of all these anthracene derivatives $\Delta G^{CT} > 0$ because of the low E_T values. Thus both these studies are in agreement with the original suggestion by Gijzeman et al (2, 3) that CT interactions are more important for molecules with high triplet energies.

CONCLUSIONS

The efficiency of singlet oxygen $O_2^*(^1\Delta_g)$ formation, f_{Δ}^T, and $k_{O_2}^T$, the rate constant for triplet state quenching by $O_2(^3\Sigma_g^-)$, have been measured for a range of substituted naphthalenes in acetonitrile, benzene and cyclohexane. An inverse correlation between $k_{O_2}^T$ and f_{Δ}^T exists which is almost independent of solvent (Figure 5). Both $k_{O_2}^T$ and f_{Δ}^T are strongly dependent on ΔG^{CT}, the free energy change for charge transfer state formation from the triplet state of the substituted naphthalene to $O_2(^3\Sigma_g^-)$, which is evidence for the participation of charge transfer interactions during the quenching. The data is consistent with quenching showing a free energy of activation $\Delta G^{\ddagger}$ for the formation of the charge transfer state during quenching or for the formation of exciplexes in which there is substantial charge transfer character. Finally our f_{Δ}^T measurements in acetonitrile and cyclohexane show clearly that f_{Δ}^T for naphthalene in these two solvents as in the case of the solvent benzene is less than unity.

ACKNOWLEDGEMENTS

Table 1

Photophysical Properties of Substituted Naphthalenes in Acetonitrile.

Sensitiser	f_Δ^T(a)	$k_{O_2}^T$(b) $(10^9 \, dm^3 \, mol^{-1} s^{-1})$	E_T(c) $(kJ \, mol^{-1})$	E_M^{OX}(d) (V vs SCE)	ΔG^{CT}(e) $(kJ \, mol^{-1})$
1-Methoxynaphthalene	0.33	7.2	251[h]	1.38	-43
Acenaphthene	0.41	6.5	248	1.41	-37
2-Methoxynaphthalene	0.44	5.3	260[h]	1.52	-38
1-Methylnaphthalene	0.60	3.2	249	1.54	-25
1-Ethylnaphthalene	0.56	3.3	250[h]	-	-
2-Methylnaphthalene	0.61	3.1	254	1.52	-32
2-Ethylnaphthalene	0.61	3.3	-	-	-
Naphthalene	0.62	2.6 [2.7(8)]	255	1.63	-22
2-Bromonaphthalene	0.68	1.8	252	1.90	+7
1-Fluoronaphthalene	0.71	2.2	251	-	-
1-Bromonaphthalene	0.77	1.8	247	1.85	+7
1-Chloronaphthalene	0.74	1.9	248	-	-
1-Cyanonaphthalene	0.74	1.4	241	1.95[j]	+22
1-Nitronaphthalene	0.89[f]	1.5	231	1.92	+30
Benzophenone	0.38	3.0 [2.3(21)]	287	-	-
Phenazine	0.86[g]	-	186[i]	-	-
Acridine	0.82[g]	-	189[i]	-	-

(a)   Relative to Φ_Δ (acridine) = 0.82 (31), error ± 10%

(b)   Error ± 15% (values in square brackets are literature values).

(c)   From reference 22 unless stated otherwise.

(d)   From reference 42 unless stated otherwise.

(e)   Calculated using equation 4, error ± 10 kJ mol⁻¹.

(f)   Calculated assuming an intersystem crossing yield of 0.63 (28).

(g)   Number refers to ϕ_Δ and not f_Δ^T.

(h)   Determined using oxygen-perturbation in CCl_4 (see text).

(i)   From reference 19.

(j)   Calculated from the ionisation potential (43) using an average value obtained from the equations of Pysh and Yang (44) and Neikam et al (45).

Table 2

Photophysical Properties of Substituted Naphthalenes in Benzene and Cyclohexane

Sensitser	Cyclohexane		Benzene	
	f_Δ^T(a)	$k_{O_2}^T$(b) $(10^9 \, dm^3 \, mol^{-1}s^{-1})$	f_Δ^T(c)	$k_{O_2}^T$(b) $(10^9 \, dm^3 \, mol^{-1}s^{-1})$
1-Methoxynaphthalene	0.56	3.4	0.34	5.0
Acenaphthene	0.61	2.9	0.40	4.4
2-Methoxynaphthalene	0.80	2.4	0.50	3.5
1-Methylnaphthalene	0.84	1.8	0.56	2.6
1-Ethylnaphthalene	0.86	1.8	0.57	2.6
2-Methylnaphthalene	0.91	1.8	0.57	2.5
2-Ethylnaphthalene	0.88	1.8	0.59	2.5
Naphthalene	0.92	1.4	0.62	2.1 [2.2(46)]
2-Bromonaphthalene	0.94	1.2	0.66	1.5
1-Fluoronaphthalene	0.94	1.4	0.68	1.9
1-Bromonaphthalene	1.04	1.2	0.73	1.5
1-Chloronaphthalene	1.01	1.3	0.75	1.6
1-Cyanonaphthalene	1.03	1.1	0.75	1.2
1-Nitronaphthalene	0.91[d]	1.5	0.83[d]	1.3
Phenazine	0.96[e]	-	0.82[e]	2.0 [2.0(19)]
Biphenyl	0.86	0.9	-	-
Benzophenone	-	-	0.33	2.5[2.3(21)]
pMAP	-	-	0.25	6.3[6.0(21)]
TPP	-	-	0.58[e]	-

(a)   Relative to f_Δ^T (naphthalene) = 0.92 (32), error ± 10%

(b)   Error ± 15% (values in square brackets are literature values).

(c)   Relative to f_Δ^T (naphthalene) = 0.62 (9, 18), error ± 10%.

(d)   Calculated assuming an intersystem crossing yield of 0.63 (28).

(e)   Number refers to Φ_Δ and not f_Δ^T.

18.

REFERENCES

1. Birks, J.B., Photophysics of Aromatic Molecules; Wiley-Interscience, London, 1970; chapter 10 (pp 492-517) and references therein.

2. Gijzeman, O.L.J.; Kaufman, F.; Porter, G. *J. Chem. Soc., Faraday Trans. 2.* 1973, **69**, 708.

3. Gijzeman, O.L.J.; Kaufman, F. *J. Chem. Soc., Faraday Trans. 2.* 1973, **69**, 721.

4. Garner, A.; Wilkinson, F. *Chem. Phys. Lett.* 1977, **45**, 432.

5. Saltiel, J.; Atwater, B.W. *Advan. Photochem.* 1988, **14**, 1.

6. McLean, A.J.; McGarvey, D.J.; Truscott, T.G.; Lambert, C.R.; Land, E.J. *J. Chem. Soc., Faraday Trans.* 1990, **86**, 3075.

7. Ogilby, P.R.; Sanetra, J. *J. Phys. Chem.* 1993, **97**, 4689.

8. McLean, A.J.; Rodgers, M.A.J. *J. Am. Chem. Soc.* 1993, **115**, 4786.

9. McGarvey, D.J.; Szekeres, P.G.; Wilkinson, F. *Chem. Phys. Lett.* 1992, **199**, 314.

10. McGarvey, D.J.; Wilkinson, F.; Worrall, D.R.; Hobley, J.; Shaikh, W. *Chem. Phys. Lett.* 1993, **202**, 528.

11. Logunov, S.L.; Rodgers, M.A.J. *J. Phys. Chem.* 1993, **97**, 5643.

12. Olea, A.F.; McGarvey, D.J.; Wilkinson, F. *J. Amer. Chem. Soc.*, in press.

13. Kikuchi, K.; Sato, C.; Watabe, M.; Ikedo, H.; Takahashi, Y.; Miyashi, T. *J. Amer. Chem. Soc.* 1993, **115**, 5180.

14. Darmanyan, A.P.; Foote, C.S. *J. Phys. Chem.* 1993, **97**, 4573.

15. Darmanyan, A.P.; Foote, C.S. *J. Phys. Chem.* 1993, **97**, 5032.

16. Krasnovsky, A.A.; Foote, C.S. *J. Amer. Chem. Soc.* 1993, **115**, 6013.

17. Usui, Y.; Shimizu, N.; Mori, S. *Bull. Chem. Soc. J.* 1992, **65**, 897.

18. Wilkinson, F.; Helman, W.P.; Ross, A.B. *J. Phys. Chem. Ref. Data,* 1993, **22**, 113.

19. Redmond, R.W.; Braslavsky, S.E. *Chem. Phys. Lett.* 1988, **148**, 523.

20. Kristiansen, M.; Scurlock, R.D.; Iu, K-K.; Ogilby, P.R. *J. Phys. Chem.* 1991, **95**, 5190.

21. Chattopadhyay, S.K.; Kumor, C.V.; Das, P.K. *J. Photochem.* 1985, **30**, 81.

22. Murov, S.L.; Carmichael, I; Hug, G.L., Handbook of Photochemistry; Marcel Dekker, Inc., New York, 1993.

23. Darmanyan, A.P.; Arbogast, J.W.; Foote, C.S. *J. Phys. Chem.* 1991, **95**, 7308.

24. Wilkinson, F.; Worrall, D.R. ; McGarvey, D.J.; Goodwin, A.; Langley, A. *J. Chem. Soc., Faraday Trans.* 1993, **89**, 2385.

25. Evans, D.F. *J. Chem. Soc.* 1957, p 1351.

26. Garner, A.; Wilkinson, F. In Singlet Oxygen, Reactions with Organic Compounds and Polymers; Ranby, B.; Rabek, J.F., eds.; Wiley, New York, 1976; p 48.

27. Gorman, A.A.; Hamblett, I.; Lambert, C.; Prescott, A.L.; Rodgers, M.A.J.; Spence, H.M. *J. Amer. Chem. Soc.* 1987, **109**, 3091.

28. Hurley, R.; Testa, A.C. *J. Amer. Chem. Soc.* 1968, **90**, 1949.

29 (a) Land, E.J. *Proc. Roy. Soc.* 1968, **A305**, 457.

   (b) Carmichael, I.; Hug, G.L. *J. Phys. Chem. Ref. Data* , 1986, **15**, 1.

30. Gorman, A.A.; Rodgers, M.A.J. In Handbook of Organic Photochemistry, Vol. 2, Scaiano, J.C., Ed; CRC Press, Boca Raton, 1989, p 229.

31. Redmond, R.W.; Braslavsky, S.E. In Photosensitisation, NATO ASI Series, Vol H15; Moreno, G.; Pottier, R.H.; Truscott, T.G., Eds; Springer, Berlin, 1988; p 93.

32. Gorman, A.A.; Krasnovsky, A.A.; Rodgers, M.A.J. *J. Phys. Chem.* 1991, **95**, 598.

33. Rossbroich, G.; Garcia, N.A.; Braslavsky, S.E. *J. Photochem.* 1985, **31** 37.

34. Olea, A.F.; McGarvey, D.J.; Wilkinson, F. unpublished results (work in progress).

35. Rehm, D.; Weller, A. *Israel, J. Chem.* 1970, **8**, 259.

36. Wilkinson, F.; Tsiamis, C. *J. Amer. Chem. Soc.* 1983, **105**, 767.

37. Kavarnos, G.J.; Turro, N.J. *Chem. Rev.* 1986, **86**, 401.

38. Marcus, R.A. *Angev. Chem. Int.* Ed. Engl. 1993, **32**, 1111.

39. Knibbe, H.; Rehm, D.; Weller, A. *Ber. Bunsenges. Phys. Chem.* 1969, **73**, 839.

40. Ware, W.R. *J. Phys. Chem.* 1962, **66**, 455.

41. Marcus, R.A. *J. Chem. Phys.* 1957, **26**, 867.

42. Mann, C.K.; Barnes, K.K., Electrochemical Reactions in Nonaqueous Systems; Marcel Dekker, New York, 1970.

43. Utsunomiya, C; Kobayashi, T; Nagakura, S. *Bull. Chem. Soc. Jpn*, 1975, **48**, 1852.

44. Pysh, E.S.; Yang, N.C. *J. Amer. Chem. Soc.* 1963, **85**, 2124.

45. Neikam, W.C.; Dimeler, G.R.; Desmond, M.M. *J. Electrochem. Soc.* 1964, **111**, 1190.

46. Smith, G.J. *J. Chem. Soc. Faraday Trans. 2.* 1982, **78**, 769.

FIGURE CAPTIONS

Figure 1

Representative plots of $O_2^*(^1\Delta_g)$ luminscence intensity (I_o) versus laser intensity in

(A) benzene: $\square$ = phenazine, $\blacktriangle$ = benzophenone/1-cyanonaphthalene,

O = benzophenone/naphthalene, $\blacksquare$ = benzophenone/1-methoxynaphthalene,

(B) acetonitrile: $\square$ = acridine, $\blacktriangle$ = benzophenone/1-cyanonaphthalene,

O = benzophenone/naphthalene, $\blacksquare$ = benzophenone/1-methoxynaphthalene,

(C) cyclohexane: $\square$ = phenazine, $\blacktriangle$ = p-methoxyacetophenone/1-cyanonaphthalene,

O = p-methoxyacetophenone/naphthalene, $\blacksquare$ = p-methoxyacetophenone/1-methoxynaphthalene.

Figure 2

Schematic electronic energy level diagram for substituted naphthalenes (M), molecular oxygen and

$(M..O_2)$ complexes. The band of $^{1,3}(M^+..O_2^-)$ energy levels (E_{CT}) indicates the range over which

E_{CT} may vary depending on the nature of the substituent on M and the solvent.

Figure 3

Dependence of the rate constant $(k_{O_2}^T)$ for oxygen quenching of aromatic hydrocarbon triplet states in

benzene versus the triplet state energy (E_T); $\square$ = $k_{O_2}^T$ data of Gijzeman et al (2), $\blacktriangle$ = $k_{O_2}^T$ data for

substituted naphthalenes in benzene (Table 2).

Figure 4

(A) Dependence of $k_{O_2}^T$ on the free energy change (ΔG^{CT}) for charge transfer from $^3M^*$ to $O_2(^3\Sigma_g^-)$;

$\square$ = $k_{O_2}^T$ data in acetonitrile (Table 1), $\blacktriangle$ = $k_{O_2}^T$ data in benzene (Table 2), O = $k_{O_2}^T$ data in

cyclohexane (Table 2),

(B) Dependence of $k_{O_2}^T/k_d$ on ΔG^{CT}, where k_d is the solvent dependent bimolecular rate constant at

the diffusion limit, $\square$ = $k_{O_2}^T$ data in acetonitrile (Table 1), $\blacktriangle$ = $k_{O_2}^T$ data in benzene (Table 2), $\bullet$ =

$k_{O_2}^T$ data in cyclohexane (Table 2). The values of k_d used are 3×10^{10} dm^3 mol^{-1} s^{-1} in both benzene

and cyclohexane and 3.7×10^{10} dm^3 mol^{-1} s^{-1} in acetonitrile. The curve passing through the data is

as predicted by theory, see text.

Figure 5

Dependence of the efficiency of $O_2^*(^1\Delta_g)$ production (f_Δ^T) during oxygen quenching of substituted naphthalene triplet states versus $k_{O_2}^T$ in benzene (▲), acetonitrile (□) and cyclohexane (O).
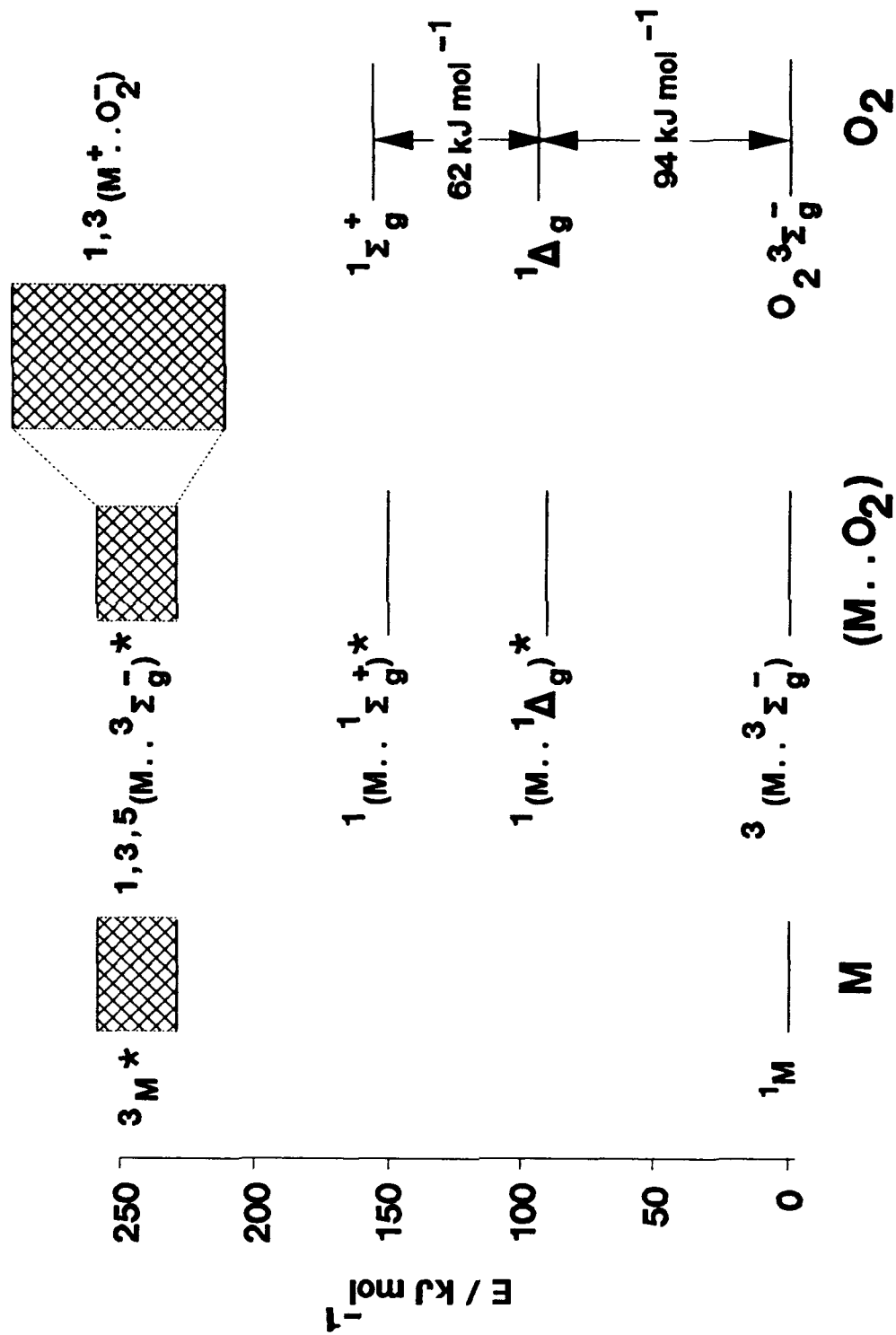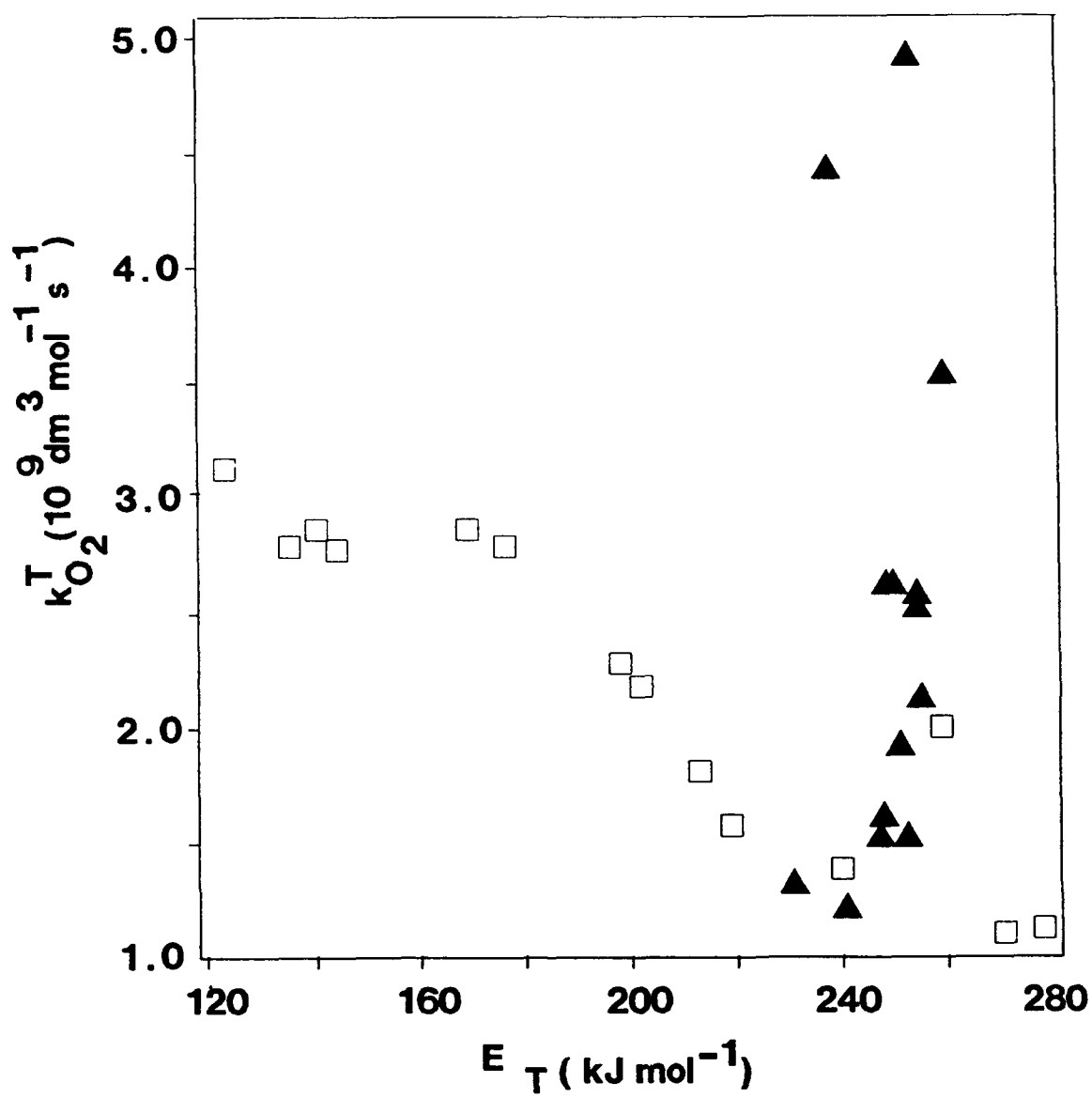
Figure 6

Dependence of the rate constant ($k_{O_2}^3$) for enhanced intersystem crossing on ΔG^{CT}. The $k_{O_2}^3$ data was evaluated using equation (8). The curve passing through the data is the predicted dependence of $k_{O_2}^3$ on ΔG^{CT} from equations (12) and (13) with $\lambda = 78$ kJ mol^{-1}, see text.
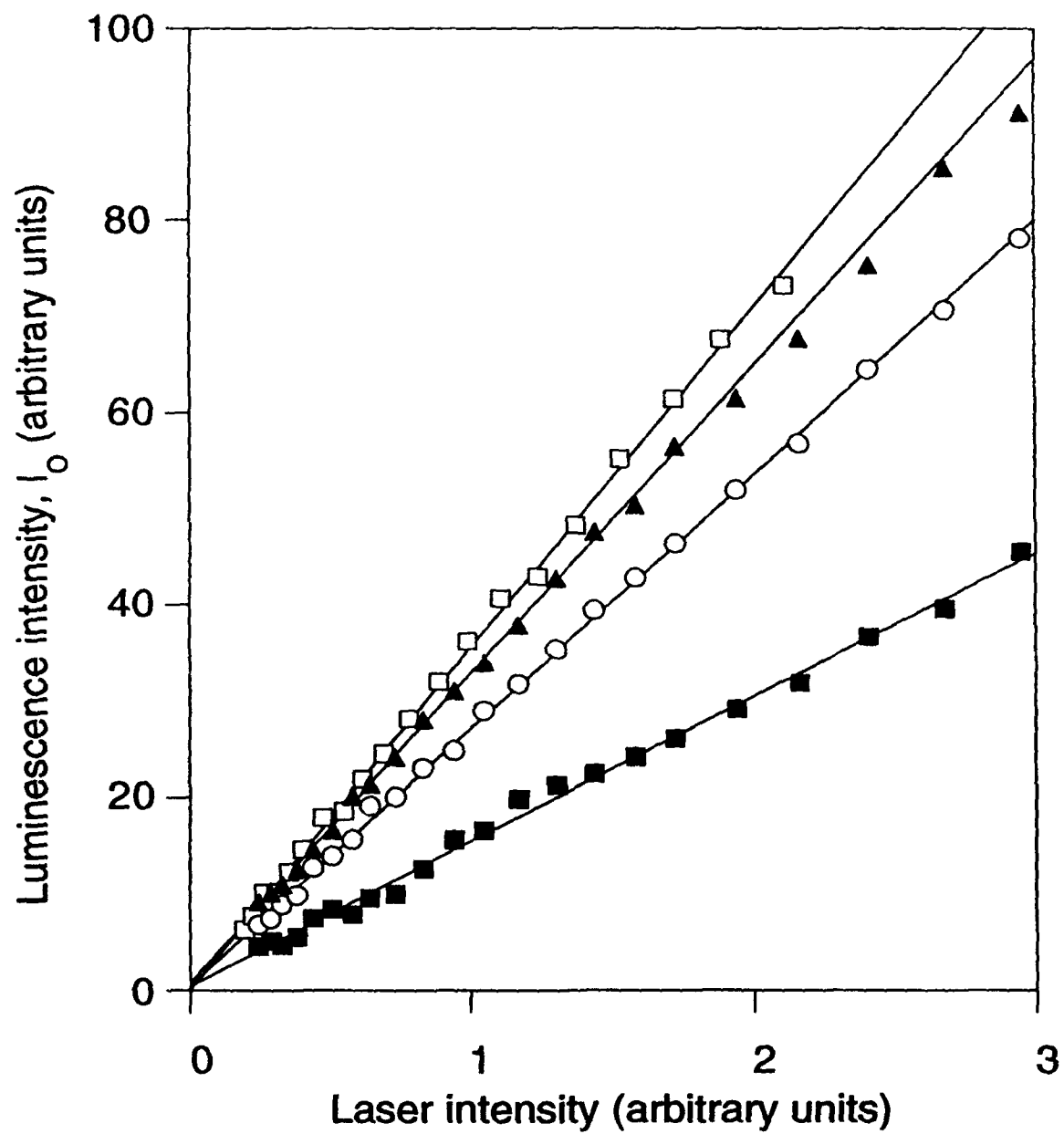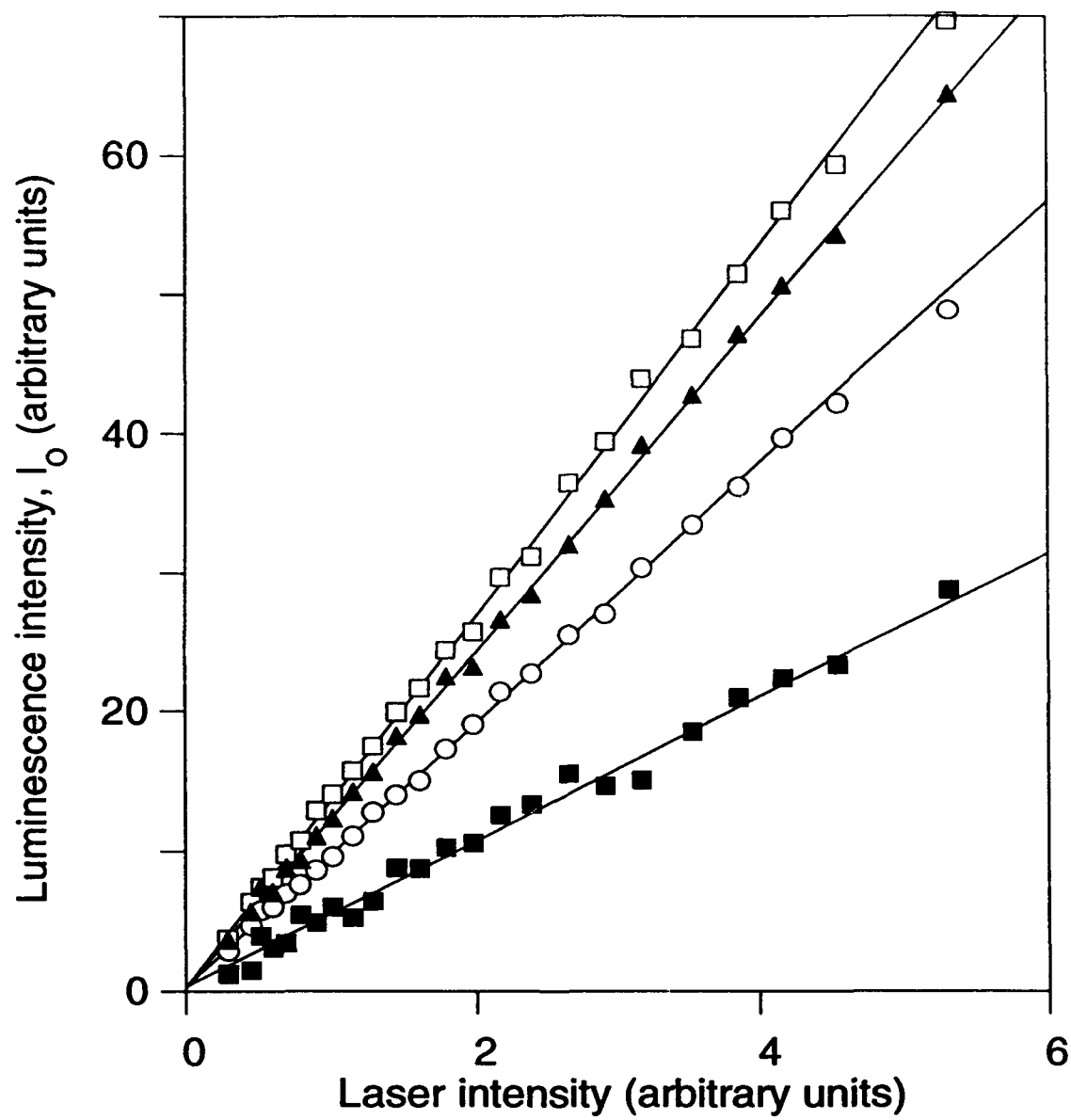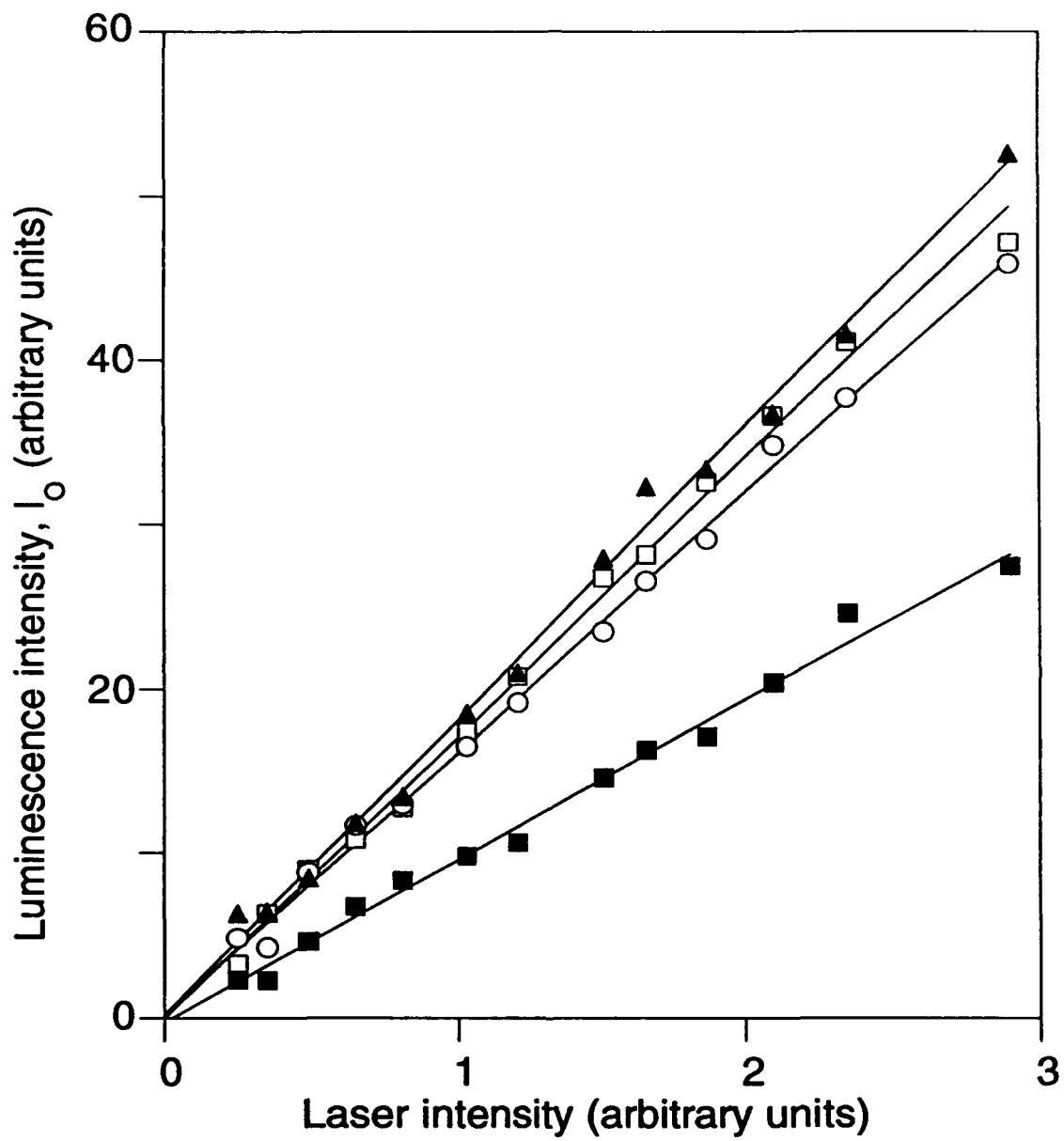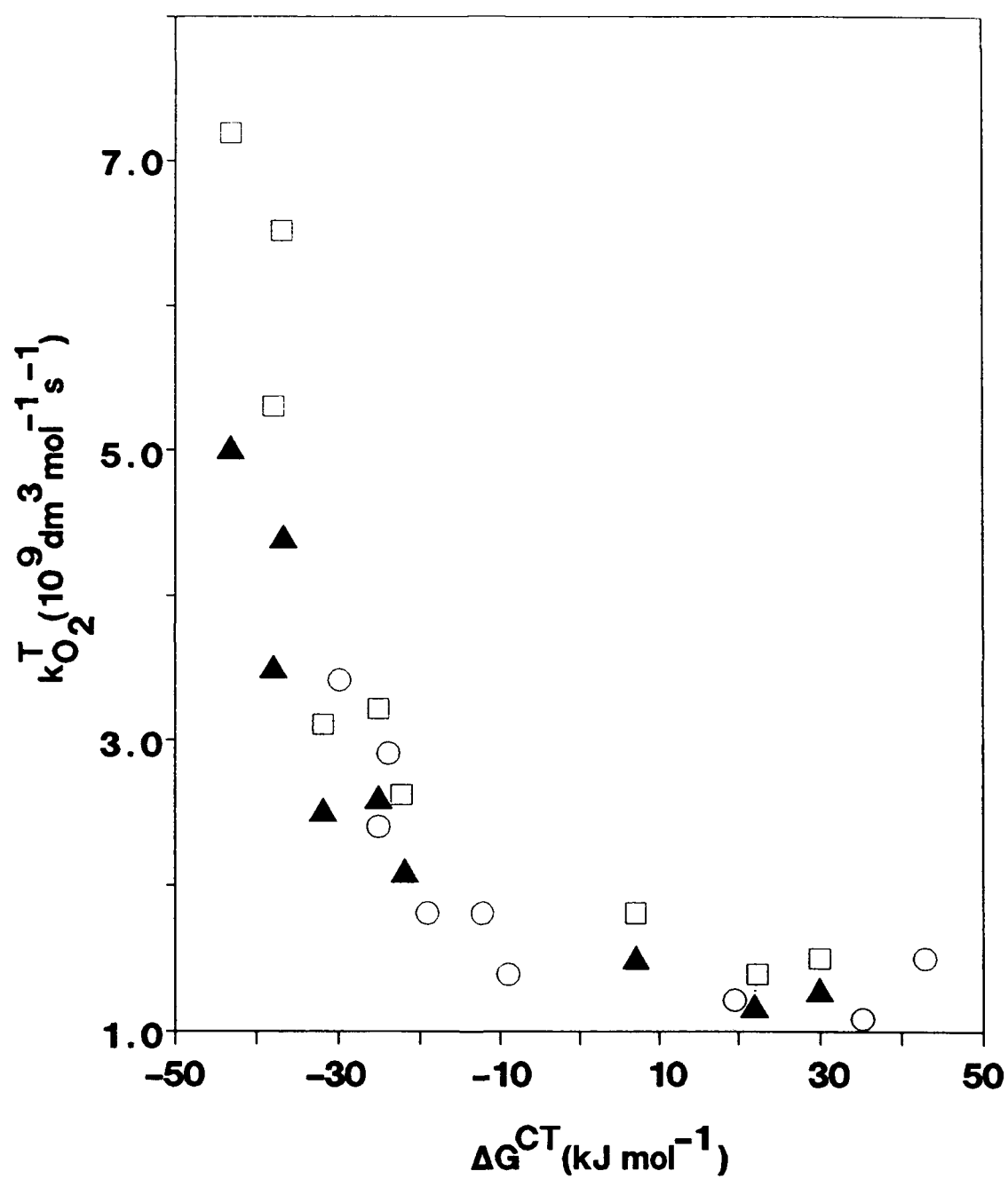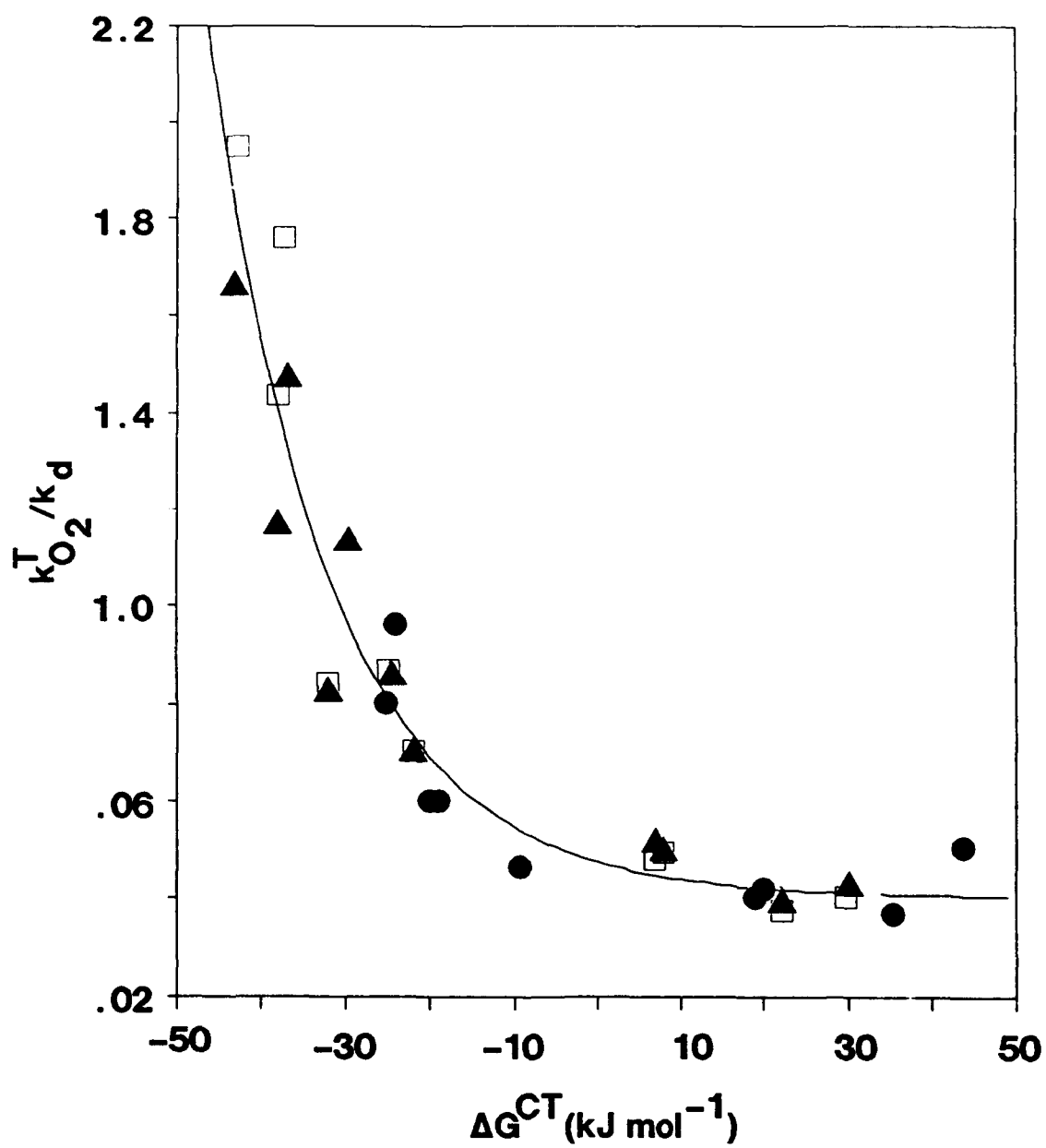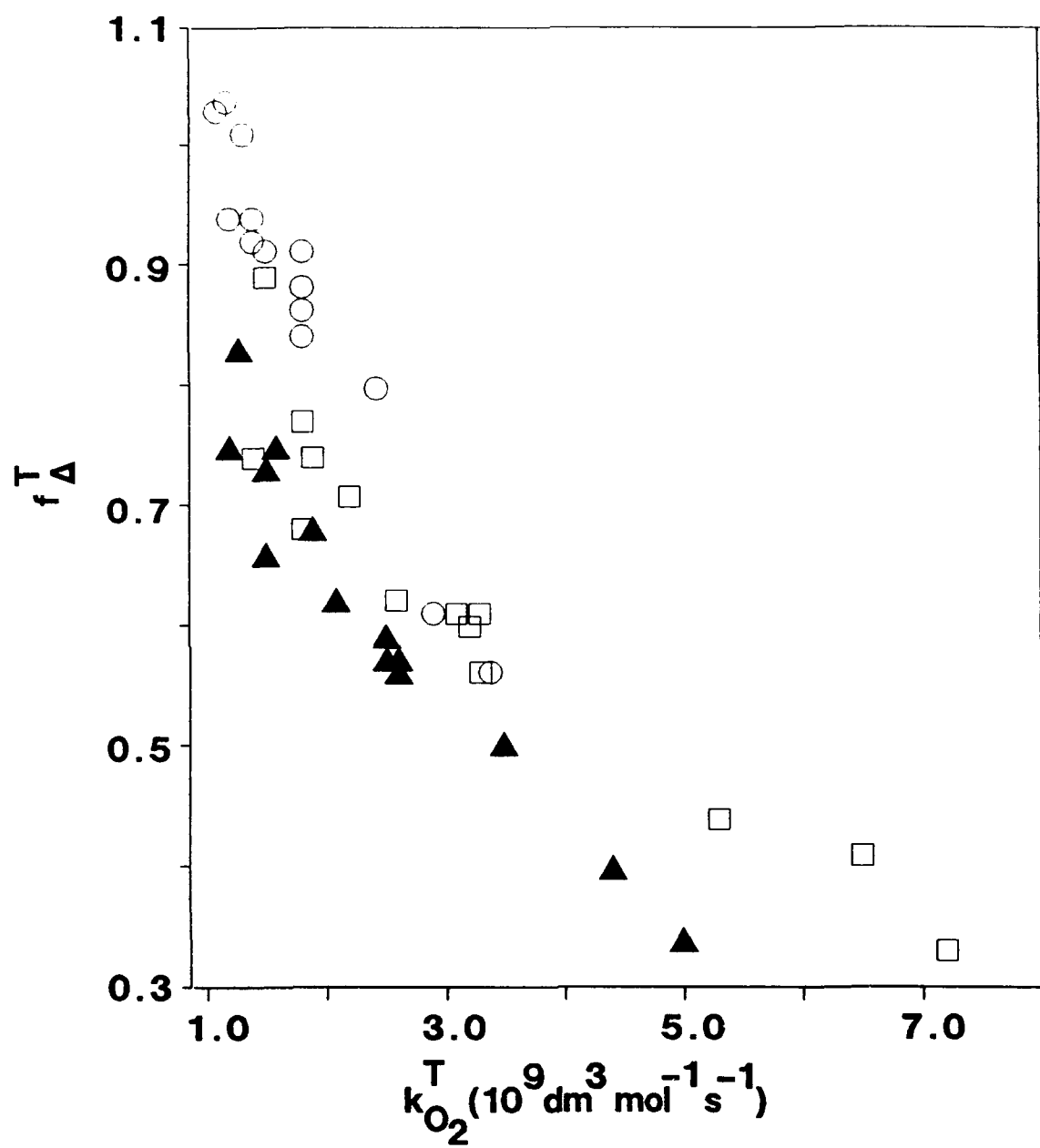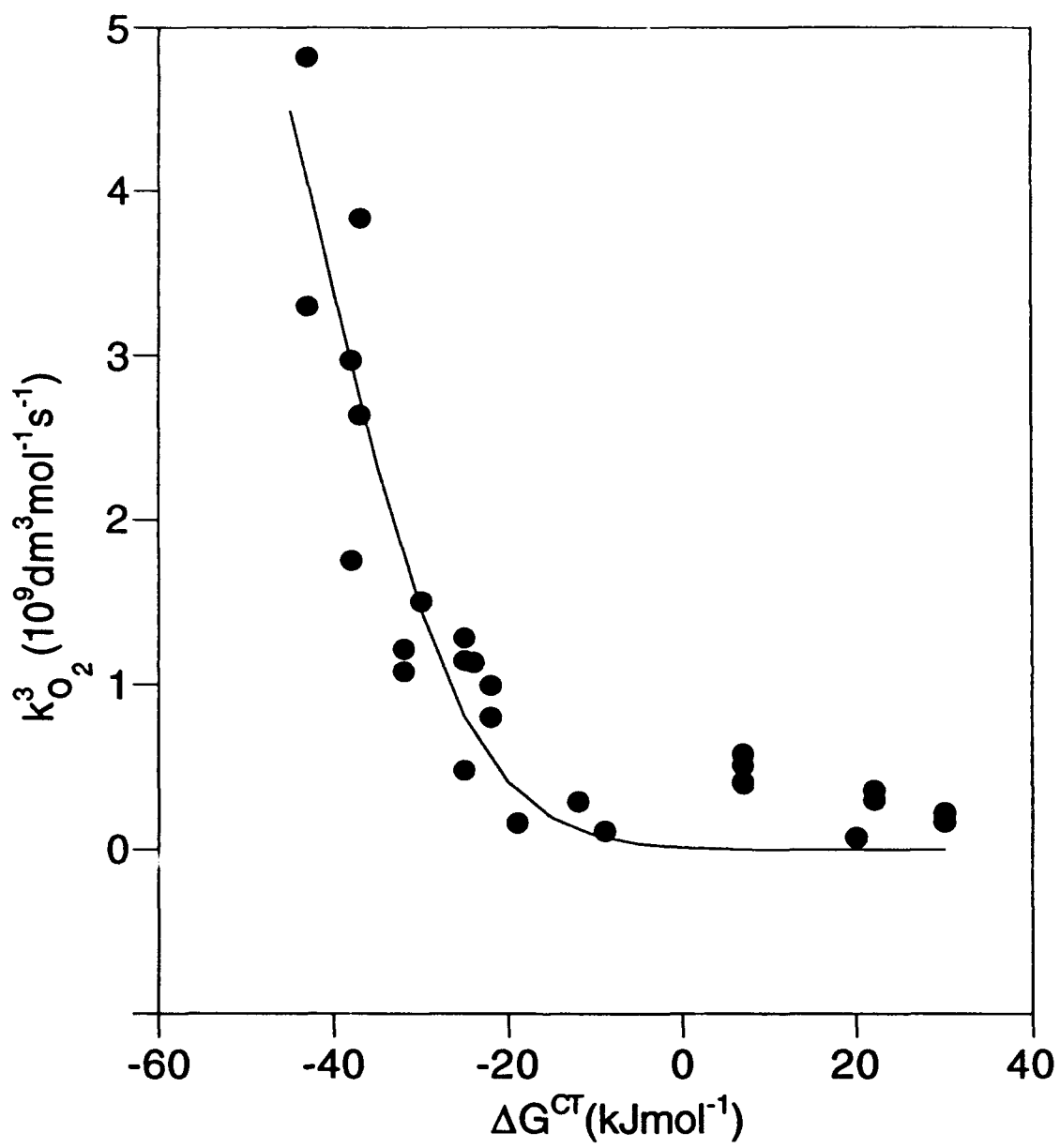
Nanosecond and Picosecond Laser Flash Photolysis Studies of Charge Transfer Interactions in the Mechanisms of Quenching by Molecular Oxygen.

by F. Wilkinson
Department of Chemistry
Loughborough University of Technology
Loughborough, Leicestershire, LE11 3TU, U.K.

Laser Flash Photolysis studies on nanosecond and picosecond timescales have been carried out in order to demonstrate the importance of charge transfer interactions during quenching of excited states by molecular oxygen. An inverse correlation between the rate constants for oxygen quenching of the triplet states of naphthalene and several of its derivatives and the efficiency of singlet state generation is established for a range of substituted naphthalenes containing electron donating and electron withdrawing substituents in several solvents [1]. The only property which varies significantly with the substituent is the oxidation potential of the naphthalene derivative and we have established correlations between the singlet oxygen yields and the triplet quenching rate constants with the free energy change for charge transfer, thereby demonstrating the participation of charge transfer interactions in the quenching mechanism. Singlet oxygen yields vary from 0.34 to 0.75 and triplet quenching rate constants from 5×10^9 to 1.2×10^9 l. mol^{-1} s^{-1}. for 1-methoxynaphthalene and 1-cyanonaphthalene respectively. These results will be compared with those we have recently obtained for anthracene derivatives where singlet oxygen is produced as a result of oxygen quenching of both singlet and triplet states [2].

Pump-probe picosecond studies [3] in which direct excitation into the charge transfer bands of oxygenated hydrocarbon solutions have been carried out for the first time. Exciting into the charge transfer bands of oxygenated solutions of 1-ethylnaphthalene, we observed a rapidly formed long-lived absorption which is attributed to the triplet state. The efficiency of production of the triplet state from the excited charge-transfer complex exhibits a marked solvent dependence, for example, in acetonitrile the yield is only 0.4 while in cyclohexane it is 0.8. We have also measured the yield of singlet oxygen following excitation into 1-ethylnaphthalene-oxygen charge transfer complexes, relative to the singlet oxygen yields when the triplet state is produced following sensitisation with the triplet state of an aromatic ketone. The yields of singlet oxygen observed following charge transfer absorption are greater than that which would be expected on the basis of the measured triplet yields. Mechanisms of quenching of excited states by oxygen which explain these results will be discussed.

References

[1]   D.J. McGarvey, P.G. Szekeres and F. Wilkinson, Chem. Phys. Letters 199 (1992) 314.

[2]   F. Wilkinson, D.J. McGarvey and A Olea, J Amer Chem Soc. In press.

[3]   D.J. McGarvey, F. Wilkinson, D.R. Worrall, J. Hobley and W. Shaikh,
      Chem. Phys. Letters 202 (1993) 528.

Oxygen Quenching of Excited States and Quantum Yields of Sensitized Production of Singlet Oxygen.

F. Wilkinson

Department of Chemistry, Loughborough University of Technology,
Leicestershire, LE11 3TU, UK

It is well known that $O_2(^3\Sigma_g^-)$ is a potent quencher of the excited states of organic molecules (M) and that the quenching rate constants (k_q) and singlet oxygen production efficiencies (f_Δ^T) vary considerably depending on the nature of M* (its energy, multiplicity, electronic configuration, structure, oxidation potential etc) as well as on the nature of the solvent. Numerous organic molecule oxygen complexes may be postulated following interaction of M with O_2 in a variety of initial electronically excited states in which M or O_2 (or both M and O_2) are excited. In addition to these complexes, excited charge transfer states which may be written $(M^+..O_2^-)^*$ can significantly influence excited state quenching rates and f_Δ^T. We are investigating the oxygen quenching of the triplet states of substituted naphthalenes [1] in which the substituents span a wide range from the electron donating group OCH_3 to the electron withdrawing group CN. In this way the energy levels of the charge transfer states are selectively varied while other parameters remain essentially constant, e.g., the triplet energy, E_T, the nature of the electronically excited state, the solvent etc. Our results demonstrate an inverse correlation between the rate constants for oxygen quenching of triplet states and the efficiency of singlet oxygen generation for naphthalene derivatives in various solvents. Correlations between f_Δ^T, k_q^T and the free energy change ΔG_{CT} for charge transfer have also been found with values of f_Δ^T ranging from 0.34 to 1.0 and and k_q^T the quenching rate constants from 7 x 10^9 to 6 x 10^8 dm^3 mol^{-1} s^{-1}. Solvent polarity has a marked influence on the k_q^T values and these results are accounted for by invoking charge transfer states of the type $(M^+..O^-)^*$ which are low lying and increase the probability of quenching by an enhanced intersystem crossing channel (triplet channel) leading to ground state products, especially when ΔG_{CT} is exoergenic.

Oxygenated hydrocarbon solutions show CT absorption bands and enchanced $S_0 \rightarrow T_1$ absorption. These additional absorption bands originate from electronic transitions within $^3(M..O_2)$ ground state contact complexes. Thus, in principle it is possible to selectivity populate the excited state complexes which are actually formed during excited state quenching by $O_2(^3\Sigma_g^-)$. Picosecond pump-probe measurements from oxygenated hydrocarbon solutions excited directly and exclusively into the charge transfer absorption bands have been carried out. Following excitation at 353 nm which precludes population of the lowest excited singlet states of various naphthalenes their triplet states have been observed to be produced rapidly in less than 10 ps in both oxygenated acetonitrile and cyclohexane solutions. The efficiency of this triplet state production exhibits a pronounced sensitivity to the solvent being high in cyclohexane but considerably smaller in acetonitrile. Measurements of the efficiency of singlet oxygen production following charge transfer excitation [2] demonstrates that dynamic quenching of the triplet state is not the sole route to singlet oxygen.

References

[1] D.J. McGarvey, P.G. Szekeres and F. Wilkinson, Chem. Phys. Letters 199 (1992) 314.

[2] D.J. McGarvey, F. Wilkinson, D.R. Worrall, J. Hobley and W. Shaikh, Chem. Phys. Letters 202 (1993) 528.

TIME RESOLVED DIFFUSE REFLECTANCE SPECTROSCOPY INVOLVING MOLECULES ADSORBED ON OXIDE MINERALS.

by F. Wilkinson

Department of Chemistry
Loughborough University of Technology
Loughborough, Leicestershire, LE11 3TU, U.K.

Recently we have extended to heterogeneous, opaque and often highly scattering systems the advantages of being able to subject them to flash photolysis investigation by using diffuse reflected light instead of transmitted light as the analysing source on timescales extending from several seconds to picoseconds [1-3]. Laser induced transient spectra and decay kinetics have been observed from a wide variety of solid samples including fractions of monolayers of organic molecules adsorbed on catalytic metal oxide surfaces, and included within the hydrophobic man-made zeolite silicalite, from paper pulp, from semiconductor powders and sintered porous electrodes doped and undoped, from organic and inorganic microcrystals, and from dyes adsorbed on fabrics and chemically bound to polymers.

In this lecture we shall discuss the technique of diffuse reflectance laser flash photolysis and its application to the study of photoinduced transient species formed when various solid samples are subjected to nanosecond and picosecond laser flash photolysis. Firstly, experimental details will be described as will typical experimental results obtained from microcrystalline organic dyes, from dyes adsorbed on metal oxide surfaces and on fabrics. Time resolved spectra showing laser induced changes in diffuse reflectance decaying as a function of time, often show isosbestic behaviour and the methods we have developed to extract from raw experimental data, transient spectra, decay kinetics, extinction coefficients and quantum yields of production etc., will be illustrated. The potential of the technique to study photochemical reactions at interfaces is demonstrated with particular reference to bimolecular reactions including, triplet-triplet annihilation, ion-electron recombination, radical recombination,and energy transfer between adsorbed molecules on porous silica surfaces.

REFERENCES

R.W. Kessler and F. Wilkinson, *J. Chem. soc., Faraday Trans I*, 77, (1981), 309.

F. Wilkinson and G.P. Kelly,(1990) In "Handbook of rganic Photochemistry. Vol 1." J.C.Scaiano (Ed), CRC Press, Ch 12.

G.P. Kelly, P.A. Leicester, F. Wilkinson, D.R. Worrall, L.F.V. Ferreira, R. Chittock and W. Toner, *Spectrochim. Acta.*, 46A, (1990), 975.

NANOSECOND AND PICOSECOND STUDIES OF THE EFFECTS OF CHARGE TRANSFER INTERACTIONS ON OXYGEN QUENCHING OF EXCITED STATES AND ON SINGLET OXYGEN YIELDS

F. Wilkinson and D.J McGarvey

Department of Chemistry, Loughborough University of Technology,
Leicestershire, LE11 3TU, UK

It is well known that $O_2(^3\Sigma_g^-)$ is a potent quencher of the excited states of organic molecules (M) and that the quenching rate constants (k_q) and singlet oxygen production efficiencies (S_Δ) vary considerably depending on the nature of M* (its energy, multiplicity, electronic configuration, structure, oxidation potential etc) as well as on the nature of the solvent. These studies aim to enhance the understanding of the interactions between the excited states of organic molecules and molecular oxygen which determine excited state quenching rates and singlet oxygen production, processes which are poorly understood and potentially very complex. It is believed that quenching proceeds through excited state complexes (M..O_2*) of the excited organic molecules with oxygen. Numerous organic molecule oxygen complexes may be postulated following interaction of M with O_2 in a variety of initial electronically excited states in which M or O_2 (or both M and O_2) are excited. In addition to these complexes, excited charge transfer states which may be written (M$^+$..O_2^-)* can significantly influence excited state quenching rates and S_Δ. We are investigating the oxygen quenching of the triplet states of substituted naphthalenes [1] and biphenyls in which the substituents span a wide range from the electron donating group OCH_3 to the electron withdrawing group CN. In this way the energy levels of the charge transfer states are selectively varied while other parameters remain essentially constant, e.g., the triplet energy, E_T, the nature of the electronically excited state, the structure, solvent etc. Thus the only significant parameter which is varying is the oxidation potential of the organic molecule. Our results demonstrate an inverse correlation between the rate constants for oxygen quenching of triplet states and the efficiency of singlet oxygen generation for both naphthalene and biphenyl derivatives in various solvents. Correlations between S_Δ, k_q^T and the free energy change ΔG_{CT} for charge transfer have also been found with values of S_Δ and k_q^T ranging from 0.34 to 1.0 and quenching rate constants from 7×10^9 to 6×10^8 dm^3 mol^{-1} s^{-1} respectively. Solvent polarity has a marked influence on the k_q^T values and these results are accounted for by invoking charge transfer states of the type (M$^+$..O$^-$)* which are low lying and increase the probability of quenching by an enhanced intersystem crossing channel (triplet channel) leading to ground state products, especially when ΔG_{CT} is exoergenic.

Mulliken [2] and Evans [3] have previouly reported the observation of CT absorption bands and enchanced $S_0 \rightarrow T_1$ absorption bands in oxygenated hydrocarbon solutions. These additional absorption bands originate from electronic transitions within ^{3}(M..O_2) ground state contact complexes. Thus, in principle it is possible to selectivity populate the excited state complexes which are actually formed during excited state quenching by $O_2(^3\Sigma_g^-)$.
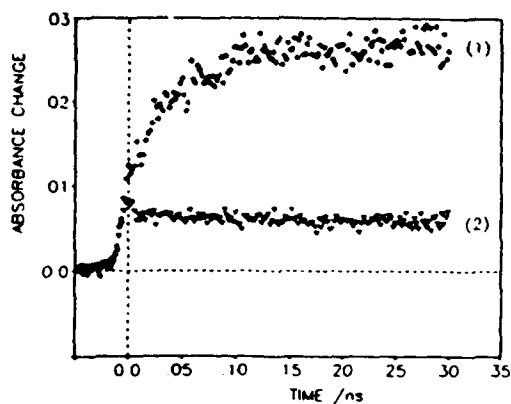
Figure 1. Subnanosecond absorption traces obtained following 7ps, 353nm excitation of (1) 1M 1-methoxynaphthalene in air-equilibrated acetonitrile containing an aromatic ketone as a sensitiser, (2) 1M 1-methoxy naphthalene in acetonitrile equilibrated with three atmospheres of oxygen. Solutions were optically matched at 353nm.
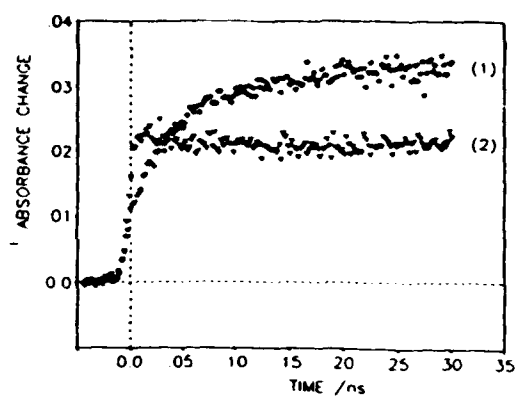
Figure 2. Subnanosecond absorption traces obtained following 7ps, 353nm excitation of (1) 1M 1-methoxynaphthalene in air-equilibrated cyclohexane containing an aromatic ketone as a sensitiser, (2) 1M 1-methoxy naphthalene in cyclohexane equilibrated with 3 atmospheres of oxygen. Solutions were optically matched at 353nm.

Picosecond pump-probe measurements from oxygenated hydrocarbon solutions excited directly and exclusively into the charge transfer absorption bands have been carried out. Following excitation at 353 nm which precludes population of the lowest excited singlet states of various naphthalenes their triplet states have been observed to be produced rapidly in less than 10 ps in both oxygenated acetonitrile and cyclohexane solutions. The efficiency of this triplet state production exhibits a pronounced sensitivity to the solvent being high in cyclohexane but considerably smaller in acetonitrile. Measurements of the efficiency of singlet oxygen production following charge transfer excitation [4] demonstrates that dynamic quenching of the triplet state is not the sole route to singlet oxygen.

References

[1]   D.J. McGarvey, P.G. Szekeres and F. Wilkinson, Chem. Phys. Letters 199 (1992) 314.
[2]   H. Tsubomura and R.S. Mulliken, J. Am. Chem. Soc. 82 (1960) 5966.
[3]   D.F. Evans, J. Chem. Soc. (1957) 1351.
[4]   D.J. McGarvey, F. Wilkinson, D.R. Worrall, J. Hobley and W. Shaikh, Chem. Phys. Letters 202 (1993) 528.

'The Role of Charge Transfer Interactions in the Mechanisms of Quenching of Triplet States by Molecular Oxygen - Nanosecond and Picosecond Laser Flash Photolysis Studies.'

by F. Wilkinson and D.J. McGarvey
Department of Chemistry
Loughborough University of Technology
Loughborough, Leicestershire, LE11 3TU, U.K.

Laser Flash Photolysis studies on nanosecond and picosecond timescales have been carried out in order to demonstrate the importance of charge transfer interactions during quenching of excited states by molecular oxygen. An inverse correlation between the rate constants for oxygen quenching of the triplet states of naphthalene and several of its derivatives and the efficiency of singlet state generation is established for a range of substituted naphthalenes containing electron donating and electron withdrawing substituents in several solvents. The only property which varies significantly with the substituent is the oxidation potential of the naphthalene derivative and we have established correlations between the singlet oxygen yields and the triplet quenching rate constants with the free energy change for charge transfer, thereby demonstrating the participation of charge transfer interactions in the quenching mechanism. Singlet oxygen yields vary from 0.34 to 0.75 and triplet quenching rate constants from 5×10^9 to 1.2×10^9 l. mol^{-1} s^{-1}. for 1-methoxynaphthalene and 1-cyanonaphthalene respectively.

Pump-probe picosecond studies in which direct excitation into the charge transfer bands of oxygenated hydrocarbon solutions have been carried out for the first time. Exciting into the charge transfer bands of oxygenated solutions of 1-ethylnaphthalene, we observed a rapidly formed long-lived absorption which is attributed to the triplet state. The efficiency of production of the triplet state from the excited charge-transfer complex exhibits a marked solvent dependence, for example, in acetonitrile the yield is only 0.4 while in cyclohexane it is 0.8. We have also measured the yield of singlet oxygen following excitation into 1-ethylnaphthalene-oxygen charge transfer complexes, relative to the singlet oxygen yields when the triplet state is produced following sensitisation with the triplet state of an aromatic ketone. The yields of singlet oxygen observed following charge transfer absorption are greater than that which would be expected on the basis of the measured triplet yields. Mechanisms of quenching of excited states by oxygen which explain these results will be discussed.

VI-1 / O 1 DIFFUSE REFLECTANCE LASER PHOTOLYSIS STUDIES OF LIGHT-INDUCED REACTIONS IN HETEROGENEOUS SYSTEMS

F. Wilkinson
Department of Chemistry, Loughborough University of Technology, Loughborough,
Leicestershire, LE11 3TU, England

Photochemical investigations in heterogeneous systems constitute a great challenge because of the potential such studies have for increased understanding of many photobiological processes. Hetrogeneity makes the analysis of the photochemical and photophysical data much more complicated than in homogeneous media, but its major importance justifies efforts which have been made to cope with the inherent complexity. Recently we have extended to heterogeneous opaque and often highly scattering systems, the advantages of being able to subject them to flash photolysis investigations by using diffuse reflected light instead of transmitted light as the analysing source on timescales extending from several seconds[1] to picoseconds[2]. Laser induced transient spectra and decay kinetics have been observed for a wide variety of samples including fractions of monolayers of organic molecules absorbed on catalytic metal oxide surfaces and included within zeolites, from semiconductor powders and porous electrodes doped and undoped, from ruthenium complexes within ion exchange resins from organic microcrystals and organic dyes absorbed on fabrics and on microcrystaline cellulose, from natural fibres such as wool and from paper pulp. Experimental details are reviewed in brief with some typical experimental results. The potential of the technique to study photochemical reactions at interfaces is demonstrated and the potential for studying several photobiological systems will be discussed.

References:
1. Kessler R W and Wilkinson F (1981)*J. Chem. Soc., Faraday Trans, I* , 77, 309.
2. Kelly G P, Leicester P A, Wilkinson F, Worrall D R, Ferreira L F V, Chittock R and Toner W (1990) *Spectrochim. Acta* , A46, 975.

LUMINESCENCE, TRANSIENT ABSORPTION AND ENERGY TRANSFER

INVOLVING MONOMERIC AND DIMERIC ADSORBED DYES ON SURFACES

by F. Wilkinson, L.F.V. Ferreira and D.R. Worrall

Department of Chemistry, University of Technology,

Loughborough, Leicestershire, LE11 3TU, England

The properties of molecules adsorbed at surfaces are modified to a greater or lesser extent depending on the nature of the adsorbate-adsorbent interaction. We have investigated the ground and excited state absorption and emission properties for oxazine, rhodamine and acridine dyes when they are adsorbed on the surface of microcrystalline cellulose. Ground state absorption and fluorescence measurements provide evidence for aggregation of these dyes on the surface, often in marked contrast to their behaviour in dilute fluid solution. Monomer and dimer spectra have been elucidated and the equilibrium constants for dimerisation measured for several systems.

Both fluorescent and non-fluorescent dimers have been detected. For example at low loadings of acridine orange on cellulose ($< 1 \, \mu$mol g^{-1}) the fluorescence emission is mainly due to the monomer and is similar to that observed in ethanolic solutions where little aggregation occurs, and fluorescence peaks at 530 nm [1]. A linear dependence of the fluorescence intensity on the amount of light absorbed by the dye was established for these "dilute" samples. However, at higher loadings ($> 20 \, \mu$mol g^{-1}), the fluorescence intensity decreases, and the emission is broad with its maximum at 620 nm, and is mainly due to the dimer. Different excitation spectra are obtained from dimer and monomer emissions which confirms the ground state absorption studies.

PICOSECOND ABSORPTION STUDIES OF ORGANIC MOLECULE - MOLECULAR OXYGEN EXCITED CHARGE TRANSFER COMPLEXES

by D.J. McGarvey and F. Wilkinson

Loughborough University of Technology,

Loughborough, Leicestershire, LE11 3TU

The importance of organic molecule - molecular oxygen excited charge transfer (C.T.) complexes derives from their probable participation in the oxygen quenching of excited states. Direct population of these excited C.T. states is possible by exciting into the C.T. absorption bands evident in oxygen saturated concentrated solutions of the organic molecule.

We have employed picosecond and nanosecond time resolved spectroscopy to investigate these excited C.T. complexes, in particular the rate of decay of the C.T. state, the identification of the principal product channels and the measurement of singlet oxygen yields. Picosecond absorption measurements on naphthalene and ethylnaphthalene - O_2 excited C.T. complexes employing 353nm excitation and probing at 424nm for the naphthalene triplet state have indicated rapid formation of a long-lived absorption (triplet) within the time resolution of the apparatus (5 ps).

Combining picosecond and nanosecond absorption measurements and near-i.r. luminescence measurements allows us to determine the fate of these excited C.T. complexes in different solvent environments and to advance our understanding of the quenching of excited states by oxygen.

DYNAMIC ENERGY AND ELECTRON TRANSFER ON SURFAC_S

by D.J. McGarvey, S. McHugh and F. W lkinson

Department of Chemistry, University of Technology
Loughborough, Leicestershire, LE11 3TU, England

Dynamic energy and electron transfer on solid surfa. s provides an insight to the behaviour of adsorbed molecules, particularly regarding diffusional mobility.

We have been investigating several energy and elect. o transfer systems adsorbed onto silica in order to a quire information on adsorbate interactions with the surface.

Dynamic energy transfer on silica is observed, for example, from [3]eosin to anthracene. In this case it has een established that anthracene is the mobile partner in the quenching process.

Electron transfer studies have been less conclusive, however. Excited state quenching by electron donors or acceptors is observed although radical products have yet to be detected possibly due to rapid back electron transfer. For example, we have yet to observe the products of the electron transfer between [3]anthracene and methyl viologen on silica, although the triplet state of anthracene is quenched efficiently. Dat for other energy/electron transfer systems will also e presented.

PRIMARY PHOTOCHEMICAL PROCESSES OF ORGANIC DYES ADSORBED ON SURFACES

by F. Wilkinson[a], D.R. Worrall[a] and L.F. Vierra Ferreira[b]

[a]Department of Chemistry, University of Technology, Loughborough, Leicestershire, LE11 3TU, England.

[b]Centro de Quimica Fisica Molecular, Universidade Tecnica de Lisboa, 1096 Lisboa Codex, Portugal,

The properties of molecules adsorbed at surfaces are modified to a greater or lesser extent depending on the nature of the adsorbate-adsorbent interaction. We have investigated the ground and excited state absorption and emission properties for oxazine and acridine dyes when they are adsorbed on the surface of microcrystalline cellulose. Ground state absorption and fluorescence measurements provide evidence for aggregation of these dyes on the surface, often in marked contrast to their behaviour in dilute fluid solution. Monomer and dimer spectra have been elucidated and the equilibrium constants for dimerisation measured for several systems. Both fluorescent and non-fluorescent dimers have been detected.

The absorption spectra of the triplet states of acridine orange and other dyes adsorbed on cellulose surfaces have been measured, using the technique of diffuse reflectance laser flash photolysis. Triplet lifetimes which are often considerably longer than in fluid solution have been measured. Triplet-triplet energy transfer, with triplet benzophenone as sensitizer, has been used to allow relative triplet extinction coefficients to be obtained for the first time. Both static and dynamic quenching mechanism pertain and the determining parameters controlling dynamic aspects of light induced heterogeneous reactions are discussed.